Development of radioligand binding and functional assays for the characterization of dopamine D$_2$-like receptor ligands

Dissertation

zur Erlangung des Doktorgrades der Naturwissenschaften
(Dr. rer. nat.)
an der Fakultät für Chemie und Pharmazie der Universität Regensburg

vorgelegt von
Lisa Forster
aus München

2021

Die vorliegende Arbeit entstand in der Zeit von Februar 2016 bis Mai 2021 unter der Leitung von Herrn Prof. Dr. Armin Buschauer, Herrn Prof. Dr. Günther Bernhardt und Herrn PD Dr. Max Keller an der Fakultät für Chemie und Pharmazie der Universität Regensburg.

Acknowledgements and declaration of collaborations

Publications, presentations and professional training

Peer-reviewed journal articles
(published prior to the submission of this thesis)

L. Forster, L. Grätz, D. Mönnich, G. Bernhardt, S. Pockes, A split luciferase complementation assay for the quantification of β-arrestin2 recruitment to dopamine D_2-like receptors, *Int J Mol Sci* 21 (**2020**)

S. Biselli, M. Bresinsky, K. Tropmann, L. Forster, C. Hönisch, A. Buschauer, G. Bernhardt, S. Pockes, Pharmacological characterization of a new series of carbamoylguanidines reveals potent agonism at the H_2R and D_3R, *Eur J Med Chem* 214 (**2021**)

K. Tropmann, M. Bresinsky*, L. Forster*, D. Mönnich, A. Buschauer, H.-J. Wittmann, H. Hübner, P. Gmeiner, S. Pockes, A. Strasser, Abolishing dopamine D_{2long}/D_3 receptor affinity of subtype-selective carbamoylguanidine-type histamine H_2 receptor agonists, *J Med Chem* (**2021**)
*contributed equally

Poster presentations
(only contributions as presenting author are listed)

L. Forster, N. Plank, H. Hübner, G. Bernhardt, P. Gmeiner, A. Buschauer, Aminothiazole-type histamine H_2 receptor agonists: Investigations on dopamine D_{2short} and D_3 receptor binding, *8th International Summer School "Medicinal Chemistry", September 2016, Regensburg, Germany*

L. Forster, J. Felixberger, G. Bernhardt, A. Buschauer, Development of a split luciferase-based β-arrestin recruitment assay for the D_{2long} and D_3 receptor, *9th International Summer School "Medicinal Chemistry", September 2018, Regensburg, Germany*

L. Forster, G. Bernhardt, A. Buschauer, Investigation of GPCR – β-arrestin interactions using a split luciferase complementation assay: Application to the D_{2long} and D_3 receptor, *4th German Pharm-Tox Summit, February 2019, Stuttgart, Germany*

L. Forster, A. Buschauer, G. Bernhardt, Dopamine D_2 receptor signaling: Toward deconvolution of the holistic readout obtained by dynamic mass redistribution, *DPhG Annual Meeting, September 2019, Heidelberg, Germany*

L. Forster, L. Grätz, D. Mönnich, G. Bernhardt, S. Pockes, A split luciferase complementation assay for the quantification of β-arrestin2 recruitment to dopamine D_2-like receptors, *6th German Pharm-Tox Summit, March 2021, digital*

Short oral presentation

L. Forster, L. Grätz, D. Mönnich, G. Bernhardt, S. Pockes, A split luciferase complementation assay for the quantification of β-arrestin2 recruitment to dopamine D_2-like receptors, *9th GDR3545-GPCR international meeting, November 2020, digital*

Professional training

Since 02/2016:	Member of the "ChemPharm" Graduate School of the University of Regensburg
03/2017:	Fortbildung für Projektleiter und Beauftragte für Biologische Sicherheit (§§ 15 und 17 Gentechniksicherheitsverordnung), Regensburg
12/2020:	Fachapothekerin für pharmazeutische Analytik, Bayerische Landesapothekerkammer

Chapter 1
General introduction

1.1.   The discovery of dopamine receptors: a historical overview

The accidental discovery of the first antipsychotic in 1952[1], chlorpromazine, paved the way for the identification of the first dopamine receptor more than two decades later in 1975[2,3]. At the time, a series of antihistamines was used to enhance analgesia, whereby in some patients treated with chlorpromazine a "euphoric quietude" was observed[4]. In 1965 dopamine was described to excite or inhibit neurons[5] and in 1971 reports of a dopamine-sensitive adenylyl cyclase (AC) became the first evidence for the existence of dopamine receptors in the central nervous system (CNS)[6,7]. What was then called the "antipsychotic receptor", later described as the dopamine D_2 receptor[8], was identified by means of [^{3}H]haloperidol binding experiments and a direct correlation between clinical doses of antipsychotics and IC_{50} values for blocking [^{3}H]haloperidol binding was found[2,3]. Shortly afterwards, the existence of two distinct dopamine receptors was postulated, excitation-mediating dopamine receptors on the one hand and inhibition-mediating receptors on the other hand[9]. It became obvious that certain dopamine receptors are linked to the stimulation of adenylyl cyclase and cyclic AMP accumulation[6,10], whereas others were found to inhibit adenylyl cyclase[11]. Based on these findings, the classification in D_1 and D_2 receptors was introduced in 1979[8]. About ten years later Grandy et al.[12] cloned the human dopamine D_2 receptor and showed that due to alternative splicing of the receptor's mRNA two isoforms of this receptor exist, the D_{2short} and the D_{2long} receptor[13]. In the years 1990 and 1991, the dopamine D_1 and D_5 receptors were cloned[14-16], as well as the D_3[17] and the D_4 receptor[18], completing the family of dopamine receptors. Shortly after, a polymorphism of the coding sequence of the D_4 receptor in the human population, i.e. a varying number of repeats of a 48 base pair sequence in the region coding for the third intracellular loop (ICL3), was reported[19].

1.2.   Classification of dopamine receptors

G protein-coupled receptors (GPCRs) can be classified into five main families according to phylogenetic analysis[20]. The rhodopsin family is the largest of these groups and dopamine receptors are members of this family[21]. Within the dopamine receptor family, the receptors can be classified according to their biochemical, structural and pharmacological properties into D_1-like (D_1 and D_5) and D_2-like receptors (D_2, D_3 and D_4)[7]. This classification roots in the observation of a stimulatory as well as an inhibitory modulation of the AC by dopamine receptors, namely that D_1 receptors are positively coupled to AC, whereas D_2 receptors inhibit cAMP synthesis[22]. Now it is commonly accepted that D_1-like receptors exert this effect via activation of G proteins of the $G\alpha_{s/olf}$ family, whereas D_2-like receptor activation leads to inhibition of the AC through coupling to $G\alpha_{i/o}$ proteins[23]. Another distinguishing characteristic is that genes encoding the D_2-like receptors contain multiple introns, which leads to the occurrence of receptor variants due to alternative splicing of the mRNA[7]. At the level of the receptor structure, the two dopamine receptor classes can be distinguished due to the length of the C-terminus and the size

of the third intracellular loop (ICL3), as shown in **Figure 1.1**. The C-terminus of D_1-like receptors is about seven times longer than that of D_2-like receptors, whereas the D_2-like receptors share the feature of a long third intracellular loop[24], which appears to be a prerequisite for $G\alpha_i$ coupling[25].

D₁ receptor   **D₂long receptor**
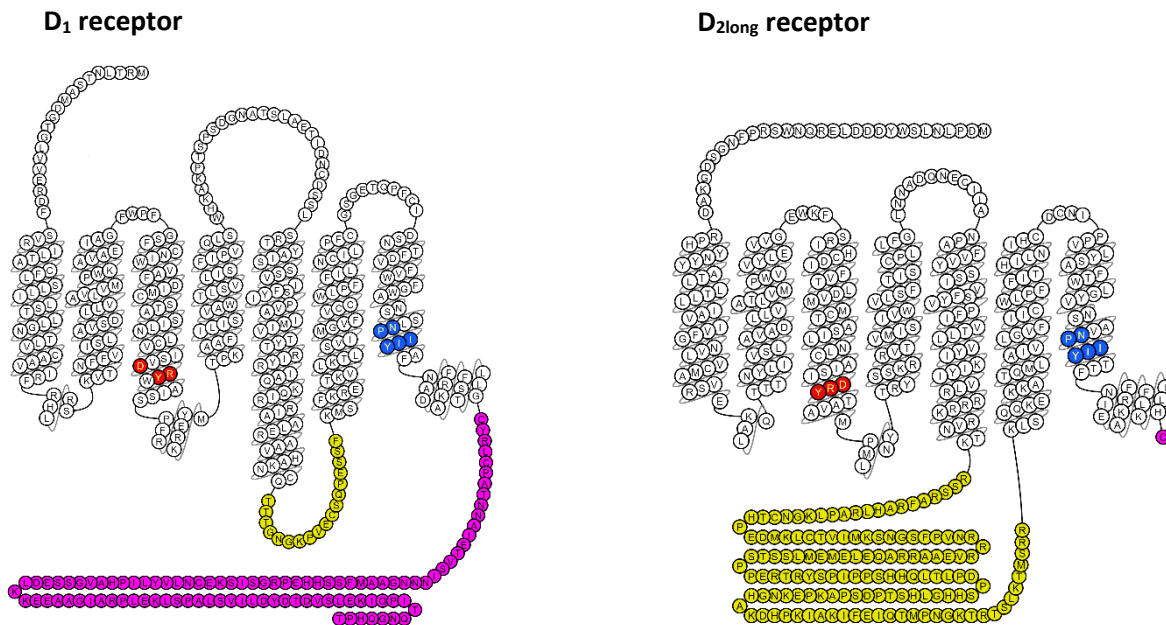
Figure 1.1. Two-dimensional schemes of the dopamine D_1 and the D_{2long} receptors. Highly conserved motifs among all class A GPCRs are shown in red and blue. The DRY motif (red) stabilizes the inactive receptor conformation, the NPXXY motif (blue) is associated with conformational changes during receptor activation and other properties, such as receptor phosphorylation and down-regulation[26,27]. The ICL3 are shown in yellow and the C-termini in pink[28,29].

1.3. Structures, expression and function of dopamine D_2-like receptors

Belonging to the superfamily of seven transmembrane (7TM) receptors alias GPCRs, the dopamine D_1- and D_2-like receptors exhibit an extracellular N-terminus, seven membrane spanning α-helices, which are connected by three extra- (ECL) and three intracellular loops (ICL), and an intracellular C-terminus[7]. In their TM regions, the D_2-like receptors share a high sequence identity, amounting to 79% for D_2/D_3 receptors, 51% for D_2/D_4 receptors and 53% for D_3/D_4 receptors[30]. Of every D_2-like receptor subtype, different variants were found. Due to alternative splicing, the D_2 receptor exists in three variants, of which the short and the long isoform are the predominant forms, differing by a 29 amino acid insert in ICL3[13]. Seeman et al.[31] discovered a third splicing variant of the D_2R, the $D_{2longer}R$ with two additional amino acids in ICL3 compared to the $D_{2long}R$, which appears to play only a minor role (found in 2.3% of the investigated population) compared to the D_{2short} (18%) and $D_{2long}R$ (79%). Shorter variants of the D_3R were reported, also resulting from alternative splicing, however they seem to be nonfunctional[32]. The D_4R was found in polymorphic variants, with different numbers of a 16 amino acid sequence repeat in the ICL3. The fourfold repeat ($D_{4.4}$) is the most common form (60%), followed by the sevenfold repeat

(D$_{4.7}$R; 14%) and the two repeat sequence (D$_{4.2}$R; 10%)[32]. The physiological role of the differing number of repeats is not fully understood yet and regarding the pharmacological properties of the variants, only minor differences have been observed[19].

Crystal structures of all three dopamine D$_2$-like receptors have been reported, the D$_3$ receptor in complex with the D$_2$/D$_3$ selective antagonist eticlopride being the first in 2010[33], followed by the D$_4$ receptor bound to nemonapride in 2017[34] and the D$_{2long}$ receptor bound to risperidone in 2018[35]. The crystallization of the receptors led to the discovery of extended binding pockets characteristic of each subtype[35], which could facilitate the development of subtype selective ligands.

The dopamine D$_{2long}$ receptor shows the highest expression level and the widest distribution of the D$_2$-like receptor family[36]. In certain brain regions, such as the hippocampus and the substantia nigra, all three D$_2$-like receptor subtypes are expressed[7,37]. The D$_2$R was furthermore detected at high levels in the olfactory tubercle, the striatum and different structures associated with the limbic systems, such as the hypothalamus and the amygdala[7,36]. Over the years, increasing evidence on different functions of the two main splicing variants of the D$_2$R has emerged. The short isoform was found to be a mainly presynaptically expressed autoreceptor, controlling dopamine release[38], while the long variant primarily mediates postsynaptic effects[39]. In comparison to the D$_2$R, the expression of the D$_3$R is more limited to the limbic system[40], but it was also found in low amounts in the striatum and the cerebellum[23,41]. As the D$_2$R, the D$_3$R is found pre- and postsynaptically[42]. The D$_4$R exhibits the lowest expression levels of the D$_2$-like receptors and was found in the cerebral cortex and the amygdala, among others[37], where it is almost exclusively expressed postsynaptically[43]. The D$_2$-like receptors can also be found in the periphery, for example in the kidney, being involved in the regulation of renal functions or the adrenal gland, where D$_2$-like receptors inhibit aldosterone secretion. Additionally, D$_2$-like receptors are expressed in the heart (D$_4$R), retina (D$_4$R) and blood vessels (D$_2$R)[7,23,37].

In general, the presynaptically expressed dopamine receptors regulate the synthesis and the release of neurotransmitters, working as negative feedback mechanisms[23]. The physiological role of brain D$_2$ receptors has been extensively studied and ranges from involvement in controlling locomotor activity[44] or reward mechanisms[45] to functions regarding memory and learning[46]. Moreover, dysregulation of D$_2$ receptor signaling is critically involved in the pathophysiology of schizophrenia or bipolar disorder[23,47]. The specific functions of the D$_3$ and the D$_4$ receptor are less well understood. D$_3$ receptors exert a less pronounced effect on locomotion compared to D$_2$ receptors[44] and are thought to be involved in cognition, together with D$_4$ receptors[48].

1.4. Dopamine D$_2$-like receptor signaling and desensitization

D$_2$-like receptors transduce signals from the extra- to the intracellular site of the plasma membrane resulting in the activation of heterotrimeric G proteins, composed of Gα, Gβ and Gγ subunits, which is referred to as G protein dependent signaling[49]. Furthermore, D$_2$-like receptors recruit β-arrestins, another major class of effector proteins, involved in the termination of G protein mediated signaling but also in so called G protein independent signaling[23].

1.4.1. G protein-dependent signaling

In general, after being activated, GPCRs undergo conformational changes, followed by coupling to G proteins[50]. In the inactive state the Gα subunit of the heterotrimeric G protein is bound to GDP, which is released upon the formation of the receptor-G protein complex. Subsequently, GTP is rapidly bound to the nucleotide binding site of the Gα subunit, which undergoes a conformational change, followed by the dissociation of the Gα and the Gβγ subunits[49]. Both subunits target different downstream effectors until the Gα-bound GTP is hydrolyzed to GDP, due to the intrinsic GTPase activity of the α-subunit, and the heterotrimeric G protein is reassociated[49]. All dopamine D$_2$-like receptors activate G proteins of the Gα$_{i/o}$ family[51] but exhibit slightly differing coupling specificities towards different Gα$_{i/o}$ isoforms. The D$_2$R was shown to activate several Gα$_i$ subtypes, as well as Gα$_o$ and Gα$_z$[52,53]. Since the two predominant variants of the D$_2$ receptor differ in the length of the ICL3, which was demonstrated to be relevant for G protein coupling in the case of adrenergic receptors[54], it was assumed that the difference in this structural element is responsible for differential G protein coupling features. However, investigations that have been made in this regard have led to inconsistent findings. It seems likely that both isoforms couple to multiple Gα$_i$ subtypes[55-57]. The D$_3$R seems to preferentially activate Gα$_o$ proteins[58,59] and generally appears to activate G proteins less effectively compared to the D$_2$R[60,61]. Additionally, the D$_3$R was reported to signal through Gα$_{q/11}$[60]. The D$_4$R activates multiple Gα$_{i/o}$ isoforms[58,62] and the varying lengths of the ICL3 in the different polymorphic variants of the receptor do not appear to have an impact on G protein coupling specificity or efficiency[62]. Via activation of Gα$_{i/o}$ proteins, D$_2$ and D$_4$ receptors distinctly inhibit the activity of the AC[48,63]. The D$_3$R also inhibits cAMP formation by ACs, but in a less pronounced manner and was reported to selectively inhibit AC type 5[64]. Through this mechanism, the D$_2$-like receptors inhibit the accumulation of cAMP, thereby decreasing protein kinase A (PKA) activity and thus may have effects on PKA substrates[23]. In the case of the D$_2$R, downstream effects on, for example, ionotropic glutamate receptors (AMPA, NMDA) and DARPP-32 (32-kDa dopamine and cAMP regulated phosphoprotein) were observed, as depicted schematically in **Figure 2**[23]. This contributes to slow synaptic transmission in the brain, whereby dopamine receptors modulate the action of fast acting neurotransmitters, such as glutamate or γ-aminobutyric acid[65].
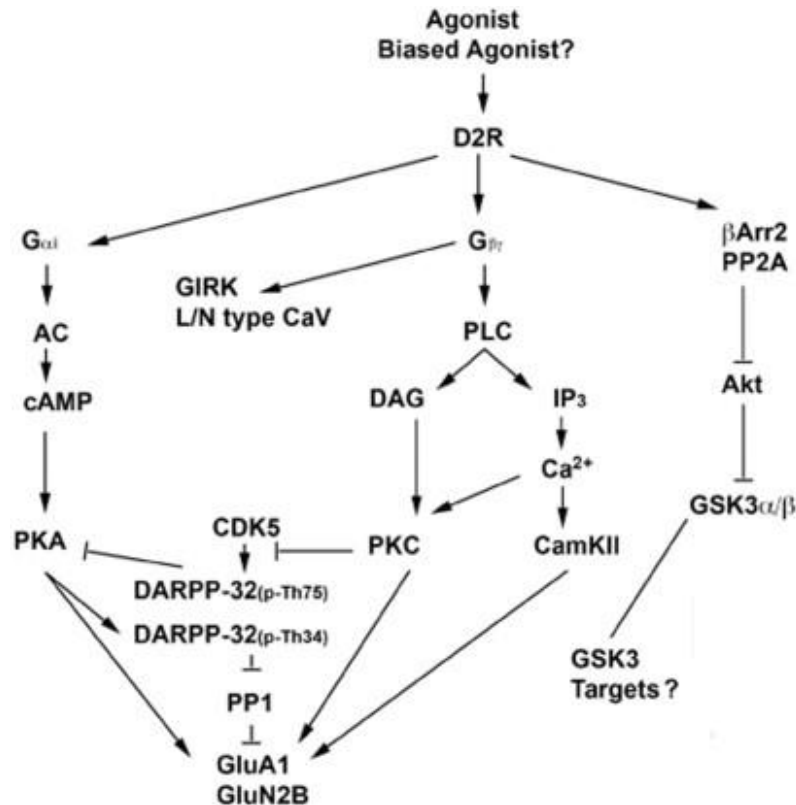
Figure 1.2. Schematic representation of dopamine D_2 receptor-mediated signaling. Extracted and modified from Beaulieu et al.[24] with permission from John Wiley & Sons, Inc.; license number: 5113560138742. CamKII, Ca^{2+}/calmodulin-dependent protein kinase II; CDK5, cyclin-dependent kinase 5; DAG, diacylglycerol; GSK3, glycogen synthase kinase 3; PKC, protein kinase C; PP1, protein phosphatase 1; PP2A, protein phosphatase 2A.

After dissociation of the heterotrimeric G protein, the Gβγ subunit regulates multiple other processes, as shown in **Figure 1.2**. Among others, Gβγ subunits were reported to activate phospholipase C (PLC) resulting in an increase in intracellular Ca^{2+} [66]. Furthermore, a reduction of Ca^{2+} currents through voltage gated Ca^{2+} channels was observed after activation of D_2 and D_3 receptors, contributing to the inhibitory properties of the D_2-like receptors[67,68]. On G protein-coupled inwardly rectifying potassium channels (GIRKs), the Gβγ subunits were reported to have stimulatory effects, which results in a decreased cell excitability[69].

1.4.2. Desensitization and β-arrestin-mediated signaling

Many of the existing paradigms concerning the regulation of GPCRs have been established based on investigations of prototypical receptors, such as the β₂ adrenergic receptor. The mechanism of homologous desensitization of such receptors is described as follows: the agonist occupied GPCR is phosphorylated by a G protein-coupled receptor kinase (GRK) at serine and threonine residues within the C-terminal tail or the ICL3. This promotes binding of β-arrestins, which terminates the G protein coupling of the receptor and links the GPCR to clathrin-dependent endocytosis. Then, the receptor can be recycled to the plasma membrane or becomes subject to degradation[70]. This applies to many GPCRs, but there is growing evidence for exceptions from this general scheme[71]. For instance, using the

metabotropic glutamate receptor-1 (mGluR1) it was shown that GRK2-mediated receptor phosphorylation is not a mandatory prerequisite for desensitization or internalization[72]. Deviations from the general mechanism were also described for the dopamine D_2-like receptors. Activation of the D_2R is followed by GRK-mediated phosphorylation, β-arrestin recruitment and internalization[73]. However, it was shown that phosphorylation is not necessarily required for arrestin binding, desensitization or endocytosis[74]. It was postulated that an agonist-induced conformational change is the primary driver for arrestin recruitment and that arrestin association is relevant for the internalization process[74]. Interestingly, GRK2 was reported to attenuate dopamine D_2 receptor signaling, but in contrast to the generally accepted paradigm, in a phosphorylation-independent manner[71]. The exact mechanism is yet to be elucidated. Phosphorylation mediated by GRK2 was suggested to dictate whether the receptor is recycled back to the cell membrane or degraded, with phosphorylated receptors being more likely to be recycled[71,75]. In contrast to the D_2R, the D_3R only undergoes subtle agonist-mediated phosphorylation, recruits β-arrestin2 to a much lesser extent and exhibits constitutive interaction with β-arrestin2[76,77]. For the phosphorylation-independent desensitization of the D_3R a completely novel mechanism was postulated[78]. It was observed that the D_3R mediates, independent of agonist binding, translocation of Mdm2 from the nucleus to the cytosol, a ubiquitin ligase which ubiquitinates β-arrestin2[79]. After agonist stimulation of the D_3R, Mdm2 translocates to the nucleus and β-arrestin2 is deubiquitinated, subsequently forming a tight complex with the Gβγ subunit and thereby preventing D_3R signaling and reassociation of the heterotrimeric G protein[78]. In the case of the D_4 receptor, neither agonist-promoted phosphorylation nor β-arrestin recruitment could be observed[80,81].

Besides their functions in the termination of G protein-mediated signaling or receptor internalization, β-arrestins mediate further signaling processes. D_2 receptors have been shown to regulate Akt, a protein kinase, through β-arrestin2 (**Figure 1.2**)[82]. Stimulation of the receptor leads to the formation of a signaling complex of receptor, β-arrestin2, Akt and protein phosphatase 2A (PP2A), whereas the latter deactivates Akt. Subsequently, GSK3 (glycogen synthase kinase) signaling is stimulated, which has been shown to be involved in the regulation of behavior by dopamine, such as locomotor activity[83]. In addition, β-arrestins act as scaffolding proteins for other cytoplasmic signaling complexes[84] and play a complementary role in the negative regulation of G protein signaling by recruiting enzymes, that catalyze second messenger degradation, such as cAMP phosphodiesterases[85].

1.5. Drugs targeting dopamine D_2-like receptors

Drugs targeting GPCRs represent about a quarter of the global therapeutic drug market of which 11% are drugs addressing dopaminergic receptors[86]. Due to the expression pattern and the physiological functions of the D_2-like receptors, they are involved in the etiology and therapy of different

pathological conditions, such as Parkinson's disease, schizophrenia, Tourette's syndrome or attention deficit hyperactivity disorder (ADHD)[23]. In general, D_2-like receptor agonists, such as pramipexole or apomorphine (**Figure 1.3**), are applied in the therapy of Parkinson's disease to counteract the consequences of the loss of dopamine-producing neurons in the substantia nigra[87]. Compounds, antagonizing D_2-like receptor functions, such as haloperidol or sulpiride (**Figure 1.3**) exert antipsychotic effects and are therefore indicated in the therapy of schizophrenia or ADHD. High concentrations of $D_{2/3}$ receptors can be found in the chemoreceptive trigger zone located in the brainstem, which is implicated in the control of nausea and vomiting[88]. Dopamine D_2-like receptor antagonists like domperidone (**Figure 1.3**) or the non-specific dopamine D_2/serotonin 5-HT_3 receptor antagonist metoclopramide are therefore also used to control nausea and vomiting[88]. However, the pharmacology of more recently developed antipsychotics, such as aripiprazole (**Figure 1.3**) or cariprazine is more complex and remains controversial. Aripiprazole was reported to exhibit activities of a partial agonist in inhibiting cAMP accumulation[89,90] but antagonized binding of GTPγS to G-proteins[91]. The findings regarding β-arrestin recruitment are also controversial, since aripiprazole was described as a partial agonist in recruiting β-arrestin2 to the D_2R[92] and as an antagonist, a feature commonly described for antipsychotics[93]. Cariprazine displays comparable actions at the D_2R but other than aripiprazole, exhibits a higher affinity for the D_3R[94].

The development of subtype selective ligands remains difficult due to the high amino acid homology within the transmembrane spanning domains of the D_2-like receptors and clinically used dopaminergic drugs are not subtype selective[95,96]. D_2 receptor subtype selective antagonists were thought to be a valuable remedy in the treatment of psychosis or schizophrenia, but the development has proven difficult[95]. Few ligands with only moderate selectivity have been reported. A promising compound (indole derivative **1.1**, **Figure 1.3**) was reported by Vangveravong et al.[97], however, following studies revealed a short half-life due to metabolic instability[95]. D_3 receptor selective antagonists are potential drug candidates for the treatment of substance abuse[98]. In an approach to develop compounds that occupy the orthosteric binding site as well as the secondary binding pocket of the D_3R, which was discovered by means of the crystal structure of the receptor[33], compound **1.2** (**Figure 1.3**) was developed, exhibiting about 1700-fold selectivity for the D_3R over the D_2R[98]. Many potent D_2/D_3/D_4 ligands belong to the class of 1,4-disubstituted aromatic piperazines and piperidines (1,4-DAPs), such as haloperidol (**Figure 1.3**) and it was discovered that 1,4-DAPs containing a short methylene linker exhibit enhanced D_4R selectivity[96]. FAUC 213 (**Figure 1.3**) is a 1,4-disubstituted piperazine that exhibits antagonistic properties and high D_4 receptor selectivity[99]. Another structure-based approach to the development of D_4R selective ligands in the context of the determination of the D_4R crystal structure led to the partial agonist **1.3** (**Figure 1.3**), which occupies the orthosteric binding site of the D_4R, as well as the secondary binding pocket[34]. The first reported D_2R selective agonist was suminarole, however,

subsequent studies revealed only a moderate selectivity towards the D_2 receptor[95]. Based on the sumanirole scaffold other D_2 agonists were developed by attaching molecular fragments, aiming at the design of ligands that occupy the OBS and the secondary binding pocket of the receptor simultaneously[100]. The developed compounds, such as compound **1.4** (**Figure 1.3**), exhibit G_o protein bias, but show also only moderate subtype selectivity[100]. D_3 receptor agonists have potential neuroprotective and neurorestorative properties[95]. Since numerous known agonists, such as dopamine or pramipexole slightly prefer the D_3 over the D_2 receptor[95], Chen et al. developed highly selective D_3R agonists based on the pramipexole scaffold (compound **1.5**, **Figure 1.3**), which could help to investigate the physiological role of the D_3R in different processes[101].

(partial) agonists
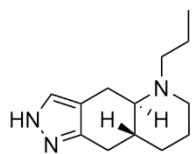
(-)-quinpirole
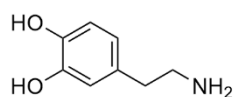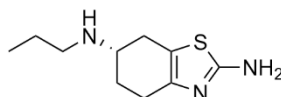
dopamine

pramipexole
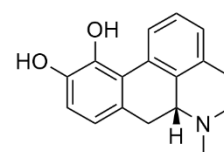
R-(-)-apomorphine
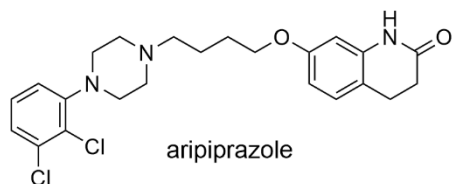
aripiprazole
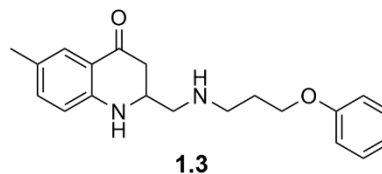
1.3
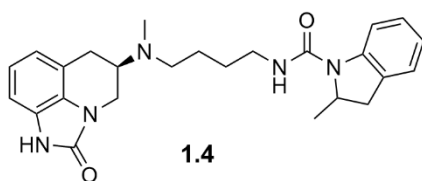
1.4
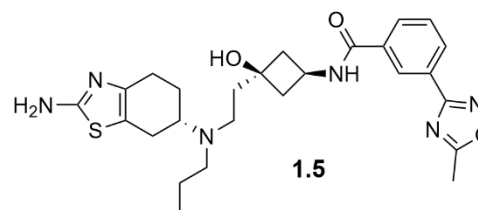
1.5

antagonists
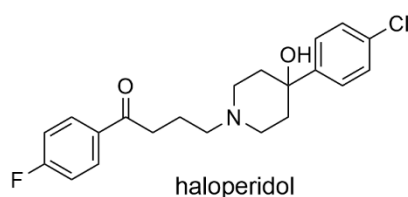
haloperidol
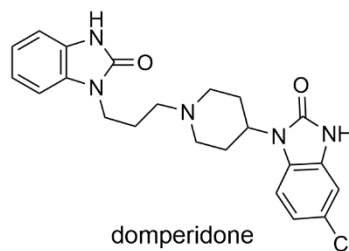
domperidone
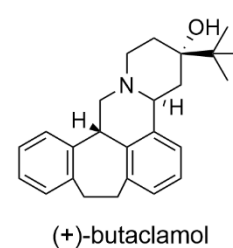
(+)-butaclamol
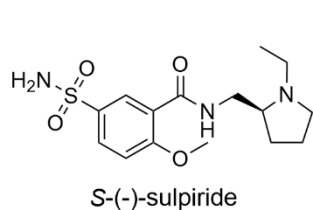
S-(-)-sulpiride
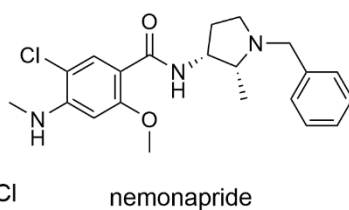
nemonapride
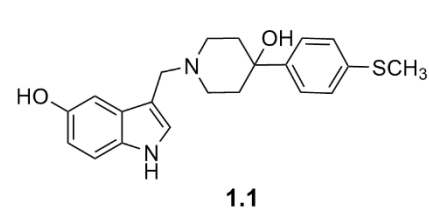
1.1
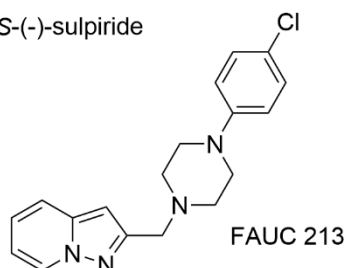
FAUC 213
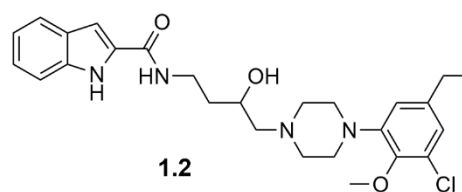
1.2

Figure 1.3. Structures of compounds targeting dopamine D$_2$-like receptors.

1.6. Methods in GPCR drug discovery

GPCRs represent intensively studied drug targets and there is a variety of assays available to investigate ligands acting at GPCRs. A small selection of binding and functional assays is presented in **Table 1.1**, where advantages and disadvantages of the different techniques are briefly addressed.

Table 1.1. A selection of common binding and functional assays for investigations at GPCRs.

assay type	measurement	advantages	disadvantages	equilibrium
binding	quantification of ligand-GPCR interaction			
radioligand binding	binding of a radiolabelled ligand is quantified by the measurement of radioactivity	• theoretically applicable to any GPCR • no artificial modifications of ligands (if isotopes ^{3}H or ^{14}C are used) or receptors • ligand depletion, if occurring, can be easily quantified	• availability of radiolabelled ligands with high affinity • ionizing radiation • high costs for disposal of radioactive waste • separation step required	equilibrium, but can be disturbed by the separation of bound/unbound ligand
fluorescence polarisation/anisotropy	ligand binding is monitored by changes in the polarization of emitted light when a fluorescently labelled ligand is bound to a receptor[102]	• no separation step required • real-time monitoring	• ligand is modified (fluorescently labelled) • low signal-to-noise-ratio • ligand depletion is unavoidable	equilibrium
flow cytometry	binding of a fluorescently labelled ligand is detected by measuring the fluorescence intensity of single cells	• no separation step required • neglectable ligand depletion	• ligand is modified (fluorescently labelled)	equilibrium
high content imaging	combination of high-resolution fluorescence microscopy with automated image analysis[103]	• real-time monitoring possible • neglectable ligand depletion • no separation/wash step required (depends on the affinity and extent of unspecific binding of the fluorescent ligand)	• high costs • ligand is modified (fluorescently labelled)	equilibrium (if no separation step is required)
BRET binding	BRET occurs when a fluorescently labelled ligand binds to a receptor, which is fused to a luciferase, such as NanoLuc, in the presence of a substrate[104]	• no separation step required • no need for excitation light • real-time monitoring	• artificial modifications of the receptors/ligands	equilibrium

functional assays

[^{35}S]GTPγS	direct measurement of G protein activation using a non-hydrolysable GTP analogue[105]	• proximal readout • discrimination between different modes of ligand action	• often low signal-to-noise-ratios with $Gα_s$ or $Gα_q$ coupling receptors[106] • ionizing radiation • separation step required	no equilibrium
Ca^{2+}	fluorescent indicators change their optical properties upon Ca^{2+} binding/expression of Ca^{2+}-sensitive aequorin, that generates a luminescent signal in the presence of substrate[107]	• high sensitivity • real-time monitoring • discrimination between different modes of ligand action • homogenous	• not applicable to investigations of inverse agonists	no equilibrium, transient signal
cAMP	different methods available: • BRET-based cAMP sensor (CAMYEL)[108] • permuted firefly luciferase that undergoes conformational change upon cAMP binding concomitant with an increased luciferase activity (cAMP Glosensor™ by Promega)[109] • split enzyme complementation using β-galactosidase (HitHunter™ by DiscoverX)[109]	• real-time monitoring • homogenous • Glosensor: very sensitive, applicable to $Gα_i$-coupling receptors without forskolin prestimulation	• investigating antagonists at $Gα_{i/o}$-coupled receptors can be difficult • no real-time monitoring	no equilibrium
gene reporter assays	GPCR-mediated changes in second messengers alter the expression of conveniently detectable gene products[107]	• high sensitivity • theoretically applicable to any GPCR	• distal readout, comparably high risk of false positives due to interferences with other signaling pathways • long incubation times	equilibrium
high content imaging	combination of high-resolution fluorescence microscopy with automated image analysis[103]	• monitoring of diverse GPCR functions • real-time monitoring of spatio-temporal events possible	• high costs • complex assay protocols, labour and data intensive • modification of proteins and ligands of interest	depends on the process under investigation

label-free methods				
DMR (dynamic mass redistribution)	• cells are grown on optical biosensors, which transform changes in cell shape or redistribution of cellular constituents into an optical readout[110]	• highly sensitive (exceeds sensitivity of traditional methods)[110] • real-time monitoring • discrimination between different modes of ligand action • no artificial modifications of receptors or ligands required	• potentially higher risk for false positives and negatives • further pathway analysis needed	no equilibrium
ECIS (electric cell-substrate impedance sensing)	• cells are cultured on small gold electrodes, to which an alternating current is applied and changes in impedance are monitored[111]			

1.7 Scope of this thesis

In our research group, the development of subtype selective histamine H_2 receptor ligands as pharmacological tools for investigating the physiological role of H_2 receptors especially in the CNS has been of great interest. During the optimization process of histamine H_2 receptor ligands, the need for assays to characterize compounds in binding and functional assays at dopamine D_2-like receptors emerged, since carbamoylguanidine-type H_2R ligands containing a 2-aminothiazole moiety share structural similarities with reported dopamine D_2-like receptor agonists. As both histamine H_2 and dopamine receptors are expressed in the CNS[24,112,113], pharmacological tools for the investigation of central H_2 receptors must be characterized with respect to dopamine receptor binding.

Overall, binding assays are indispensable for the characterization of GPCR ligands. In order to provide means for the determination of D_2-like receptor affinities, this thesis aimed at the establishment of a radioligand binding assay for all three D_2-like receptor subtypes. For this purpose, HEK293T cell lines stably expressing the physiologically most dominant receptor isoforms of the human D_2-like receptor subtypes ($hD_{2long}R$, hD_3R, $hD_{4.4}R$) had to be generated. The binding of the used radioligand to every receptor subtype had to be investigated and the assay needed to be validated by screening of reported D_2-like receptor ligands and comparing the data with literature reports.

Furthermore, an assay to probe β-arrestin recruitment to D_2-like receptors, using the split luciferase complementation technique[114] was aimed at, enabling the functional characterization of dopamine receptor ligands. HEK293T cells stably co-expressing the fusion constructs of β-arrestin2 with a split luciferase fragment and the hD_{2long}, hD_3 or $hD_{4.4}$ receptor fused to the complementary luciferase fragment had to be developed for this purpose. For the validation of the assay, sets of reported D_2-like receptor (partial) agonists and antagonists had to be screened and again the results compared with literature data.

Label-free assays, such as the dynamic mass redistribution (DMR) assay, yield holistic information resulting from live cell responses to GPCR stimulation, utilizing optical biosensors. In contrast to assays that quantify the activation of a distinct signaling pathway, DMR represents a readout resulting from an integrated cell response to receptor stimulation. For the investigation of ligand agonism and antagonism at the D_{2long} receptor with the DMR technique, a stable CHO-K1 $hD_{2long}R$ cell line was intended to be used. Results from the screening of known D_2 receptor ligands with the DMR assay under optimized conditions had to be compared with data derived from more traditional functional assays. Additionally, using specific pathway inhibitors, the signaling pathway in CHO-K1 $hD_{2long}R$ cells had to be explored.

1.8 References

1. M. Lacomme, H. Laborit, G. Le Lorier, M. Pommier, Obstetric analgesia potentiated by associated intravenous dolosal with RP 4560. *Bull Féd Soc Gynecol Obstétr Lang Fr* **4**, 558-562 (1952).

2. P. Seeman, M. Chau-Wong, J. Tedesco, K. Wong, Brain receptors for antipsychotic drugs and dopamine: direct binding assays. *Proc Nat Acad Sci USA* **72**, 4376-4380; doi:10.1073/pnas.72.11.4376 (1975).

3. P. Seeman, T. Lee, Antipsychotic drugs: direct correlation between clinical potency and presynaptic action on dopamine neurons. *Science* **188**, 1217-1219; doi:10.1126/science.1145194 (1975).

4. P. Seeman, in *The Dopamine Receptors,* K. Neve, Ed. (Humana Press, 2010), vol. 2, chap. 1.

5. F. E. Bloom, E. Costa, G. C. Salmoiraghi, Anesthesia and the responsiveness of individual neurons of the caudate nucleus of the cat to acetylcholine, norepinephrine and dopamine administered by microelectrophoresis. *J Pharmacol Exp Ther* **150**, 244-252 (1965).

6. J. W. Kebabian, P. Greengard, Dopamine-sensitive adenyl cyclase: possible role in synaptic transmission. *Science* **174**, 1346-1349; doi:10.1126/science.174.4016.1346 (1971).

7. C. Missale, S. R. Nash, S. W. Robinson, M. Jaber, M. G. Caron, Dopamine receptors: from structure to function. *Physiol Rev* **78**, 189-225; doi:10.1152/physrev.1998.78.1.189 (1998).

8. J. W. Kebabian, D. B. Calne, Multiple receptors for dopamine. *Nature* **277**, 93-96; doi:10.1038/277093a0 (1979).

9. A. R. Cools, J. M. Van Rossum, Excitation-mediating and inhibition-mediating dopamine-receptors: a new concept towards a better understanding of electrophysiological, biochemical, pharmacological, functional and clinical data. *Psychopharmacologia* **45**, 243-254; doi:10.1007/BF00421135 (1976).

10. E. M. Brown, R. J. Carroll, G. D. Aurbach, Dopaminergic stimulation of cyclic AMP accumulation and parathyroid hormone release from dispersed bovine parathyroid cells. *Proc Nat Acad Sci USA* **74**, 4210-4213; doi:10.1073/pnas.74.10.4210 (1977).

11. P. De Camilli, D. Macconi, A. Spada, Dopamine inhibits adenylate cyclase in human prolactin-secreting pituitary adenomas. *Nature* **278**, 252-254; doi:10.1038/278252a0 (1979).

12. D. K. Grandy, M. A. Marchionni, H. Makam, R. E. Stofko, M. Alfano, L. Frothingham, J. B. Fischer, K. J. Burke-Howie, J. R. Bunzow, A. C. Server, et al., Cloning of the cDNA and gene for a human D_2 dopamine receptor. *Proc Nat Acad Sci USA* **86**, 9762-9766 (1989).

13. B. Giros, P. Sokoloff, M. P. Martres, J. F. Riou, L. J. Emorine, J. C. Schwartz, Alternative splicing directs the expression of two D_2 dopamine receptor isoforms. *Nature* **342**, 923-926; doi:10.1038/342923a0 (1989).

14. R. K. Sunahara, H. B. Niznik, D. M. Weiner, T. M. Stormann, M. R. Brann, J. L. Kennedy, J. E. Gelernter, R. Rozmahel, Y. L. Yang, Y. Israel, et al., Human dopamine D_1 receptor encoded by an intronless gene on chromosome 5. *Nature* **347**, 80-83; doi:10.1038/347080a0 (1990).

15. R. K. Sunahara, H. C. Guan, B. F. O'Dowd, P. Seeman, L. G. Laurier, G. Ng, S. R. George, J. Torchia, H. H. Van Tol, H. B. Niznik, Cloning of the gene for a human dopamine D_5 receptor with higher affinity for dopamine than D_1. *Nature* **350**, 614-619; doi:10.1038/350614a0 (1991).

16. Q. Y. Zhou, D. K. Grandy, L. Thambi, J. A. Kushner, H. H. Van Tol, R. Cone, D. Pribnow, J. Salon, J. R. Bunzow, O. Civelli, Cloning and expression of human and rat D_1 dopamine receptors. *Nature* **347**, 76-80; doi:10.1038/347076a0 (1990).

17. P. Sokoloff, B. Giros, M.-P. Martres, M.-L. Bouthenet, J.-C. Schwartz, Molecular cloning and characterization of a novel dopamine receptor (D_3) as a target for neuroleptics. *Nature* **347**, 146-151; doi:10.1038/347146a0 (1990).

18. H. H. Van Tol, J. R. Bunzow, H. C. Guan, R. K. Sunahara, P. Seeman, H. B. Niznik, O. Civelli, Cloning of the gene for a human dopamine D_4 receptor with high affinity for the antipsychotic clozapine. *Nature* **350**, 610-614; doi:10.1038/350610a0 (1991).

19. H. H. Van Tol, C. M. Wu, H. C. Guan, K. Ohara, J. R. Bunzow, O. Civelli, J. Kennedy, P. Seeman, H. B. Niznik, V. Jovanovic, Multiple dopamine D_4 receptor variants in the human population. *Nature* **358**, 149-152; doi:10.1038/358149a0 (1992).

20. R. Fredriksson, M. C. Lagerstrom, L. G. Lundin, H. B. Schioth, The G-protein-coupled receptors in the human genome form five main families. Phylogenetic analysis, paralogon groups, and fingerprints. *Mol Pharmacol* **63**, 1256-1272; doi:10.1124/mol.63.6.1256 (2003).

21. S. M. Foord, T. I. Bonner, R. R. Neubig, E. M. Rosser, J. P. Pin, A. P. Davenport, M. Spedding, A. J. Harmar, International Union of Pharmacology. XLVI. G protein-coupled receptor list. *Pharmacol Rev* **57**, 279-288; doi:10.1124/pr.57.2.5 (2005).

22. J.-M. Beaulieu, S. Espinoza, R. R. Gainetdinov, Dopamine receptors – IUPHAR Review 13. *Br J Pharmacol* **172**, 1-23; doi:10.1111/bph.12906 (2015).

23. J. M. Beaulieu, R. R. Gainetdinov, The physiology, signaling, and pharmacology of dopamine receptors. *Pharmacol Rev* **63**, 182-217; doi:10.1124/pr.110.002642 (2011).

24. J. A. Gingrich, M. G. Caron, Recent advances in the molecular biology of dopamine receptors. *Annu Rev Neurosci* **16**, 299-321; doi:10.1146/annurev.ne.16.030193.001503 (1993).

25. B. F. O'Dowd, Structures of dopamine receptors. *J Neurochem* **60**, 804-816; doi:10.1111/j.1471-4159.1993.tb03224.x (1993).

26. D. M. Rosenbaum, S. G. Rasmussen, B. K. Kobilka, The structure and function of G-protein-coupled receptors. *Nature* **459**, 356-363; doi:10.1038/nature08144 (2009).

27. L. S. Barak, L. Menard, S. S. Ferguson, A. M. Colapietro, M. G. Caron, The conserved seven-transmembrane sequence NP(X)2,3Y of the G-protein-coupled receptor superfamily regulates multiple properties of the beta 2-adrenergic receptor. *Biochemistry* **34**, 15407-15414; doi:10.1021/bi00047a003 (1995).

28. A. J. Kooistra, S. Mordalski, G. Pándy-Szekeres, M. Esguerra, A. Mamyrbekov, C. Munk, G. M. Keserű, David E. Gloriam, GPCRdb in 2021: integrating GPCR sequence, structure and function. *Nucleic Acids Res* **49**, D335-D343; doi:10.1093/nar/gkaa1080 (2021).

29. V. Isberg, S. Mordalski, C. Munk, K. Rataj, K. Harpsøe, A. S. Hauser, B. Vroling, A. J. Bojarski, G. Vriend, D. E. Gloriam, GPCRdb: an information system for G protein-coupled receptors. *Nucleic Acids Res* **44**, D356-D364; doi:10.1093/nar/gkv1178 (2016).

30. F. Boeckler, P. Gmeiner, The structural evolution of dopamine D_3 receptor ligands: structure-activity relationships and selected neuropharmacological aspects. *Pharmacol Ther* **112**, 281-333; doi:10.1016/j.pharmthera.2006.04.007 (2006).

31. P. Seeman, D. Nam, C. Ulpian, I. S. Liu, T. Tallerico, New dopamine receptor, D_2(Longer), with unique TG splice site, in human brain. *Brain Res Mol Brain Res* **76**, 132-141; doi:10.1016/s0169-328x(99)00343-5 (2000).

32. P. Seeman, H. H. Van Tol, Dopamine receptor pharmacology. *Trends Pharmacol Sci* **15**, 264-270; doi:10.1016/0165-6147(94)90323-9 (1994).

33. E. Y. Chien, W. Liu, Q. Zhao, V. Katritch, G. W. Han, M. A. Hanson, L. Shi, A. H. Newman, J. A. Javitch, V. Cherezov, R. C. Stevens, Structure of the human dopamine D_3 receptor in complex with a D_2/D_3 selective antagonist. *Science* **330**, 1091-1095; doi:10.1126/science.1197410 (2010).

34. S. Wang, D. Wacker, A. Levit, T. Che, R. M. Betz, J. D. McCorvy, A. J. Venkatakrishnan, X. P. Huang, R. O. Dror, B. K. Shoichet, B. L. Roth, D_4 dopamine receptor high-resolution structures enable the discovery of selective agonists. *Science* **358**, 381-386; doi:10.1126/science.aan5468 (2017).

35. S. Wang, T. Che, A. Levit, B. K. Shoichet, D. Wacker, B. L. Roth, Structure of the D_2 dopamine receptor bound to the atypical antipsychotic drug risperidone. *Nature* **555**, 269-273; doi:10.1038/nature25758 (2018).

36.   D. Vallone, R. Picetti, E. Borrelli, Structure and function of dopamine receptors. *Neurosci Biobehav Rev* **24**, 125-132(2000).

37.   P. Rondou, G. Haegeman, K. Van Craenenbroeck, The dopamine D_4 receptor: biochemical and signalling properties. *Cell Mol Life Sci* **67**, 1971-1986; doi:10.1007/s00018-010-0293-y (2010).

38.   Z. U. Khan, L. Mrzljak, A. Gutierrez, A. de la Calle, P. S. Goldman-Rakic, Prominence of the dopamine D2 short isoform in dopaminergic pathways. *Proc Natl Acad Sci USA* **95**, 7731-7736; doi:10.1073/pnas.95.13.7731 (1998).

39.   N. Lindgren, A. Usiello, M. Goiny, J. Haycock, E. Erbs, P. Greengard, T. Hokfelt, E. Borrelli, G. Fisone, Distinct roles of dopamine D_{2L} and D_{2S} receptor isoforms in the regulation of protein phosphorylation at presynaptic and postsynaptic sites. *Proc Natl Acad Sci USA* **100**, 4305-4309; doi:10.1073/pnas.0730708100 (2003).

40.   B. Landwehrmeyer, G. Mengod, J. M. Palacios, Dopamine D_3 receptor mRNA and binding sites in human brain. *Brain Res Mol Brain Res* **18**, 187-192; doi:10.1016/0169-328x(93)90188-u (1993).

41.   J. Diaz, D. Levesque, C. H. Lammers, N. Griffon, M. P. Martres, J. C. Schwartz, P. Sokoloff, Phenotypical characterization of neurons expressing the dopamine D_3 receptor in the rat brain. *Neuroscience* **65**, 731-745; doi:10.1016/0306-4522(94)00527-c (1995).

42.   P. Sokoloff, J. Diaz, B. Le Foll, O. Guillin, L. Leriche, E. Bezard, C. Gross, The dopamine D_3 receptor: a therapeutic target for the treatment of neuropsychiatric disorders. *CNS Neurol Disord Drug Targets* **5**, 25-43; doi:10.2174/187152706784111551 (2006).

43.   A. Rivera, B. Cuellar, F. J. Giron, D. K. Grandy, A. de la Calle, R. Moratalla, Dopamine D_4 receptors are heterogeneously distributed in the striosomes/matrix compartments of the striatum. *J Neurochem* **80**, 219-229; doi:10.1046/j.0022-3042.2001.00702.x (2002).

44.   D. R. Sibley, New insights into dopaminergic receptor function using antisense and genetically altered animals. *Annu Rev Pharmacol Toxicol* **39**, 313-341; doi:10.1146/annurev.pharmtox.39.1.313 (1999).

45.   G. Di Chiara, V. Bassareo, S. Fenu, M. A. De Luca, L. Spina, C. Cadoni, E. Acquas, E. Carboni, V. Valentini, D. Lecca, Dopamine and drug addiction: the nucleus accumbens shell connection. *Neuropharmacology* **47 Suppl 1**, 227-241; doi:10.1016/j.neuropharm.2004.06.032 (2004).

46.   T. X. Xu, T. D. Sotnikova, C. Liang, J. Zhang, J. U. Jung, R. D. Spealman, R. R. Gainetdinov, W. D. Yao, Hyperdopaminergic tone erodes prefrontal long-term potential via a D_2 receptor-operated protein phosphatase gate. *J Neurosci* **29**, 14086-14099; doi:10.1523/JNEUROSCI.0974-09.2009 (2009).

47.   P. Seeman, Schizophrenia and dopamine receptors. *Eur Neuropsychopharmacol* **23**, 999-1009; doi:10.1016/j.euroneuro.2013.06.005 (2013).

48.   J. N. Oak, J. Oldenhof, H. H. Van Tol, The dopamine D(4) receptor: one decade of research. *Eur J Pharmacol* **405**, 303-327; doi:10.1016/s0014-2999(00)00562-8 (2000).

49.   D. Hilger, M. Masureel, B. K. Kobilka, Structure and dynamics of GPCR signaling complexes. *Nat Struct Mol Biol* **25**, 4-12; doi:10.1038/s41594-017-0011-7 (2018).

50.   K. L. Pierce, R. T. Premont, R. J. Lefkowitz, Seven-transmembrane receptors. *Nat Rev Mol Cell Biol* **3**, 639-650; doi:10.1038/nrm908 (2002).

51.   A. Sidhu, H. B. Niznik, Coupling of dopamine receptor subtypes to multiple and diverse G proteins. *Int J Dev Neurosci* **18**, 669-677; doi:10.1016/s0736-5748(00)00033-2 (2000).

52.   Y. F. Liu, K. H. Jakobs, M. M. Rasenick, P. R. Albert, G protein specificity in receptor-effector coupling. Analysis of the roles of G_0 and G_{i2} in GH4C1 pituitary cells. *J Biol Chem* **269**, 13880-13886(1994).

53.   J. Obadiah, T. Avidor-Reiss, C. S. Fishburn, S. Carmon, M. Bayewitch, Z. Vogel, S. Fuchs, B. Levavi-Sivan, Adenylyl cyclase interaction with the D2 dopamine receptor family; differential coupling to G_i, G_z, and G_s. *Cell Mol Neurobiol* **19**, 653-664; doi:10.1023/a:1006988603199 (1999).

54. J. P. Montmayeur, E. Borrelli, Transcription mediated by a cAMP-responsive promoter element is reduced upon activation of dopamine D_2 receptors. *Proc Natl Acad Sci USA* **88**, 3135-3139 (1991).

55. S. E. Senogles, The D_2 dopamine receptor isoforms signal through distinct Gi alpha proteins to inhibit adenylyl cyclase. A study with site-directed mutant G_i alpha proteins. *J Biol Chem* **269**, 23120-23127 (1994).

56. J. P. Montmayeur, J. Guiramand, E. Borrelli, Preferential coupling between dopamine D_2 receptors and G-proteins. *Mol Endocrinol* **7**, 161-170; doi:10.1210/mend.7.2.7682286 (1993).

57. K. A. Neve, J. K. Seamans, H. Trantham-Davidson, Dopamine receptor signaling. *J Recept Signal Transduct Res* **24**, 165-205; doi:10.1081/rrs-200029981 (2004).

58. L. X. Liu, L. H. Burgess, A. M. Gonzalez, D. R. Sibley, L. A. Chiodo, D_{2S}, D_{2L}, D_3, and D_4 dopamine receptors couple to a voltage-dependent potassium current in N18TG2 x mesencephalon hybrid cell (MES-23.5) via distinct G proteins. *Synapse* **31**, 108-118; doi:10.1002/(SICI)1098-2396(199902)31:2<108::AID-SYN3>3.0.CO;2-V (1999).

59. P. G. Zaworski, G. L. Alberts, J. F. Pregenzer, W. B. Im, J. L. Slightom, G. S. Gill, Efficient functional coupling of the human D_3 dopamine receptor to G(o) subtype of G proteins in SH-SY5Y cells. *Br J Pharmacol* **128**, 1181-1188; doi:10.1038/sj.bjp.0702905 (1999).

60. A. Newman-Tancredi, D. Cussac, V. Audinot, V. Pasteau, S. Gavaudan, M. J. Millan, G protein activation by human dopamine D3 receptors in high-expressing Chinese hamster ovary cells: A guanosine-5'-O-(3-[^{35}S]thio)- triphosphate binding and antibody study. *Mol Pharmacol* **55**, 564-574(1999).

61. D. I. Cho, M. Zheng, K. M. Kim, Current perspectives on the selective regulation of dopamine D(2) and D(3) receptors. *Arch Pharm Res* **33**, 1521-1538; doi:10.1007/s12272-010-1005-8 (2010).

62. M. A. Kazmi, L. A. Snyder, A. M. Cypess, S. G. Graber, T. P. Sakmar, Selective reconstitution of human D_4 dopamine receptor variants with G_i alpha subtypes. *Biochemistry* **39**, 3734-3744; doi:10.1021/bi992354c (2000).

63. C. M. O'Hara, L. Tang, R. Taussig, R. D. Todd, K. L. O'Malley, Dopamine D_{2L} receptor couples to G alpha i2 and G alpha i3 but not G alpha i1, leading to the inhibition of adenylate cyclase in transfected cell lines. *J Pharmacol Exp Ther* **278**, 354-360 (1996).

64. S. W. Robinson, M. G. Caron, Selective inhibition of adenylyl cyclase type V by the dopamine D_3 receptor. *Mol Pharmacol* **52**, 508-514; doi:10.1124/mol.52.3.508 (1997).

65. P. Greengard, The neurobiology of slow synaptic transmission. *Science* **294**, 1024-1030; doi:10.1126/science.294.5544.1024 (2001).

66. S. Hernandez-Lopez, T. Tkatch, E. Perez-Garci, E. Galarraga, J. Bargas, H. Hamm, D. J. Surmeier, D_2 dopamine receptors in striatal medium spiny neurons reduce L-type Ca^{2+} currents and excitability via a novel PLC[beta]1-IP3-calcineurin-signaling cascade. *J Neurosci* **20**, 8987-8995; doi:10.1523/JNEUROSCI.20-24-08987.2000 (2000).

67. E. V. Kuzhikandathil, G. S. Oxford, Activation of human D_3 dopamine receptor inhibits P/Q-type calcium channels and secretory activity in AtT-20 cells. *J Neurosci* **19**, 1698-1707; doi:10.1523/JNEUROSCI.19-05-01698.1999 (1999).

68. Z. Yan, W. J. Song, J. Surmeier, D_2 dopamine receptors reduce N-type Ca^{2+} currents in rat neostriatal cholinergic interneurons through a membrane-delimited, protein-kinase-C-insensitive pathway. *J Neurophysiol* **77**, 1003-1015; doi:10.1152/jn.1997.77.2.1003 (1997).

69. E. V. Kuzhikandathil, W. Yu, G. S. Oxford, Human dopamine D_3 and D_{2L} receptors couple to inward rectifier potassium channels in mammalian cell lines. *Mol Cell Neurosci* **12**, 390-402; doi:10.1006/mcne.1998.0722 (1998).

70. S. S. Ferguson, Evolving concepts in G protein-coupled receptor endocytosis: the role in receptor desensitization and signaling. *Pharmacol Rev* **53**, 1-24(2001).

71. Y. Namkung, C. Dipace, E. Urizar, J. A. Javitch, D. R. Sibley, G protein-coupled receptor kinase-2 constitutively regulates D_2 dopamine receptor expression and signaling independently of receptor phosphorylation. *J Biol Chem* **284**, 34103-34115; doi:10.1074/jbc.M109.055707 (2009).

72. G. K. Dhami, S. S. Ferguson, Regulation of metabotropic glutamate receptor signaling, desensitization and endocytosis. *Pharmacol Ther* **111**, 260-271; doi:10.1016/j.pharmthera.2005.01.008 (2006).

73. K. M. Kim, K. J. Valenzano, S. R. Robinson, W. D. Yao, L. S. Barak, M. G. Caron, Differential regulation of the dopamine D_2 and D_3 receptors by G protein-coupled receptor kinases and beta-arrestins. *J Biol Chem* **276**, 37409-37414; doi:10.1074/jbc.M106728200 (2001).

74. Y. Namkung, C. Dipace, J. A. Javitch, D. R. Sibley, G protein-coupled receptor kinase-mediated phosphorylation regulates post-endocytic trafficking of the D_2 dopamine receptor. *J Biol Chem* **284**, 15038-15051; doi:10.1074/jbc.M900388200 (2009).

75. D. Cho, M. Zheng, C. Min, L. Ma, H. Kurose, J. H. Park, K. M. Kim, Agonist-induced endocytosis and receptor phosphorylation mediate resensitization of dopamine D(2) receptors. *Mol Endocrinol* **24**, 574-586; doi:10.1210/me.2009-0369 (2010).

76. C. Min, M. Zheng, X. Zhang, M. G. Caron, K. M. Kim, Novel roles for beta-arrestins in the regulation of pharmacological sequestration to predict agonist-induced desensitization of dopamine D_3 receptors. *Br J Pharmacol* **170**, 1112-1129; doi:10.1111/bph.12357 (2013).

77. E. Y. Cho, D. I. Cho, J. H. Park, H. Kurose, M. G. Caron, K. M. Kim, Roles of protein kinase C and actin-binding protein 280 in the regulation of intracellular trafficking of dopamine D_3 receptor. *Mol Endocrinol* **21**, 2242-2254; doi:10.1210/me.2007-0202 (2007).

78. M. Zheng, X. Zhang, N. Sun, X. Min, S. Acharya, K. M. Kim, A novel molecular mechanism responsible for phosphorylation-independent desensitization of G protein-coupled receptors exemplified by the dopamine D_3 receptor. *Biochem Biophys Res Commun* **528**, 432-439; doi:10.1016/j.bbrc.2020.05.197 (2020).

79. X. Zhang, X. Min, S. Wang, N. Sun, K. M. Kim, Mdm2-mediated ubiquitination of beta-arrestin2 in the nucleus occurs in a Gbetagamma- and clathrin-dependent manner. *Biochem Pharmacol* **178**, 114049; doi:10.1016/j.bcp.2020.114049 (2020).

80. A. Spooren, P. Rondou, K. Debowska, B. Lintermans, L. Vermeulen, B. Samyn, K. Skieterska, G. Debyser, B. Devreese, P. Vanhoenacker, U. Wojda, G. Haegeman, K. Van Craenenbroeck, Resistance of the dopamine D_4 receptor to agonist-induced internalization and degradation. *Cell Signal* **22**, 600-609; doi:10.1016/j.cellsig.2009.11.013 (2010).

81. D. I. Cho, S. Beom, H. H. Van Tol, M. G. Caron, K. M. Kim, Characterization of the desensitization properties of five dopamine receptor subtypes and alternatively spliced variants of dopamine D_2 and D_4 receptors. *Biochem Biophys Res Commun* **350**, 634-640; doi:10.1016/j.bbrc.2006.09.090 (2006).

82. J. M. Beaulieu, R. R. Gainetdinov, M. G. Caron, Akt/GSK3 signaling in the action of psychotropic drugs. *Annu Rev Pharmacol Toxicol* **49**, 327-347; doi:10.1146/annurev.pharmtox.011008.145634 (2009).

83. J. M. Beaulieu, R. R. Gainetdinov, M. G. Caron, The Akt-GSK-3 signaling cascade in the actions of dopamine. *Trends Pharmacol Sci* **28**, 166-172; doi:10.1016/j.tips.2007.02.006 (2007).

84. R. J. Lefkowitz, S. K. Shenoy, Transduction of receptor signals by beta-arrestins. *Science* **308**, 512-517; doi:10.1126/science.1109237 (2005).

85. L. M. Luttrell, D. Gesty-Palmer, Beyond desensitization: physiological relevance of arrestin-dependent signaling. *Pharmacol Rev* **62**, 305-330; doi:10.1124/pr.109.002436 (2010).

86. A. S. Hauser, M. M. Attwood, M. Rask-Andersen, H. B. Schioth, D. E. Gloriam, Trends in GPCR drug discovery: new agents, targets and indications. *Nat Rev Drug Discov* **16**, 829-842; doi:10.1038/nrd.2017.178 (2017).

87. J. Lotharius, P. Brundin, Pathogenesis of Parkinson's disease: dopamine, vesicles and alpha-synuclein. *Nature reviews. Neuroscience* **3**, 932-942; doi:10.1038/nrn983 (2002).

88.   L. Belkacemi, N. A. Darmani, Dopamine receptors in emesis: Molecular mechanisms and potential therapeutic function. *Pharmacol Res* **161**, 105124; doi:10.1016/j.phrs.2020.105124 (2020).

89.   K. D. Burris, T. F. Molski, C. Xu, E. Ryan, K. Tottori, T. Kikuchi, F. D. Yocca, P. B. Molinoff, Aripiprazole, a novel antipsychotic, is a high-affinity partial agonist at human dopamine D_2 receptors. *J Pharmacol Exp Ther* **302**, 381-389; doi:10.1124/jpet.102.033175 (2002).

90.   T. F. Brust, M. P. Hayes, D. L. Roman, V. J. Watts, New functional activity of aripiprazole revealed: Robust antagonism of D2 dopamine receptor-stimulated Gbetagamma signaling. *Biochem Pharmacol* **93**, 85-91; doi:10.1016/j.bcp.2014.10.014 (2015).

91.   D. A. Shapiro, S. Renock, E. Arrington, L. A. Chiodo, L. X. Liu, D. R. Sibley, B. L. Roth, R. Mailman, Aripiprazole, a novel atypical antipsychotic drug with a unique and robust pharmacology. *Neuropsychopharmacology* **28**, 1400-1411; doi:10.1038/sj.npp.1300203 (2003).

92.   J. A. Allen, J. M. Yost, V. Setola, X. Chen, M. F. Sassano, M. Chen, S. Peterson, P. N. Yadav, X. P. Huang, B. Feng, N. H. Jensen, X. Che, X. Bai, S. V. Frye, W. C. Wetsel, M. G. Caron, J. A. Javitch, B. L. Roth, J. Jin, Discovery of beta-arrestin-biased dopamine D_2 ligands for probing signal transduction pathways essential for antipsychotic efficacy. *Proc Natl Acad Sci USA* **108**, 18488-18493; doi:10.1073/pnas.1104807108 (2011).

93.   B. Masri, A. Salahpour, M. Didriksen, V. Ghisi, J. M. Beaulieu, R. R. Gainetdinov, M. G. Caron, Antagonism of dopamine D_2 receptor/beta-arrestin 2 interaction is a common property of clinically effective antipsychotics. *Proc Natl Acad Sci USA* **105**, 13656-13661; doi:10.1073/pnas.0803522105 (2008).

94.   B. Kiss, A. Horvath, Z. Nemethy, E. Schmidt, I. Laszlovszky, G. Bugovics, K. Fazekas, K. Hornok, S. Orosz, I. Gyertyan, E. Agai-Csongor, G. Domany, K. Tihanyi, N. Adham, Z. Szombathelyi, Cariprazine (RGH-188), a dopamine D(3) receptor-preferring, D(3)/D(2) dopamine receptor antagonist-partial agonist antipsychotic candidate: in vitro and neurochemical profile. *J Pharmacol Exp Ther* **333**, 328-340; doi:10.1124/jpet.109.160432 (2010).

95.   A. E. Moritz, R. B. Free, D. R. Sibley, Advances and challenges in the search for D_2 and D_3 dopamine receptor-selective compounds. *Cell Signal* **41**, 75-81; doi:10.1016/j.cellsig.2017.07.003 (2018).

96.   S. Lober, H. Hubner, N. Tschammer, P. Gmeiner, Recent advances in the search for D3- and D4-selective drugs: probes, models and candidates. *Trends Pharmacol Sci* **32**, 148-157; doi:10.1016/j.tips.2010.12.003 (2011).

97.   S. Vangveravong, E. McElveen, M. Taylor, J. Xu, Z. Tu, R. R. Luedtke, R. H. Mach, Synthesis and characterization of selective dopamine D_2 receptor antagonists. *Bioorg Med Chem* **14**, 815-825; doi:10.1016/j.bmc.2005.09.008 (2006).

98.   V. Kumar, A. Bonifazi, M. P. Ellenberger, T. M. Keck, E. Pommier, R. Rais, B. S. Slusher, E. Gardner, Z. B. You, Z. X. Xi, A. H. Newman, Highly Selective Dopamine D_3 Receptor (D_3R) Antagonists and Partial Agonists Based on Eticlopride and the D_3R Crystal Structure: New Leads for Opioid Dependence Treatment. *J Med Chem* **59**, 7634-7650; doi:10.1021/acs.jmedchem.6b00860 (2016).

99.   S. Lober, H. Hubner, W. Utz, P. Gmeiner, Rationally based efficacy tuning of selective dopamine D_4 receptor ligands leading to the complete antagonist 2-[4-(4-chlorophenyl)piperazin-1-ylmethyl]pyrazolo[1,5-a]pyridine (FAUC 213). *J Med Chem* **44**, 2691-2694; doi:10.1021/jm015522j (2001).

100.   A. Bonifazi, H. Yano, A. M. Guerrero, V. Kumar, A. F. Hoffman, C. R. Lupica, L. Shi, A. H. Newman, Novel and Potent Dopamine D_2 Receptor G_o-Protein Biased Agonists. *ACS Pharmacol Transl Sci* **2**, 52-65; doi:10.1021/acsptsci.8b00060 (2019).

101.   J. Chen, C. Jiang, B. Levant, X. Li, T. Zhao, B. Wen, R. Luo, D. Sun, S. Wang, Pramipexole derivatives as potent and selective dopamine D(3) receptor agonists with improved human microsomal stability. *ChemMedChem* **9**, 2653-2660; doi:10.1002/cmdc.201402398 (2014).

102.   M. Allen, J. Reeves, G. Mellor, High throughput fluorescence polarization: a homogeneous alternative to radioligand binding for cell surface receptors. *J Biomol Screen* **5**, 63-69; doi:10.1177/108705710000500202 (2000).

103. F. Zanella, J. B. Lorens, W. Link, High content screening: seeing is believing. *Trends Biotechnol* **28**, 237-245; doi:10.1016/j.tibtech.2010.02.005 (2010).

104. L. A. Stoddart, E. K. M. Johnstone, A. J. Wheal, J. Goulding, M. B. Robers, T. Machleidt, K. V. Wood, S. J. Hill, K. D. G. Pfleger, Application of BRET to monitor ligand binding to GPCRs. *Nat Methods* **12**, 661-663; doi:10.1038/nmeth.3398 (2015).

105. C. Harrison, J. R. Traynor, The [^{35}S]GTPgammaS binding assay: approaches and applications in pharmacology. *Life Sci* **74**, 489-508; doi:10.1016/j.lfs.2003.07.005 (2003).

106. G. Milligan, Principles: extending the utility of [^{35}S]GTP gamma S binding assays. *Trends Pharmacol Sci* **24**, 87-90; doi:10.1016/s0165-6147(02)00027-5 (2003).

107. W. Thomsen, J. Frazer, D. Unett, Functional assays for screening GPCR targets. *Curr Opin Biotechnol* **16**, 655-665; doi:10.1016/j.copbio.2005.10.008 (2005).

108. L. I. Jiang, J. Collins, R. Davis, K.-M. Lin, D. DeCamp, T. Roach, R. Hsueh, R. A. Rebres, E. M. Ross, R. Taussig, I. Fraser, P. C. Sternweis, Use of a cAMP BRET sensor to characterize a novel regulation of cAMP by the sphingosine 1-phosphate/G13 pathway. *J Biol Chem* **282**, 10576-10584; doi:10.1074/jbc.M609695200 (2007).

109. R. Zhang, X. Xie, Tools for GPCR drug discovery. *Acta Pharmacologica Sin* **33**, 372-384 (2012).

110. C. W. Scott, M. F. Peters, Label-free whole-cell assays: expanding the scope of GPCR screening. *Drug Discov Today* **15**, 704-716; doi:10.1016/j.drudis.2010.06.008 (2010).

111. I. Giaever, C. R. Keese, Micromotion of mammalian cells measured electrically. *Proc Nat Acad Sci USA* **88**, 7896-7900; doi:10.1073/pnas.88.17.7896 (1991).

112. S. Biselli, M. Bresinsky, K. Tropmann, L. Forster, C. Honisch, A. Buschauer, G. Bernhardt, S. Pockes, Pharmacological characterization of a new series of carbamoylguanidines reveals potent agonism at the H_2R and D_3R. *Eur J Med Chem* **214**, 113190; doi:10.1016/j.ejmech.2021.113190 (2021).

113. E. Traiffort, H. Pollard, J. Moreau, M. Ruat, J. C. Schwartz, M. I. Martinez-Mir, J. M. Palacios, Pharmacological characterization and autoradiographic localization of histamine H_2 receptors in human brain identified with [^{125}I]iodoaminopotentidine. *J Neurochem* **59**, 290-299; doi:10.1111/j.1471-4159.1992.tb08903.x (1992).

114. N. Misawa, A. K. Kafi, M. Hattori, K. Miura, K. Masuda, T. Ozawa, Rapid and high-sensitivity cell-based assays of protein-protein interactions using split click beetle luciferase complementation: an approach to the study of G-protein-coupled receptors. *Anal Chem* **82**, 2552-2560; doi:10.1021/ac100104q (2010).

.

Chapter 2
Radioligand binding assays for dopamine D$_{2long}$, D$_3$ and D$_{4.4}$ receptors

2.1   Introduction

Radioligand binding studies have been widely used for studying ligand-receptor interactions since the 1970's[1]. They play an important role in high-throughput screening of compound libraries in drug development[2], serve as an irreplaceable tool for the determination of receptor ligand selectivities[3] and, with the aid of radioligand binding studies, mechanisms of ligand-receptor interactions could be explored[3]. With respect to the D_2-like family of dopamine receptors (comprising D_2, D_3 and D_4 receptors), radioligand binding assays have been extensively used in the development and study of antipsychotic drugs[4] and therapeutics used for the treatment of other neurological disorders, such as Parkinson's, Tourette's syndrome or attention deficit hyperactivity disorder (ADHD)[5].

For these purposes, a variety of radioligands have been used, a selection is displayed in **Figure 2.1**. The antagonist spiperone was already widely used in the 1970's as a radioligand with a sub-nanomolar equilibrium dissociation constant (0.3 nM[6]) for investigations on dopamine D_2 receptors[6-8]. It should be noted that, at this time, the D_3R and the D_4R were yet to be discovered. A few years later the spiperone derivative [³H]*N*-methylspiperone was mentioned for the first time, exhibiting comparable properties with K_d values of 0.11 nM or 0.44 nM determined at different human brain tissues[9]. [³H]Domperidone was described in 1978 by Martres et al.[10] with an equilibrium dissociation constant of 0.8 – 1.0 nM (determined at mouse striata, where the D_2 receptor is predominantly expressed over the D_3 and the D_4 receptor[11]) and the advantageous features of low non-specific binding and higher selectivity towards dopamine D_2-like receptors compared to spiperone, the latter showing also considerable affinity to serotoninergic receptors like the 5-HT$_{2A}$ receptor (pK_i = 8.60)[12]. In the early decades of radioligand binding studies, recombinant systems were not available, i.e. native tissues had to be used. Thus, the lack of receptor-ligand specificity (binding to receptors of different receptor families) or selectivity (binding to different subtypes within a receptor family) represented a greater obstacle than today. Spiperone exhibits comparable affinities to all D_2-like receptors[13] and domperidone also does not clearly discriminate between the D_2 and the D_3 receptor binding site[14]. A radioligand claimed to be selective for the D_3R with a sub-nanomolar K_d is [³H]7-OH-DPAT (K_d (rD$_3$R) = 0.67 nM)[15]. Besides these antagonistic radioligands, tritiated agonists like [³H]dopamine[16] or [³H]pramipexole[17] have also been used.
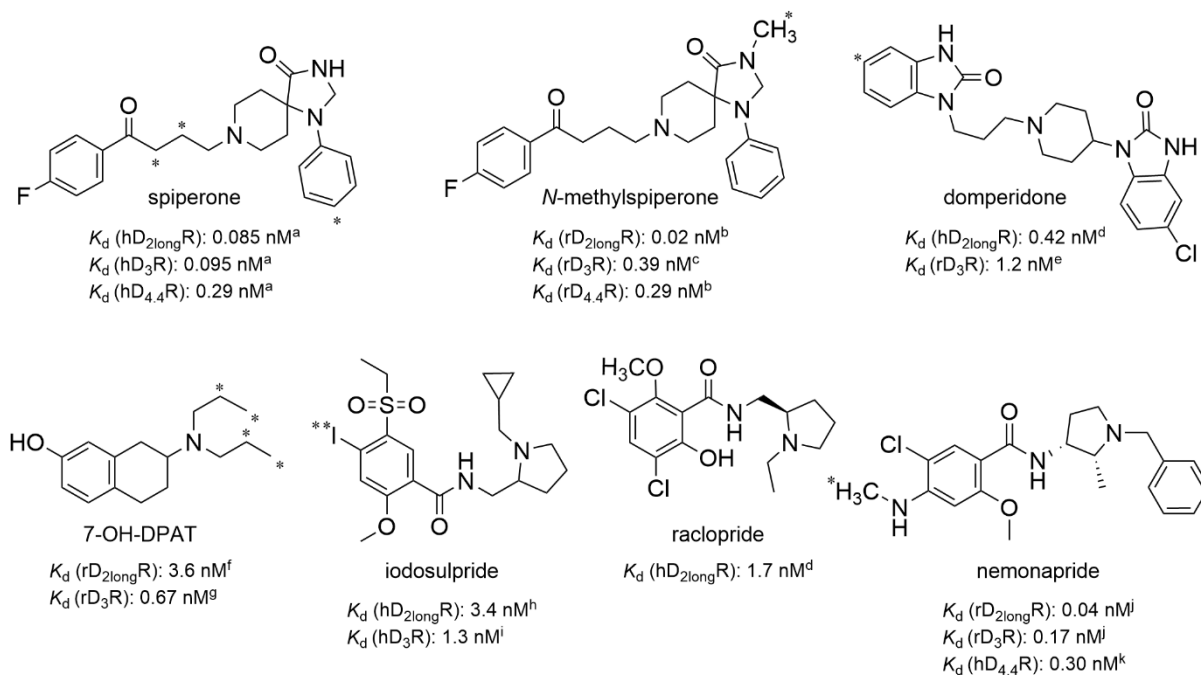
Figure 2.1. Structures of selected antagonistic dopamine D$_2$-like receptor radioligands. * ^{3}H-labeled position(s). ** ^{125}I-labeled position. [a]Möller et al. 2015[13] [b]Schetz et al. 2000[18] [c]Skinbjerg et al. 2009[19] [d]Seeman et al. 2003[16] [e]Seeman et al.2009[20] [f]Gonzalez et al. 1995[21] [g]Levesque et al. 1992[15] [h]Vanhauwe et al. 1999[22] [i]Sokoloff et al. 1992[14] [j]Vile et al. 1995[23] [k]Hidaka et al. 1995[24]

It is well known that binding assays involving high-affinity radioligands, such as [^{3}H]spiperone or [^{3}H]N-methylspiperone, are prone to radioligand depletion. This means that, upon binding of the radioligand to the receptor, the free concentration of radioligand is markedly decreased compared to the total concentration of added radioligand, which can lead to misinterpretation of experimental data if not taken into account. Regarding determinations of equilibrium dissociation constants in saturation binding experiments, unnoticed radioligand depletion would lead to an underestimation of the affinity[25]. In addition, in competition binding experiments, radioligand depletion can result in an apparently lower affinity of the competitor[25]. Seeman et al.[26] presented how different levels of radioligand depletion can affect the determination of dissociation constants with the example of [^{3}H]spiperone. Reported [^{3}H]spiperone dissociation constants vary over a broad range from 13 pM to 1.6 nM, which can be explained by greatly varying amounts of protein/receptor (high amounts of protein result in more pronounced ligand depletion) and varying materials used in the different studies, resulting in radioligand depletion through different processes[26]. It is recommended that the portion of receptor bound radioligand should not exceed 10%, in order to obtain a good estimate of the dissociation constant from saturation binding assays[3]. If this requirement cannot be met, there are other means available to counteract ligand depletion or its consequences, but these are often not straightforward to implement. For example, the receptor concentration can be reduced to 10% of the K_d value of the radioligand, resulting in lower ratios of bound over free radioligand[27]. However, for tritiated ligands, this is often not feasible due to their relatively low specific activity. A low

concentration of receptor bound radioligand could result in an insufficient number of counts. Another approach is to increase the assay volume, which may be limited by technical conditions. To reduce the fraction of bound radioligand, one could also increase the radioligand concentration while keeping the amount of protein constant. Nevertheless, this would be accompanied by an increase in unspecific binding resulting in lower ratios of specific/unspecific binding[25]. Regarding the analysis of saturation binding data obtained from assays under conditions of radioligand depletion, misinterpretation can partly be avoided by estimating the concentration of free radioligand (difference between totally added and bound radioligand)[2]. Direct measurements of the free radioligand concentration would be preferable but are difficult to achieve in homogeneous assay formats. Alternatively, the data could be analysed according to a model described by Swillens[28]. This model considers that under conditions of radioligand depletion, non-specific binding will be overestimated. With respect to the analysis of competition binding assays, Carter et al.[25] showed that valid estimates of inhibition constants (dissociation constant K_i) can be obtained by applying the Cheng-Prusoff equation with a reliably determined K_d of the radioligand.

Another important aspect concerning radioligand binding studies on dopamine D_2-like receptors is the occurrence of different affinity states of the receptor in agonist/[³H]antagonist competition binding studies[17,29]. This phenomenon was also reported for other GPCRs such as muscarinic receptors[30], β-adrenergic receptors[31] or the histamine H_2 receptor[32]. A two-stage binding reaction, as postulated by the ternary complex model[33], is discussed as the underlying mechanism of biphasic displacement curves of agonists yielding two distinct dissociation constants (K_{iH} for the high-affinity and K_{iL} for the low-affinity state)[17]. It is assumed that the high-affinity state reflects the G-protein bound receptor, whereas the low-affinity state resembles the G-protein unbound receptor[34]. The high-affinity component is detectable in systems, where the ternary complex of agonist, receptor and G protein can be stabilized, such as membrane preparations, where the concentration of GTP is low[35]. A complete conversion of the high-affinity state of agonist binding to the low-affinity state can be achieved by the presence of non-hydrolysable guanine nucleotide analogues, such as GTPγS or guanylylimidodiphosphate (Gpp(NH)p), causing the ternary complex to be persistently dissociated[36].

The objective of this project was to establish a radioligand binding assay that allows a reliable determination of receptor affinities of dopamine D_2, D_3 and D_4 receptor ligands. The need for such dopamine receptor binding assays in our group arose from the development of subtype selective histamine H_2 receptor ligands. In the process of optimizing the histamine H_2 receptor ligands, representing derivatives of the bisalkylguanidine impromidine (**Figure 2.2**), different structural changes were implemented. The introduction of an acylated guanidine group resulted in lower basicity and improved bioavailability, and the bioisosteric replacement of the imidazole ring by a 2-amino-4-methylthiazol-5-yl moiety as in UR-PG267 (**Figure 2.2**) gave access to selective H_2R ligands[37].

Subsequently, with the replacement of the acylguanidine moiety by a carbamoylguanidine group, compounds with increased stability against hydrolytic cleavage were obtained[38]. However, the developed compounds share a structural feature, i.e. the aminomethylthiazole moiety, with reported dopamine D$_2$, D$_3$ and D$_4$ receptor agonists, such as pramipexole[17] or (–)-**19**[39] (**Figure 2.2**). In order to investigate a potential binding of aminomethylthiazole-type H$_2$R ligands to D$_2$-like receptors, dopamine receptor binding assays were required.

For the establishment of the binding assays, HEK293T cell lines, expressing the human dopamine D$_{2long}$R, D$_3$R or D$_{4.4}$R, were generated. [³H]*N*-methylspiperone was chosen as a radioligand. Binding of [³H]*N*-methylspiperone was determined using cell homogenates and, in some cases, experiments were also performed with whole cells for comparison. The problem of radioligand depletion is discussed in the following. The detectability of the high-affinity states of dopamine receptor agonists was studied. Furthermore, several carbamoylguanidine-type histamine H$_2$ receptor ligands were investigated with respect to their affinities to receptors of the dopamine D$_2$-like family.
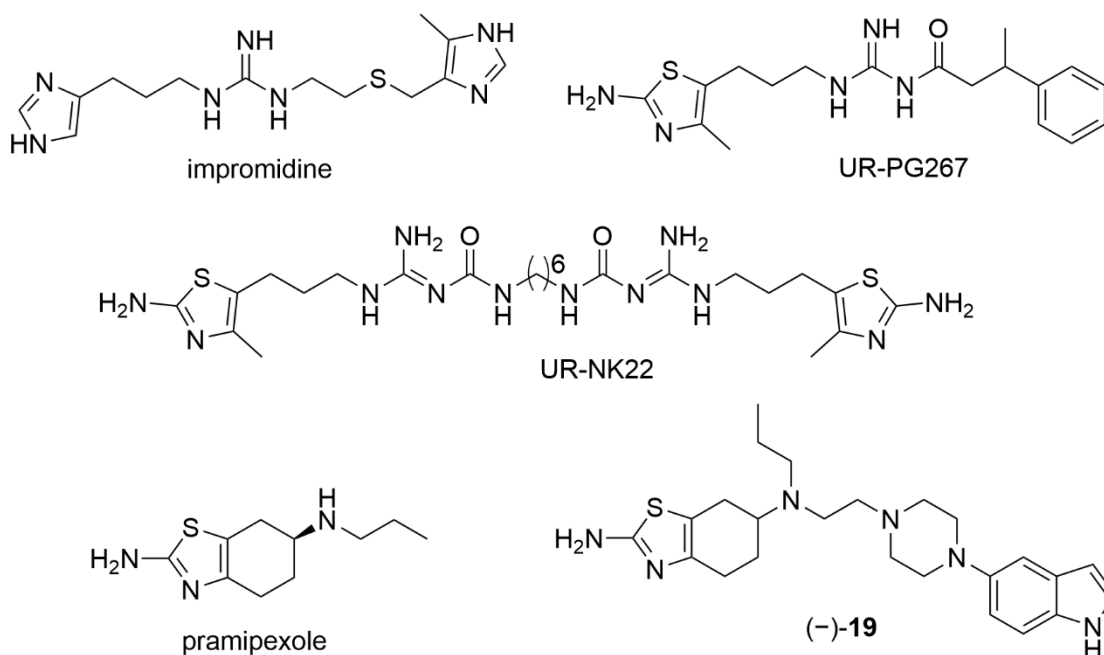
Figure 2.2. Structures of histamine H$_2$ receptor agonists (impromidine, UR-PG267, UR-NK22) and dopamine D$_2$-like receptor agonists (pramipexole and (–)-**19**).

2.2   Results

2.2.1   Preparation of monoclonal cell lines expressing dopamine receptors

As monoclonal, genetically uniform cell lines allow a stable receptor expression over a long period of time, monoclonal cell lines, expressing the $D_{2long}R$, the D_3R or the $D_{4.4}R$, were generated.

HEK293T cells stably expressing the firefly luciferase under the control of a cyclic AMP response element (HEK293T CRE Luc)[40] were used for the transfection with the $D_{2long}R$ or the D_3R. For the transfection with the $D_{4.4}R$, wild type HEK293T cells were used. Several clones of each transfectant were picked for further cultivation (*cf*. Materials and Methods 2.3.4) and subjected to a screening of the signal-to-background (S/B) ratio (radioligand binding). Unfortunately, in the case of the D_3R only two clones were found after antibiotic selection. All clones were studied with respect to total
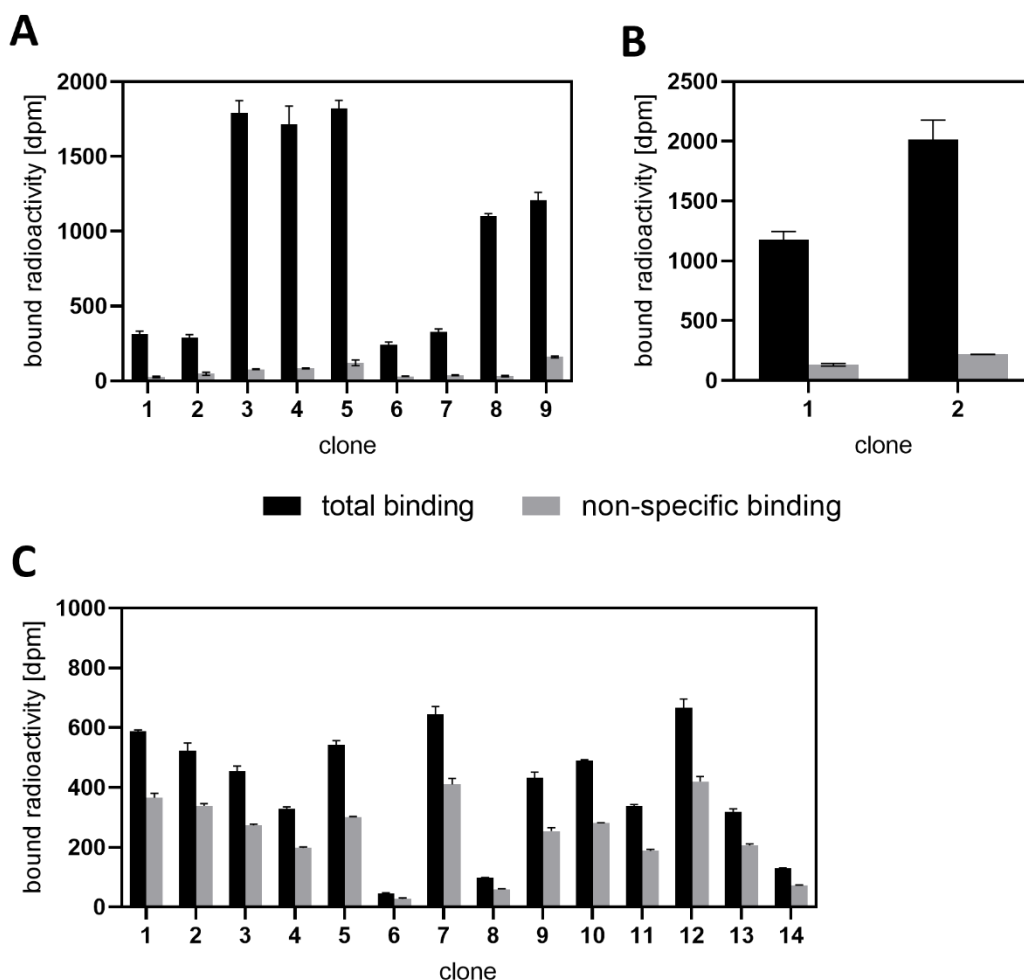
Figure 2.3. Single clones of HEK293T CRE Luc cells expressing the $D_{2long}R$ (**A**) or the D_3R (**B**) and clones of HEK293T cells expressing the $D_{4.4}R$ (**C**) were studied for total and non-specific binding of 0.05 nM [^{3}H]spiperone (**A**,**B**) or 0.05 nM [^{3}H]N-methylspiperone (**C**) (incubation time: 60 min). For the determination of non-specific binding, the antagonist (+)-butaclamol (250 nM) was additionally added. Either 24,000 (**A, B**) or 16,000 (**C**) cells were applied per well. Data are shown as means ± SEM from one experiment performed in triplicate (**A, B**) or duplicate (**C**).

radioligand binding and non-specific radioligand binding (NSB) using the tritiated antagonists [³H]spiperone or [³H]N-methylspiperone (**Figure 2.3**). Based on the expression level of the respective receptor, reflected by the S/B ratio, single clones were chosen for further cultivation, for the preparation of cell homogenates and for radioligand binding studies (D$_{2long}$R: clone 5 (S/B ratio of 15), D$_3$R: clone 1 (S/B ratio of 9), D$_{4.4}$R: clone 7 (S/B ratio of 1.6)). In the case of the D$_{4.4}$R, (+)-butaclamol appeared to be inadequate for the determination of non-specific binding. The high degree of non-specifically bound radioligand (**Figure 2.3C**) indicates that (+)-butaclamol is not able to fully displace [³H]N-methylspiperone from the D$_{4.4}$R. Therefore, the antagonist nemonapride was used for the determination of non-specific binding in the following radioligand binding experiments at the D$_{4.4}$R.

2.2.2   Saturation binding studies with [³H]N-methylspiperone

Saturation binding experiments with the radiolabeled antagonist [³H]N-methylspiperone were performed with whole HEK293T CRE Luc D$_{2long}$R, HEK293T CRE Luc D$_3$R or HEK293T D$_{4.4}$R cells as well as with cell homogenates prepared from these cells (as described in Materials and Methods 2.3.6). In
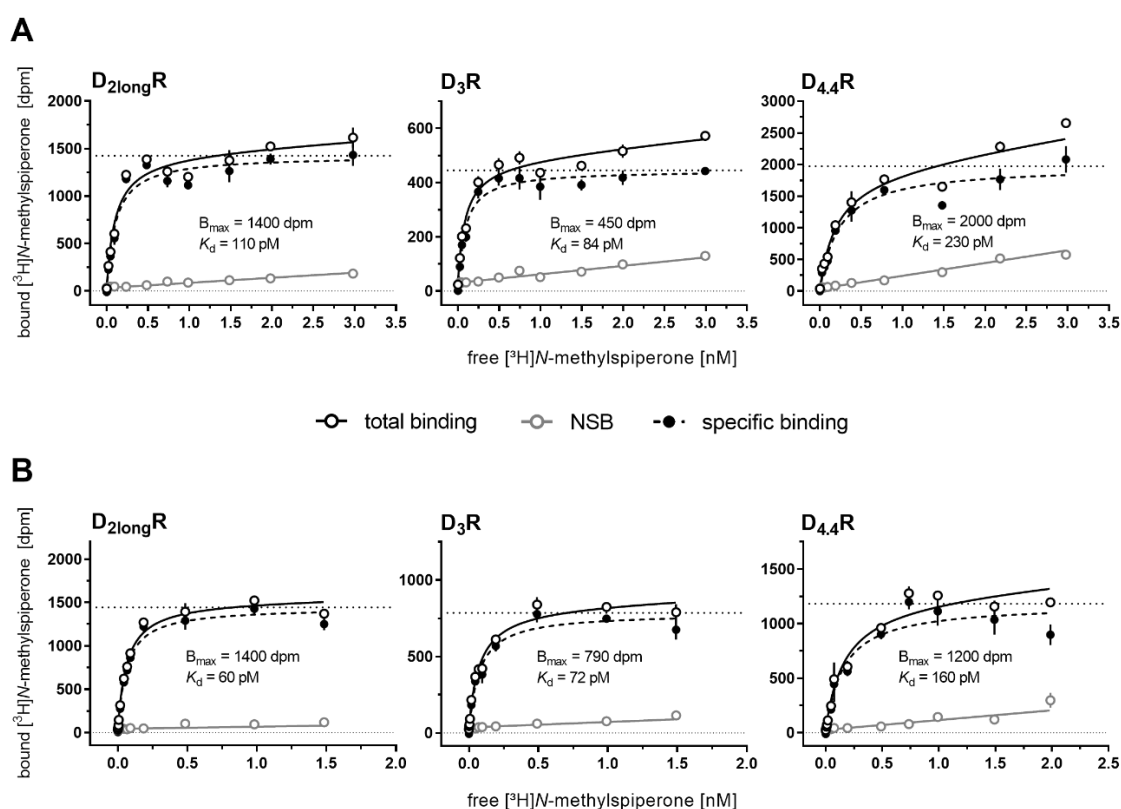
Figure 2.4. Representative saturation isotherms (specific binding) obtained from saturation binding experiments with [³H]N-methylspiperone at whole HEK293T CRE Luc cells co-expressing the hD$_{2long}$R or the hD$_3$R and at whole HEK293T cells expressing the hD$_{4.4}$R (**A**), as well as at cell homogenates prepared from the aforementioned cell lines (**B**). Non-specific binding was determined in the presence of a 2000-fold excess of the antagonist (+)-butaclamol (D$_{2long}$R, D$_3$R) or nemonapride (D$_{4.4}$R). Experiments were performed in triplicate. Error bars of specific binding represent propagated errors. Error bars of total and non-specific binding represent the SEM.

the case of whole cell experiments, [³H]N-methylspiperone bound to all three dopamine receptor subtypes in a saturable manner, affording K_d values of 97 pM, 95 pM and 406 pM for the D$_{2long}$R, D$_3$R and D$_{4.4}$R, respectively (mean values from three independent experiments performed in triplicate) (**Figure 2.4A**, **Table 2.1**). Non-specific binding of the radioligand was low for all three cell lines amounting to 8-13% of total binding at concentrations around the K_d. From the experimentally determined B$_{max}$ values and the number of cells applied in the saturation binding experiments, the cellular receptor expression was calculated and resulted in about 390,000, 120,000 and 480,000 receptors per cell for the D$_{2long}$R, D$_3$R and D$_{4.4}$R, respectively.

The saturation binding curves obtained from experiments performed with cell homogenates prepared from the aforementioned cell lines could be also best described by a one-site fit, being in accordance with the law of mass action (**Figure 2.4B**). The dissociation constants K_d for the D$_{2long}$R, D$_3$R and D$_{4.4}$R were 33, 43 and 100 pM respectively (**Table 2.1**). Non-specific binding of [³H]N-methylspiperone was low for all three dopamine receptor subtypes amounting to 7-9% of total binding at concentrations around the K_d. The maximal number of binding sites (B_{max}) resulted in approximately 21 (D$_{2long}$R), 10 (D$_3$R) and 19 (D$_{4.4}$R) pmol per mg soluble protein of the cell homogenates.

Table 2.1. D$_{2long}$R, D$_3$R and D$_{4.4}$R affinities of [³H]N-methylspiperone determined in saturation binding experiments using whole cells or cell homogenates.

receptor subtype	pK_d ± SEM (K_d, nM)			
	whole cells	N	homogenates	N
D$_{2long}$R	10.02 ± 0.05 (0.097)	3	10.52 ± 0.07 (0.033)	6
D$_3$R	10.02 ± 0.02 (0.095)	3	10.39 ± 0.05 (0.043)	6
D$_{4.4}$R	9.43 ± 0.10 (0.41)	3	10.01 ± 0.06 (0.10)	4

K_d values from individual experiments, obtained by one-site hyperbolic fitting, were transformed to pK_d values, for which mean and SEM values were calculated. N denotes the number of independent experiments, each performed in triplicate.

It can be noticed, that [³H]N-methylspiperone consistently showed a slightly higher affinity to the respective dopamine receptor in experiments performed with cell homogenates compared to whole cell experiments. As this difference was low (< 0.6 log unit), the data were in good agreement.

Equilibrium dissociation constants of [³H]N-methylspiperone at the D$_{2long}$R reported in the literature range from 20 pM[18] over 72 pM[41] to 230 pM[42], determined under varying assay conditions. The herein obtained K_d values from experiments with whole cells as well as those determined with cell homogenates fit well into this range. For the D$_3$R, K_d values ranging from 390 pM[19] to 580 pM[42] were published, being about 9-fold higher compared to the dissociation constant determined at cell homogenates in this study. Regarding the D$_{4.4}$R, reported K_d values of [³H]N-methylspiperone were

294 pM[18] and 480 pM[43], being in good agreement with the K_d determined in the whole cell saturation binding experiments. Differences in the data could arise, for example, from different assay conditions, such as different compositions of buffers, the use of other expression vehicles than HEK293T cells, different assay volumes or the use of whole cells *vs.* membrane preparations *vs.* cell homogenates.

As mentioned in the introduction, the event of radioligand depletion can affect the determination of binding constants, especially in miniaturized assay formats with a limited assay volume[25]. In the performed experiments, the portion of receptor bound radioligand at concentrations around the K_d amounted to 26%, 19% and 5% (in average) for the D_{2long}R, D_3R and $D_{4.4}$R, respectively. To counteract the depletion effect, the bound radioactivity was plotted against the free concentration of radioligand, which was calculated by subtracting bound radioactivity from totally added radioactivity (*cf.* Materials and Methods 2.3.7). The K_d values obtained from this analysis are presented in **Table 2.1**. Applying the model described by Swillens[28] for the evaluation of saturation binding data obtained under conditions of radioligand depletion would have been another option, but since the non-specific binding in the herein performed saturation assays is low, its influence was considered negligible. It should also be noted that non-specific binding at the material of the 96-well plates, being undetectable by the used method (suction and filtration), amounted to approximately 2% of totally added radioactivity at concentrations around the K_d value (investigated by desorption using DMSO, data not shown).

2.2.3   Binding kinetics of [³H]*N*-methylspiperone

Kinetic experiments with [³H]*N*-methylspiperone were conducted with the same homogenate preparations as used for saturation binding experiments. Association to the D_{2long}R, D_3R and $D_{4.4}$R could be best described by an exponential one-phasic fit. [³H]*N*-methylspiperone completely associated to the receptors within 50 min (D_{2long}R), 60 min (D_3R) or 200 min ($D_{4.4}$R), resulting in observed association rate constants (k_{obs}) of 0.078 ± 0.012 (D_{2long}R), 0.11 ± 0.01 (D_3R) and 0.037 ± 0.009 ($D_{4.4}$R) min^{-1} (**Figure 2.5A**). For all three receptor subtypes, the dissociation from the receptors was monophasic reaching plateaus at 34% (D_{2long}R), 7.5% (D_3R) and 19% ($D_{4.4}$R) when analyzed with a three-parameter equation (**Figure 2.5B**). The plateaus were significantly different from zero (one-tailed t-test, $p < 0.05$). Dissociation of [³H]*N*-methylspiperone from the D_{2long}R was slower compared to the dissociation from the D_3R and D_4R (for dissociation rate constants k_{off} see **Table 2.2**). From the observed association rate constant k_{obs} and the k_{off} values the association rate constant k_{on} was calculated ($k_{on} = (k_{obs}-k_{off})/[\text{ligand}]$) (**Table 2.2**). The resulting k_{on} values for the D_{2long}R and the D_3R were markedly higher compared to the $D_{4.4}$R (**Table 2.2**). The k_{on} value obtained for the D_{2long}R ($k_{on} = 3.5$ min^{-1}·nM^{-1}) was not far from a reported k_{on} of the structurally related radioligand [³H]spiperone (k_{on} (D_{2long}R) $= 0.95$ min^{-1}·nM^{-1})[44].

When comparing the kinetically derived equilibrium dissociation constants of [³H]*N*-methylspiperone calculated from k_{off} and k_{on} (K_d(kin) $= k_{off}/k_{on}$) with the K_d values determined in saturation binding

experiments, discrepancies of varying extents, depending on the receptor subtype, were found. The K_d values derived from saturation binding experiments are consistently higher than the kinetic K_d values. The most pronounced difference (15-fold) was observed for the $D_{2long}R$ and the lowest discrepancy (2-fold) was found for the $D_{4.4}R$ (**Table 2.2**). As already mentioned in the previous section, radioligand depletion of high affinity radioligands can lead to an incorrect determination of binding data. At the concentrations applied in the kinetic experiments, about 37%, 25% or 14% of the radioligand were bound to D_{2long}, D_3 or $D_{4.4}$ receptors, respectively (calculated from saturation experiment data). Interestingly, the magnitude of discrepancies between dissociation constants determined in saturation binding experiments and kinetic experiments correlated with the amount of receptor bound radioligand. It might have been advantageous to choose higher radioligand concentrations than the applied concentrations of 0.02 nM ($D_{2long}R$), 0.03 nM (D_3R) and 0.08 nM ($D_{4.4}R$) for the association experiments.
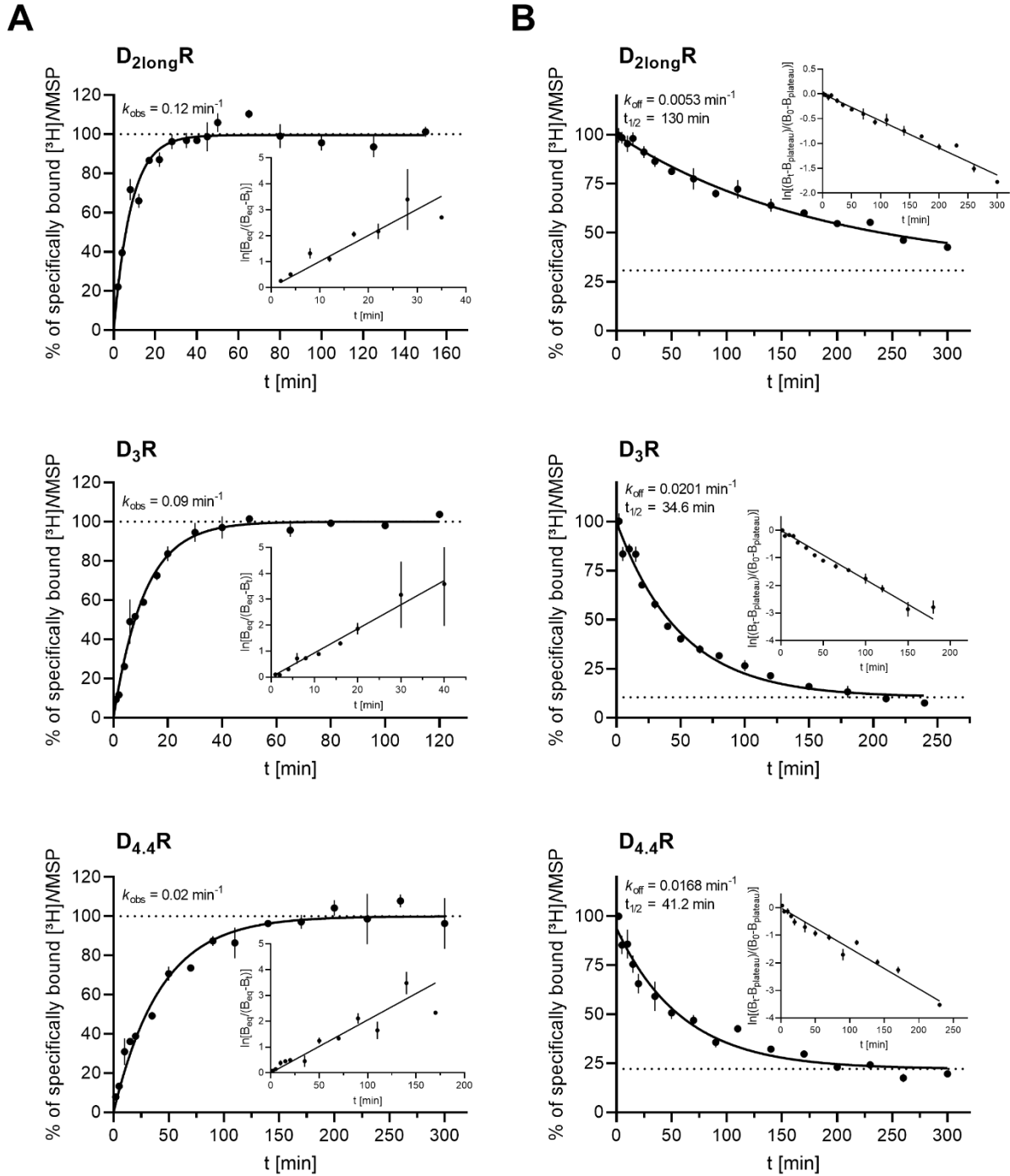
Figure 2.5. Kinetic binding data from experiments with [³H]*N*-methylspiperone at homogenates of HEK293T CRE Luc cells expressing the D$_{2long}$R or D$_3$R or homogenates of HEK293T cells expressing the D$_{4.4}$R performed at 22 ± 1 °C. (**A**) Representative associations of [³H]*N*-methylspiperone (c = 0.02 nM (D$_{2long}$R), 0.03 nM (D$_3$R) or 0.08 nM (D$_{4.4}$R)) as a function of time (k_{obs}, observed association rate constant). Insets: $\ln[B_{(eq)}/(B_{(eq)} - B_{(t)})]$ plotted versus time. (**B**) Representative dissociations of [³H]*N*-methylspiperone (preincubation: 60 min (D$_{2long}$R, D$_3$R) or 150 min (D$_{4.4}$R); *c* = 0.02 nM (D$_{2long}$R), 0.03 nM (D$_3$R) or 0.08 nM (D$_{4.4}$R)) as a function of time (k_{off}, dissociation rate constant), showing an incomplete monophasic exponential decline (plateaus: 34% (D$_{2long}$R), 7.5% (D$_3$R), 20% (D$_{4.4}$R)). Insets: $\ln[(B_t - B_{plateau})/(B_0 - B_{plateau})]$ plotted versus time. Non-specific binding was determined in the presence of a 2000-fold excess of (+)-butaclamol (D$_{2long}$R, D$_3$R) or nemonapride (D$_{4.4}$R). Each experiment was performed in triplicate.

Table 2.2. $D_{2long}R$, D_3R and $D_{4.4}R$ binding data of [^{3}H]N-methylspiperone determined at cell homogenates.

receptor	$pK_d \pm$ SEM (K_d(sat), nM)[a]	K_d(kin) [nM][b]	k_{obs} [min^{-1}]	k_{on} [min^{-1}·nM^{-1}][c]	k_{off} [min^{-1}][d] $t_{1/2}$ [min][d]
$D_{2long}R$	10.52 ± 0.07 (0.033)	0.0022 ± 0.0007	0.078 ± 0.012	3.5 ± 0.7	0.0078 ± 0.001 94 ± 15
D_3R	10.39 ± 0.05 (0.043)	0.0079 ± 0.0018	0.11 ± 0.01	2.9 ± 0.4	0.023 ± 0.002 30 ± 2
$D_{4.4}R$	10.01 ± 0.06 (0.10)	0.048 ± 0.025	0.037 ± 0.009	0.29 ± 0.13	0.014 ± 0.001 51 ± 5

[a]Equilibrium dissociation constant determined by saturation binding. [b]Kinetically derived dissociation constant as mean ± propagated error (K_d(kin) = k_{off}/k_{on}). [c]Association rate constant presented as mean ± propagated error (k_{on} = (k_{obs}–k_{off})/[radioligand]). [d]Dissociation rate constant and derived half-life; mean ± SEM. Data are from at least three independent experiments each performed in triplicate.

2.2.4 Competition binding experiments with [^{3}H]N-methylspiperone and reported dopamine receptor ligands

Aiming at the development of a binding assay suitable to determine DR affinities of newly synthesized compounds, literature known dopamine receptor ligands with different modes of action were studied and the obtained binding constants were compared with literature data. The affinities of the endogenous ligand dopamine, the partial agonist R-(−)-apomorphine[45] and the antagonist haloperidol (**Figure 1.3**, general introduction) at the $D_{2long}R$, D_3R and $D_{4.4}R$ were determined in whole cell competition binding assays using [^{3}H]N-methylspiperone. Resulting competition binding curves are shown in **Figure 2.6**. Haloperidol as well as R-(−)-apomorphine were able to fully displace [^{3}H]N-methylspiperone from the receptors. The determined inhibition constants (K_i values) of haloperidol were in agreement with reported data (**Table 2.3**). However, the obtained K_i values of the partial agonist R-(−)-apomorphine were consistently higher at all three dopamine receptor subtypes
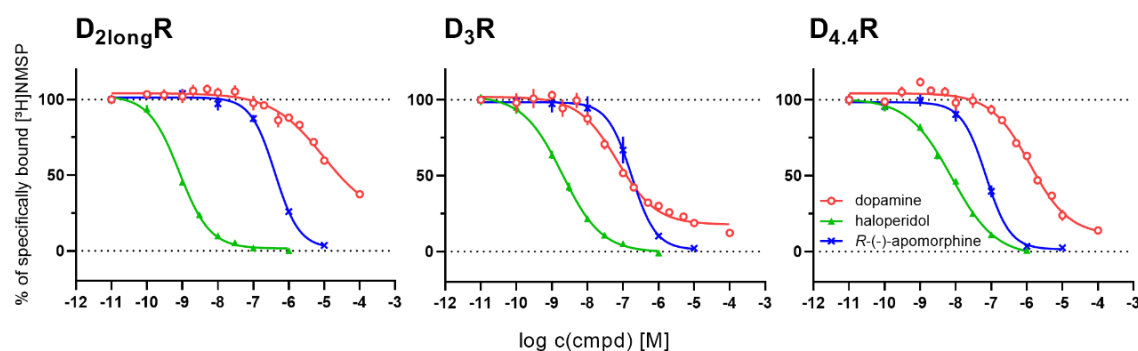
Figure 2.6. Radioligand displacement curves from competition binding experiments performed with [^{3}H]N-methylspiperone and dopamine, haloperidol or R-(−)-apomorphine at whole HEK293T CRE Luc $D_{2long}R$, HEK293T CRE Luc D_3R or HEK293T $D_{4.4}R$ cells. [^{3}H]N-Methylspiperone was applied in concentrations of 0.25 nM ($D_{2long}R$, D_3R) or 0.30 nM ($D_{4.4}R$). Data represent means ± SEM from at least three independent experiments performed in triplicate.

compared to reported literature values. The endogenous ligand dopamine could not fully displace the radioligand at any dopamine receptor subtype (**Figure 2.6**) and the resulting K_i values did not correspond to reference values found in the literature (**Table 2.3**). Regarding the D$_{2long}$R and the D$_{4.4}$R, the obtained K_i values were markedly higher. Furthermore, high and low affinity inhibition constants were reported for dopamine at the D$_{2long}$R, D$_3$R and D$_{4.4}$R[14,46]. However, the data obtained in the whole cell competition binding assays in this study were best described by a one-site binding model.

Table 2.3. Comparison of D$_{2long}$, D$_3$ and D$_{4.4}$ receptor affinities of selected dopamine receptor ligands, obtained from whole cell radioligand competition binding studies, with reported data.

cmpd.	D$_{2long}$R pK$_i$ ± SEM (K$_i$, nM)	N	D$_3$R pK$_i$ ± SEM (K$_i$, nM)	N	D$_{4.4}$R pK$_i$ ± SEM (K$_i$, nM)	N	Ref. K$_i$ [nM] D$_{2long}$R/D$_3$R/D$_{4.4}$R
R-(−)-apomorphine	6.86 ± 0.05 (140)	3	7.35 ± 0.15 (53)	3	7.40 ± 0.12 (44)	3	24/20[47]/4.1[48]
dopamine	5.53 ± 0.19 (4500)	4	7.81 ± 0.10 (20)	3	6.16 ± 0.05 (710)	3	15, 3300*[36]/50, 1600*[46]/28[48]
haloperidol	9.56 ± 0.06 (0.28)	3	9.30 ± 0.08 (0.53)	3	8.36 ± 0.02 (4.4)	3	0.91[49]/2.9[4]/5.1[48]

Data are presented as means ± SEM. *N* denotes the number of independent experiments, each performed in triplicate.

*K_i values for the high- and the low-affinity state.

These results suggested that the whole cell competition binding assay is no ideal system for the determination of DR affinities of agonists and partial agonists. As described in the introduction, the high-affinity binding component is detectable in systems, which allow an accumulation of the ternary complex of agonist, receptor and G-protein[35]. In whole cells the intracellular GTP concentration is high, thus intervening the persistence of the ternary complex[35]. This does not apply to cell homogenates or membrane preparations, so the assay procedure was adapted and the experiments were performed with cell homogenates prepared from the same cell lines (*cf*. Materials and Methods, section 2.3.5). This approach led to results that were in better agreement with reported data (**Table 2.4**). Results from agonist/[³H]*N*-methylspiperone competition binding studies are discussed in chapter 2.2.6. In addition to the compounds that were tested in the whole cell competition binding experiments, the partial agonist aripiprazole and the antagonists (+)-butaclamol, domperidone, nemonapride and *S*-(−)-sulpiride were included in the investigations (**Figure 1.3**, general introduction). All competition binding curves were best fitted with a one-site model (**Figure 2.7**). Obtained IC$_{50}$ values were converted to inhibition constants (K_i) using the Cheng-Prusoff equation[50]. The determined ligand affinities were in good agreement with reference data found in in the literature, with no more than half an order of magnitude difference in pK_i values (**Table 2.4**). Exceptions were, with larger discrepancies,

nemonapride at the $D_{2long}R$ and (+)-butaclamol and domperidone at the $D_{4.4}R$. In the reference, reporting the $D_{4.4}R$ affinities of (+)-butaclamol and domperidone, it was not specified which isoform of the D_4R was used. Possibly, the differences in affinities might be due to the use of different isoforms of the D_4 receptor.

As already mentioned in the previous sections, binding assays employing high affinity radioligands are prone to ligand depletion. In terms of competition binding experiments, radioligand depletion can lead to an underestimation of the affinity of the competitor[25]. The bound fraction of [³H]N-methylspiperone in the $D_{2long}R$ and D_3R binding assays amounted to approximately 26% and 19%, respectively (in average). Radioligand depletion did not play a role in experiments with the $D_{4.4}R$, where the bound fraction of [³H]N-methylspiperone was ca. 6%. Carter et al.[25] showed that employing radioligand concentrations around the K_d value in competition binding experiments and the use of a correctly determined K_d value in the Cheng-Prusoff equation to convert IC_{50} values to K_i values, reduces the impact of ligand depletion.
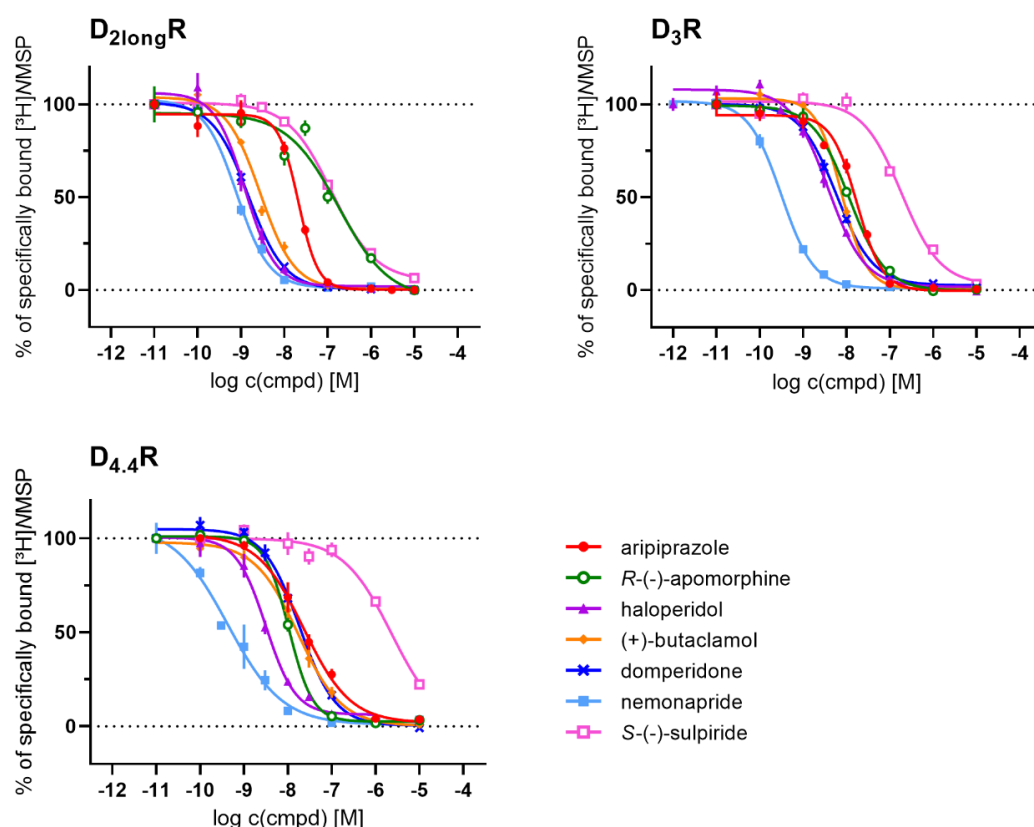

Figure 2.7. Radioligand displacement curves from competition binding experiments performed with [³H]N-methylspiperone and various DR ligands at cell homogenates prepared from HEK293T CRE Luc cells co-expressing the $D_{2long}R$ or the D_3R, or from HEK293T cells expressing the $D_{4.4}R$. [³H]N-methylspiperone was applied at concentrations of 0.05 nM ($D_{2long}R$, D_3R) or 0.10 nM ($D_{4.4}R$). The lower curve plateau of the displacement curve of S-(−)-sulpiride at the $D_{4.4}R$ was constrained to 0 to obtain an IC_{50} value since S-(−)-sulpiride was not able to fully displace the radioligand at a concentration of 10 μM. Data represent mean values ± SEM from at least three independent experiments, each performed in triplicate.

Table 2.4. D_{2long}, D_3 and $D_{4.4}$ receptor affinities of selected dopamine receptor ligands obtained by competition binding with [^{3}H]N-methylspiperone using cell homogenates.

cmpd.	D_{2long}R pK$_i$ ± SEM (K$_i$, nM)	N	D_3R pK$_i$ ± SEM (K$_i$, nM)	N	$D_{4.4}$R pK$_i$ ± SEM (K$_i$, nM)	N	Ref. K$_i$ [nM] D_{2long}R/D_3R/$D_{4.4}$R
R-(-)-apomorphine	7.33 ± 0.13 (57)	4	8.26 ± 0.03 (5.5)	3	8.27 ± 0.02 (5.4)	3	24[47]/20[47]/4.1[48]
aripiprazole	8.08 ± 0.02 (8.3)	3	8.12 ± 0.01 (7.5)	3	7.79 ± 0.08 (17)	3	2.58[51]/10[52]/46.5[53]
(+)-butaclamol	8.90 ± 0.06 (1.3)	3	8.46 ± 0.02 (2.8)	3	8.01 ± 0.09 (11)	3	4.1[49]/4.0[54]/550[55]
domperidone	9.23 ± 0.07 (0.62)	3	8.58 ± 0.04 (2.7)	4	8.05 ± 0.07 (9.3)	3	0.87[49]/2.9[56]/90[55]
haloperidol	9.44 ± 0.13 (0.44)	4	8.78 ± 0.04 (1.7)	6	8.95 ± 0.08 (1.2)	4	0.91[49]/2.9[4]/5.1[48]
nemonapride	9.52 ± 0.08 (0.32)	3	9.86 ± 0.06 (0.14)	3	9.53 ± 0.13 (0.35)	4	0.02[54]/0.06[54]/0.09*[57]
S-(-)-sulpiride	7.27 ± 0.09 (58)	3	7.07 ± 0.03 (86)	4	5.94 ± 0.04 (1300)	3	15.9[49]/70[58]/1900[55]

Data represent means ± SEM. *N* denotes the number of independent experiments, each performed in triplicate.

*K$_d$ value.

2.2.5 Detection of high and low affinity receptor states for DR agonists

The dopamine D_2-like receptor agonists dopamine, quinpirole and pramipexole were investigated in equilibrium competition binding experiments with [^{3}H]N-methylspiperone to assess the corresponding affinities for the D_{2long}, the D_3 and the $D_{4.4}$ receptor. Furthermore, the detectability of different affinity states of the receptors in the used recombinant systems was studied. To investigate the interconvertible affinity states in detail, the competition binding experiments with dopamine and quinpirole were additionally performed in the presence of guanylylimidodiphosphate (Gpp(NH)p), a non-hydrolysable GTP analogue. The obtained competition binding curves are depicted in **Figure 2.8**, where for illustration purposes, the data obtained from experiments in the absence of Gpp(NH)p were fitted according to both a two-site model (grey line) and a one-site model (red dashed line). Results obtained from experiments in the presence of Gpp(NH)p are shown in green. Whether the data were best described by a one-site (One site – fit logIC$_{50}$, slope constrained to unity) or a two-site (Two site – fit logIC$_{50}$, slopes constrained to unity) model (GraphPad Prism 9) was decided after comparing both

fits using the extra sum-of-squares F-test, which accounts for the difference in the degrees of freedom between the two models. *P*-values < 0.05 were considered to indicate statistical significance and the more complex model (alternative hypothesis) was favored over the one-site model (null hypothesis).

Competition binding of the agonists dopamine, quinpirole or pramipexole with [^{3}H]*N*-methylspiperone at the D$_{2long}$ receptor resulted in shallow displacement curves (**Figure 2.8**), indicating a more complex binding interaction of the receptors with these ligands. The data were best described by a two-site model (**Figures 2.8B**-**C**, grey lines) providing affinities for a high and a low affinity state (pK_{iH} and pK_{iL}, **Table 2.5**). The obtained pK_i values of quinpirole and dopamine for the high and low affinity states of the D$_{2long}$R aligned well with reported data, whereas the pK_i values obtained for pramipexole were different from reported data by about one log unit (**Table 2.5**). However, reported binding data of pramipexole are very inconsistent and in some cases only one inhibition constant for pramipexole was determined. For instance, Millan et al.[59] and Sautel et al.[60] reported single K_i values for pramipexole at the D$_{2long}$R, amounting to 1.7 µM and 790 nM, respectively.

The dopamine competition binding curve at the D$_3$R was also shallow and best described by a two-site model (**Figure 2.8A**, grey line), yielding pK_i values that correlated well with reported data (**Table 2.5**). In contrast, the competition binding curves of quinpirole and pramipexole were steeper and the results of the extra sum-of-squares F-test suggested a single binding state of the D$_3$R. However, for both agonists distinct inhibition constants for the high affinity and the low affinity state of the D$_3$R were reported[17,58]. The pK_i values obtained from curve fitting according to a one-site model were in good agreement with the reported inhibition constants for the high affinity state of the receptor, differing less than half a log unit (**Table 2.5**).

The situation is similar for the D$_{4.4}$R, where displacement of the radioligand by dopamine resulted in a shallow curve and was best analysed according to a two-site model (**Figure 2.8A**). For the competition binding curves of quinpirole and pramipexole (**Figures 2.8B** + **C**) the results of the extra sum-of-squares F-test did not support the two-site model, being in disagreement with reported biphasic radioligand displacement curves for these DR agonists at the D$_{4.4}$R[17,58]. The inhibition constant obtained for quinpirole from the one-site fit (pK_i: 7.94) fell between the values reported in the literature for the high affinity and the low affinity states (pK_{iH}: 9.64, pK_{iL}: 6.75). Regarding pramipexole, the obtained inhibition constant at the D$_{4.4}$R (7.68 ± 0.05) was in good agreement with the pK_{iH} reported for the high affinity state (pK_{iH}: 7.56[17]) (**Table 2.5**).

Whereas the fraction of D$_{2long}$ receptors in the high affinity state (% R$_h$, **Table 2.5**) ranged from 24 to 40%, 57% or 58% of the total population of binding sites of the D$_3$R and the D$_{4.4}$R, respectively, accounted for the high affinity binding state.
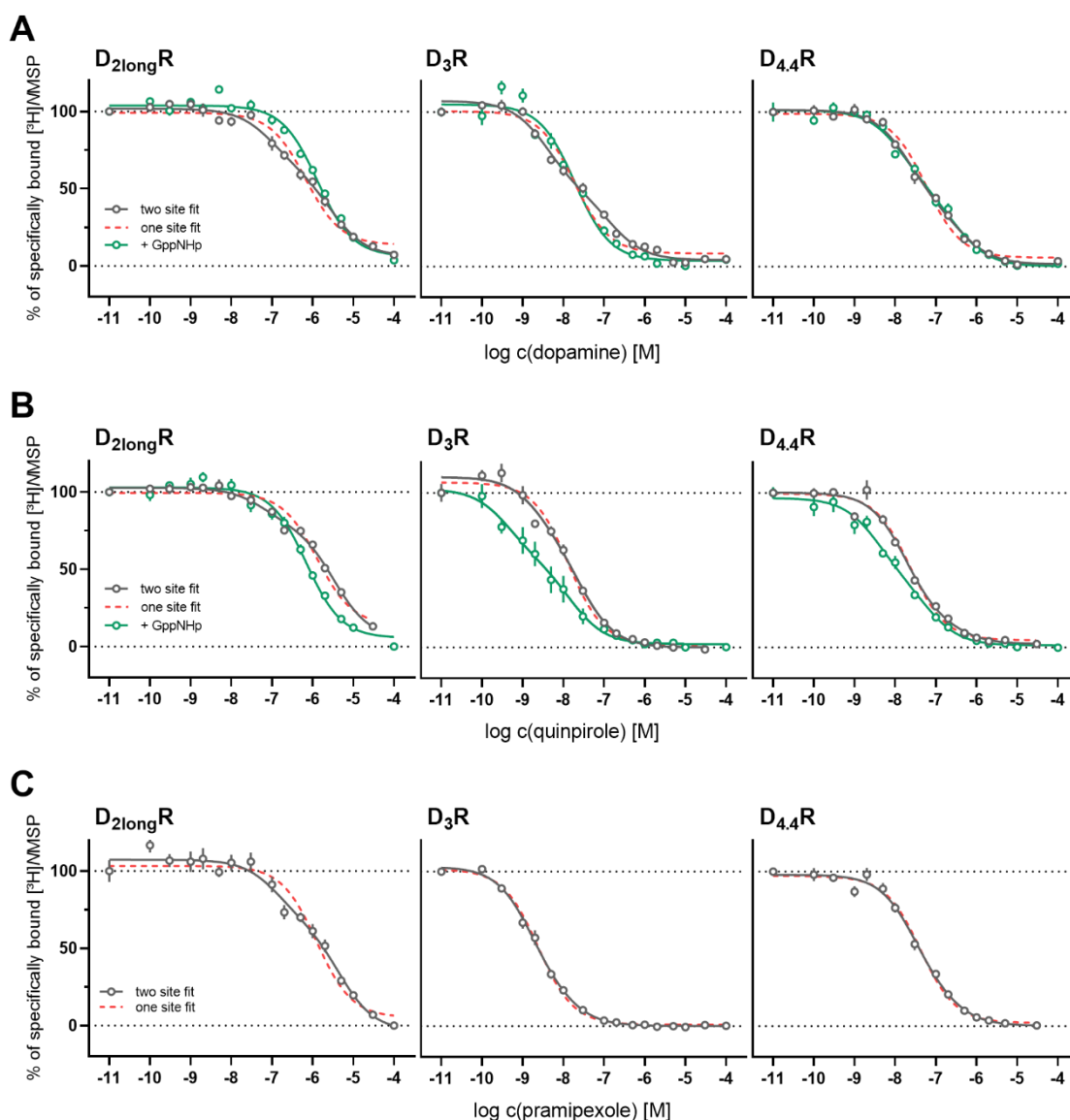
***Figure 2.8.*** Radioligand displacement curves from competition binding experiments performed with [^{3}H]*N*-methylspiperone and dopamine (**A**), quinpirole (**B**) or pramipexole (**C**) at cell homogenates prepared from HEK293T CRE Luc cells co-expressing the D$_{2long}$R or the D$_3$R, or from HEK293T cells expressing the D$_{4.4}$R. Data obtained from experiments in the absence of Gpp(NH)p were fitted according to a two-site (grey line) and a one-site (red broken line) model. Data derived from experiments in the presence of Gpp(NH)p are depicted in green and were fitted according to a one-site model in the case of dopamine at the D$_{2long}$R and D$_3$R and quinpirole at the D$_{2long}$R and D$_{4.4}$R. In the case of dopamine at the D$_{4.4}$R and quinpirole at the D$_3$R (in the presence of Gpp(NH)p), data were fitted according to a two-site model. Note: Both fitting models used constrained slope factors (slope = −1). Data represent mean values ± SEM from at least three independent experiments, each performed in triplicate.

To further investigate the occurrence of two interconvertible affinity states of the D$_2$-like receptors, competition binding experiments with dopamine and quinpirole were performed in the presence of 50 µM Gpp(NH)p. The resulting competition binding curves are shown in **Figure 2.8A** and **B** in green. At the D$_{2long}$R, the addition of Gpp(NH)p led to a steepening of the curves and in the case of dopamine also to a rightward shift. The second binding state was abolished, i.e. the competition binding curves

were best described by a one-site model yielding pK_i values closer to the pK_{iL} determined in the absence of Gpp(NH)p. The same was observed for the dopamine competition binding curve at the D$_3$R. Interestingly, the quinpirole competition binding curve was flattened in the presence of Gpp(NH)p and the comparison of the fits yielded a *p*-value < 0.05, indicating that the two-site model was more likely to be correct. The determined pK_i values amounted to 9.77 ± 0.32 for the high affinity and 7.53 ± 0.54 for the low affinity state. However, these results should be treated with caution, since for some of the individual experiments no 95% confidence intervals of the IC$_{50}$ values or the fraction of high affinity sites could be calculated. Consequently, it might be reasonable to assume a single binding site, yielding a pK_i of 8.90 ± 0.30.

At the D$_{4.4}$R, neither the slope of the competition binding curve of dopamine nor the obtained pK_i values for the high and low affinity site were markedly affected by the addition of Gpp(NH)p (**Figure 2.8A**). Similar to the D$_3$R, the competition binding curve of quinpirole was flattened in the presence of Gpp(NH)p and a two-site fit yielded a pK_{iH} of 10.06 ± 1.02 and a pK_{iL} of 7.59 ± 0.20. The calculated *p*-value for the depicted competition binding curve (**Figure 2.8B**) was 0.0012. However, taking the high error of the pK_{iH} value into account, as well as the fact that for some of the individual experiments no or a very large 95% confidence interval was obtained for some of the parameters of the two-site model analysis, the one-site model should be favored. The reason for the partially ambiguous results could be that the GTP analogue Gpp(NH)p was not applied in a saturating concentration. Kent et al.[31] investigated the effect of different concentrations of Gpp(NH)p at β-adrenergic receptors and the receptors were completely converted to the low affinity state in the presence of 100 μM Gpp(NH)p. However, they noted a concentration-dependent effect of nucleotides starting from Gpp(NH)p concentrations of 0.1 μM.

Table 2.5. D$_{2\text{long}}$, D$_3$ and D$_{4.4}$ receptor binding data of the DR agonists dopamine, quinpirole and pramipexole obtained from [^{3}H]N-methylspiperone competition binding studies in the absence or presence of guanylylimidodiphosphate (Gpp(NH)p).

		pK$_{iH}$ ± SEM (K$_{iH}$, nM)	% R$_h$	pK$_{iL}$ ± SEM (K$_{iL}$, nM)	pK$_i$ ± SEM (K$_i$, nM)	N	+ Gpp(NH)p pK$_{iH}$ ± SEM (K$_{iH}$, nM)	% R$_h$	pK$_{iL}$ ± SEM (K$_{iL}$, nM)	pK$_i$ ± SEM (K$_i$, nM)	N	Ref. pK$_{iH}$/ pK$_{iL}$
D$_{2\text{long}}$R	dopamine	7.53 ± 0.21 (41)	40 ± 3	5.96 ± 0.10 (1200)	-	3	-	-	-	6.27 ± 0.07 (560)	4	7.82/5.48[36]
	quinpirole	7.66 ± 0.10 (24)	24 ± 1	5.87 ± 0.02 (1300)	-	3	-	-	-	6.56 ± 0.03 (280)	3	7.81/5.62[58]
	pramipexole	7.35 ± 0.12 (50)	35 ± 4	5.76 ± 0.03 (1700)	-	3	n.d.	-	-	-	-	8.68/6.87[17]
D$_3$R	dopamine	8.64 ± 0.09 (2.5)	57 ± 5	7.10 ± 0.09 (86)	-	4	-	-	-	8.06 ± 0.02 (7)	3	8.41/7.14[14]
	quinpirole	-	-	-	8.20 ± 0.07 (6.6)	3	9.77 ± 0.32 (0.29)	52 ± 17	7.53 ± 0.54 (200)	-	3	7.71/6.58[58]
	pramipexole	-	-	-	8.97 ± 0.08 (1.2)	4	n.d.	-	-	-	-	9.31/8.56[17]
D$_{4.4}$R	dopamine	8.02 ± 0.02 (10)	58 ± 8	6.72 ± 0.13 (220)	-	3	8.11 ± 0.06 (8.0)	52 ± 7	6.81 ± 0.07 (160)	-	3	8.92/7.21[46]
	quinpirole	-	-	-	7.93 ± 0.07 (12)	3	-	-	-	8.20 ± 0.06 (6.6)	3	7.47[55]
	pramipexole	-	-	-	7.68 ± 0.05 (22)	3	n.d.	-	-	-	-	7.56/6.86[17]

Data were analysed as described in Materials and Methods. If data were best described by a two-site binding model, affinities for the high (K$_{iH}$) and the low (K$_{iL}$) affinity state of the respective receptor and the percentage of high affinity states (%R$_h$) are given. Data represent mean values ± SEM from N independent experiments, each performed in triplicate.

2.2.6 Dopamine receptor binding of carbamoylguanidine-type histamine H$_2$ receptor ligands

As already described in the introduction, the establishment of DR binding assays was prompted by the synthesis of histamine H$_2$ receptor ligands (performed by other doctoral students), which might also bind to receptors of the D$_2$-like family. A selection of these ligands, shown in **Figure 2.9**, was studied with respect to the capability of displacing [^{3}H]N-methylspiperone from the dopamine D$_{2long}$ and D$_3$ receptor. Some of these data were already published (Biselli et al.[61] and Tropmann et al.[62]). The most promising ligands regarding histamine H$_2$ receptor selectivity and those that were selected as representatives of the different heterocyclic moieties were also investigated with respect to D$_{4.4}$ receptor binding. Competition binding curves of the compounds studied at all three dopamine receptor subtypes are shown in **Figure 2.10**, radioligand displacement curves obtained from the remaining H$_2$-receptor ligands are given in **Figure A1** (Appendix). If the compounds were able to displace the radioligand by more than 50% (at a concentration of 10 or 100 µM), the curves were fitted by a four-parameter logistic fit with variable slope as depicted in **Figure 2.10**. Obtained IC$_{50}$ values were converted to inhibition constants K_i using the Cheng-Prusoff equation (K_i values presented in **Table 2.6** and **Table A1** (Appendix)).

The dimeric carbamoylguanidine UR-NK22 showed affinities to the D$_2$-like receptors in the nanomolar range, with the highest affinity to the D$_3$R (pK_i = 8.57, **Table 2.6**). In comparison, monomeric compounds carrying a 2-amino-4-methylthiazole heterocycle (UR-SB283, UR-KAT523, UR-CH22, UR-MB-69 and UR-KAT580) exhibited a slightly lower affinity to the studied dopamine receptor subtypes. However, especially in the case of the D$_3$R, low binding constants in the two-digit nanomolar range were determined (*cf*. **Table 2.6**). With few exceptions, the affinities of the 2-amino-4-methylthiazoles at the studied receptors can be ranked according to D$_3$R > D$_{4.4}$R > D$_{2long}$R, with UR-Po563 showing the highest affinity at the D$_3$R (pK_i = 7.88, *cf*. **Table 2.6** and **Figure A1**, Appendix). Ligands containing an aminothiazole heterocycle, such as UR-KAT580 or UR-KAT583, still showed moderate to high affinities to the D$_2$-like receptors, again especially to the D$_3$ receptor (**Table 2.6**, **Figure 2.10** and **Figure A1**, Appendix). With the introduction of the heterocycles 2-amino-1,3,4-thiadiazole (UR-KAT505, UR-KAT533) or 1H-1,2,4-triazole (UR-MB-159), the D$_2$-like receptor binding could be abolished. These ligands displayed lower affinities at the D$_{2long}$, D$_3$ and D$_{4.4}$ receptors (pK_i < 6; except for UR-KAT533 at the D$_{4.4}$R, pK_i = 6.17). The compounds UR-SB238 and UR-SB239 with a rigidized aminothiazolylpropyl moiety also showed very low affinities for the D$_{2long}$R and the D$_3$R, however, they also exhibited only moderate to low affinities to the histamine H$_2$ receptor[61].

dimeric carbamoylguanidines

R
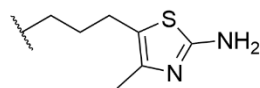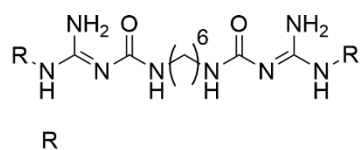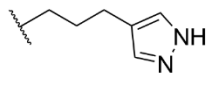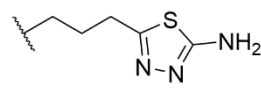
UR-NK22 UR-SB146 UR-KAT512

monomeric carbamoylguanidines and thiocarbamoylguanidines
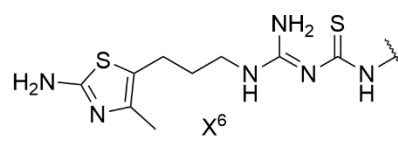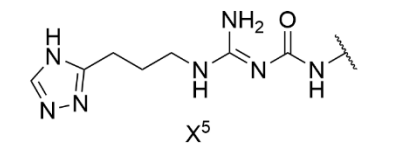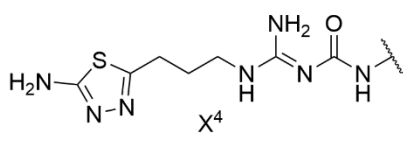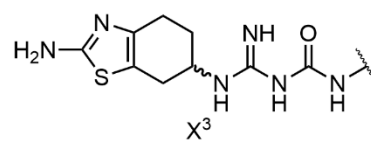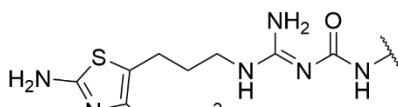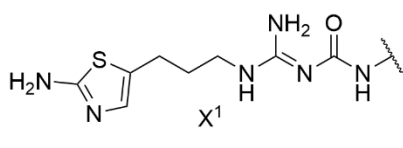
R

X^1: UR-KAT583
X^2: UR-KAT523
X^4: UR-KAT505

X^1: UR-SB232
X^2: UR-CH20
X^3: UR-SB239
X^4: UR-KAT528
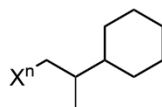
X^2: UR-SB291
X^4: UR-KAT508
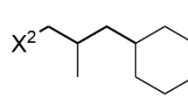
UR-SB294
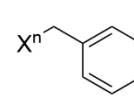
X^1: UR-KAT584
X^2: UR-CH22
X^3: UR-SB238
X^4: UR-KAT533
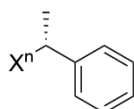
X^2: UR-Po563
X^4: UR-MB-158
X^5: UR-MB-159
X^6: UR-Po586
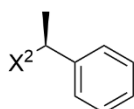
UR-Po564
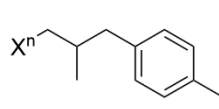
X^1: UR-KAT580
X^2: UR-SB257
X^4: UR-KAT501
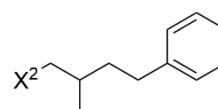
UR-SB283
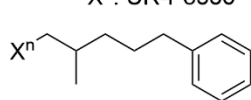
X^2: UR-KAT527
X^4: UR-KAT524
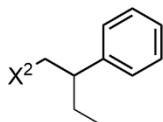
UR-SB295
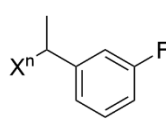
X^2: UR-MB-69
X^4: UR-MB-165
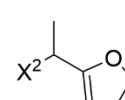
UR-MB-72
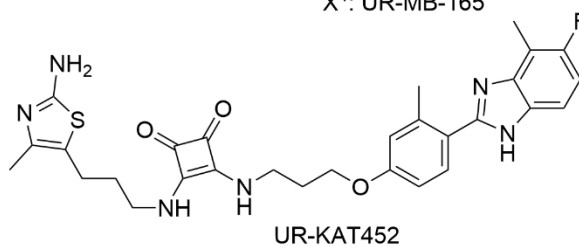
UR-KAT452

Figure 2.9. Structures of the investigated carbamoylguanidine-type and thiocarbamoylguanidine-type H$_2$R agonists.
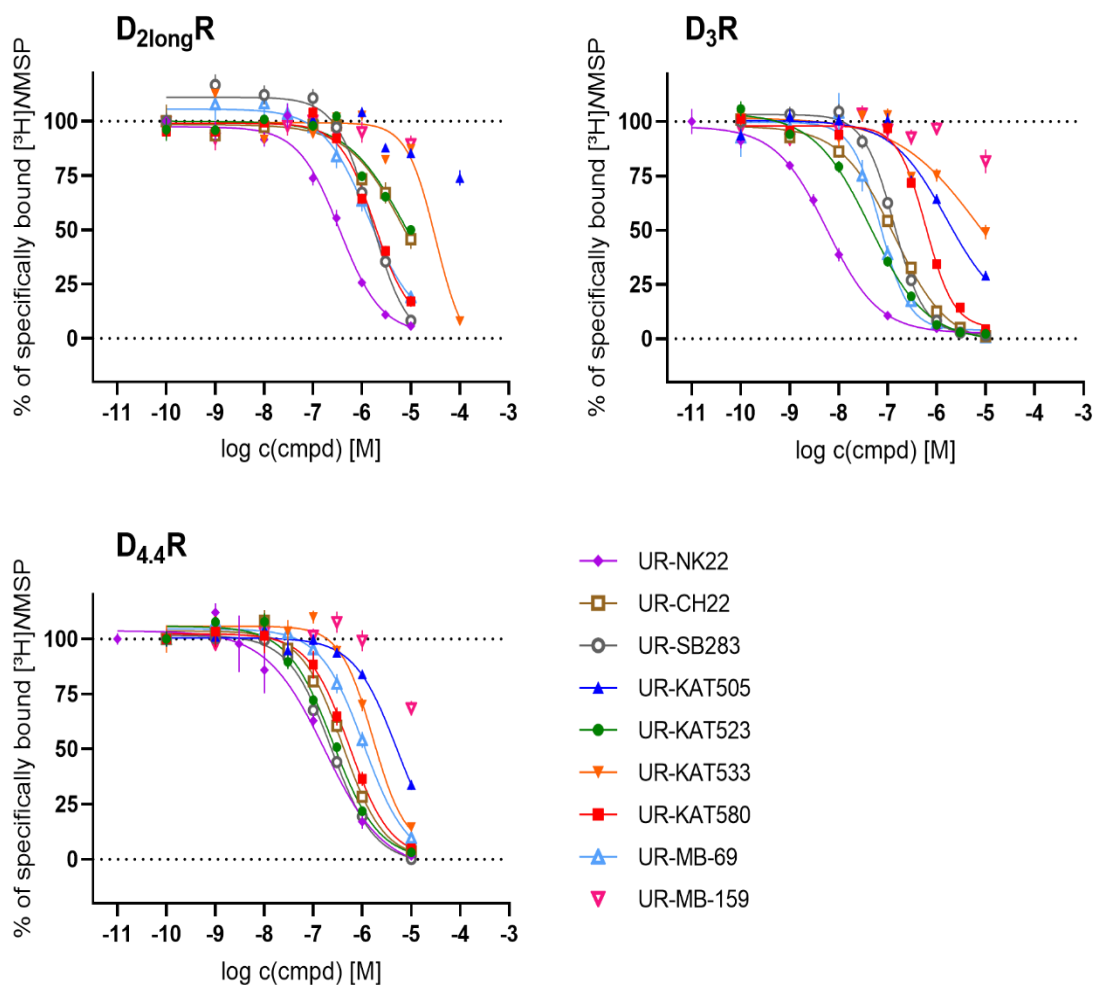
Figure 2.10. Radioligand displacement curves from competition binding experiments performed with [³H]*N*-methylspiperone and various histamine H$_2$ receptor ligands (structures see **Figure 2.9**) at cell homogenates of HEK293T CRE Luc cells co-expressing the D$_{2long}$R or the D$_3$R or of HEK293T cells expressing the D$_{4.4}$R. If radioligand displacement was incomplete (< 90%) at 10 or 100 µM, but more than 50% of the radioligand was displaced, data were fitted constraining the lower curve plateau to 0. Data represent mean values ± SEM from at least three independent experiments, each performed in triplicate.

Table 2.6. D$_{2long}$, D$_3$ and D$_{4.4}$ receptor affinities of selected carbamoylguanidine-type histamine H$_2$-receptor ligands obtained by competition binding with [^{3}H]*N*-methylspiperone using cell homogenates.

cmpd.	D$_{2long}$R pK$_i$ ± SEM (K$_i$, nM)	N	D$_3$R pK$_i$ ± SEM (K$_i$, nM)	N	D$_{4.4}$R pK$_i$ ± SEM (K$_i$, nM)	N
UR-NK22	6.85 ± 0.07 (120)	3	8.57 ± 0.04 (2.7)	3	7.15 ± 0.03 (72)	3
UR-CH22	5.98 ± 0.08 (1100)	3	7.21 ± 0.02 (63)	3	6.77 ± 0.04 (170)	3
UR-SB283	6.14 ± 0.04 (640)	3	7.20 ± 0.03 (63)	4	7.01 ± 0.07 (100)	3
UR-KAT523	6.05 ± 0.05 (910)	3	7.67 ± 0.09 (23)	3	6.96 ± 0.01 (110)	3
UR-Po563	6.03 ± 0.12 (1100)	3	7.88 ± 0.16 (16)	3	n.d.	
UR-MB-69	6.32 ± 0.09 (520)	3	7.70 ± 0.08 (21)	3	6.39 ± 0.06 (420)	3
UR-KAT580	6.06 ± 0.06 (900)	3	6.46 ± 0.02 (350)	3	6.64 ± 0.08 (210)	3
UR-KAT583	<5	3	7.31 ± 0.02 (49)	3	n.d.	
UR-KAT505	<4	3	6.0 ± 0.05 (1000)	4	5.65 ± 0.02 (2300)	3
UR-KAT533	4.93 ± 0.03 (12000)	3	5.39 ± 0.15 (4800)	3	6.14 ± 0.10 (740)	3
UR-MB-159	<5	3	<5	3	<5	3
UR-SB238	4.41 ± 0.09 (41000)	3	5.08 ± 0.04 (8400)	3	n.d.	
UR-SB239	<5	3	5.49 ± 0.06 (3300)	3	n.d.	

Data represent means ± SEM. *N* denotes the number of independent experiments, each performed in triplicate. n.d.: not determined.

2.3   Materials and methods

2.3.1   Materials

Dulbecco's modified Eagle's medium (DMEM) and L-glutamine were from Sigma (Taufkirchen, Germany). Leibovitz' L-15 medium (L-15) was from Fisher Scientific (Nidderau, Germany). Fetal calf serum (FCS), trypsin/EDTA and geneticin (G418) were from Merck Biochrom (Darmstadt, Germany) and hygromycin B was from MoBiTec (Göttingen, Germany). Cell culture flasks and dishes were from Sarstedt (Nümbrecht, Germany). The cDNAs of the $hD_{2long}R$ and hD_3R were kindly provided by Dr. Harald Hübner (Department of Chemistry and Pharmacy, Friedrich-Alexander-University, Erlangen). The cDNA of the $D_{4.4}R$ was purchased from the cDNA Resource Center (Rolla, MO, USA). The pIRESneo3 vector was a gift from Prof. G. Meister (Institute of Biochemistry, Genetics, and Microbiology, University of Regensburg, Germany). Bacitracin was from SERVA Electrophoresis GmbH (Heidelberg, Germany). If possible, stock solutions of receptor ligands were prepared using H_2O (millipore); otherwise DMSO was used (Merck, Darmstadt, Germany). (+)-Butaclamol, dopamine, pramipexole and quinpirole were from Sigma (Taufkirchen, Germany), aripiprazole and haloperidol were from TCI Deutschland GmbH (Eschborn, Germany). *R*-(−)-Apomorphine, nemonapride, *S*-(−)-sulpiride and domperidone were from Tocris Bioscience (Bristol, United Kingdom).

2.3.2   Cell cultivation

HEK293T cells obtained as a kind gift from Prof. Dr. Wulf Schneider (Institute for Medical Microbiology and Hygiene, Regensburg, Germany) were cultured in DMEM supplemented with 10% FCS at 37 °C in a water-saturated atmosphere containing 5% CO_2. Cells were routinely tested for mycoplasma contamination using the Venor GeM Mycoplasma Detection Kit (Minerva Biolabs, Germany) and were negative.

2.3.3   Generation of plasmids

The $hD_{2long}R$, hD_3R and $hD_{4.4}R$ were cloned into a pIRESneo3 vector via Gibson assembly. The pIRESneo3-SP-FLAG-hH$_4$R vector, described elsewhere[63], was used as a template. First, the vector was linearized using standard PCR techniques (Q5 high fidelity DNA polymerase; New England Biolabs, Ipswich, MA, USA). The sequences of the dopamine receptors were amplified and, simultaneously, overlaps complementary to both ends of the linearized vector were attached to the dopamine receptors using specific primers and the Q5 high fidelity DNA polymerase. Subsequently, receptors were cloned into pIRESneo3 according to the NEBuilder HiFi DNA Assembly Reaction Protocol (New England Biolabs GmbH, Frankfurt/Main, Germany) resulting in receptors that are N-terminally fused to the membrane signal peptide (SP) of the murine 5-HT$_{3A}$ receptor and tagged with a codon-optimized FLAG tag. The quality of the vectors was controlled by sequencing (Eurofins Genomics GmbH, Ebersberg, Germany).

2.3.4   Generation of stable transfectants

For the generation of a cell line stably expressing the human D_{2long} or the human D_3 receptor, the previously described[40] HEK293T CRE Luc cell line stably expressing a CRE controlled luciferase was used. For generating the cell line stably expressing the human $D_{4.4}$R, HEK293T wild-type cells were used. Cells were seeded in a 6-well plate (Sarstedt, Nümbrecht, Germany) one day prior to transfection with 2 µg of cDNA. The transfection was performed using the reagent XtremeGene HP (Roche Diagnostics, Mannheim, Germany) according to the manufacturer's protocol. After incubation of the cells with the cDNA at 37 °C for 48 h, cells were detached with trypsin/EDTA and transferred to 15-cm cell culture dishes (Sarstedt, Nümbrecht, Germany). Selection was achieved by the addition of 1 mg/mL G418. After stable growth had been observed, the concentration of G418 was reduced to 600 µg/mL. Subsequently, a clonal selection was performed for every cell line aiming at the isolation of a clone with high receptor expression. For this purpose, the stably transfected cells were seeded in a 15-cm dish at a density of 1000–2000 cells/dish. After 2 weeks, single clones were picked and screened by radioligand binding for the highest S/B ratios as described in section 2.2.1.

2.3.5   Preparation of cell homogenates

Homogenates were prepared as previously described[46] with minor modifications. HEK293T CRE Luc cells stably expressing the D_{2long}R or the D_3R or HEK293T cells stably expressing the $D_{4.4}$R were grown in 15-cm dishes (Sarstedt) to 80-90% confluency. Cells were rinsed with ice-cold PBS (137 mM NaCl, 2.7 mM KCl, 10 mM Na_2HPO_4, 1.8 mM KH_2PO_4; pH 7.4), then covered with harvest buffer (10 mM Tris-HCl, 0.5 mM EDTA, 5.5 mM KCl, 140 mM NaCl; pH 7.4) supplemented with protease inhibitors (SigmaFAST, Cocktail Tablets, EDTA-free, Sigma-Aldrich, Deisenhofen, Germany), followed by detachment from the dishes using a cell scraper. After centrifugation (500 g, 5 min), the D_{2long}R expressing cells were resuspended in homogenate buffer (50 mM Tris-HCl, 5 mM EDTA, 1.5 mM $CaCl_2$, 5 mM $MgCl_2$, 5 mM KCl, 120 mM NaCl; pH 7.4), whereas the D_3R or $D_{4.4}$R expressing cells were resuspended in Tris-$MgSO_4$ buffer (10 mM Tris-HCl, 5 mM $MgSO_4$; pH 7.4). All cell suspensions were stored at −80 °C. After thawing, the cells were resuspended in homogenate buffer or Tris-$MgSO_4$ buffer and homogenized under ice-cooling using an Ultraturrax (IKA-Werke, Germany) (5 times for 5 s). The homogenates were centrifuged (6 °C, 50,000 g, 15 min), the pellet was resuspended in binding buffer (50 mM Tris-HCl, 1 mM EDTA, 5 mM $MgCl_2$, 100 µg/mL bacitracin; pH 7.4) and homogenized using a syringe and needle (i.d. = 0.4 mm). The homogenates were stored as small aliquots at −80 °C. Protein concentrations were determined with the Bio-Rad protein assay according to the manufacturer's protocol (Bio-Rad Laboratories, Munich, Germany).

2.3.6 Radioligand binding assays

All radioligand binding experiments were performed at $22 \pm 1\,°C$. For whole cell binding assays, HEK293T CRE Luc $D_{2long}R$, HEK293T CRE Luc D_3R or HEK293T $D_{4.4}R$ cells were grown in a 75-cm² flask to a confluency of approximately 80%. On the day of the experiment, the cells were detached with trypsin/EDTA and suspended in Leibovitz' L-15 medium supplemented with 10% FCS, followed by centrifugation ($22 \pm 1\,°C$, 700 g, 5 min). The supernatant was discarded and cells were resuspended in L-15 containing 100 µg/mL bacitracin to a density of 100,000 cells/mL. The assay was carried out in a final volume of 200 µL in 96-well round-bottom polypropylene plates. All compounds were added as 10-fold concentrated solutions (20 µL per well). The radioligand [³H]N-methylspiperone (specific activity: 77 Ci/mmol, Novandi Chemistry AB, Södertälje, Sweden) was used in saturation and competition binding assays as well as for single clone screening of the cells transfected with the $D_{4.4}R$ as described in section 2.2.1. For single clone screening of the cells transfected with the $D_{2long}R$ or the D_3R, [³H]spiperone (specific activity: 79 Ci/mmol, Biotrend Chemicals, Cologne, Germany) was used. In saturation binding experiments with cells expressing the $D_{2long}R$ or D_3R, the radioligand was applied in concentrations ranging from 0.025 nM to 3 nM, in assays with cells expressing the $D_{4.4}R$, the radioligand was used in concentrations ranging from 0.03 nM to 3 nM. Non-specific binding was determined in the presence of (+)-butaclamol (2000-fold, $D_{2long}R$, D_3R) or nemonapride (2000-fold, $D_{4.4}R$). The incubation period was 60 min ($D_{2long}R$, D_3R) or 150 min ($D_{4.4}R$). After incubation, bound radioligand was separated from free radioligand by filtration through poly(ethyleneimine)-pretreated (0.3% in water, w/v) GF/C filters (Whatman) using a 96-well Brandel harvester (Brandel Inc., Unterföhring, Germany). After three washing steps with cold PBS, filter pieces were punched out and transferred to (flexible) 1450-401 96-well sample plates (PerkinElmer, Rodgau, Germany). Scintillation cocktail (Rotiszint eco plus, Carl Roth, Karlsruhe, Germany) (200 µL) was added, followed by an incubation period for at least 4 h and measurement of the radioactivity using a MicroBeta2 plate counter (PerkinElmer, Waltham, MA, USA). Competition binding experiments with whole cells were carried out in analogy to saturation binding experiments. For experiments with the $D_{2long}R$ and the D_3R, [³H]N-methylspiperone was applied in a final concentration of 0.25 nM, whereas in experiments with the $D_{4.4}R$ the final concentration of the radioligand was 0.3 nM. Non-specific binding was determined in the presence of 2 µM (+)-butaclamol ($D_{2long}R$, D_3R) or 2 µM nemonapride ($D_{4.4}R$).

Radioligand binding experiments with cell homogenates were performed as described for whole cells with the following modifications. Homogenates were resuspended in binding buffer (50 mM Tris-HCl, 1 mM EDTA, 5 mM $MgCl_2$, 100 µg/mL bacitracin, pH = 7.4) to a final concentration of 0.3-0.5 µg ($D_{2long}R$), 0.7 µg (D_3R) or 0.3-0.4 µg ($D_{4.4}R$) protein/well. In saturation binding experiments, [³H]N-methylspiperone was applied in concentrations ranging from 0.002 nM to 1.5 nM ($D_{2long}R$, D_3R) or from 0.008 nM to 2 nM ($D_{4.4}R$). Non-specific binding was determined in the presence of a 2000-fold excess

of (+)-butaclamol ($D_{2long}R$, D_3R) or nemonapride ($D_{4.4}R$). For competition binding experiments, [³H]*N*-methylspiperone was used at a concentration of 0.05 nM ($D_{2long}R$, D_3R) or 0.1 nM ($D_{4.4}R$). Non-specific binding was determined in the presence of 2 µM (+)-butaclamol ($D_{2long}R$, D_3R) or 2 µM nemonapride ($D_{4.4}R$). For kinetic experiments, cell homogenates were prepared as described above. In the case of association experiments, [³H]*N*-methylspiperone was added to the homogenates at different times at a final concentration of 0.02 nM ($D_{2long}R$), 0.03 nM (D_3R) or 0.08 nM ($D_{4.4}R$). Non-specific binding was determined for each incubation time in the presence of (+)-butaclamol ($D_{2long}R$, D_3R) or nemonapride ($D_{4.4}R$) (2000-fold excess to the applied radioligand concentration). During incubation, plates were shaken at 300 rpm (Titramax 101, Heidolph Instruments, Germany). In the case of dissociation experiments, cell homogenates were incubated with the same concentrations of [³H]*N*-methylspiperone as applied in association experiments for 60 min ($D_{2long}R$, D_3R) or 150 min ($D_{4.4}R$) before dissociation was initiated by the addition of a 2000-fold excess of (+)-butaclamol ($D_{2long}R$, D_3R) or nemonapride ($D_{4.4}R$). The dissociation was stopped after different periods of time by separating bound from free radioligand by filtration. Determination of non-specific binding was carried out as described for association experiments.

2.3.7   Data analysis

For the analysis of saturation binding experiments, specific binding data (dpm) were plotted against the free radioligand concentration (nM) and analysed by a two-parameter fit describing hyperbolic binding to obtain K_d and B_{max} values. K_d values from single experiments were transformed to pK_d values, from which mean values were calculated. Free radioligand concentrations were calculated by conversion of totally bound radioactivity (dpm) to the concentration of totally bound radioligand (mol/L) (based on the specific activity of [³H]*N*-methylspiperone and the assay volume) and subsequent subtraction from the initially applied, total radioligand concentration. Non-specific binding was fitted by linear regression.

For radioligand competition binding experiments, specific binding data (non-specific binding subtracted from total binding) were normalized (100% = specifically bound radioligand in the absence of competitor) and plotted as % over log(concentration of competitor) followed by analysis using a four-parameter logistic equation (log(inhibitor) vs. response - variable slope, GraphPad Prism 9.0) to obtain IC_{50} and pIC_{50} values for each individual experiment. The pIC_{50} values were converted to pK_i values by applying the Cheng-Prusoff equation[50]. From the individual pK_i values, mean values were calculated. In the case of the competition binding experiments with agonists, data were analysed by a three-parameter fit (One site – fit $logIC_{50}$, slope constrained to unity) or a five-parameter fit (Two sites – fit $logIC_{50}$, slopes constrained to unity) provided by GraphPad Prism 9.0. Comparison of both fits was performed with the "extra sum-of-squares F-test" (GaphPad Prism 9.0), accounting for the differences

in degrees of freedom. P-values < 0.05 were considered to indicate statistical significance and the "two sites – fit logIC$_{50}$" model (alternative hypothesis) was favoured over the one-site model (null hypothesis). IC$_{50}$ values of the high and low affinity states were processed as described above.

Specific binding data (dpm) from association experiments were fitted by a one-phase association equation to obtain k_{obs} (observed association rate constant) and $B_{(eq)}$ (maximum of specifically bound radioligand). The latter was used for calculating specifically bound radioligand $B_{(t)}$ in %, which was plotted over time. Specific binding data (dpm) from dissociation experiments were fitted by a three-parameter one-phase decay equation, yielding k_{off}. The association rate constant k_{on} was calculated using the following equation: $k_{on} = (k_{obs} - k_{off})/[\text{ligand}]$. The dissociation half-life t$_{1/2}$ was calculated according to: t$_{1/2}$ = ln(2)/k_{off}. Kinetic dissociation constants $K_{d(kin)}$ were calculated according to: $K_{d(kin)} = k_{off}/k_{on}$. Analyses were performed using GraphPad Prism 9.0 (La Jolla, CA, USA).

Propagated errors were calculated according to the general equation (maximum error propagation):

$$\Delta z = \left| \frac{\partial f}{\partial x_1} \right| \Delta x_1 + \left| \frac{\partial f}{\partial x_2} \right| \Delta x_2 + \ldots$$

f: function of x_1, x_2, etc. (f(x_1, x_2, …) = z); Δx_1, Δx_2: error (in this work represented by the SEM) of x_1 and x_2; Δz: (propagated) error of z

2.4   Summary and conclusions

Radioligand binding assays for the family of D_2-like receptors were established for the determination of $D_{2long}R$, D_3R and $D_{4.4}R$ affinities of (potential) DR ligands, not least required for the evaluation of the specificity of ligands of other GPCR families. Stably transfected cell lines showing a sufficiently high expression of the $D_{2long}R$, D_3R or $D_{4.4}R$ were generated. Taking ligand depletion into account (use of low receptor concentrations, analysis of saturation binding data based on the free radioligand concentration), affinity measures (pK_d, pK_i) could be reliably determined for the dopamine D_2-like receptor antagonists [³H]N-methylspiperone and haloperidol using both whole cells or cell homogenates. However, this study revealed that cell homogenates should be used when investigating (partial) agonists, since the use of cell homogenates, containing low amounts of GTP, enables the detection of the high-affinity binding component. The high-affinity state of the dopamine D_2-like receptors has been repeatedly referred to as the functional state: the concentrations of dopamine receptor agonists that are able to suppress prolactin release in the anterior pituitary were found to correlate with the inhibition constants determined for the high affinity state[64]. Additionally, it was reported that therapeutically effective concentrations of drugs used for the treatment of Parkinson's disease also correlate with their affinities for the high affinity state of the D_2 receptor[65]. Consequently, for screening newly synthesized DR ligands whose mode of action is unknown, binding studies should be performed using cell homogenates. The established assays were used to confirm the assumption that carbamoylguanidine-type H_2 receptor ligands carrying an amino(methyl)thiazole residue exhibit considerable affinity to D_2-like receptors. Furthermore, it was shown that H_2 receptor ligands containing other heterocycles such as an aminothiadiazole or a triazole moiety displayed only very low affinity to D_2-like receptors. Using the endogenous DR agonist dopamine, it was possible to detect two affinity states of the $D_{2long}R$, the D_3R and the $D_{4.4}R$. Experiments with the non-hydrolysable GTP analogue Gpp(NH)p (anticipated to promote the low affinity state) led in part to ambiguous results regarding quinpirole binding to the D_3R and the $D_{4.4}R$. It should be mentioned, in this respect, that the discrimination between the high and the low affinity binding components for the D_2 receptor was also not always obvious when [³H]spiperone (structurally closely related to [³H]N-methylspiperone) was used as radioligand, due to its hydrophobic nature[66]. With a different radioligand, such as [³H]domperidone, as suggested by Durdagi et al.[66], a clearer distinction between the different affinity states might have been achieved.

2.5   References

1.   R. J. Lefkowitz, Historical review: a brief history and personal retrospective of seven-transmembrane receptors. *Trends Pharmacol Sci* **25**, 413-422; doi:10.1016/j.tips.2004.06.006 (2004).

2.   S. Lazareno, Quantification of receptor interactions using binding methods. *J Recept Signal Transduct Res* **21**, 139-165; doi:10.1081/RRS-100107426 (2001).

3.   E. C. Hulme, M. A. Trevethick, Ligand binding assays at equilibrium: validation and interpretation. *Br J Pharmacol* **161**, 1219-1237; doi:10.1111/j.1476-5381.2009.00604.x (2010).

4.   J. C. Schwartz, J. Diaz, C. Pilon, P. Sokoloff, Possible implications of the dopamine D(3) receptor in schizophrenia and in antipsychotic drug actions. *Brain Res Brain Res Rev* **31**, 277-287; doi:10.1016/s0165-0173(99)00043-0 (2000).

5.   J. M. Beaulieu, R. R. Gainetdinov, The physiology, signaling, and pharmacology of dopamine receptors. *Pharmacol Rev* **63**, 182-217; doi:10.1124/pr.110.002642 (2011).

6.   I. Creese, R. Schneider, S. H. Snyder, ^{3}H-Spiroperidol labels dopamine receptors in pituitary and brain. *Eur J Pharmacol* **46**, 377-381; doi:10.1016/0014-2999(77)90232-1 (1977).

7.   D. R. Howlett, S. R. Nahorski, A comparative study of [^{3}H]haloperidol and [^{3}H]spiroperidol binding to receptors on rat cerebral membranes. *FEBS Lett* **87**, 152-156; doi:10.1016/0014-5793(78)80155-0 (1978).

8.   N. Fujita, K. Saito, N. Yonehara, H. Yoshida, Lisuride inhibits ^{3}H-spiroperidol binding to membranes isolated from striatum. *Neuropharmacology* **17**, 1089-1091; doi:10.1016/0028-3908(78)90047-3 (1978).

9.   R. A. Lyon, M. Titeler, J. J. Frost, P. J. Whitehouse, D. F. Wong, H. N. Wagner, Jr., R. F. Dannals, J. M. Links, M. J. Kuhar, ^{3}H-3-N-methylspiperone labels D_2 dopamine receptors in basal ganglia and S_2 serotonin receptors in cerebral cortex. *J Neurosci* **6**, 2941-2949; doi:10.1523/JNEUROSCI.06-10-02941.1986 (1986).

10.   M. P. Martres, M. Baudry, J. C. Schwartz, Characterization of ^{3}H-domperidone binding on striatal dopamine receptors. *Life Sci* **23**, 1781-1784; doi:10.1016/0024-3205(78)90108-x (1978).

11.   K. Y. Araki, J. R. Sims, P. G. Bhide, Dopamine receptor mRNA and protein expression in the mouse corpus striatum and cerebral cortex during pre- and postnatal development. *Brain Res* **1156**, 31-45; doi:10.1016/j.brainres.2007.04.043 (2007).

12.   A. J. Sleight, N. J. Stam, V. Mutel, P. M. Vanderheyden, Radiolabelling of the human 5-HT$_{2A}$ receptor with an agonist, a partial agonist and an antagonist: effects on apparent agonist affinities. *Biochem Pharmacol* **51**, 71-76; doi:10.1016/0006-2952(95)02122-1 (1996).

13.   D. Moller, R. C. Kling, M. Skultety, K. Leuner, H. Hubner, P. Gmeiner, Functionally selective dopamine D(2), D(3) receptor partial agonists. *J Med Chem* **57**, 4861-4875; doi:10.1021/jm5004039 (2014).

14.   P. Sokoloff, M. Andrieux, R. Besancon, C. Pilon, M. P. Martres, B. Giros, J. C. Schwartz, Pharmacology of human dopamine D_3 receptor expressed in a mammalian cell line: comparison with D_2 receptor. *Eur J Pharmacol* **225**, 331-337; doi:10.1016/0922-4106(92)90107-7 (1992).

15.   D. Levesque, J. Diaz, C. Pilon, M. P. Martres, B. Giros, E. Souil, D. Schott, J. L. Morgat, J. C. Schwartz, P. Sokoloff, Identification, characterization, and localization of the dopamine D_3 receptor in rat brain using 7-[^{3}H]hydroxy-N,N-di-n-propyl-2-aminotetralin. *Proc Natl Acad Sci USA* **89**, 8155-8159; doi:10.1073/pnas.89.17.8155 (1992).

16.   P. Seeman, T. Tallerico, F. Ko, Dopamine displaces [^{3}H]domperidone from high-affinity sites of the dopamine D_2 receptor, but not [^{3}H]raclopride or [^{3}H]spiperone in isotonic medium: Implications for human positron emission tomography. *Synapse* **49**, 209-215; doi:10.1002/syn.10232 (2003).

17. J. Mierau, F. J. Schneider, H. A. Ensinger, C. L. Chio, M. E. Lajiness, R. M. Huff, Pramipexole binding and activation of cloned and expressed dopamine D$_2$, D$_3$ and D$_4$ receptors. *Eur J Pharmacol* **290**, 29-36 (1995).

18. J. A. Schetz, P. S. Benjamin, D. R. Sibley, Nonconserved residues in the second transmembrane-spanning domain of the D(4) dopamine receptor are molecular determinants of D(4)-selective pharmacology. *Mol Pharmacol* **57**, 144-152 (2000).

19. M. Skinbjerg, Y. Namkung, C. Halldin, R. B. Innis, D. R. Sibley, Pharmacological characterization of 2-methoxy-N-propylnorapomorphine's interactions with D$_2$ and D$_3$ dopamine receptors. *Synapse* **63**, 462-475; doi:10.1002/syn.20626 (2009).

20. P. Seeman, H. C. Guan, Glutamate agonists for treating schizophrenia have affinity for dopamine D$_2$High and D$_3$ receptors. *Synapse* **63**, 705-709; doi:10.1002/syn.20673 (2009).

21. A. M. Gonzalez, D. R. Sibley, [³H]7-OH-DPAT is capable of labeling dopamine D$_2$ as well as D$_3$ receptors. *Eur J Pharmacol* **272**, R1-3 (1995).

22. J. F. Vanhauwe, N. Fraeyman, B. J. Francken, W. H. Luyten, J. E. Leysen, Comparison of the ligand binding and signaling properties of human dopamine D(2) and D(3) receptors in Chinese hamster ovary cells. *J Pharmacol Exp Ther* **290**, 908-916 (1999).

23. J. M. Vile, U. M. D'Souza, P. G. Strange, [³H]nemonapride and [³H]spiperone label equivalent numbers of D$_2$ and D$_3$ dopamine receptors in a range of tissues and under different conditions. *J Neurochem* **64**, 940-943; doi:10.1046/j.1471-4159.1995.64020940.x (1995).

24. K. Hidaka, M. Matsumoto, S. Tada, Y. Tasaki, T. Yamaguchi, Differential effects of [³H]nemonapride and [³H]spiperone binding on human dopamine D$_4$ receptors. *Neurosci Lett* **186**, 145-148; doi:10.1016/0304-3940(95)11306-h (1995).

25. C. M. Carter, J. R. Leighton-Davies, S. J. Charlton, Miniaturized receptor binding assays: complications arising from ligand depletion. *J Biomol Screen* **12**, 255-266; doi:10.1177/1087057106297788 (2007).

26. P. Seeman, C. Ulpian, K. A. Wreggett, J. W. Wells, Dopamine receptor parameters detected by [³H]spiperone depend on tissue concentration: analysis and examples. *J Neurochem* **43**, 221-235 (1984).

27. K. J. Chang, S. Jacobs, P. Cuatrecasas, Quantitative aspects of hormone-receptor interactions of high affinity. Effect of receptor concentration and measurement of dissociation constants of labeled and unlabeled hormones. *Biochim Biophys Acta* **406**, 294-303; doi:10.1016/0005-2736(75)90011-5 (1975).

28. S. Swillens, Interpretation of binding curves obtained with high receptor concentrations: practical aid for computer analysis. *Mol Pharmacol* **47**, 1197-1203 (1995).

29. D. R. Sibley, A. De Lean, I. Creese, Anterior pituitary dopamine receptors. Demonstration of interconvertible high and low affinity states of the D$_2$ dopamine receptor. *J Biol Chem* **257**, 6351-6361; doi:10.1016/S0021-9258(20)65148-1 (1982).

30. N. J. Birdsall, A. S. Burgen, E. C. Hulme, The binding of agonists to brain muscarinic receptors. *Mol Pharmacol* **14**, 723-736 (1978).

31. R. S. Kent, A. De Lean, R. J. Lefkowitz, A quantitative analysis of beta-adrenergic receptor interactions: resolution of high and low affinity states of the receptor by computer modeling of ligand binding data. *Mol Pharmacol* **17**, 14-23 (1980).

32. R. Leurs, M. J. Smit, W. M. Menge, H. Timmerman, Pharmacological characterization of the human histamine H$_2$ receptor stably expressed in Chinese hamster ovary cells. *Br J Pharmacol* **112**, 847-854; doi:10.1111/j.1476-5381.1994.tb13157.x (1994).

33. A. De Lean, J. M. Stadel, R. J. Lefkowitz, A ternary complex model explains the agonist-specific binding properties of the adenylate cyclase-coupled beta-adrenergic receptor. *J Biol Chem* **255**, 7108-7117 (1980).

34. M. Skinbjerg, D. R. Sibley, J. A. Javitch, A. Abi-Dargham, Imaging the high-affinity state of the dopamine D_2 receptor in vivo: fact or fiction? *Biochem Pharmacol* **83**, 193-198; doi:10.1016/j.bcp.2011.09.008 (2012).

35. T. P. Kenakin, in *A Pharmacology Primer (Fourth Edition),* T. P. Kenakin, Ed. (Academic Press, San Diego, 2014), pp. 63-83.

36. B. Gardner, P. G. Strange, Agonist action at D_2(long) dopamine receptors: ligand binding and functional assays. *Br J Pharmacol* **124**, 978-984; doi:10.1038/sj.bjp.0701926 (1998).

37. A. Kraus, P. Ghorai, T. Birnkammer, D. Schnell, S. Elz, R. Seifert, S. Dove, G. Bernhardt, A. Buschauer, N(G)-acylated aminothiazolylpropylguanidines as potent and selective histamine H(2) receptor agonists. *ChemMedChem* **4**, 232-240; doi:10.1002/cmdc.200800296 (2009).

38. N. Kagermeier, K. Werner, M. Keller, P. Baumeister, G. Bernhardt, R. Seifert, A. Buschauer, Dimeric carbamoylguanidine-type histamine H_2 receptor ligands: A new class of potent and selective agonists. *Bioorg Med Chem* **23**, 3957-3969; doi:10.1016/j.bmc.2015.01.012 (2015).

39. M. Johnson, T. Antonio, M. E. Reith, A. K. Dutta, Structure-activity relationship study of N(6)-(2-(4-(1H-Indol-5-yl)piperazin-1-yl)ethyl)-N(6)-propyl-4,5,6,7-tetrahydrobenzo[d]thiazole-2,6-diamine analogues: development of highly selective D_3 dopamine receptor agonists along with a highly potent D_2/D_3 agonist and their pharmacological characterization. *J Med Chem* **55**, 5826-5840; doi:10.1021/jm300268s (2012).

40. U. Nordemann, D. Wifling, D. Schnell, G. Bernhardt, H. Stark, R. Seifert, A. Buschauer, Luciferase reporter gene assay on human, murine and rat histamine H_4 receptor orthologs: correlations and discrepancies between distal and proximal readouts. *PLoS One* **8**, e73961; doi:10.1371/journal.pone.0073961 (2013).

41. L. J. Zhang, J. E. Lachowicz, D. R. Sibley, The D_{2S} and D_{2L} dopamine receptor isoforms are differentially regulated in Chinese hamster ovary cells. *Mol Pharmacol* **45**, 878-889 (1994).

42. N. Schmieg, C. Rocchi, S. Romeo, R. Maggio, M. J. Millan, C. Mannoury la Cour, Dysbindin-1 modifies signaling and cellular localization of recombinant, human D(3) and D(2) receptors. *J Neurochem* **136**, 1037-1051; doi:10.1111/jnc.13501 (2016).

43. S. Wang, D. Wacker, A. Levit, T. Che, R. M. Betz, J. D. McCorvy, A. J. Venkatakrishnan, X. P. Huang, R. O. Dror, B. K. Shoichet, B. L. Roth, D_4 dopamine receptor high-resolution structures enable the discovery of selective agonists. *Science* **358**, 381-386; doi:10.1126/science.aan5468 (2017).

44. C. Klein Herenbrink, D. A. Sykes, P. Donthamsetti, M. Canals, T. Coudrat, J. Shonberg, P. J. Scammells, B. Capuano, P. M. Sexton, S. J. Charlton, J. A. Javitch, A. Christopoulos, J. R. Lane, The role of kinetic context in apparent biased agonism at GPCRs. *Nat Commun* **7**, 10842; doi:10.1038/ncomms10842 (2016).

45. A. Newman-Tancredi, D. Cussac, V. Audinot, J. P. Nicolas, F. De Ceuninck, J. A. Boutin, M. J. Millan, Differential actions of antiparkinson agents at multiple classes of monoaminergic receptor. II. Agonist and antagonist properties at subtypes of dopamine D(2)-like receptor and alpha(1)/alpha(2)-adrenoceptor. *J Pharmacol Exp Ther* **303**, 805-814; doi:10.1124/jpet.102.039875 (2002).

46. H. Hübner, C. Haubmann, W. Utz, P. Gmeiner, Conjugated Enynes as Nonaromatic Catechol Bioisosteres: Synthesis, Binding Experiments, and Computational Studies of Novel Dopamine Receptor Agonists Recognizing Preferentially the D_3 Subtype. *J Med Chem* **43**, 756-762; doi:10.1021/jm991098z (2000).

47. P. Sokoloff, B. Giros, M.-P. Martres, M.-L. Bouthenet, J.-C. Schwartz, Molecular cloning and characterization of a novel dopamine receptor (D_3) as a target for neuroleptics. *Nature* **347**, 146-151; doi:10.1038/347146a0 (1990).

48. H. H. Van Tol, J. R. Bunzow, H. C. Guan, R. K. Sunahara, P. Seeman, H. B. Niznik, O. Civelli, Cloning of the gene for a human dopamine D_4 receptor with high affinity for the antipsychotic clozapine. *Nature* **350**, 610-614; doi:10.1038/350610a0 (1991).

49. S. W. Castro, P. G. Strange, Differences in the ligand binding properties of the short and long versions of the D_2 dopamine receptor. *J Neurochem* **60**, 372-375 (1993).

50. Y. Cheng, W. H. Prusoff, Relationship between the inhibition constant (K1) and the concentration of inhibitor which causes 50 per cent inhibition (I50) of an enzymatic reaction. *Biochem Pharmacol* **22**, 3099-3108; doi:10.1016/0006-2952(73)90196-2 (1973).

51. Y. Tadori, R. A. Forbes, R. D. McQuade, T. Kikuchi, Functional potencies of dopamine agonists and antagonists at human dopamine D(2) and D(3) receptors. *Eur J Pharmacol* **666**, 43-52; doi:10.1016/j.ejphar.2011.05.050 (2011).

52. M. Wood, C. Reavill, Aripiprazole acts as a selective dopamine D$_2$ receptor partial agonist. *Exp Opin Investig Drugs* **16**, 771-775; doi:10.1517/13543784.16.6.771 (2007).

53. C. P. Lawler, C. Prioleau, M. M. Lewis, C. Mak, D. Jiang, J. A. Schetz, A. M. Gonzalez, D. R. Sibley, R. B. Mailman, Interactions of the novel antipsychotic aripiprazole (OPC-14597) with dopamine and serotonin receptor subtypes. *Neuropsychopharmacology* **20**, 612-627; doi:10.1016/S0893-133X(98)00099-2 (1999).

54. R. G. MacKenzie, D. VanLeeuwen, T. A. Pugsley, Y. H. Shih, S. Demattos, L. Tang, R. D. Todd, K. L. O'Malley, Characterization of the human dopamine D$_3$ receptor expressed in transfected cell lines. *Eur J Pharmacol* **266**, 79-85; doi:10.1016/0922-4106(94)90212-7 (1994).

55. S. Patel, S. Patel, R. Marwood, F. Emms, D. Marston, P. D. Leeson, N. R. Curtis, J. J. Kulagowski, S. B. Freedman, Identification and pharmacological characterization of [^{125}I]L-750,667, a novel radioligand for the dopamine D$_4$ receptor. *Mol Pharmacol* **50**, 1658-1664 (1996).

56. S. B. Freedman, S. Patel, R. Marwood, F. Emms, G. R. Seabrook, M. R. Knowles, G. McAllister, Expression and pharmacological characterization of the human D$_3$ dopamine receptor. *J Pharmacol Exp Ther* **268**, 417-426 (1994).

57. P. Seeman, H. C. Guan, H. H. Van Tol, H. B. Niznik, Low density of dopamine D$_4$ receptors in Parkinson's, schizophrenia, and control brain striata. *Synapse* **14**, 247-253; doi:10.1002/syn.890140402 (1993).

58. L. Tang, R. D. Todd, A. Heller, K. L. O'Malley, Pharmacological and functional characterization of D$_2$, D$_3$ and D$_4$ dopamine receptors in fibroblast and dopaminergic cell lines. *J Pharmacol Exp Ther* **268**, 495-502 (1994).

59. M. J. Millan, L. Maiofiss, D. Cussac, V. Audinot, J. A. Boutin, A. Newman-Tancredi, Differential actions of antiparkinson agents at multiple classes of monoaminergic receptor. I. A multivariate analysis of the binding profiles of 14 drugs at 21 native and cloned human receptor subtypes. *J Pharmacol Exp Ther* **303**, 791-804; doi:10.1124/jpet.102.039867 (2002).

60. F. Sautel, N. Griffon, D. Levesque, C. Pilon, J. C. Schwartz, P. Sokoloff, A functional test identifies dopamine agonists selective for D$_3$ versus D$_2$ receptors. *Neuroreport* **6**, 329-332; doi:10.1097/00001756-199501000-00026 (1995).

61. S. Biselli, M. Bresinsky, K. Tropmann, L. Forster, C. Honisch, A. Buschauer, G. Bernhardt, S. Pockes, Pharmacological characterization of a new series of carbamoylguanidines reveals potent agonism at the H$_2$R and D$_3$R. *Eur J Med Chem* **214**, 113190; doi:10.1016/j.ejmech.2021.113190 (2021).

62. K. Tropmann, M. Bresinsky, L. Forster, D. Mönnich, A. Buschauer, H.-J. Wittmann, H. Hübner, P. Gmeiner, S. Pockes, A. Strasser, Abolishing Dopamine D$_{2long}$/D$_3$ Receptor Affinity of Subtype-Selective Carbamoylguanidine-Type Histamine H$_2$ Receptor Agonists. *J Med Chem*; doi:10.1021/acs.jmedchem.1c00692 (2021).

63. E. Bartole, L. Gratz, T. Littmann, D. Wifling, U. Seibel, A. Buschauer, G. Bernhardt, UR-DEBa242: A Py-5-Labeled Fluorescent Multipurpose Probe for Investigations on the Histamine H$_3$ and H$_4$ Receptors. *J Med Chem* **63**, 5297-5311; doi:10.1021/acs.jmedchem.0c00160 (2020).

64. S. R. George, M. Watanabe, T. Di Paolo, P. Falardeau, F. Labrie, P. Seeman, The functional state of the dopamine receptor in the anterior pituitary is in the high affinity form. *Endocrinology* **117**, 690-697; doi:10.1210/endo-117-2-690 (1985).

65. P. Seeman, Antiparkinson therapeutic potencies correlate with their affinities at dopamine D$_2$(High) receptors. *Synapse* **61**, 1013-1018; doi:10.1002/syn.20453 (2007).

66. S. Durdagi, R. E. Salmas, M. Stein, M. Yurtsever, P. Seeman, Binding Interactions of Dopamine and Apomorphine in D_2High and D_2Low States of Human Dopamine D_2 Receptor Using Computational and Experimental Techniques. *ACS Chem Neurosci* **7**, 185-195; doi:10.1021/acschemneuro.5b00271 (2016).

Chapter 3

A split luciferase complementation assay for the quantification of β-arrestin2 recruitment to dopamine D_2-like receptors

Prior to the submission of this thesis, parts of this chapter were published in cooperation with partners:

L. Forster, L. Grätz, D. Mönnich, G. Bernhardt, S. Pockes, A Split Luciferase Complementation Assay for the Quantification of beta-Arrestin2 Recruitment to Dopamine D_2-Like Receptors. *International journal of molecular sciences* **21**, doi:10.3390/ijms21176103 (2020).

Author contributions: Conceptualization, L.F., S.P. and G.B.; methodology, L.F. and L.G.; formal analysis, L.F. and D.M.; investigation, L.F. and D.M.; resources, S.P. and G.B.; data curation, L.F.; writing—original draft preparation, L.F. and S.P.; writing—review and editing, L.F., S.P., D.M., G.B. and L.G.; visualization, L.F. and S.P.; supervision, S.P. and G.B.; project administration, L.F., S.P. and G.B.

3.1 Introduction

The neurotransmitter dopamine exerts its effects via five dopamine receptor (DR) subtypes (D_1, D_2, D_3, D_4 and D_5), all being members of the superfamily of G-protein-coupled receptors (GPCRs)[1-5]. Within the family of dopamine receptors, there is a classification into D_1-like receptors (D_1 and D_5) and D_2-like receptors (D_2, D_3 and D_4) according to their preferred G-protein signaling[6]. While D_1-like receptors predominantly couple to $G\alpha_{s/olf}$ proteins and stimulate the adenylyl cyclase (AC), thereby increasing the intracellular cAMP level[7], D_2-like receptors are associated with coupling to $G\alpha_{i/o}$ proteins and inhibiting the formation of cAMP[8-10]. Dopamine receptors are targeted by a variety of pharmacological agents since anomalous dopamine receptor signaling is implicated in numerous neuropsychiatric disorders in the human body such as schizophrenia[11], Parkinson's disease[12,13], drug addiction[14,15], genetic hypertension[16], bipolar disorder[17,18] and restless legs syndrome[19,20].

Apart from G-protein-mediated signaling, many GPCRs are known to recruit β-arrestin, which is involved in receptor desensitization, internalization processes and also in signaling (β-arrestin-dependent signaling)[21-23]. It is generally accepted that phosphorylation of GPCRs by G-protein receptor kinases (GRKs) or protein kinase C (PKC) at specific clusters of serine and threonine residues located in the receptor C-terminus precedes β-arrestin binding[21,24-26]. However, β-arrestin recruitment to agonist-activated non-phosphorylated receptors has also been described, but with lower affinity[21]. Furthermore, β-arrestins also participate in receptor sequestration and play a role in desensitization and subsequent resensitization of GPCR responsiveness[22]. The most abundantly expressed arrestins in mammals are β-arrestin1 and β-arrestin2[27]. Based on their binding preference towards β-arrestins and their behavior during the internalization, GPCRs can be subdivided in two major classes (class A and B)[28]. A precise classification of the respective dopamine receptors according to this model is very difficult due to the complexity of available data[29,30]. However, in terms of D_2-like receptors, the D_2R

and the D$_3$R are frequently described to be phosphorylated by GRKs, resulting in the recruitment of β-arrestins[31-34], while no recruitment is described for the D$_4$R[35,36]. The D$_2$ and D$_3$ receptors share a high sequence homology[37] but are regulated differently and show different levels of basal phosphorylation[33,34,38].

In current drug development of antipsychotics, the need for biased ligands to reduce adverse drug effects is the subject of lively debate. A study by Masri et al. led to the assumption that functionally selective D$_2$ receptor antagonists, specifically preventing β-arrestin2 recruitment may lead to new antipsychotics with reduced extrapyramidal side effects, while retaining their therapeutic benefit[39]. Therefore, the functional characterization of potential future drug candidates, with respect to β-arrestin2 recruitment, is of high relevance particularly in the very early stage of in vitro testing. Different assay techniques have been described for investigating β-arrestin2 recruitment in live cells. Commercially available split reporter assays currently used for high throughput screening do not give temporal information about the receptor/β-arrestin interaction, since they require cell lysis[40] or real-time measurements are hampered by relatively long maturation times of the reporter protein (Venus, a variant of yellow fluorescent protein)[41]. A β-arrestin recruitment assay utilizing a transcription factor is the TANGO assay. Here, β-arrestin is fused to a protease, while a transcription factor, which is able to induce transcription of β-lactamase, is C-terminally attached to the receptor via a linker containing the respective protease cleavage sequence. Once β-arrestin is recruited, the transcription factor is cleaved off, translocated into the nucleus and β-lactamase is expressed. For detection, a substrate is added and the cells need to by lysed[42]. Another approach for the quantification of β-arrestin recruitment to GPCRs is the LinkLight assay using a permuted luciferase reporter[43]. Here, the GPCR of interest is fused to a viral protease and β-arrestin is fused to a permuted firefly luciferase containing a protease cleavage sequence. After arrestin recruitment, the permuted luciferase is cleaved and reconstituted to an active enzyme[43]. In transcription-based assays, the obtained signal is prone to amplification and no kinetic information can be gained from this experimental setup. There are optimized luciferases available now, that show a higher luminescence output and pH independence of the spectra[44]. We aimed to develop a β-arrestin recruitment assay that overcomes the aforementioned limitations. For this purpose, the split Emerald luciferase complementation technique, first described by Misawa et al.[45], seemed to be appropriate. The employed Emerald luciferase (ELuc) was cleaved into two fragments. The N-terminal part was fused to β-arrestin2 (referred to as ELucN-βarr2) and the C-terminal part to the respective receptor (**Figure 3.1**).
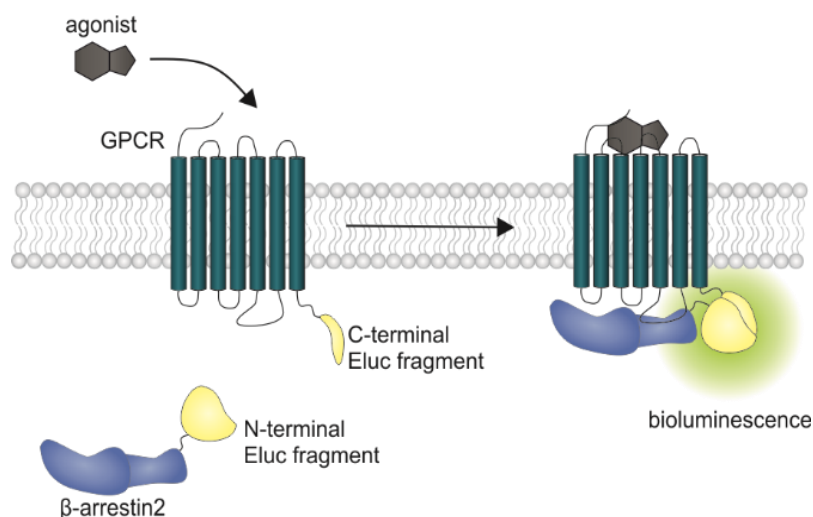
Figure 3.1. Schematic illustration of the split luciferase β-arrestin2 recruitment assay. Upon agonist stimulation of the receptor, β-arrestin2 is recruited and the luciferase fragments come into close proximity to form a functional enzyme, which catalyzes the oxidation of D-luciferin to oxyluciferin, accompanied by the emission of light (λ_{max} = 535 nm).

The ability to perform measurements in living cells allows to retrieve kinetic information about protein-protein interactions[40,46]. Additionally, the utilized ELuc results in improved sensitivity of the test system, as the signal brightness is increased compared to commercially available test kits[45]. Moreover, this homogeneous assay can be conducted very rapidly without the necessity for any washing or separation step, facilitating the development of high-throughput screening campaigns[45]. To investigate the interaction of β-arrestin with the D_2-like receptors upon agonist stimulation, a β-arrestin recruitment assay, based on the split luciferase complementation technique, was established. The complementary fragments of the Emerald luciferase were fused to the N-terminal end of β-arrestin2 and the C-terminus of the $D_{2long}R$, the D_3R or the $D_{4.4}R$. A possible impact of this modification of the receptors on the affinity of selected reference ligands was investigated and various described dopamine receptor ligands were pharmacologically characterized using the developed β-arrestin2 recruitment assays. Additionally, the influence of GRK2, GRK3 and PKC on the recruitment of β-arrestin2 was studied.

3.2 Results and discussion

3.2.1 Characterization of the receptor fusion proteins

To verify the membrane expression of the receptor-luciferase fusion constructs and to investigate a potential influence of the receptor modification on ligand affinities, radioligand saturation binding experiments were performed with the radiolabeled antagonist [^{3}H]N-methylspiperone at all three generated receptor constructs. Saturable binding (see Appendix **Figure A2**) was found for all of them and the pK_d values of 10.30 (D_{2long}R-ELucC), 10.21 (D_3R-ELucC) and 9.37 ($D_{4.4}$R-ELucC) at the respective receptor fusion protein were in good agreement with pK_d values determined at receptors devoid of the luciferase fragment (subsequently referred to as wild-type, *cf*. Methods) (**Table 3.1** and Appendix **Figure A2**). This shows that the fusion of the luciferase fragment to the respective receptor did not markedly impair the affinity to the ligand. Expression of the D_{2long}R-ELucC, the D_3R-ELucC and the ELucN-βarr2 fusion constructs was additionally confirmed by western blot analysis (*cf*. Appendix **Figure A3**).

Table 3.1. Dissociation constants (pK_d values) of [^{3}H]N-methylspiperone determined in radioligand saturation binding experiments at receptors fused to the C-terminal fragment of the Emerald luciferase using whole cells and at wild-type (wt) receptors using homogenates.

	D_{2long}R		D_3R		$D_{4.4}$R	
	ELucC fusion protein	wt	ELucC fusion protein	wt	ELucC fusion protein	wt
pK_d	10.30 ± 0.04	10.52 ± 0.07	10.21 ± 0.05	10.39 ± 0.05	9.37 ± 0.08	10.01 ± 0.06

Data represent means ± SEM determined in three independent experiments, each performed in triplicate.

Results from radioligand displacement experiments at the receptor-ELucC constructs, which were compared with the results obtained at the wild-type receptors (**Table 3.2**), supported the finding that the fusion protein did not markedly affect the receptor affinity to the ligands. At all three investigated dopamine receptor subtypes, the pK_i values of the tested antagonists haloperidol and nemonapride determined at the receptor fusion proteins correspond very well with the affinities determined at wild-type receptors. In case of the agonist quinpirole and the partial agonist aripiprazole, slight discrepancies but no general pattern was identified. With a pK_i of 9.11 compared to 8.08, aripiprazole showed a higher affinity to the D_{2long}R-ELucC fusion protein than to the wild-type receptor (**Table 3.2**). The same observations were made for aripiprazole at the D_3R with a pK_i value of 8.58 at the ELucC construct compared to 8.12 at the wild-type receptor (**Table 3.2**). However, the data for the $D_{4.4}$R-ELucC and the wild-type $D_{4.4}$R were in very good agreement with each other. For quinpirole a biphasic displacement curve was observed at the wild-type D_{2long}R, yielding a high- and a low-affinity inhibition constant (**Table 3.2**), which is in line with published data[47]. By contrast, a monophasic displacement

curve was obtained at the ELucC fusion protein with a pK_i value that was in between the high- and low-affinity inhibition constant determined at the wild-type D$_{2long}$R (**Table 3.2**). At the D$_3$R and the D$_{4.4}$R, only monophasic displacement curves could be fitted. For both receptors, quinpirole showed a higher affinity to the wild-type receptor. It must be noted that binding experiments with the ELucC fusion proteins were carried out using whole cells, whereas in experiments with the wild-type receptors cell homogenates were employed. It is known that the use of whole cells can strongly affect the determination of ligand affinities, especially of agonists[48], hence this could be the reason for the observed differences rather than the fusion of the luciferase fragment to the C-terminus of the receptor.

Table 3.2. Inhibition constants (pK_i) of selected standard ligands determined in radioligand displacement experiments. pK_i values were determined at receptors fused to the C-terminal fragment of the Emerald luciferase using whole cells and at wild-type receptors using homogenates.

cmpd.	D$_{2long}$R ELucC fusion protein		wt	D$_3$R ELucC fusion protein	wt	D$_{4.4}$R ELucC fusion protein	wt
aripiprazole	9.11 ± 0.16		8.08 ± 0.02	8.58 ± 0.15	8.12 ± 0.01	7.60 ± 0.15	7.79 ± 0.08
quinpirole	7.14 ± 0.07	hi	7.66 ± 0.10	7.57 ± 0.05	8.21 ± 0.07	6.55 ± 0.01	7.94 ± 0.08
		lo	5.87 ± 0.02				
haloperidol	9.30 ± 0.05		9.44 ± 0.13	8.92 ± 0.08	8.78 ± 0.04	8.24 ± 0.02	8.95 ± 0.08
nemonapride	9.81 ± 0.13		9.52 ± 0.08	9.76 ± 0.02	9.86 ± 0.06	9.66 ± 0.08	9.53 ± 0.13

Data represent mean pK_i ± SEM determined in three independent experiments, each performed in triplicate.

Aiming at the development of an assay, allowing not only the measurement of reliable potencies and efficacies but also the possibility to conduct live cell measurements as well as kinetic observations of β-arrestin2 recruitment, each transfectant was tested for the feasibility of a real-time experiment. The D$_{2long}$R-ELucC expressing cells showed robust concentration-dependent responses and high signal-to-background (S/B) ratios to stimulation with quinpirole when the substrate D-luciferin was added to live cells (**Figure 3.2**). Unfortunately, no β-arrestin2 recruitment could be observed in live-cell measurements at HEK293T cells expressing the D$_3$R-ELucC. It was previously reported that the D$_3$R recruits β-arrestin2 to a very small extent[33], but by performing lysis-based measurements, we could obtain reliable results with reasonable S/B ratios (**Figure 3.2**). In consistence with published data[35], the cells expressing the D$_{4.4}$R did not show any response to agonistic stimulation in either real-time or lytic endpoint measurements.
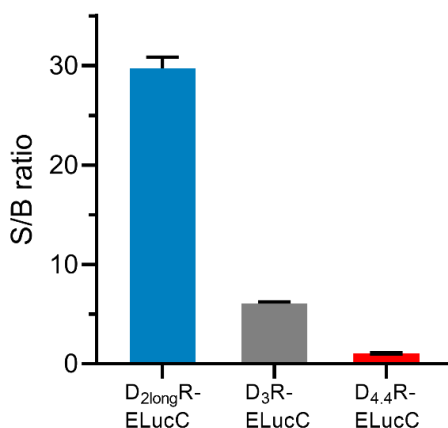
Figure 3.2. S/B ratios of the complemented ELuc after stimulation of the analyzed receptors with the agonist quinpirole. The cells were stimulated with quinpirole at a concentration of 1 µM. In the case of the D$_{2long}$R, live-cell measurements were performed and the resulting area under the curve (AUC) (interval: 0-50 min) was divided by the area obtained from a solvent control to obtain S/B ratios. For D$_3$R and the D$_{4.4}$R studies, S/B ratios of were retrieved by performing lysis-based endpoint measurements (90 min). Data represent means ± SEM from at least three independent experiments performed in triplicate.

3.2.2 Pharmacological characterization of dopamine receptor ligands in the β-arrestin2 split luciferase complementation assay

Standard agonists and antagonists were tested to explore the suitability of the β-arrestin2 split luciferase complementation assay to pharmacologically characterize dopamine receptor ligands of different qualities of action, regarding their potencies (pEC$_{50}$), efficacies (E$_{max}$) or antagonistic activities (pK_b). As agonists, the endogenous ligand dopamine, pramipexole, a widely used drug for the treatment of Parkinson's disease, and the full agonist quinpirole, were chosen. With *R*-(-)-apomorphine and aripiprazole, a "third generation" antipsychotic drug, exhibiting a unique activity profile, two partial agonists were included in the study as well (see **Figure 1.3**, general introduction)[49,50]. For defining the efficacy of each compound at the respective receptor, quinpirole was set as the reference agonist (100%), since it shows a higher chemical stability with respect to oxidation compared to the endogenous ligand dopamine. Dopamine decomposes to a certain extent in aqueous solution over the time-course of several hours, which renders it unsuitable as a reference ligand for assays with longer incubation periods. The stability of dopamine was investigated by a UHPLC method (see Appendix **Figure A4**).

All agonists showed a time-dependent increase in luminescence in a concentration-dependent manner, which could be converted to concentration-response curves (**Figure 3.3** and **4A**). The pEC$_{50}$ values for all agonists determined at the D$_{2long}$R (**Table 3.3**) were in very good agreement with data reported in the literature derived from commonly used assays such as [^{35}S]GTPγS binding[49] or cAMP

assays[51], not differing more than 0.5 orders of magnitude. The endogenous ligand dopamine exhibited full intrinsic activity in the experiment, whereas pramipexole was only able to elicit 86% of the maximal response induced by quinpirole (**Table 3.3**). It was previously reported that pramipexole acts as a partial agonist at the dopamine $D_{2long}R$[52]. Aripiprazole appeared as a partial agonist in recruiting β-arrestin2
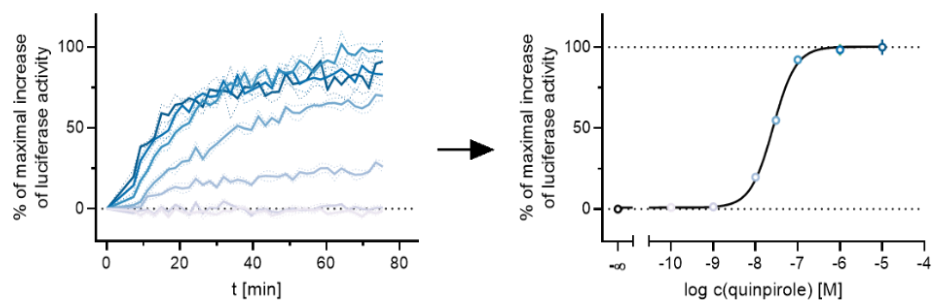
Figure 3.3. Exemplary results of a live-cell measurement at the $D_{2long}R$. HEK293T cells stably expressing ELucN-βarr2 and $D_{2long}R$-ELucC were stimulated with different concentrations of the standard agonist quinpirole. The time-dependent increase in luminescence was recorded and the AUC after 50 min was used to generate a concentration-response curve.
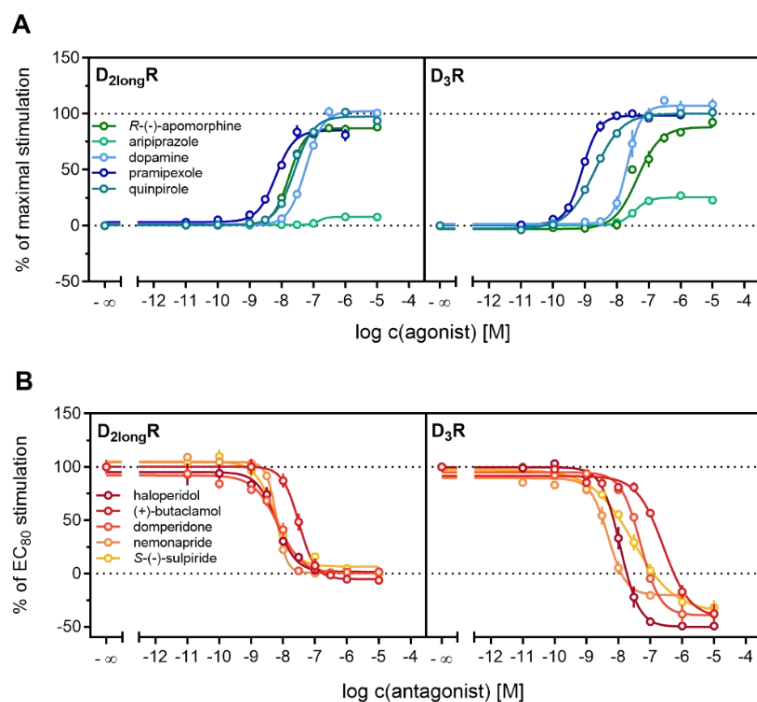
Figure 3.4. Characterization of standard ligands in the β-arrestin2 recruitment assay. A set of agonists (**A**) and antagonists (**B**) were tested for their ability to promote or inhibit (the quinpirole-induced) β-arrestin recruitment at the $D_{2long}R$ and the D_3R. Data of agonists were normalized to the maximal stimulation induced by 1 μM quinpirole (100%) and a solvent control (0%). Antagonist data were normalized to the signal elicited by quinpirole at a concentration corresponding to the EC_{80} (100%) and a solvent control (0%). Obtained pEC_{50}, E_{max} and pK_b values are presented in **Table 3.3**. Data represent means ± SEM from at least three independent experiments, each performed in triplicate.
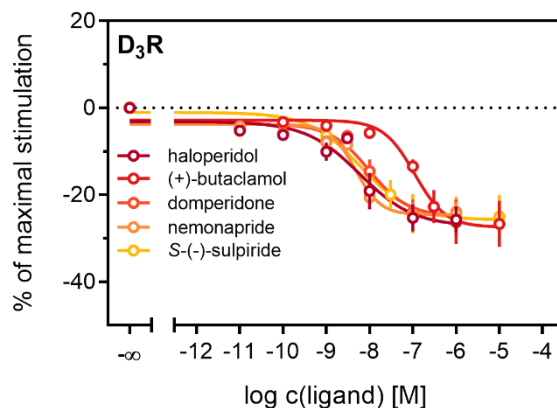
Figure 3.5. Detection of inverse agonism at the D_3R. Inhibition of constitutive β-arrestin2 recruitment to the D_3R by various D_3R ligands. Results are presented as percent maximal stimulation as that observed with quinpirole [1 µM]. Data represent means ± SEM from three independent experiments, each performed in triplicate.

to the $D_{2long}R$ with a very low intrinsic activity (E_{max} = 8 ± 2%) (**Table 3.3**). The efficacy of aripiprazole at the $D_{2long}R$ is controversial, with publications claiming that it is an antagonist[39] and others describing it as a partial agonist in recruiting β-arrestin2 with efficacies ranging from 47% to 73% depending on the assay[50]. For *R*-(-)-apomorphine, we determined an efficacy of 87% (**Table 3.3**), thus it acts as a partial agonist, which is in very good agreement with the literature[52]. At the D_3R, the potencies of all agonistic compounds (**Figure 3.4A**) also correlate very well with published data. Dopamine and pramipexole acted as full agonists, whereas *R*-(-)-apomorphine and aripiprazole exhibited E_{max} values of 91% and 26%, respectively (**Table 3.3**). For both compounds, a partial agonism at the D_3R has been described elsewhere[49,53], with efficacies in a comparable range. Antagonistic activities (pK_b) of (+)-butaclamol, domperidone, haloperidol and nemonapride at the $D_{2long}R$ (**Figure 3.4B**) also correlated very well with data described in the literature (**Table 3.3**), with the minor exception of *S*-(-)-sulpiride. The same generally applies to the D_3R (**Figure 3.4B**), with nemonapride and (+)-butaclamol showing slight differences (**Table 3.3**). A constitutive interaction of the D_3R with β-arrestin has been reported repeatedly[37,54], which we also observed in our assay, as all antagonists lowered the arrestin-dependent luminescence signal at the D_3R below the baseline. Therefore, the set of antagonists was also tested for inverse agonism in the developed assay (agonist mode) as shown in **Figure 3.5**. All these ligands exhibited negative efficacy at the D_3R and potencies, which were comparable with the respective pK_b values (**Table 3.3**).

Table 3.3. pEC$_{50}$, E$_{max}$ and pK_b values of standard DR ligands analyzed in the newly developed β-arrestin2 recruitment assay. For comparison, pK_i values determined in radioligand displacement studies utilizing homogenates from HEK293T cells stably expressing the wild-type receptors (*cf*. **Table 3.2**) and published data from different assays are included.

receptor	cmpd	β-arrestin2 recruitment			N		radioligand displacement	Ref.
		pEC$_{50}$	E$_{max}$ [%]	pK_b			pK_i	
D$_{2long}$R	R-(-)-apomorphine	7.77 ± 0.04	87 ± 3		4		7.33 ± 0.13	7.66[49]
	aripiprazole	6.65 ± 0.15	8 ± 2		3		8.08 ± 0.02	6.84[50]
	dopamine	7.24 ± 0.04	104 ± 3		3	hi	7.53 ± 0.21	7.05[55]
						lo	5.96 ± 0.10	
	pramipexole	8.19 ± 0.05	86 ± 4		4	hi	7.35 ± 0.12	8.51[56]
						lo	5.76 ± 0.03	
	quinpirole	7.55 ± 0.07	100		5	hi	7.66 ± 0.10	7.11[51]
						lo	5.87 ± 0.02	
	(+)-butaclamol			8.29 ± 0.10	3		8.90 ± 0.06	8.04[57]
	domperidone			9.13 ± 0.09	3		9.23 ± 0.07	8.87[58]
	haloperidol			8.90 ± 0.05	3		9.44 ± 0.13	8.89[59]
	nemonapride			8.90 ± 0.05	3		9.52 ± 0.08	9.32[60]
	S-(-)-sulpiride			8.86 ± 0.10	3		7.27 ± 0.09	8.22[61]
D$_3$R	R-(-)-apomorphine	7.43 ± 0.17	91 ± 5		3		8.26 ± 0.03	7.93[49]
	aripiprazole	7.44 ± 0.05	26 ± 1		3		8.12 ± 0.01	7.00[62]
	dopamine	7.66 ± 0.14	105 ± 8		3	hi	8.64 ± 0.09	7.95[63]
						lo	7.10 ± 0.09	
	pramipexole	9.09 ± 0.06	99 ± 4		4		8.99 ± 0.09	8.65[49]
	quinpirole	8.75 ± 0.07	100		6		8.21 ± 0.07	9.07[56]
	(+)-butaclamol	7.16 ± 0.17	-27 ± 9	7.35 ± 0.08	3/3		8.46 ± 0.02	7.95[64]
	domperidone	8.02 ± 0.14	-26 ± 4	8.06 ± 0.09	3/3		8.58 ± 0.04	8.12[58]
	haloperidol	8.29 ± 0.29	-27 ± 5	8.68 ± 0.12	3/3		8.78 ± 0.04	8.70[65]
	nemonapride	8.43 ± 0.13	-25 ± 4	9.07 ± 0.12	3/3		9.86 ± 0.06	9.77[66]
	S-(-)-sulpiride	8.33 ± 0.10	-26 ± 8	8.23 ± 0.07	3/4		7.07 ± 0.03	7.70[58]

Data represent means ± SEM from *N* independent experiments, each performed in triplicate.

3.2.3 Influence of GRK2/3 on β-arrestin2 recruitment to the D$_{2long}$R and the D$_3$R

According to a generally accepted paradigm, G-protein coupled receptor kinases (GRKs) directly link the attenuation of G-protein signaling to arrestin recruitment and therefore play an important role in the desensitization and internalization processes of GPCRs[21]. However, a large body of this knowledge was gained from studies with the β$_2$-adrenergic receptor[21] and it has been shown that there are significant differences among GPCRs. In the case of the D$_2$-like receptors, it was shown that especially GRK2 and 3 play an important role in these processes[67]. The exact mechanism is not fully understood yet. Therefore, we decided to investigate the influence of these kinases in the developed method. Firstly, effects of the selective GRK2/3 inhibitor cpd101[68] were investigated. The cells co-expressing the ELucN-βarr2 and the D$_{2long}$R-ELucC or D$_3$R-ELucC were pre-incubated with the inhibitor at increasing concentrations and concentration-response curves of quinpirole were generated, as displayed in **Figure 3.6**. Surprisingly, the inhibition of GRK2/3 in the cells expressing the D$_{2long}$R led to an increase in the luminescence signal to almost 400% (p < 0.05) (**Figure 3.6A**) and the potency was decreased by almost one log unit (p < 0.05). Regarding the D$_3$R, the use of cpd101 had no significant effect on the
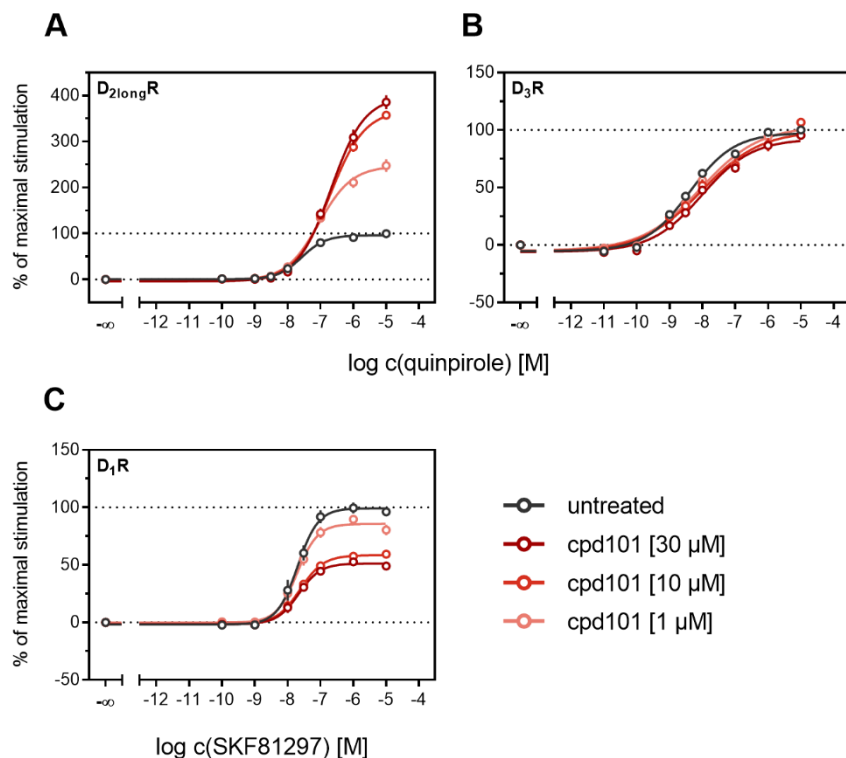
Figure 3.6. Influence of the GRK2/3 inhibitor cpd101 on β-arrestin2 recruitment. HEK293T cells stably expressing ELucN-βarr2 and the indicated D$_x$R-ELucC were incubated with cpd101 at different concentrations for 40 min prior to agonist addition (**A-C**). Data represent means ± SEM from three independent experiments, each performed in triplicate.

efficacy (p = 0.21) or potency (p = 0.19) of quinpirole (**Figure 3.6B**). Since for the D$_1$R it is described that phosphorylation by GRK2 precedes the association of the D$_1$R with β-arrestin2[69], we constructed an analogous β-arrestin2 recruitment assay for the D$_1$R (*cf*. Methods) as a control. The D$_1$R-ELucC construct was validated by radioligand saturation binding and β-arrestin2 recruitment experiments and the results are presented in the Appendix (*cf*. **Figures A5** and **A6**, **Tables A2** and **A3**). The data were in agreement with data obtained from wild-type receptors. Subsequently, the influence of the inhibition of GRK2/3 by using cpd101 was investigated. As expected, inhibition of the kinases led to a concentration-dependent decrease in maximal response induced by the D$_1$R standard agonist SKF81297 (*cf*. **Figure 3.6C**) by about 47% (p < 0.05) and the potency was only affected to a minor extent (p = 0.87). To further unravel the effects of the GRKs, the impact of exogenous overexpression of GRK2 and/or GRK3 on β-arrestin2 recruitment to the D$_{2long}$R and D$_3$R was investigated. The HEK293T cells expressing ELucN-βarr2 and D$_{2long}$R-ELucC or D$_3$R-ELucC were transiently transfected with a plasmid encoding GRK2 or GRK3. Their response to stimulation with quinpirole was compared to the response of cells that were mock transfected with the empty vector. As illustrated in **Figure 3.7A**, GRK2 overexpression in the D$_{2long}$R-ELucC expressing cells led to a slight increase in luminescence signal,
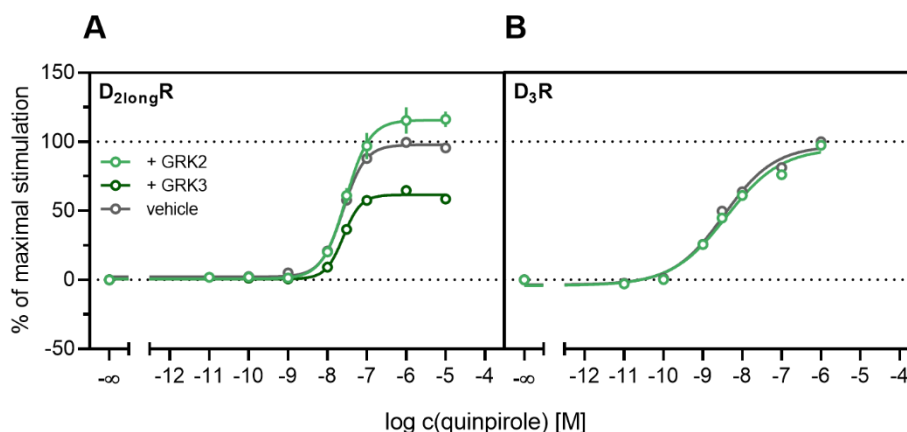
Figure 3.7. Influence of exogenous GRK2 or GRK3 overexpression on β-arrestin2 recruitment. HEK293T cells stably co-expressing ELucN-βarr2 and the D_xR-ELucC were transiently transfected with GRK2/GRK3 or empty vector (**A, B**). Data represent means ± SEM from three independent experiments, each performed in triplicate or quadruplicate.

although this was not statistically significant (p = 0.17). Interestingly, the overexpression of GRK3 led to a marked decrease in luminescence signal (p < 0.05) to about 59% of the maximum signal exhibited by the mock transfected cells. This led to the assumption that the increase of the luminescence signal in the experiments with cpd101 (**Figure 3.6**) is mainly caused by the inhibition of GRK3. The β-arrestin2 recruitment to the D_3R (**Figure 3.7B**) was not affected (p = 0.21) by exogenous GRK2 overexpression, suggesting that endogenous levels of the GRKs are sufficient to ensure β-arrestin2 recruitment or that GRKs are only marginally involved in this process. Additionally, the potency of quinpirole at either receptor was not altered (p > 0.05).

Our results regarding the D_1R are in line with previous findings, confirming that phosphorylation of the receptor by GRK2 initiates or facilitates the interaction of the D_1R with β-arrestin2[69]. In contrast to the D_1R, the involvement of GRK2 in β-arrestin2 recruitment to the $D_{2long}R$ is controversially discussed in the literature. It has been reported that inhibition of the kinase activity of GRK2 leads to reduction of arrestin recruitment[70]. However, it has also been reported that GRK-mediated phosphorylation of the $D_{2long}R$ is not necessary for arrestin association[71] and that GRK2 is constitutively associated with the receptor, whereby $D_{2long}R$ signaling is constitutively suppressed[67]. To the best of our knowledge, the contribution of the GRK3 to phosphorylation or trafficking processes of the $D_{2long}R$ has not been subject to extensive studies so far. Our findings suggest that the GRK3 somehow hampers the recruitment of β-arrestin2 to the receptor. The inhibitor cpd101 binds to the active site of GRK2/3 and thus blocks the binding of ATP to the enzyme[68]. Since application of the inhibitor led to a marked increase in luminescence signal (**Figure 3.6A**), this led to the assumption that the kinase activity of the enzyme hampers β-arrestin recruitment to the $D_{2long}R$. With respect to the D_3R, the findings are consistent with

earlier publications, in that D$_3$Rs only undergo subtle phosphorylation by GRKs and that they are regulated differently than D$_2$Rs[72].

The kinetic profiles of β-arrestin2 recruitment to the D$_{2long}$R and the D$_1$R under the influence of cpd101 are shown in **Figure 3.8**. In both cases, the time courses of the GPCR/β-arrestin interaction with and without cpd101 were similar; only the efficacy was influenced in opposite directions. It is noteworthy that the kinetic courses of β-arrestin2 recruitment to both receptors differ markedly. For the D$_1$R, it has been described that β-arrestin2 is recruited rapidly, whereas the complex of receptor and arrestin is relatively unstable and already dissociates at the plasma membrane[28]. These findings are reflected by the course of our kinetic measurement, where we observed a steep increase in luminescence signal followed by a rapid decline after reaching a maximum (**Figure 3.8B**). This contrasts with the kinetic behavior at the D$_{2long}$R, where the luminescent signal appears to stabilize (**Figure 3.8A**), suggesting that there is a more stable interaction between the D$_{2long}$R and β-arrestin2.
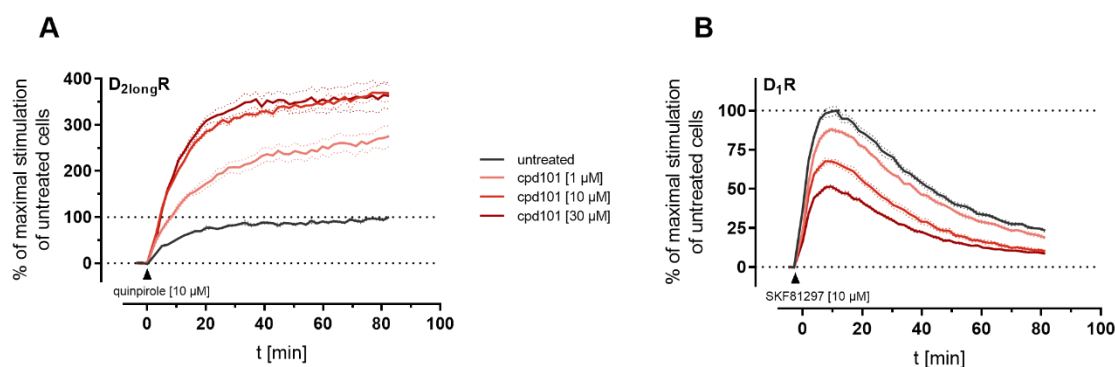

Figure 3.8. Impact of the specific GRK2/3 inhibitor cpd101 on the kinetics of β-arrestin2 recruitment to the D$_{2long}$R (**A**) and the D$_1$R (**B**). Data represent means ± SEM from three independent experiments, each performed in triplicate.

3.2.4 Influence of PKC on β-arrestin2 recruitment to the D$_3$R

Different studies on the internalization of D$_3$ receptors have confirmed that the GRK/arrestin-dependent pathway plays a subordinate role for these receptors, which is consistent with our results described above (*cf*. **Figures 3.6** and 3.**7**). It has been reported that D$_3$Rs are mainly internalized after phosphorylation by PKC[38,73]. PKC is known to be involved in heterologous desensitization of GPCRs[38], so we tested whether it contributes to agonist-induced β-arrestin2 recruitment to the D$_3$R. We used Gö6983, an inhibitor of different PKC isoenzymes, to abrogate the PKC-dependent phosphorylation of the D$_3$R[73]. The cells were treated with increasing concentrations of the inhibitor before the concentration-response curves of quinpirole were recorded. As shown in **Figure 3.9**, inhibition of the PKC led to a significant decrease ($p < 0.05$) of the maximum response elicited by quinpirole. Moreover, the potency of quinpirole was decreased when cells were treated with the inhibitor before the

measurement, but not with statistical significance (p = 0.19). Altogether, these results suggest that PKC-dependent phosphorylation facilitates β-arrestin2 recruitment to the D_3R.
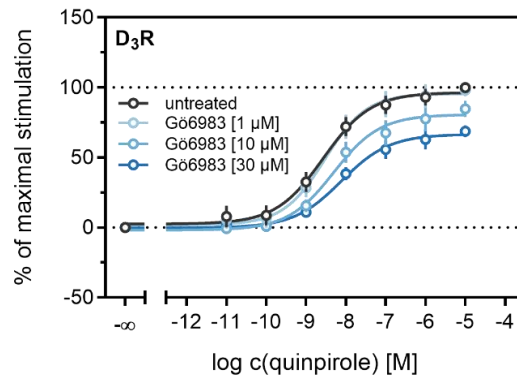

Figure 3.9. Influence of the PKC inhibitor Gö6983 on β-arrestin2 recruitment. HEK293T cells stably expressing ELucN-βarr2 and D_3R-ELucC were incubated with Gö6983 at different concentrations 40 min prior to addition of agonist. Data represent means ± SEM from three independent experiments, each performed in triplicate.

3.3 Materials and methods

3.3.1 Materials

Dulbecco's modified Eagle's medium (DMEM) was from Sigma (Taufkirchen, Germany). Leibovitz' L-15 medium (L-15) was from Fisher Scientific (Nidderau, Germany). Fetal calf serum (FCS), trypsin/EDTA and geneticin (G418) were from Merck Biochrom (Darmstadt, Germany). Zeocin was purchased from Invivogen Europe (Toulouse, France). The cDNAs of the hD$_{2long}$R and hD$_3$R were kindly provided by Dr. Harald Hübner (Department of Chemistry and Pharmacy, Friedrich-Alexander-University, Erlangen). cDNAs of the D$_1$R and the D$_{4.4}$R were purchased from the cDNA Resource Center (Rolla, MO, USA). pcDNA3.1/myc-HIS (B) containing the sequence of the β-arrestin2 fusion construct with the N-terminal fragment of the click beetle luciferase was kindly provided by Prof. Dr. Takeaki Ozawa (Department of Chemistry, School of Science, University of Tokyo). The pIRESneo3 vector was a gift from Prof. G. Meister (Institute of Biochemistry, Genetics, and Microbiology, University of Regensburg, Germany). pcDNA-GRK3 was a gift from Robert Lefkowitz[74] (Addgene plasmid # 32,689; http://n2t.net/addgene:32689; RRID: Addgene_32689). If possible, ligands were dissolved in H$_2$O (millipore); otherwise in DMSO (Merck, Darmstadt, Germany). (+)-butaclamol, dopamine, Gö6983, pramipexole, quinpirole and SKF81297 were from Sigma (Taufkirchen, Germany), aripiprazole and haloperidol were from TCI Deutschland GmbH (Eschborn, Germany), *R*-(-)-apomorphine, nemonapride, *S*-(-)-sulpiride, domperidone and Takeda compound 101 (cpd 101) were from Tocris Bioscience (Bristol, United Kingdom). Pierce D-luciferin was purchased as a potassium salt from Fisher Scientific GmbH (Schwerte, Germany).

3.3.2 Cell culture

HEK293T cells obtained as a kind gift from Prof. Dr. Wulf Schneider (Institute for Medical Microbiology and Hygiene, Regensburg, Germany) were cultured in DMEM supplemented with 10% fetal calf serum at 37 °C in a water-saturated atmosphere containing 5% CO$_2$. Cells were routinely tested for mycoplasma contamination using the Venor GeM Mycoplasma Detection Kit (Minerva Biolabs, Germany) and were negative.

3.3.3 Generation of plasmids for cells used in the β-arrestin2 recruitment assay

The fusion construct of the respective dopamine receptor and the C-terminal fragment of the luciferase was generated by using the previously described pcDNA4/V5-HIS (B) vector containing the hH$_1$R-ELucC construct[75]. The sequence of the hH$_1$R was replaced by the cDNA of the hD$_1$R, hD$_{2long}$R, hD$_3$R or the hD$_{4.4}$R. The cDNAs were amplified by standard polymerase chain reaction (PCR) using gene specific primers and the Q5 high fidelity DNA polymerase (New England Biolabs, Ipswich, USA). The sequences encoding the receptor-ELucC fusion constructs were cloned into the vector by standard

restriction and ligation techniques. The quality of the vectors was controlled by sequencing (Eurofins Genomics GmbH, Ebersberg, Germany).

3.3.4   Generation of plasmids for cells used for homogenate preparation

The hD_1R, $hD_{2long}R$, hD_3R and $hD_{4.4}R$ were cloned into a pIRESneo3 vector via Gibson Assembly. The pIRESneo3-SP-FLAG-hH$_4$R vector, described elsewhere[76], was linearized using standard PCR techniques. Overlaps, complementary to the vector backbone were attached to the dopamine receptors using PCR. Subsequently, receptors were cloned into pIRESneo3 according to the NEBuilder HiFi DNA Assembly Reaction Protocol, resulting in receptors that are N-terminally fused to the membrane signal peptide (SP) of the murine 5-HT$_{3A}$ receptor and tagged with a codon-optimized FLAG tag, subsequently referred to as wild-type receptors. The quality of the vectors was controlled by sequencing.

3.3.5   Generation of stable transfectants

HEK293T cells stably expressing the β-arrestin2 fusion construct were generated as previously described[45]. The cells were seeded into a 6-well plate 24 h prior to transfection. For the transfection with the pcDNA3.1/myc-HIS (B) vector encoding the ELucN-βarr2 fusion construct, Fugene HD transfection reagent (Promega, Mannheim, Germany) was used. Cells were incubated with 2 µg of plasmid DNA at 37 °C for 48 h. Before starting with the antibiotic selection, cells were detached with trypsin/EDTA and transferred to a 75-cm^2 culture flask. G418 at a final concentration of 1000 µg/mL was added to the culture medium until stable growth was observed (for up to 3 weeks). Subsequently, cells were transfected with 2 µg of the pcDNA4/V5-HIS (B) vector encoding the cDNAs for the dopamine receptor fusion proteins (D_1R-ELucC, $D_{2long}R$-ELucC, D_3R-ELucC, $D_{4.4}R$-ELucC) as described above with the exception that X-tremeGENE HP (Roche, Basel, Switzerland) was used as transfection reagent. Selection was performed with 400 µg/mL zeocin. Subsequently, a clonal selection was performed with every cell line for high expression of the modified receptor and β-arrestin2 fusion construct. Therefore, stably transfected cells (see above) were seeded on a 15 cm dish at a density of 1000–2000 cells/dish. After 2 weeks, single clones were picked and screened for the highest S/B ratios as described in **Figure 2** by using 1 µM quinpirole. HEK293T cells stably expressing the wild-type receptors were generated in an analogous manner. Briefly, 2 µg of the pIRESneo3 SP-FLAG-D_1R/$D_{2long}R$/D_3R/$D_{4.4}R$ vector were used and selection was achieved in the presence of 1000 µg/mL of G418.

3.3.6   Preparation of cell homogenates

Homogenates were prepared as previously described[77] with minor modifications. HEK293T cells stably expressing the D_1R, $D_{2long}R$, the D_3R or the $D_{4.4}R$ were grown in 15 cm dishes to 80–90% confluency. Cells were rinsed with ice-cold PBS (137 mM NaCl, 2.7 mM KCl, 10 mM Na$_2$HPO$_4$, 1.8 mM KH$_2$PO$_4$,

pH 7.4) and detached from the dishes using a cell scraper in the presence of harvest buffer (10 mM Tris·HCl, 0.5 mM EDTA, 5.5 mM KCl, 140 mM NaCl; pH 7.4) supplemented with protease inhibitors (SigmaFAST, Cocktail Tablets, EDTA-free, Sigma-Aldrich, Deisenhofen, Germany). After centrifugation (500 g, 5 min), the D$_{2long}$R expressing cells were resuspended in homogenate buffer (50 mM Tris·HCl, 5 mM EDTA, 1.5 mM CaCl$_2$, 5 mM MgCl$_2$, 5 mM KCl, 120 mM NaCl; pH 7.4), whereas the D$_3$R or D$_{4.4}$R expressing cells were resuspended in Tris-MgSO$_4$ buffer (10 mM Tris·HCl, 5 mM MgSO$_4$; pH 7.4) and stored at −80 °C. After thawing, the cells were resuspended in homogenate buffer or Tris-MgSO$_4$ buffer, and homogenized using an Ultraturrax (on ice, 5 times for 5 s). The homogenate was centrifuged (6 °C, 50,000 g, 15 min), the pellet was resuspended in binding buffer (50 mM Tris·HCl, 1 mM EDTA, 5 mM MgCl$_2$, 100 µg/mL bacitracin; pH 7.4) and homogenized using a syringe and needle (i.d. = 0.4 mm). The homogenate was stored in small aliquots at −80 °C.

3.3.7 Radioligand binding experiments with whole cells

For radioligand saturation binding with whole cells, expressing the developed D$_1$R-, D$_{2long}$R-, D$_3$R- or D$_{4.4}$R-ELucC fusion constructs, cells were cultured in a 75 cm^2 flask to a confluency of approx. 80%, detached with a cell scraper and resuspended in L-15 containing 5% FCS. After centrifugation (600 g, 5 min), the cells were resuspended in L-15 medium containing 100 µg/mL bacitracin at a density of 0.15 × 10^6 cells/mL. The assay was carried out in a final volume of 200 µL/well in 96-well polypropylene plates. The radioligand [^{3}H]SCH23390 (D$_1$R; specific activity: 81 Ci/mmol, Novandi Chemistry AB, Södertälje, Sweden) was applied for the D$_1$R in a concentration range from 0.04 nM to 4 nM. For the D$_{2,3,4.4}$R, [^{3}H]N-methylspiperone (D$_{2,3,4.4}$R; specific activity: 77 Ci/mmol, Novandi Chemistry AB, Södertälje, Sweden) was used in a concentration range from 0.025 nM to 1.5 nM for the D$_{2long}$R and the D$_3$R or 0.03 nM to 3.0 nM for the D$_{4.4}$R. After incubation for 60 min (D$_{2long,3,4.4}$R) or 120 min (D$_1$R) at room temperature, bound radioligand was separated from free radioligand by filtration through PEI-coated GF/C filters using a 96-well Brandel harvester (Brandel Inc., Unterföhring, Germany). Filters were transferred to (flexible) 1450-401 96-well sample plates (PerkinElmer, Rodgau, Germany) and after incubation with scintillation cocktail (Rotiszint eco plus, Carl Roth, Karlsruhe, Germany) for 5 h, radioactivity was measured using a MicroBeta2 plate counter (PerkinElmer, Waltham, MA, USA). Total and non-specific data were fitted by the model "one site-total and non-specific binding" using a hyperbolic curve fit for total binding and linear regression for non-specific binding. Specific binding was fitted to the model "one site-specific binding". K_d values were transformed into pK_d and means and SEMs were calculated from the respective pK_d values.

Competition binding experiments with whole cells expressing the fusion proteins were carried out analogous to saturation binding experiments with whole cells as described above. [^{3}H]N-methylspiperone was applied at a final concentration of 0.06 nM for the D$_{2long}$R and the D$_3$R or 0.5 nM

for the $D_{4.4}R$. Non-specific binding was determined in the presence of 2 µM (+)-butaclamol ($D_{2long}R$, D_3R) or nemonapride ($D_{4.4}R$). Competition binding curves were fitted using a four-parameter fit ("log(agonist) vs. response-variable slope") or a two-site fit ("two sites-fit logIC$_{50}$"). Significance of biphasic fitting was tested using the "extra sum-of-squares F Test provided by GraphPad. *P*-values < 0.05 were considered to indicate statistical significance. All calculations were conducted using Prism 8 (Graph Pad, La Jolla, CA, USA).

3.3.8   Radioligand experiments with homogenates

Radioligand binding experiments with homogenates were performed as described for whole cells (see above) with minor modifications. For saturation binding experiments homogenates containing the respective dopamine receptor were resuspended in binding buffer (50 mM Tris·HCl, 1 mM EDTA, 5 mM MgCl$_2$ and 100 µg/mL bacitracin, pH 7.4) to a final concentration of 0.3 µg (D_1R), 0.3 µg ($D_{2long}R$), 0.7 µg (D_3R) or 0.5–1.0 µg ($D_{4.4}R$) protein/well. Incubation time was 60 min for the $D_{2long}R$, D_3R and $D_{4.4}R$ or 120 min for the D_1R. Unspecific binding was determined in the presence of (+)-butaclamol (2000-fold excess, D_1R, $D_{2long}R$, D_3R) or nemonapride (2000-fold, $D_{4.4}R$). [^{3}H]SCH23390 (D_1R; specific activity: 81 Ci/mmol, Novandi Chemistry AB, Södertälje, Sweden) was used in a concentration range from 0.04 nM to 7 nM for the D_1R. [^{3}H]*N*-methylspiperone ($D_{2,3,4.4}R$; specific activity: 77 Ci/mmol, Novandi Chemistry AB, Södertälje, Sweden) was used in a concentration range from 0.025 nM to 1.5 nM for the $D_{2long}R$ and the D_3R or 3.0 nM for the $D_{4.4}R$.

For competition binding experiments, [^{3}H]*N*-methylspiperone was applied at a final concentration of 0.06 nM for the $D_{2long}R$ and the D_3R or 0.1 nM for the $D_{4.4}R$. Incubation time was 60 min.

3.3.9   Quantification of β-arrestin2 recruitment in live cells

HEK293T ELucN-βarr2 cells stably expressing the dopamine receptor-ELucC fusion protein were detached from a 75-cm^2 flask by trypsinization and centrifuged (700 g, 5 min). The pellet was resuspended in L-15 medium supplemented with 5% FCS, HEPES (10 mM), and the cell density was adjusted to 1.25 × 10^6 cells/mL. Then, 80 µL/well of this suspension were seeded into a white microtiter 96-well cellGrade plate (Brand & Co. KG, Wertheim, Germany) and incubated overnight at 37 °C in a humidified atmosphere. The next day, 10 µL of a 10 mM solution of D-luciferin in L-15 medium was added to each well and the plate was transferred to a pre-warmed (37 °C) INFINITE 200 Pro microplate reader (Tecan, Grödig, Austria). A baseline was measured for 20 min by recording the luminescence of the entire plate for 100 ms per well in 11 cycles. Serial dilutions of the respective agonists or antagonists were prepared in L-15 medium containing HEPES (10 mM) (assay buffer) and warmed to 37 °C prior to addition to the cells. Subsequently, luminescence was recorded for 45 repeats resulting in an overall period of 1 h. Negative control (assay buffer) and positive control (quinpirole ($D_{2long}R$), full agonist) were included for normalization of the data from the $D_{2long}R$. For measurements

performed in antagonist mode, 10 µL of assay buffer were removed from each well before cells were pre-incubated with the antagonist dilutions (10 µL) for 20 min. Antagonists were added simultaneously with the substrate just before starting the baseline measurement. Then, quinpirole (D$_{2long}$R) or SKF81297 (D$_1$R) was added at a concentration eliciting 80% of the maximal response and the final read was started. To correct for slight differences in cell counts or amount of substrate added to each well, the mean of the baseline values just before addition of agonists was subtracted from all subsequently recorded values. Additionally, to account for a change of luminescence that might occur over the time-course of the measurement in the absence of agonist, the recorded values of the solvent control were subtracted from all data. For generating concentration-response curves, the AUC after 50 min was used. Data were fitted to the model "log(agonist) vs. response-variable slope (four parameters)". The pK_b-values were calculated from IC$_{50}$ values according to the Cheng–Prusoff equation[78]. All calculations were conducted using Prism 8 (Graph Pad, La Jolla, CA, USA).

3.3.10 Quantification of β-arrestin2 recruitment by endpoint measurement

HEK293T ELucN-βarr2 cells stably expressing the dopamine receptor-ELucC fusion protein were prepared 24 h before as described in the preceding section. In agonist mode, 10 µL of assay buffer were added to each well before addition of 10 µL of agonist in different concentrations, resulting in an assay volume of 100 µL. In antagonist mode, cells were incubated with 10 µL of antagonist in different concentrations for 20 min, before quinpirole (10 µL) was added at a concentration eliciting 80% of the maximum response. After incubating the cells with the compounds for 90 min at room temperature, 50 µL of assay medium were removed from each well and 50 µL of Bright-Glo luciferase assay reagent were added resulting in cell lysis. Plates were vigorously shaken for 2 min and bioluminescence was recorded for 1 ms per well using an INFINITE 200 Pro microplate reader (Tecan, Grödig, Austria). Data were fitted to the model "log(agonist) vs. response-variable slope (four parameters)". The pK_b-values were calculated from IC$_{50}$ values according to the Cheng–Prusoff equation[78]. All calculations were conducted using Prism 8 (Graph Pad, La Jolla, CA, USA).

3.3.11 Statistical analysis

Statistic differences were analyzed using a t-Test or a one-way ANOVA. All reported *p*-values are two-sided, and *p*-values lower than 0.05 were considered to indicate statistical significance. All calculations were performed using the SPSS 26 software (IBM, Armonk, NY, USA).

3.4   Summary and conclusions

In this study, we developed a split luciferase complementation β-arrestin2 recruitment assay for the D$_{2long}$ and the D$_3$ receptor, which, in case of the D$_{2long}$R, is also applicable in live cells. The hypothesis that the D$_4$R does not recruit β-arrestin2 was confirmed[35], as no recruitment was measured at the D$_{4.4}$R. Our assay represents a homogeneous test principle with a cell-permeable substrate, which allows temporal (kinetic) measurements. Combined with the proximal readout and the short incubation time, it represents a significant improvement over the commercially available assays described above. For the D$_{2long}$ and D$_3$ receptors, we demonstrated that the assay is suitable for the determination of ligand potencies and efficacies. Furthermore, the test system is able to discriminate between full and partial agonists and to identify inverse agonism at the D$_3$R, which makes it a versatile tool for the characterization of dopamine receptor ligands. Although β-arrestin2 recruitment at the D$_3$R has played a rather minor role in the literature so far[33], this determination can still be an important parameter for the complete characterization and development of future biased ligands in the field of dopamine receptors. The influence of GRK2/3 and PKC at the D$_{2long}$R, D$_3$R, and D$_1$R was investigated using different kinase inhibitors, which shows that the assay can also contribute to the deciphering of signaling mechanisms. In summary, this split luciferase complementation assay is a powerful tool for the determination of β-arrestin2 recruitment in dopamine D$_2$-like receptors. Thus it represents an important methodological extension for the identification of biased agonists, e.g., in multiparametric analyses, and the characterization of D$_2$-like receptor ligands.

3.5   References

1.   A. R. Cools, J. M. Van Rossum, Excitation-mediating and inhibition-mediating dopamine-receptors: a new concept towards a better understanding of electrophysiological, biochemical, pharmacological, functional and clinical data. *Psychopharmacologia* **45**, 243-254, doi:10.1007/BF00421135 (1976).

2.   A. Dearry *et al.*, Molecular cloning and expression of the gene for a human D_1 dopamine receptor. *Nature* **347**, 72-76, doi:10.1038/347072a0 (1990).

3.   P. Sokoloff, B. Giros, M.-P. Martres, M.-L. Bouthenet, J.-C. Schwartz, Molecular cloning and characterization of a novel dopamine receptor (D_3) as a target for neuroleptics. *Nature* **347**, 146-151, doi:10.1038/347146a0 (1990).

4.   H. H. Van Tol *et al.*, Cloning of the gene for a human dopamine D_4 receptor with high affinity for the antipsychotic clozapine. *Nature* **350**, 610-614, doi:10.1038/350610a0 (1991).

5.   M. H. Polymeropoulos, H. Xiao, C. R. Merril, The human D_5 dopamine receptor (DRD_5) maps on chromosome 4. *Genomics* **11**, 777-778, doi:10.1016/0888-7543(91)90091-r (1991).

6.   P. H. Andersen *et al.*, Dopamine receptor subtypes: beyond the D_1/D_2 classification. *Trends Pharmacol Sci* **11**, 231-236, doi:10.1016/0165-6147(90)90249-8 (1990).

7.   K. A. Neve, J. K. Seamans, H. Trantham-Davidson, Dopamine receptor signaling. *J Recept Signal Transduct Res* **24**, 165-205, doi:10.1081/rrs-200029981 (2004).

8.   J. W. Kebabian, Multiple classes of dopamine receptors in mammalian central nervous system: the involvement of dopamine-sensitive adenylyl cyclase. *Life Sci* **23**, 479-483, doi:10.1016/0024-3205(78)90157-1 (1978).

9.   P. F. Spano, S. Govoni, M. Trabucchi, Studies on the pharmacological properties of dopamine receptors in various areas of the central nervous system. *Adv Biochem Psychopharmacol* **19**, 155-165 (1978).

10.   S. R. Neves, P. T. Ram, R. Iyengar, G protein pathways. *Science* **296**, 1636-1639, doi:10.1126/science.1071550 (2002).

11.   K. L. Davis, R. S. Kahn, G. Ko, M. Davidson, Dopamine in schizophrenia: a review and reconceptualization. *Am J Psychiatry* **148**, 1474-1486, doi:10.1176/ajp.148.11.1474 (1991).

12.   H. Bernheimer, W. Birkmayer, O. Hornykiewicz, K. Jellinger, F. Seitelberger, Brain dopamine and the syndromes of Parkinson and Huntington. Clinical, morphological and neurochemical correlations. *J Neurol Sci* **20**, 415-455, doi:10.1016/0022-510x(73)90175-5 (1973).

13.   G. U. Hoglinger *et al.*, Dopamine depletion impairs precursor cell proliferation in Parkinson disease. *Nat Neurosci* **7**, 726-735, doi:10.1038/nn1265 (2004).

14.   G. Di Chiara, Drug addiction as dopamine-dependent associative learning disorder. *Eur J Pharmacol* **375**, 13-30, doi:10.1016/s0014-2999(99)00372-6 (1999).

15.   G. Di Chiara *et al.*, Dopamine and drug addiction: the nucleus accumbens shell connection. *Neuropharmacology* **47 Suppl 1**, 227-241, doi:10.1016/j.neuropharm.2004.06.032 (2004).

16.   F. E. Albrecht *et al.*, Role of the D_{1A} dopamine receptor in the pathogenesis of genetic hypertension. *J Clin Investig* **97**, 2283-2288, doi:10.1172/JCI118670 (1996).

17.   M. Berk *et al.*, Dopamine dysregulation syndrome: implications for a dopamine hypothesis of bipolar disorder. *Acta Psychiatr Scand Suppl*, 41-49, doi:10.1111/j.1600-0447.2007.01058.x (2007).

18.   D. A. Cousins, K. Butts, A. H. Young, The role of dopamine in bipolar disorder. *Bipolar Disord* **11**, 787-806, doi:10.1111/j.1399-5618.2009.00760.x (2009).

19.   R. Linke *et al.*, Presynaptic dopaminergic function in patients with restless legs syndrome: are there common features with early Parkinson's disease? *Mov Disord* **19**, 1158-1162, doi:10.1002/mds.20226 (2004).

20. K. Stiasny-Kolster *et al.*, Patch application of the dopamine agonist rotigotine to patients with moderate to advanced stages of restless legs syndrome: a double-blind, placebo-controlled pilot study. *Mov Disord* **19**, 1432-1438, doi:10.1002/mds.20251 (2004).

21. M. J. Lohse, J. L. Benovic, J. Codina, M. G. Caron, R. J. Lefkowitz, beta-Arrestin: a protein that regulates beta-adrenergic receptor function. *Science* **248**, 1547-1550, doi:10.1126/science.2163110 (1990).

22. S. S. Ferguson *et al.*, Role of beta-arrestin in mediating agonist-promoted G protein-coupled receptor internalization. *Science* **271**, 363-366, doi:10.1126/science.271.5247.363 (1996).

23. S. M. DeWire, S. Ahn, R. J. Lefkowitz, S. K. Shenoy, Beta-arrestins and cell signaling. *Annu Rev Physiol* **69**, 483-510, doi:10.1146/annurev.physiol.69.022405.154749 (2007).

24. J. Inglese, N. J. Freedman, W. J. Koch, R. J. Lefkowitz, Structure and mechanism of the G protein-coupled receptor kinases. *J Biol Chem* **268**, 23735-23738, doi:10.1016/S0021-9258(20)80439-6 (1993).

25. S. Pippig *et al.*, Overexpression of beta-arrestin and beta-adrenergic receptor kinase augment desensitization of beta 2-adrenergic receptors. *J Biol Chem* **268**, 3201-3208, doi:10.1016/S0021-9258(18)53678-4 (1993).

26. R. H. Oakley, S. A. Laporte, J. A. Holt, L. S. Barak, M. G. Caron, Molecular determinants underlying the formation of stable intracellular G protein-coupled receptor-beta-arrestin complexes after receptor endocytosis. *J Biol Chem* **276**, 19452-19460, doi:10.1074/jbc.M101450200 (2001).

27. D. Hilger, M. Masureel, B. K. Kobilka, Structure and dynamics of GPCR signaling complexes. *Nature structural & molecular biology* **25**, 4-12, doi:10.1038/s41594-017-0011-7 (2018).

28. R. H. Oakley, S. A. Laporte, J. A. Holt, M. G. Caron, L. S. Barak, Differential affinities of visual arrestin, beta arrestin1, and beta arrestin2 for G protein-coupled receptors delineate two major classes of receptors. *J Biol Chem* **275**, 17201-17210, doi:10.1074/jbc.M910348199 (2000).

29. R. R. Gainetdinov, R. T. Premont, L. M. Bohn, R. J. Lefkowitz, M. G. Caron, Desensitization of G protein-coupled receptors and neuronal functions. *Annu Rev Neurosci* **27**, 107-144, doi:10.1146/annurev.neuro.27.070203.144206 (2004).

30. J. M. Beaulieu, R. R. Gainetdinov, The physiology, signaling, and pharmacology of dopamine receptors. *Pharmacol Rev* **63**, 182-217, doi:10.1124/pr.110.002642 (2011).

31. K. Ito, T. Haga, J. Lameh, W. Sadee, Sequestration of dopamine D_2 receptors depends on coexpression of G-protein-coupled receptor kinases 2 or 5. *Eur J Biochem* **260**, 112-119, doi:10.1046/j.1432-1327.1999.00125.x (1999).

32. K. Iwata, K. Ito, A. Fukuzaki, K. Inaki, T. Haga, Dynamin and rab5 regulate GRK2-dependent internalization of dopamine D_2 receptors. *Eur J Biochem* **263**, 596-602, doi:10.1046/j.1432-1327.1999.00549.x (1999).

33. K. M. Kim *et al.*, Differential regulation of the dopamine D_2 and D_3 receptors by G protein-coupled receptor kinases and beta-arrestins. *J Biol Chem* **276**, 37409-37414, doi:10.1074/jbc.M106728200 (2001).

34. K. M. Kim, M. G. Caron, Complementary roles of the DRY motif and C-terminus tail of GPCRS for G protein coupling and beta-arrestin interaction. *Biochem Biophys Res Commun* **366**, 42-47, doi:10.1016/j.bbrc.2007.11.055 (2008).

35. A. Spooren *et al.*, Resistance of the dopamine D_4 receptor to agonist-induced internalization and degradation. *Cell Signal* **22**, 600-609, doi:10.1016/j.cellsig.2009.11.013 (2010).

36. J. D. Deming *et al.*, Dopamine receptor D_4 internalization requires a beta-arrestin and a visual arrestin. *Cell Signal* **27**, 2002-2013, doi:10.1016/j.cellsig.2015.06.008 (2015).

37. C. Min, M. Zheng, X. Zhang, M. G. Caron, K. M. Kim, Novel roles for beta-arrestins in the regulation of pharmacological sequestration to predict agonist-induced desensitization of dopamine D_3 receptors. *Br J Pharmacol* **170**, 1112-1129, doi:10.1111/bph.12357 (2013).

38.   E. Y. Cho *et al.*, Roles of protein kinase C and actin-binding protein 280 in the regulation of intracellular trafficking of dopamine D$_3$ receptor. *Mol Endocrinol* **21**, 2242-2254, doi:10.1210/me.2007-0202 (2007).

39.   B. Masri *et al.*, Antagonism of dopamine D$_2$ receptor/beta-arrestin 2 interaction is a common property of clinically effective antipsychotics. *Proc Natl Acad Sci USA* **105**, 13656-13661, doi:10.1073/pnas.0803522105 (2008).

40.   T. Littmann, A. Buschauer, G. Bernhardt, Split luciferase-based assay for simultaneous analyses of the ligand concentration- and time-dependent recruitment of beta-arrestin2. *Anal Biochem* **573**, 8-16, doi:10.1016/j.ab.2019.02.023 (2019).

41.   Y. B. Song, C. O. Park, J. Y. Jeong, W. K. Huh, Monitoring G protein-coupled receptor activation using an adenovirus-based beta-arrestin bimolecular fluorescence complementation assay. *Anal Biochem* **449**, 32-41, doi:10.1016/j.ab.2013.12.017 (2014).

42.   G. Laroche, P. M. Giguere, Measurement of beta-Arrestin Recruitment at GPCRs Using the Tango Assay. *Methods Mol Biol* **1947**, 257-267, doi:10.1007/978-1-4939-9121-1_14 (2019).

43.   H. Eishingdrelo *et al.*, A cell-based protein-protein interaction method using a permuted luciferase reporter. *Curr Chem Genomics* **5**, 122-128, doi:10.2174/1875397301105010122 (2011).

44.   V. R. Viviani *et al.*, The structural origin and biological function of pH-sensitivity in firefly luciferases. *Photochem Photobiol Sci* **7**, 159-169, doi:10.1039/b714392c (2008).

45.   N. Misawa *et al.*, Rapid and high-sensitivity cell-based assays of protein-protein interactions using split click beetle luciferase complementation: an approach to the study of G-protein-coupled receptors. *Anal chem* **82**, 2552-2560, doi:10.1021/ac100104q (2010).

46.   M. Hattori *et al.*, Analysis of temporal patterns of GPCR-beta-arrestin interactions using split luciferase-fragment complementation. *Mol Biosyst* **9**, 957-964, doi:10.1039/c2mb25443c (2013).

47.   D. R. Sibley, A. De Lean, I. Creese, Anterior pituitary dopamine receptors. Demonstration of interconvertible high and low affinity states of the D$_2$ dopamine receptor. *J Biol Chem* **257**, 6351-6361, doi:10.1016/S0021-9258(20)65148-1 (1982).

48.   D. R. Sibley, L. C. Mahan, I. Creese, Dopamine receptor binding on intact cells. Absence of a high-affinity agonist-receptor binding state. *Mol pharmacol* **23**, 295-302 (1983).

49.   A. Newman-Tancredi *et al.*, Differential actions of antiparkinson agents at multiple classes of monoaminergic receptor. II. Agonist and antagonist properties at subtypes of dopamine D$_2$-like receptor and alpha$_1$/alpha$_2$-adrenoceptor. *J Pharmacol Exp Ther* **303**, 805-814, doi:10.1124/jpet.102.039875 (2002).

50.   J. A. Allen *et al.*, Discovery of beta-arrestin-biased dopamine D$_2$ ligands for probing signal transduction pathways essential for antipsychotic efficacy. *Proc Natl Acad Sci USA* **108**, 18488-18493, doi:10.1073/pnas.1104807108 (2011).

51.   S. E. George, P. J. Bungay, L. H. Naylor, Functional analysis of the D$_{2L}$ dopamine receptor expressed in a cAMP-responsive luciferase reporter cell line. *Biochem Pharmacol* **56**, 25-30, doi:10.1016/s0006-2952(98)00014-8 (1998).

52.   I. V. Klewe *et al.*, Recruitment of beta-arrestin2 to the dopamine D$_2$ receptor: insights into anti-psychotic and anti-parkinsonian drug receptor signaling. *Neuropharmacology* **54**, 1215-1222, doi:10.1016/j.neuropharm.2008.03.015 (2008).

53.   A. Frank, D. J. Kiss, G. M. Keseru, H. Stark, Binding kinetics of cariprazine and aripiprazole at the dopamine D$_3$ receptor. *Sci Rep* **8**, 12509, doi:10.1038/s41598-018-30794-y (2018).

54.   W. Xu, M. E. A. Reith, L. Y. Liu-Chen, S. Kortagere, Biased signaling agonist of dopamine D$_3$ receptor induces receptor internalization independent of beta-arrestin recruitment. *Pharmacol Res* **143**, 48-57, doi:10.1016/j.phrs.2019.03.003 (2019).

55. R. B. Free *et al.*, Discovery and characterization of a G protein-biased agonist that inhibits beta-arrestin recruitment to the D_2 dopamine receptor. *Mol pharmacol* **86**, 96-105, doi:10.1124/mol.113.090563 (2014).

56. F. Sautel *et al.*, A functional test identifies dopamine agonists selective for D_3 versus D_2 receptors. *Neuroreport* **6**, 329-332, doi:10.1097/00001756-199501000-00026 (1995).

57. W. M. McDonald, D. R. Sibley, B. F. Kilpatrick, M. G. Caron, Dopaminergic inhibition of adenylate cyclase correlates with high affinity agonist binding to anterior pituitary D_2 dopamine receptors. *Mol Cell Endocrinol* **36**, 201-209, doi:10.1016/0303-7207(84)90037-6 (1984).

58. P. Sokoloff *et al.*, Pharmacology of human dopamine D_3 receptor expressed in a mammalian cell line: comparison with D_2 receptor. *Eur J Pharmacol* **225**, 331-337, doi:10.1016/0922-4106(92)90107-7 (1992).

59. Y. Gao *et al.*, Cariprazine exerts antimanic properties and interferes with dopamine D_2 receptor beta-arrestin interactions. *Pharmacol Res Perspect* **3**, e00073, doi:10.1002/prp2.73 (2015).

60. J. F. Vanhauwe, N. Fraeyman, B. J. Francken, W. H. Luyten, J. E. Leysen, Comparison of the ligand binding and signaling properties of human dopamine D_2 and D_3 receptors in Chinese hamster ovary cells. *J Pharmacol Exp Ther* **290**, 908-916 (1999).

61. S. B. Freedman *et al.*, Expression and pharmacological characterization of the human D_3 dopamine receptor. *J Pharmacol Exp Ther* **268**, 417-426 (1994).

62. Y. Tadori, R. A. Forbes, R. D. McQuade, T. Kikuchi, Characterization of aripiprazole partial agonist activity at human dopamine D_3 receptors. *Eur J Pharmacol* **597**, 27-33, doi:10.1016/j.ejphar.2008.09.008 (2008).

63. W. Xu *et al.*, Functional Characterization of a Novel Series of Biased Signaling Dopamine D_3 Receptor Agonists. *ACS Chem Neurosci* **8**, 486-500, doi:10.1021/acschemneuro.6b00221 (2017).

64. L. Tang, R. D. Todd, A. Heller, K. L. O'Malley, Pharmacological and functional characterization of D_2, D_3 and D_4 dopamine receptors in fibroblast and dopaminergic cell lines. *J Pharmacol Exp Ther* **268**, 495-502 (1994).

65. L. A. Bruins Slot, C. Palmier, S. Tardif, D. Cussac, Action of novel antipsychotics at human dopamine D_3 receptors coupled to G protein and ERK1/2 activation. *Neuropharmacology* **53**, 232-241, doi:10.1016/j.neuropharm.2007.05.006 (2007).

66. J. M. Vile, U. M. D'Souza, P. G. Strange, [^{3}H]nemonapride and [^{3}H]spiperone label equivalent numbers of D_2 and D_3 dopamine receptors in a range of tissues and under different conditions. *J Neurochem* **64**, 940-943, doi:10.1046/j.1471-4159.1995.64020940.x (1995).

67. Y. Namkung, C. Dipace, E. Urizar, J. A. Javitch, D. R. Sibley, G protein-coupled receptor kinase-2 constitutively regulates D_2 dopamine receptor expression and signaling independently of receptor phosphorylation. *J Biol Chem* **284**, 34103-34115, doi:10.1074/jbc.M109.055707 (2009).

68. D. M. Thal, R. Y. Yeow, C. Schoenau, J. Huber, J. J. Tesmer, Molecular mechanism of selectivity among G protein-coupled receptor kinase 2 inhibitors. *Mol pharmacol* **80**, 294-303, doi:10.1124/mol.111.071522 (2011).

69. M. Lamey *et al.*, Distinct residues in the carboxyl tail mediate agonist-induced desensitization and internalization of the human dopamine D_1 receptor. *J Biol Chem* **277**, 9415-9421, doi:10.1074/jbc.M111811200 (2002).

70. T. F. Pack, M. I. Orlen, C. Ray, S. M. Peterson, M. G. Caron, The dopamine D_2 receptor can directly recruit and activate GRK2 without G protein activation. *J Biol Chem* **293**, 6161-6171, doi:10.1074/jbc.RA117.001300 (2018).

71. Y. Namkung, C. Dipace, J. A. Javitch, D. R. Sibley, G protein-coupled receptor kinase-mediated phosphorylation regulates post-endocytic trafficking of the D_2 dopamine receptor. *J Biol Chem* **284**, 15038-15051, doi:10.1074/jbc.M900388200 (2009).

72.   E. V. Gurevich, R. R. Gainetdinov, V. V. Gurevich, G protein-coupled receptor kinases as regulators of dopamine receptor functions. *Pharmacol Res* **111**, 1-16, doi:10.1016/j.phrs.2016.05.010 (2016).

73.   X. Zhang, N. Sun, M. Zheng, K. M. Kim, Clathrin-mediated endocytosis is responsible for the lysosomal degradation of dopamine D$_3$ receptor. *Biochem Biophys Res Commun* **476**, 245-251, doi:10.1016/j.bbrc.2016.05.104 (2016).

74.   J. A. Pitcher *et al.*, Phosphatidylinositol 4,5-bisphosphate (PIP2)-enhanced G protein-coupled receptor kinase (GRK) activity. Location, structure, and regulation of the PIP2 binding site distinguishes the GRK subfamilies. *J Biol Chem* **271**, 24907-24913, doi:10.1074/jbc.271.40.24907 (1996).

75.   S. Lieb *et al.*, Label-free versus conventional cellular assays: Functional investigations on the human histamine H$_1$ receptor. *Pharmacol Res* **114**, 13-26, doi:10.1016/j.phrs.2016.10.010 (2016).

76.   E. Bartole *et al.*, UR-DEBa242: A Py-5-Labeled Fluorescent Multipurpose Probe for Investigations on the Histamine H$_3$ and H$_4$ Receptors. *J Med Chem* **63**, 5297-5311, doi:10.1021/acs.jmedchem.0c00160 (2020).

77.   H. Hübner, C. Haubmann, W. Utz, P. Gmeiner, Conjugated Enynes as Nonaromatic Catechol Bioisosteres: Synthesis, Binding Experiments, and Computational Studies of Novel Dopamine Receptor Agonists Recognizing Preferentially the D$_3$ Subtype. *J Med Chem* **43**, 756-762, doi:10.1021/jm991098z (2000).

78.   Y. Cheng, W. H. Prusoff, Relationship between the inhibition constant (K$_1$) and the concentration of inhibitor which causes 50 per cent inhibition (I$_{50}$) of an enzymatic reaction. *Biochem Pharmacol* **22**, 3099-3108, doi:10.1016/0006-2952(73)90196-2 (1973).

Chapter 4

Investigation of the ligand agonism and antagonism at the D_{2long} receptor by dynamic mass redistribution (DMR)

4.1   Introduction

Traditionally, in G protein-coupled receptor (GPCR) targeted drug discovery, new compounds are characterized with respect to their pharmacological properties in binding and functional cell based assays to determine ligand-receptor affinities and to quantify distinct intracellular messengers, respectively[1,2]. A very proximate technique to measure GPCR mediated G protein activation upon agonist stimulation is, for example, the [^{35}S]GTPγS[3] assay, which is usually performed with cell membrane preparations[3]. By contrast, cell-based assays focus on the quantification of further down-stream occurring intracellular second messengers, such as cyclic AMP[4], inositol-1,4,5-trisphosphate (IP3)[5] or Ca^{2+} [6], which are regulated by Gα$_s$-, Gα$_i$- or Gα$_q$-coupled receptors. To monitor G protein independent signaling, namely the recruitment of β-arrestin, different approaches were described[7,8]. Among others, imaging-based[8] or split-luciferase complementation assays[9,10] (*cf.* chapter 3) are available, both requiring a modification of the GPCR of interest and/or β-arrestin to make the receptor-β-arrestin interaction conveniently detectable. In principle, the second messenger and effector recruitment assays can be applied for the investigation of orphan GPCRs, however this requires more efforts compared to so-called label-free technologies because for the latter the G protein coupling specificity of the receptor does not have to be known (see below).

The dopamine D$_{2long}$ receptor, a member of the rhodopsin family of GPCRs[11] and one of the natural targets of the endogenous neurotransmitter dopamine, exerts its functions primarily by activating various subtypes of Gα$_{i/o}$ proteins[12,13]. It has been shown that D$_{2long}$R signaling is multifaceted and comprises the activation of a variety of pathways[14]. By activation of the Gα$_{i/o}$ protein, the D$_{2long}$R inhibits the adenylyl cyclase and thus prevents the formation of cyclic AMP, leading to a decrease in the phosphorylation of protein kinase A (PKA) substrates[14]. Moreover, in the case of the dopamine D$_{2long}$ receptor, the Gβγ subunit, which dissociates from the heterotrimeric G protein after GTP is bound to the Gα subunit[15], mediates an increase in cytosolic calcium by activation of phospholipase C (PLC)[16]. However, as has been shown in a neuronal cell line, also exhibits an inhibitory effect on voltage gated calcium channels [16]. In addition to the aforementioned signaling pathways, the D$_{2long}$R signals through β-arrestin2, a protein, that on the one hand is involved in the desensitization of the receptor and on the other hand triggers G protein independent signaling[17]. Concerning dopamine D$_2$ receptor ligands, assays based on the quantification of cyclic AMP[18-20], β-arrestin2 recruitment[10,21] or [^{35}S]GTPγS binding[22,23] have been widely used for pharmacological characterization. Having the complex signaling mechanisms of the dopamine D$_{2long}$ receptor (or GPCRs in general) in mind, it appears to be advantageous to follow holistic approaches, i.e. label-free technologies, allowing the measurement of whole-cell responses to a ligand[2]. Dynamic mass redistribution (DMR) is a label-free technology that utilizes an optical biosensor to measure the redistribution of cellular constituents upon receptor stimulation[24]. The biosensor used for measuring DMR is a resonant waveguide grating (RWG),

consisting of a substrate and a cover layer with an embedded grating structure, and a layer of adherent cells that grow on the sensor surface[24]. As depicted in **Figure 4.1**, the bottom of the biosensor is illuminated by a broadband light source (825 – 840 nm) in a specific angle and most of the wavelengths are transmitted. The wavelength that is in resonance with the system is diffracted by the grating and couples into the grating layer, which acts as a waveguide. The light propagates within the layer until it is uncoupled again by diffraction. The wavelength that is in resonance with the system is, among others, determined by the refractive indices of the different layers, thus also by the local refractive index near the sensor surface[25]. Redistribution of cellular components, which has been reported as a complex endpoint of GPCR signaling[26,27], results in changes in the refractive index next to the sensor surface[28]. This leads to a shift of the resonance wavelength which is recorded over time[29]. The electromagnetic field that is generated by the propagated light, the evanescent wave, has a penetration depth in cells of about 150 – 200 nm, which is referred to as the sensing volume. Thus, only changes in mass distribution in the sensor-near portion of the cells are detected[30].
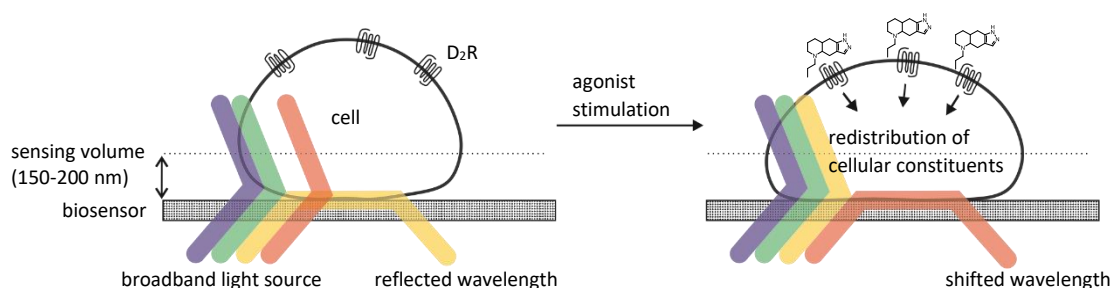

Figure 4.1. Schematic illustration of the DMR detection principle. Cells are grown in 384- or 96-well biosensor microplates that contain a biosensor within the bottom of each well. The resonant waveguide grating biosensor is illuminated by a broadband light source and the wavelength that is in resonance with the system is propagated and reflected. Other wavelengths are transmitted. The sensing volume is defined by the penetration depth of the evanescent wave that is generated by the propagated light. The resonance wavelength is a function of the refractive index near the surface of the biosensor. Stimulation of the cells can lead to a dynamic mass redistribution (DMR) of cellular constituents and subsequently a change in refractive index. This leads to a shift of the resonant wavelength in the pm range, representing the readout of the DMR assay.

Label-free techniques, such as DMR, are attractive because it is not necessary to know the G protein isoform coupling to the receptor of interest and a genetic engineering of the receptor is not required. This enables investigations under more physiological-like conditions, not least because there is no interference with cellular processes by the addition of chemical agents, often required for signal detection in conventional assays. Another strength of the DMR technique is its outstanding sensitivity, allowing the study of GPCRs at endogenous expression levels[27]. However, it should be kept in mind that extremely sensitive methods are especially error-prone.

Label-free readouts are often referred to as "black box" readouts, since the processes leading to the observed signal are not fully understood[31]. Therefore, specific antagonists or pathway inhibitors should always be included for the interpretation of data derived from DMR or other label-free assays.

In this study, well characterized dopamine D_2R-like (partial) agonists and antagonists were investigated in a dynamic mass redistribution assay using CHO-K1 cells expressing the human dopamine D_{2long} receptor. The influence of different assay conditions on pharmacological parameters of the studied DR ligands was investigated and the data were compared with data obtained from canonical assays. Furthermore, the contribution of different signaling components, such as G_s, $G_{i/o}$, $G_{q/11}$ proteins or cytosolic Ca^{2+} was investigated.

4.2   Results and discussion

4.2.1   Optimization of assay conditions

CHO cells exhibit stronger adhesion to the microplates compared to HEK293T cells and were chosen for the establishment of a DMR assay for that reason. Since the penetration depth of the biosensor is only about 200 nm, the adhesion of the cell to the sensor surface has a great impact on the sensitivity of the assay[32]. The expression of the receptor in the CHO-K1 hD$_{2long}$R cell line was determined by radioligand saturation binding, shown in **Figure A7** (Appendix). For the determination of pharmacological parameters under quasi physiological conditions in experiments involving intact cells, an assay temperature of 37 °C should be used. However, for different reasons explained in the following, a lower assay temperature was considered useful and its influence on the DMR readout was investigated. The biosensor used in the DMR technology is sensitive to the refractive index of the medium being in contact with the sensor surface[24] and the refractive index depends on the temperature. A change of 1 °C results in a 24 pm shift of the reflected wavelength (according to the manufacturer), i.e. the temperature should be kept constant during the assay procedure. Before
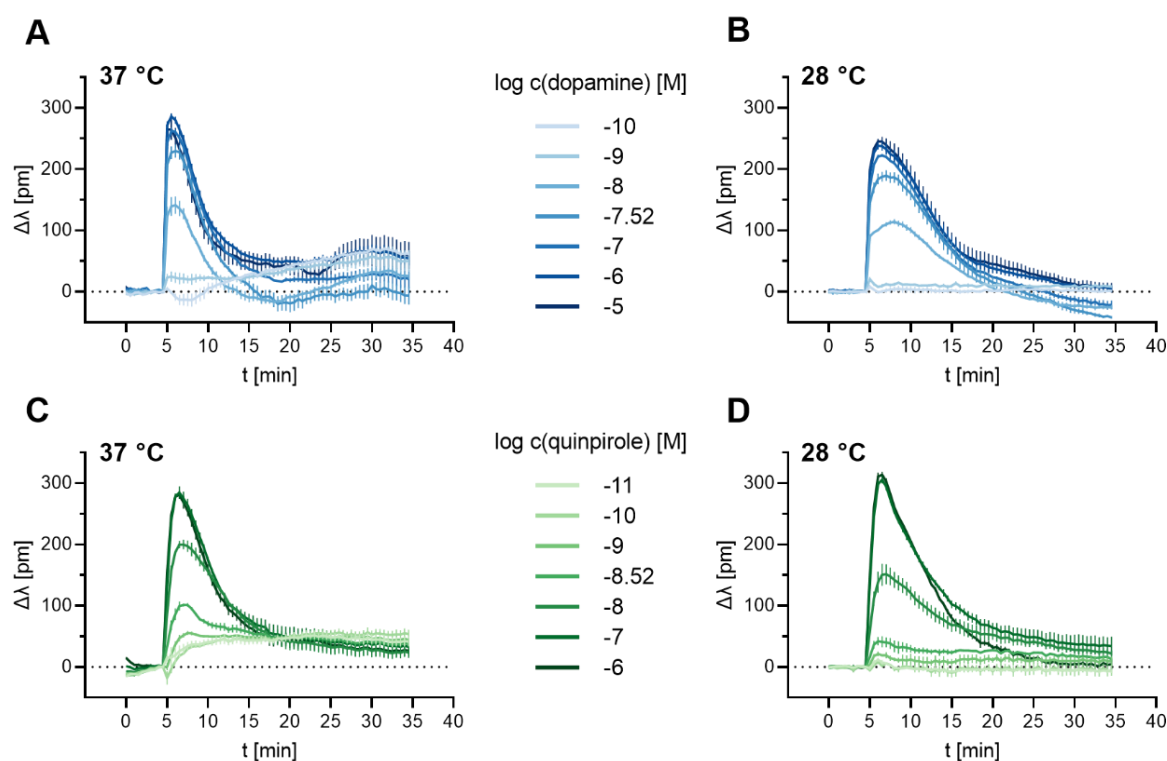
Figure 4.2. Time courses of DMR experiments performed with CHO-K1 D$_{2long}$R cells at 37 °C (**A**, **C**) or 28 °C (**B**, **D**). Cells were stimulated with the indicated concentrations of dopamine (**A**, **B**) or quinpirole (**C**, **D**) (added after 5 min baseline recording) and the wavelength shifts were monitored. Signals were corrected by subtraction of the vehicle control. Experiments were performed using 384-well microplates. Shown are means ± SEM of representative experiments, each performed in triplicate.

addition of the agonist, the microplate was kept in the plate reader for adaptation to the assay temperature and a baseline read was performed. Since the plate reader was not equipped with an automated liquid handling system, the receptor ligands were added manually outside of the device. To keep the temperature change minimal, measurements were performed at 28 °C and the resulting pEC_{50} values, the time point of the peak and the shape of the DMR traces were compared to those obtained from measurements at 37 °C. Temperature has an impact on the fluidity of the cell membrane and it was reported that the mobility of membrane-anchored proteins increases with increasing temperature[33]. As shown in **Figure 4.2**, stimulation of the cells with an agonist results in a rapid shift in wavelength, which subsequently declines to almost the baseline level. In measurements performed at 37 °C (**Figure 4.2A** and **C**), the peak appears already after 0.5 - 2 min, whereas at 28 °C (**Figure 4.2B** and **D**), the kinetics is slightly slower and the maximum wavelength shift is detected after 1.5 - 3.5 min. The temperature decrease from 37 °C to 28 °C did not seem to have another impact on the shape of the DMR traces. To determine pEC_{50} values from the DMR recordings, data were converted to concentration-response curves (CRCs; *cf.* section 4.2.2) shown in **Figure 4.3**. By comparing the obtained pEC_{50} values (**Table 4.1**), it becomes obvious that the potencies determined
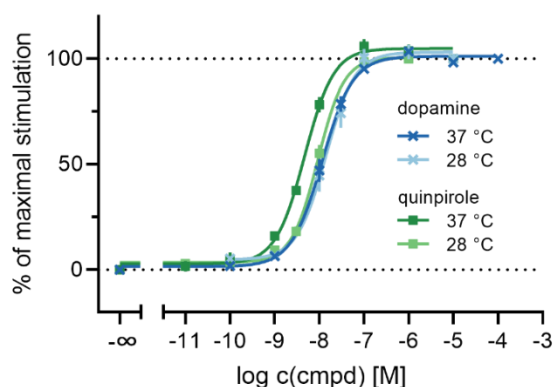

Figure 4.3. Concentration-response curves resulting from DMR recordings at different temperatures. Relative maxima in wavelength shift ($\Delta\lambda_{max}$) are plotted against the logarithmic concentration of the respective agonist. Data were normalized to $\Delta\lambda_{max}$ induced by 100 µM dopamine or 10 µM quinpirole. Data are presented as means ± SEM from three independent experiments, each performed in triplicate.

in experiments at 28 °C are lower than those obtained from experiments at 37 °C. To test for statistical significance, a t-test was performed and *p*-values < 0.05 were considered to indicate statistical significance. In the case of quinpirole, the pEC_{50} values obtained from measurements at different temperatures were significantly different (*p* = 0.03), whereas the pEC_{50} values determined for dopamine were not (*p* = 0.981). The results obtained for quinpirole indicate an impact of the assay temperature on the determined potencies. However, the rapid appearance of the peak may pose a problem when working without an automated liquid handling system (manual compound addition) as the addition of the compounds and starting the final read could take too long. Additionally it was

demonstrated that membranes of live cells do not show phase transitions within a wide range of temperatures (14-37 °C)[33]. Therefore, all subsequent experiments were performed at 28 °C. Furthermore, due to other technical reasons, the following experiments were conducted with 96-well instead of 384-well plates.

Table 4.1. pEC$_{50}$ values determined by DMR measurements performed with CHO-K1 hD$_{2long}$R cells at different temperatures.

cmpd.	pEC$_{50}$ ± SEM	
	37 °C	28 °C
dopamine	7.95 ± 0.18	7.87 ± 0.15
quinpirole	8.34 ± 0.04	8.03 ± 0.06

Data represent means ± SEM from three independent experiments, each performed in triplicate.

Another parameter investigated during the establishment of the assay was the cell density. Cells were seeded at densities of 72,000, 54,000 or 36,000 cells/well into a 96-well plate and the DMR response upon stimulation with quinpirole was recorded (**Figure 4.4A**). Concentration-response curves were constructed (**Figure 4.4B**) and the resulting signal heights and pEC$_{50}$ values were compared. As can be seen in **Figure 4.4A**, the different cell densities did not have an obvious impact on the maximal observed wavelength shift. The pEC$_{50}$ values (**Table 4.2**) obtained from CRCs (**Figure 4.4B**) decreased slightly with an increasing cell density. For statistical analysis, the potencies were compared by a one-way ANOVA with Bonferroni's correction for multiple comparisons and revealed a significant difference only between values obtained from assays with 36,000 and 72,000 seeded cells/well ($p < 0.05$). For all subsequent experiments, cells were seeded at a density of 54,000 cells/well since this led to 80-90% confluency after about 24 h of incubation.
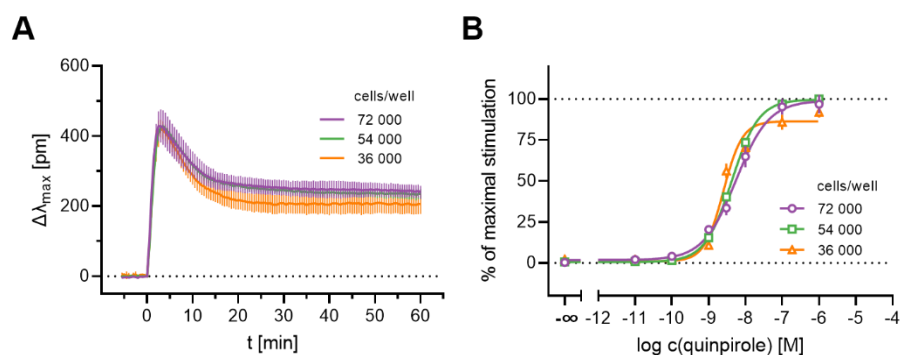
Figure 4.4. Influence of the density of seeded CHO-K1 D$_{2long}$R cells on the quinpirole induced response. (**A**) DMR recordings of CHO-K1 D$_{2long}$R cells stimulated with 1 µM quinpirole. Data show one representative experiment performed in triplicate. (**B**) Concentration-response curves of quinpirole derived from DMR measurements at different cell densities. Data are presented as means ± SEM from three independent experiments, each performed in triplicate.

Table 4.2. pEC$_{50}$ values of quinpirole (D$_{2long}$R) determined by DMR measurements with varying cell densities.

seeded cells/well	pEC$_{50}$ ± SEM (EC$_{50}$, nM)
36,000	8.58 ± 0.03 (6.0)
54,000	8.38 ± 0.04 (4.3)
72,000	8.25 ± 0.08 (2.7)

Data are presented as means ± SEM of three independent experiments, each performed in triplicate.

4.2.2   Characterization of reference ligands

After having determined the assay conditions for DMR measurements, concentration-response relationships of well-characterized reference DR agonists and antagonists were studied. The following agonists were investigated: the endogenous agonist dopamine, the full agonist quinpirole, pramipexole, a drug commonly employed in the treatment of Parkinson's disease[34], *R*-(-)-apomorphine, also a known Parkinson's therapeutic[35] described as partial agonist[36], and aripiprazole, which is considered a prototype for third generation antipsychotics[37,38]. Quinpirole was used as reference agonist for defining the efficacies of the compounds as it exhibits higher chemical stability compared to dopamine, as described in chapter 3 (section 3.2.2). A representative recording of the quinpirole induced change in wavelength shift from experiments performed with CHO-K1 hD$_{2long}$R cells is shown in **Figure 4.5.** The stimulation of the cells with quinpirole elicited a positive
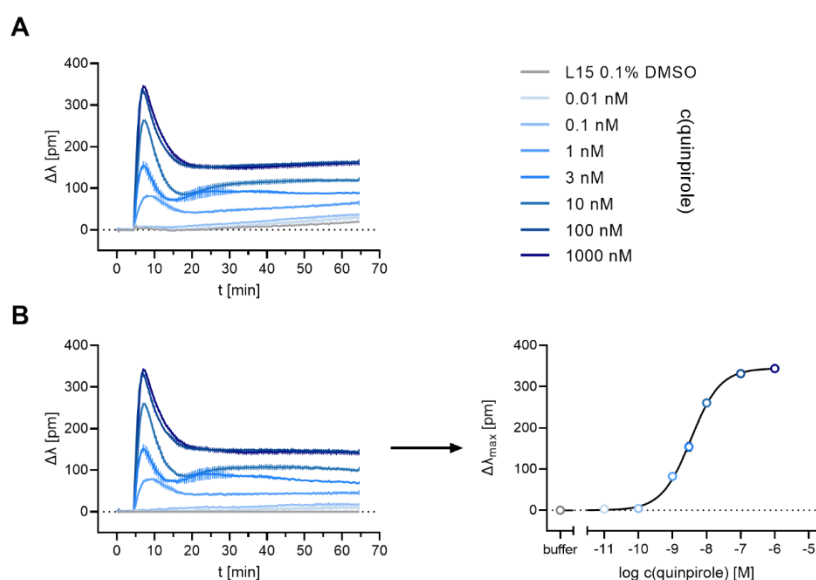
Figure 4.5. Quinpirole induced responses of CHO-K1 hD$_{2long}$R cells recorded by DMR and corresponding concentration-response curve. (**A**) Representative time courses of the change in wavelength shift after stimulating the CHO-K1 hD$_{2long}$R cells with quinpirole at various concentrations (performed in triplicate). The measurement was performed at 28 °C in a 96-well microplate. (**B**) DMR traces from **A** corrected for the vehicle control and concentration-response curves generated by plotting the maximum change in wavelength shift (Δλ$_{max}$; pm) against the logarithmic concentration of quinpirole. Data are shown as mean ± SEM.

concentration dependent DMR signal (**Figure 4.5A**). Under the applied conditions, the observed change in wavelength shift increased rapidly, reached a peak at about 3 min, followed by a rapid decline and stabilization as a plateau above the baseline level. Comparable kinetic DMR profiles have been reported for other $G_{i/o}$ coupled receptors expressed in CHO cells, such as the serotonin 5-HT$_{1B}$ receptor[39], the dopamine D$_3$ receptor[40] or the muscarinic M$_2$ receptor[41]. As the DMR traces displayed clear maxima, the maximum change in wavelength shift ($\Delta\lambda_{max}$; pm) was used to construct concentration-response curves (**Figure 4.5B**). Data fitting according to a four-parameter logistic equation (*cf.* Materials and Methods 4.3.5) afforded potencies (pEC$_{50}$ values) and efficacies (E$_{max}$) of the investigated D_{2long}R agonists (**Table 4.3**).

All agonists induced a positive DMR response in a concentration-dependent manner (**Figure 4.6**), from which CRCs could be constructed (**Figure 4.9A**). Quinpirole, dopamine and pramipexole appeared as full agonists in the DMR assay, yielding pEC$_{50}$ values of 8.48, 8.17 and 8.71, respectively (**Table 4.3**). There are only little reports on the application of the DMR technique to D_{2long} receptors, but Brust et al.[42] determined data for dopamine and pramipexole (EC$_{50}$ values of 11 nM and 8.7 nM for dopamine and pramipexole, respectively) that were in very good agreement with data obtained in present study. *R*-(-)-Apomorphine, which was reported to be a partial D$_2$R agonist in a [^{35}S]GTPγS binding assay (E$_{max}$ = 53%[36] or 90%[43] relative to dopamine, pEC$_{50}$ = 7.66[36] or 6.76[43]), appeared as full agonist in the DMR
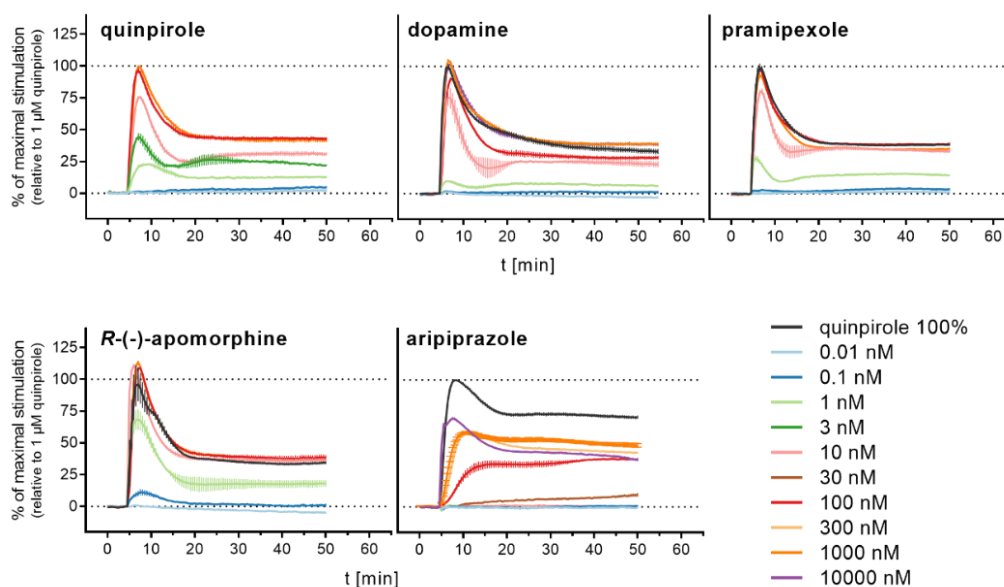
Figure 4.6. Representative DMR time courses of the concentration-dependent change in wavelength shift ($\Delta\lambda$; pm) induced by addition of the indicated reference agonists to CHO-K1 hD$_{2long}$R cells. Data were normalized to the maximum wavelength shift induced by 1 µM quinpirole (100%) and a buffer control (0%). Shown are data (means ± SEM) from representative experiments out of three independent experiments, each performed in triplicate.

assay with a high potency of 0.6 nM. Aripiprazole acted as partial agonist in the DMR assay yielding an efficacy of 62% and a pEC_{50} value of 6.44, which was in good agreement with reported data (pEC_{50} = 6.23, obtained by conversion of the reported EC_{50} value, determined in a DMR assay)[42].

A selection of D_2 receptor antagonists were studied for their ability to inhibit the quinpirole-induced DMR response mediated by the $hD_{2long}R$, confirming the specificity of the response. The investigated antagonists were the antipsychotics haloperidol, nemonapride, S-(-)-sulpiride and the antiemetic drug domperidone. All four compounds, added 8 min after the addition of the agonist, antagonized the quinpirole induced DMR response in a concentration-dependent manner and comparable kinetic DMR traces were observed. Representative DMR time courses are shown in **Figure 4.7**. Higher concentrations of the antagonists led to a steep negative DMR response below the baseline level (ca. −90%), which was reached after about 18 min. Subsequently, the DMR traces ascended slowly
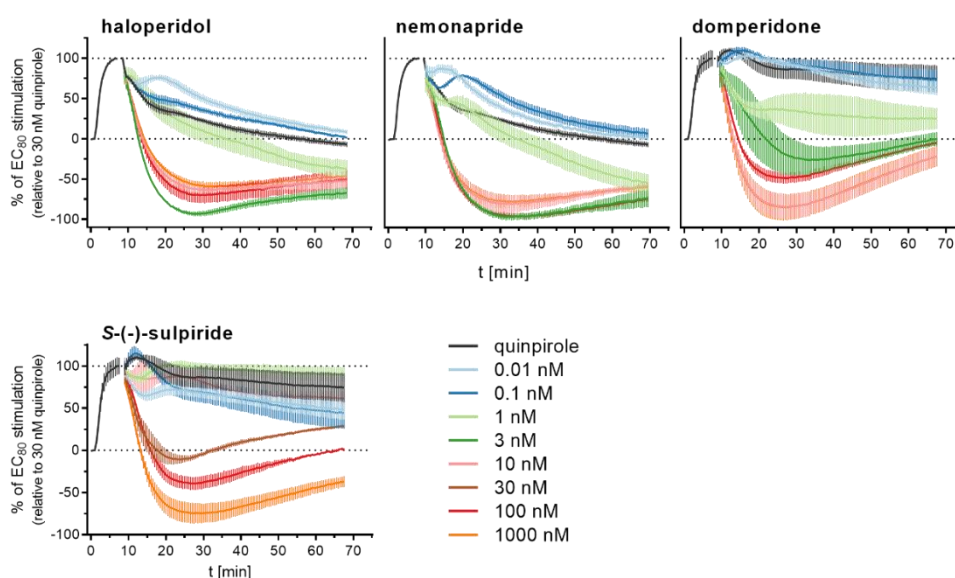

Figure 4.7. Inhibition of the quinpirole-induced DMR response by selected dopamine receptor antagonists. CHO-K1 $hD_{2long}R$ cells were stimulated with quinpirole at a concentration eliciting 80% of the maximal response (30 nM) and the DMR signal was recorded for 8 min followed by the addition of varying concentrations of the indicated antagonist. Data were normalized to the maximum wavelength shift induced by 30 nM quinpirole (100%) and a buffer control (0%). Shown are means ± SEM of representative experiments performed in triplicate, out of at least three independent experiments.

during the remaining recording. Lower concentrations of antagonists resulted in a less steep decline of the DMR traces. As will be shown in section 4.2.4, a negative DMR signal can result from activation of the adenylyl cyclase and increase in intracellular cAMP. Similar DMR traces were also observed for the G_i-coupled muscarinic M_2 receptor, expressed in Flp-In CHO cells[28]. As demonstrated in **Figure 4.8**, preincubation of the cells with the antagonists for 30 min prior to the addition of the agonist quinpirole resulted in time
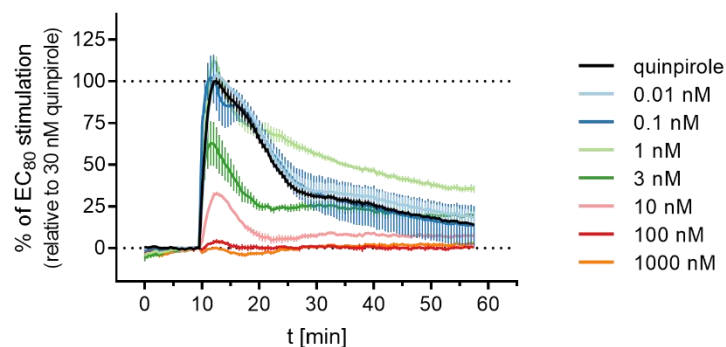
Figure 4.8. Exemplary DMR recording of haloperidol studied in antagonist mode. Before the addition of quinpirole at a concentration eliciting 80% of the maximal response (30 nM), the cells were incubated with varying concentrations of haloperidol for 30 min. Data were normalized to the maximum wavelength shift induced by 30 nM quinpirole (100%) and a buffer control (0%). Data represent means ± SEM from three independent experiments, each performed in triplicate.

courses consisting entirely of positive signals. Hence, this kind of antagonist mode allowed the construction of concentration-response curves (**Figure 4.9B**). The observed responses from experiments involving antagonists were less stable compared to the measurements with agonists and the wavelength shifts showed larger variations within individual triplicates (*cf*. **Figures 4.6** and **4.7**). The inhibition curves obtained from the measurements with antagonists displayed Hill Slopes partially deviating strongly from unity (from -1.18 for *S*-(-)-sulpiride to -1.95 for nemonapride). Therefore, the typically used Cheng-Prusoff equation was considered inappropriate for the calculation of K_b values and a "more general" modified Cheng-Prusoff equation defined by Leff and Dougall[44], that takes the Hill coefficient into account, was used to convert IC$_{50}$ values to K_b values (as described in Material and Methods, 4.3.5). The obtained pK_b values are shown in **Table 4.3**. Unfortunately, no reference data of the studied dopamine D$_2$ receptor antagonists obtained from DMR measurements were found in the literature for comparison.

All investigated D$_{2long}$R ligands were tested for off-target activity in untransfected CHO-K1 cells. As shown in **Figure A8** (Appendix) none of the agonists induced a DMR response in these cells. Regarding the antagonists, only nemonapride and haloperidol induced a slight negative DMR response.
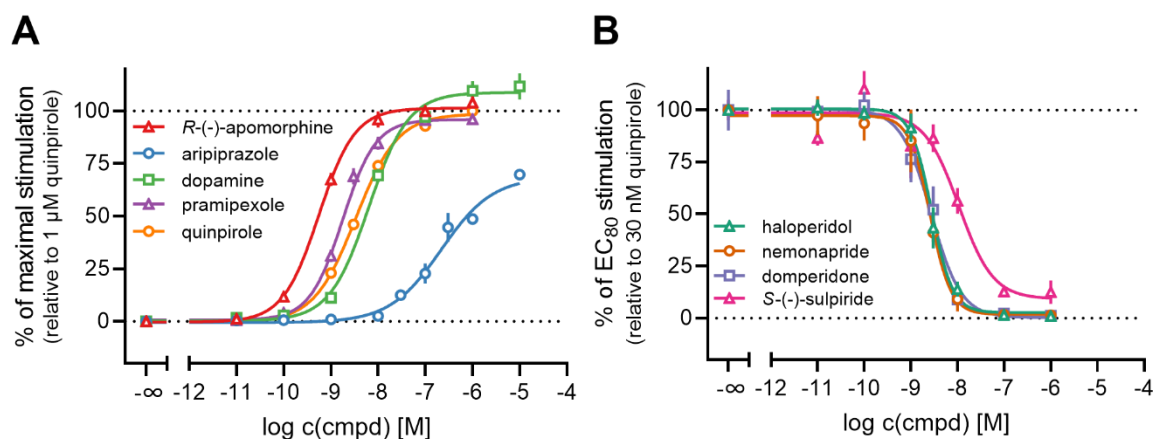
Figure 4.9. Characterization of a set of reference DR agonists (**A**) and antagonists (**B**) in the DMR assay. CHO-K1 hD$_{2long}$R cells were treated with varying concentrations of the indicated ligands and the DMR signal was recorded over a time-course of 60 min. The maximum wavelength shift ($\Delta\lambda_{max}$) was used to construct concentration-effect curves. In agonist mode (**A**), the response was normalized to a solvent control (0%) and the maximum response induced by 1 µM quinpirole (100%). In antagonist mode (**B**), the cells were preincubated with various concentrations of antagonist for 30 min before quinpirole was added at concentration (30 nM) that induces the response equal to 80% of the maximal response induced by 1 µM of quinpirole. The response was normalized to a solvent control (0%) and the response induced by 30 nM quinpirole (100%). Data represent means ± SEM of three independent experiments, performed in triplicate.

Table 4.3. pEC$_{50}$ and E$_{max}$ values of D$_2$R agonists and pK_b values of D$_2$R antagonists from DMR studies at CHO-K1 hD$_{2long}$R cells.

compound	pEC$_{50}$ ± SEM (EC$_{50}$, nM)	% E$_{max}$	N	pK_b ± SEM (K_b, nM)	N
quinpirole	8.48 ± 0.05 (3.4)	100	9		
dopamine	8.17 ± 0.10 (7.4)	110 ± 9	3		
pramipexole	8.71 ± 0.08 (2.0)	97 ± 0.1	3		
R-(-)-apomorphine	9.25 ± 0.09 (0.60)	102 ± 5	3		
aripiprazole	6.44 ± 0.13 (300)	62 ± 10	3		
haloperidol				9.17 ± 0.06 (0.71)	4
nemonapride				9.24 ± 0.13 (0.66)	3
domperidone				9.16 ± 0.20 (0.93)	3
S-(-)-sulpiride				8.82 ± 0.23 (2.3)	3

Data are presented as mean ± SEM determined in *N* independent experiments, each performed in triplicate.

4.2.3   Comparison of the data derived from DMR measurements with results from conventional assays

The results from the holistic DMR readout were compared with data obtained from radioligand binding and β-arrestin2 recruitment assays, which were described in chapters 2 and 3, respectively, as well as with data from a mini-G protein recruitment assay. Structures of the investigated ligands are given in **Figure 1.3** in the general introduction. The mini-G protein recruitment assay was developed by Höring et al.[45] for all four histamine receptor subtypes and was adapted to the dopamine hD$_{2long}$ receptor for this study. The mini-G$_i$ protein is derived from the GTPase domain of the Gα$_s$ subunit, where mutations were introduced to change its coupling specificity to that of Gα$_{i1}$ (mGsi)[46]. The assay is based on the split-luciferase complementation technique, employing an engineered luciferase from a deep-sea shrimp, the NanoLuc (NLuc)[47], to monitor the mini-G$_i$ recruitment to the receptor (leading to reconstitution of the NLuc) upon activation of the receptor with an agonist. Kinetic profiles of the mini-G$_i$ recruitment to the D$_{2long}$R are shown in **Figure A9** (Appendix).

In the case of the agonists quinpirole, dopamine and pramipexole, the pEC$_{50}$ values obtained from β-arrestin2 recruitment and mini-G$_i$ recruitment assays matched well with each other, showing a trend toward slightly higher potencies in the β-arrestin2 assay (**Table 4.4**). In the radioligand competition binding assay, binding constants for a high-affinity and a low-affinity binding state of the receptor were obtained for these agonists. When comparing the pK_{iH} and pK_{iL} values with the potencies obtained in the different functional assays, including DMR measurements, it appears that the pEC$_{50}$ values correlate better with the K_i-values for the high-affinity state (**Table 4.4**). This was in good agreement with the different reports on the high-affinity state of the D$_{2long}$ receptor being the functionally relevant state, as already mentioned in chapter 2. The concentration-response curves as well as the radar chart (**Figures 4.10A+B**) show that the potencies determined in DMR measurements are higher compared to potencies obtained from the pathway specific functional assays. The intrinsic activities exhibited by these agonists in the different assays were also highest for the DMR assay (**Figures 4.10A+C**). It has been reported that the sensitivity of DMR can be higher compared to traditional assays[41] and DMR represents the most distal readout among the applied assays, therefore, the response can be highly amplified. However, it must be kept in mind that DMR measurements were performed with CHO cells, whereas competition binding, β-arrestin2 and mini-G$_i$ recruitment were determined using HEK293T cells. Different cell populations of different cellular background can exhibit varying efficiencies in transducing signals and amplifying receptor stimuli[48,49] and potencies and intrinsic activities can depend on receptor density[50]. Ideally, for comparison of readouts obtained from different technologies, cells with an identical genetic background should be used. Therefore, the higher potencies and efficacies observed in the DMR assay could also be attributed to the different cell type or could arise from a combination of the different factors. The rank order of potencies

(pramipexole > quinpirole > dopamine) was the same in the "conventional" assays (focused on specific readouts) and the holistic technique.

R-(-)-Apomorphine, which was reported to act as $D_{2long}R$ partial agonist in a $[^{35}S]GTP\gamma S$ binding assay (*cf*. section 4.2.2), exhibited efficacies of a full agonist in the mini-G_i recruitment and the DMR assay and appeared as partial agonist only in the β-arrestin2 recruitment assay (**Figure 4.10**, **Table 4.4**). With pEC$_{50}$ values of 7.81 and 7.13 determined in the β-arrestin2 and the mini-G_i assay, respectively, the potencies are in the same range as the pK_i of 7.33 determined by radioligand competition binding. Measuring the R-(-)-apomorphine induced DMR yielded a markedly higher potency, a pEC$_{50}$ value of 9.25. The higher potency of R-(-)-apomorphine determined in the DMR assay compared to the other assays could emerge from amplification of the response due to the distal readout, as already mentioned above. However, it should be questioned whether this is an adequate explanation for such a considerably higher potency determined by DMR measurements, especially with regard to lower discrepancies found for the other agonists. Since R-(-)-apomorphine did not elicit a DMR signal in untransfected CHO-K1 cells, as shown in **Figure A8** (Appendix), it is unlikely that the observations result from stimulating other $G\alpha_{i/o}$-coupled GPCRs that bind R-(-)-apomorphine with moderate to high affinity (e.g. adrenergic α_{2A-C}-receptors or the 5-HT$_{1A}$-receptor[35]) and are potentially expressed in CHO cells. Therefore, a plausible explanation for the observed high potency of R-(-)-apomorphine in the DMR assay could not be provided in the scope of the present study.

Aripiprazole displayed a high affinity towards the $D_{2long}R$, with a pK_i of 8.08, and pEC$_{50}$ values ranged from 6.44 (DMR measurements) to 7.1 (mini-G_i recruitment assay). Its efficacies ranged from 11% in the β-arrestin2 recruitment to 62% in the DMR assay (**Figure 4.10**, **Table 4.4**). Aripiprazole was reported to be a high affinity partial agonist at the D_2 receptor[51], which is in line with the obtained results.

The data of the antagonists analyzed in the different assays are summarized in **Table 4.5** and concentration-effect curves are shown in **Figure 4.11A**. Generally, antagonistic activities determined in the mini-G_i recruitment, the β-arrestin2 recruitment and the DMR assay were in good agreement. As already observed for the potencies (pEC$_{50}$) of the agonists, a tendency to higher pK_b values in the label-free assay was observed for (+)-butaclamol, domperidone, haloperidol and nemonapride. For these compounds, the affinities determined in radioligand displacement experiments are consistently higher compared to the pK_b values. S-(-)-Sulpiride represented an exception as its affinity (pK_i) was markedly lower compared to the antagonistic activities (pK_b) determined in the "conventional" functional assays and the holistic DMR assay (**Figure 4.11B**). Moreover, in contrast to the other antagonists, the highest pK_b value of S-(-)-sulpiride was obtained in the β-arrestin2 recruitment assay.

However, the pK_b values of this antagonist obtained from the different functional assays were similar, ranging from 8.70 (mini-G$_i$ recruitment assay) to 8.99 (β-arrestin2 recruitment assay.
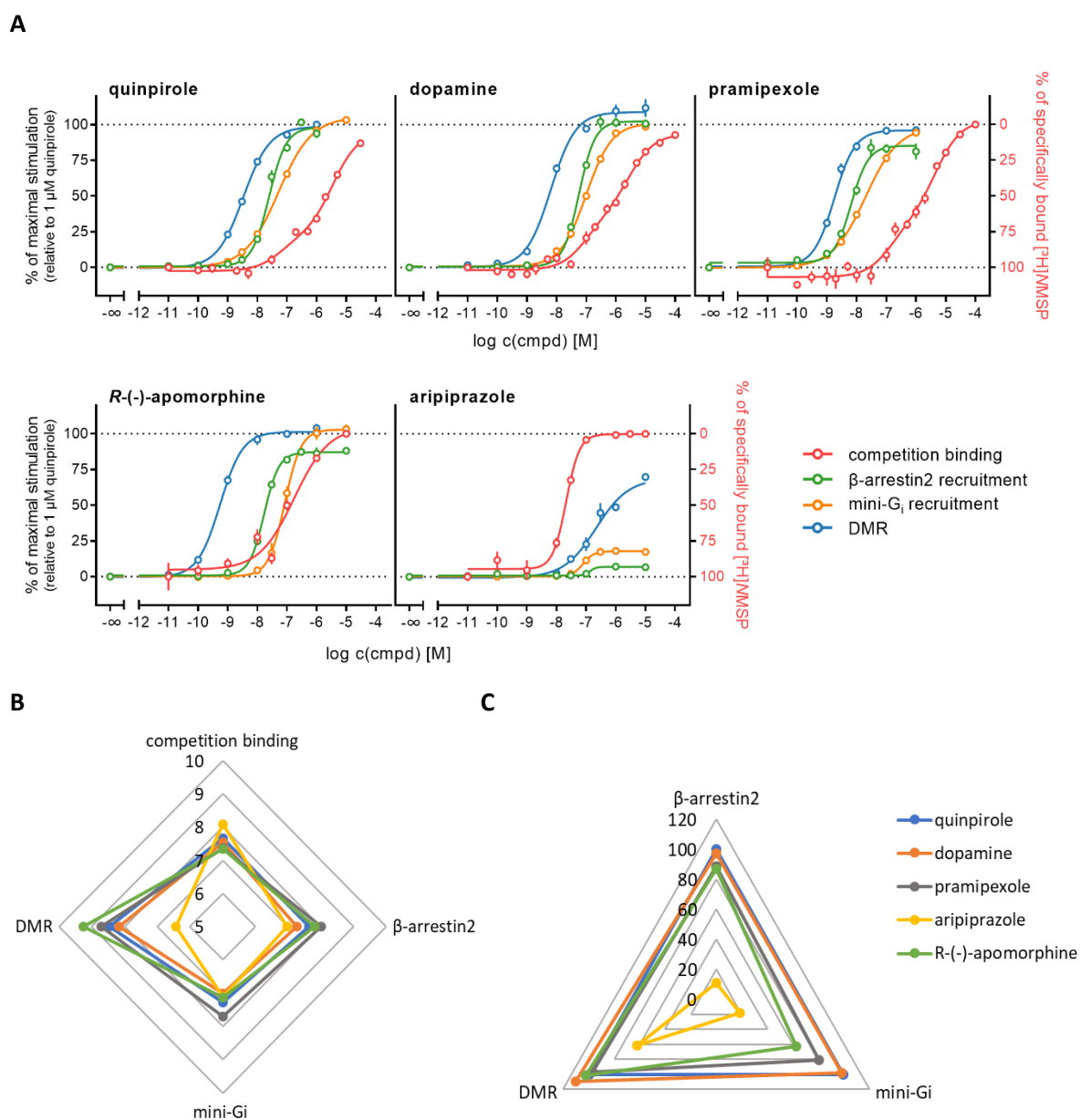
Figure 4.10. Comparative binding and functional data of selected dopamine D$_{2long}$R agonists. **A**: concentration-response curves and competition binding curves from different assay types. The right Y-axis was inverted for illustration purposes. **B**: radar plot presenting pEC$_{50}$ or pK_i values. **C**: radar plot presenting efficacies (%) obtained in the functional assays. Competition binding experiments were performed on homogenates of HEK293T CRE Luc hD$_{2long}$R cells. β-Arrestin2 recruitment assays were performed using whole HEK293T ELucN-βarr2 hD$_{2long}$R-ELucC cells, the mini-G$_i$ recruitment assay was performed with whole HEK293T NlucN-mGsi hD$_{2long}$R-NlucC cells and the DMR measurements were carried out using whole CHO-K1 hD$_{2long}$R cells. Data represent means ± SEM from at least three independent experiments, each performed in triplicate.
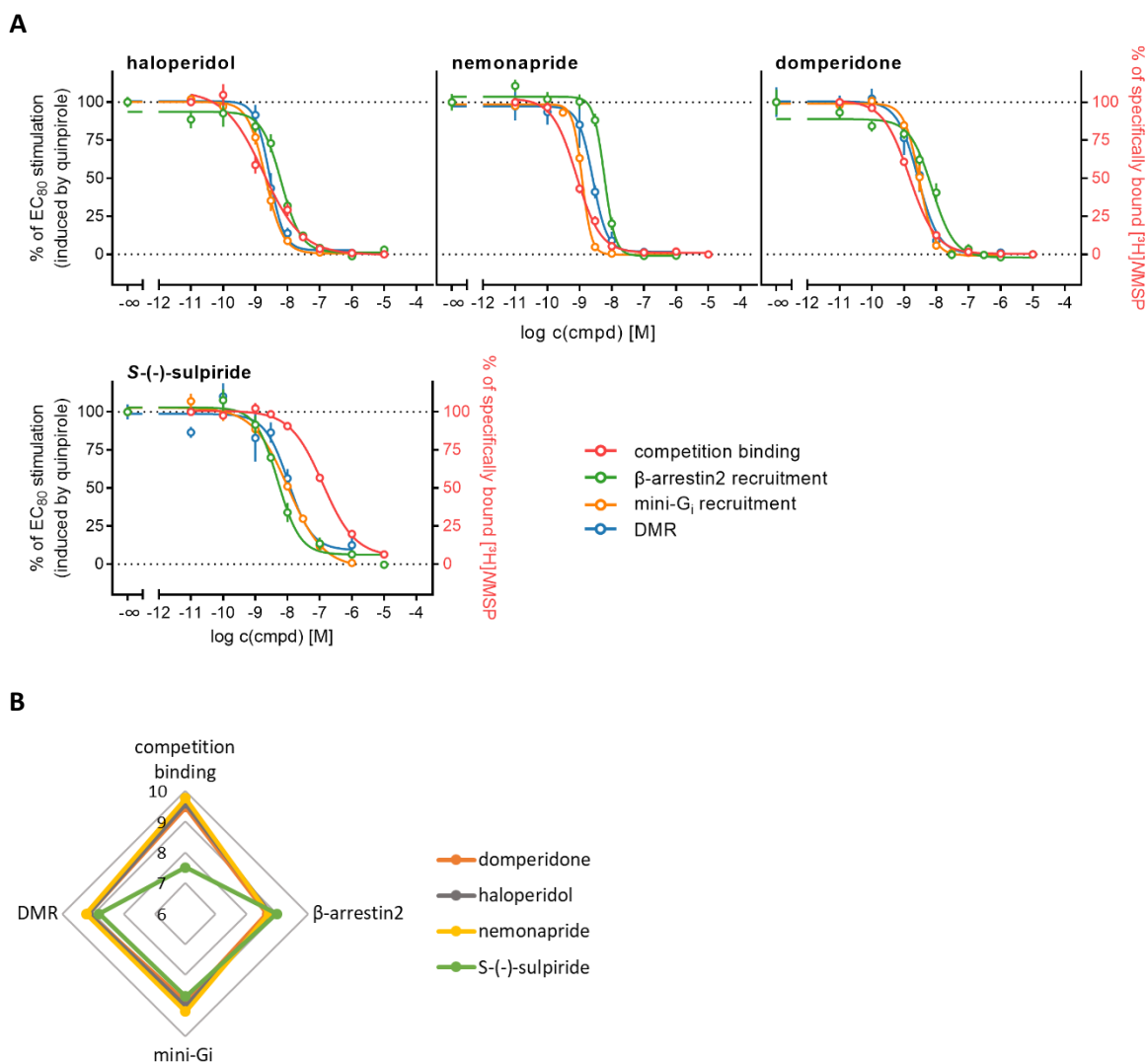
Figure 4.11. Comparative binding and functional data of selected dopamine $D_{2long}R$ antagonists. **A**: inhibition and competition binding curves of selected dopamine $D_{2long}R$ antagonists from different assay types. **B**: radar plot presenting pEC_{50} or pK_i values. Competition binding experiments were performed on homogenates of HEK293T CRE Luc $hD_{2long}R$ cells. β-Arrestin2 recruitment assays were performed using whole HEK293T ELucN-βarr2 $hD_{2long}R$-ELucC cells, the mini-G_i recruitment assay was performed with whole HEK293T NlucN-mGsi $hD_{2long}R$-NlucC cells and the DMR measurements were carried out using whole CHO-K1 $hD_{2long}R$ cells. Data were normalized to the response induced by quinpirole at concentrations of 100 nM (β-arrestin2 recruitment), 150 nM (mini-G_i recruitment) or 30 nM (DMR). Data represent means ± SEM from at least three independent experiments, each performed in triplicate.

Table 4.4. D_{2long}R affinities (pK_i values) of D_2R agonists determined in competition binding assays as well as potencies (pEC_{50} values) and efficacies (E_{max}) determined in different functional assays.

compound	competition binding		β-arrestin2 recruitment		mini-G_i recruitment		DMR	
	pK_{iH} or pK_i	pK_{iL}	pEC_{50}	E_{max} (%)	pEC_{50}	E_{max} (%)	pEC_{50}	E_{max} (%)
quinpirole	7.66 ± 0.10	5.87 ± 0.02	7.65 ± 0.08	100	7.29 ± 0.06	100	8.46 ± 0.05	100
dopamine	7.53 ± 0.21	5.96 ± 0.10	7.28 ± 0.04	97 ± 3.3	7.01 ± 0.10	99 ± 3.5	8.17 ± 0.10	110 ± 9.0
pramipexole	7.35 ± 0.12	5.76 ± 0.03	8.01 ± 0.15	89 ± 3.8	7.71 ± 0.08	96 ± 0.9	8.71 ± 0.08	97 ± 0.1
aripiprazole	8.08 ± 0.02	-	6.96 ± 0.13	11 ± 1.3	7.10 ± 0.05	17 ± 1.0	6.44 ± 0.13	62 ± 10
R-(-)-apomorphine	7.33 ± 0.13	-	7.81 ± 0.03	87 ± 4.2	7.13 ± 0.12	102 ± 0.8	9.25 ± 0.09	102 ± 5.0

Data are presented as mean ± SEM from at least three independent experiments, each performed in triplicate.

Table 4.5. D_{2long}R affinities (pK_i values) of D_2R antagonists determined in competition binding assays and pK_b values determined in different functional assays.

compound	competition binding	β-arrestin2 recruitment	mini-G_i recruitment	DMR
	pK_i	pK_b	pK_b	pK_b
(+)-butaclamol	9.14 ± 0.06	8.17 ± 0.09	8.62 + 0.03	n. d.
domperidone	9.47 ± 0.07	8.66 ± 0.12	8.87 + 0.04	9.16 ± 0.20
haloperidol	9.58 ± 0.13	8.77 ± 0.11	9.03 + 0.12	9.17 ± 0.06
nemonapride	9.76 ± 0.08	8.72 ± 0.03	9.19 + 0.04	9.24 ± 0.13
S-(-)-sulpiride	7.51 ± 0.09	8.99 ± 0.1	8.70 + 0.05	8.82 ± 0.23

Data are presented as mean ± SEM from at least three independent experiments, each performed in triplicate. K_b values were derived by converting IC_{50} values to K_b values according to a modified Cheng-Prusoff equation, as described in Material and Methods, section 4.3.5.

4.2.4   Investigations on the signaling pathway in CHO-K1 $D_{2long}R$ cells by DMR

4.2.4.1   Contributions of $G_{i/o}$, G_s or $G_{q/11}$ proteins to the $D_{2long}R$ mediated DMR response

Aiming at a deconvolution of the response pattern of CHO-K1 $hD_{2long}R$ cells observed in DMR measurements, distinct components of the signaling cascade were silenced using different pharmacological tools. For these studies, the cellular response was elicited by the D_2R agonist quinpirole. The $D_{2long}R$ couples to G proteins of the $G_{i/o}$ family[12] and it was reported that DMR measures signaling effects downstream of G protein activation[41]. To investigate the contribution of $G_{i/o}$ signaling to the DMR response, the $G\alpha_{i/o}$ protein was blocked with pertussis toxin (PTX), which prevents the interaction of the respective receptor with the G protein by ADP-ribosylation of the $G\alpha$ subunit[52]. Additionally, the effects of masking G_s and G_q signaling with cholera toxin (CTX) and the depsipeptide FR900359, respectively, were examined. CTX, like PTX, is an ADP-ribosylating toxin which inhibits the GTPase activity of $G\alpha_s$ and thus transforms the $G\alpha_s$ subunit into a permanently active state[53]. FR900359 suppresses $G\alpha_q$ signal transduction by inhibiting the dissociation of GDP from the $G\alpha$ subunit[54]. The effects of these compounds on quinpirole induced DMR responses in CHO-K1 $hD_{2long}R$ cells and the derived potencies and efficacies are shown in **Figure 4.12** and **Table 4.6**. As expected, the application of PTX resulted in a concentration-dependent decrease in the DMR response (**Figure 4.12A**), identifying $G_{i/o}$ proteins as the main elicitor of the observed response. Increasing the PTX concentration from 5 ng/mL to 10 ng/mL did not lead to a further suppression of the DMR signal, as can be seen in **Figure 4.12A**. The remaining maximal effect of quinpirole observed in the presence of 10 ng/mL PTX was 6% (**Table 4.6**), which was significantly different from zero (one-tailed t-test, $p < 0.05$). A slight rightward shift of the concentration-response curves of quinpirole appeared in the presence of increasing concentrations of PTX, resulting in decreasing pEC_{50} values (**Figure 4.12B**, **Table 4.6**). Masking G_s proteins with CTX led to an apparent increase in quinpirole efficacy (*cf*. section 4.2.4.2) without markedly shifting the concentration-response curves (**Figures 4.12C+D**, **Table 4.6**). As expected, the inhibition of the G_q protein with FR900359 did not show a pronounced effect on the quinpirole induced DMR response at any of the applied concentrations (**Figure 4.12E**). These results supported the hypothesis that the observed DMR signal after stimulation of the cells with quinpirole is triggered by $G\alpha$ proteins of the $G_{i/o}$ family and that $G\alpha_s$ and $G\alpha_q$ subunits do not considerably contribute to the response. PTX, CTX or FR900359 on their own did not induce a DMR response in CHO-K1 $hD_{2long}R$ cells (Appendix, **Figure A10**).
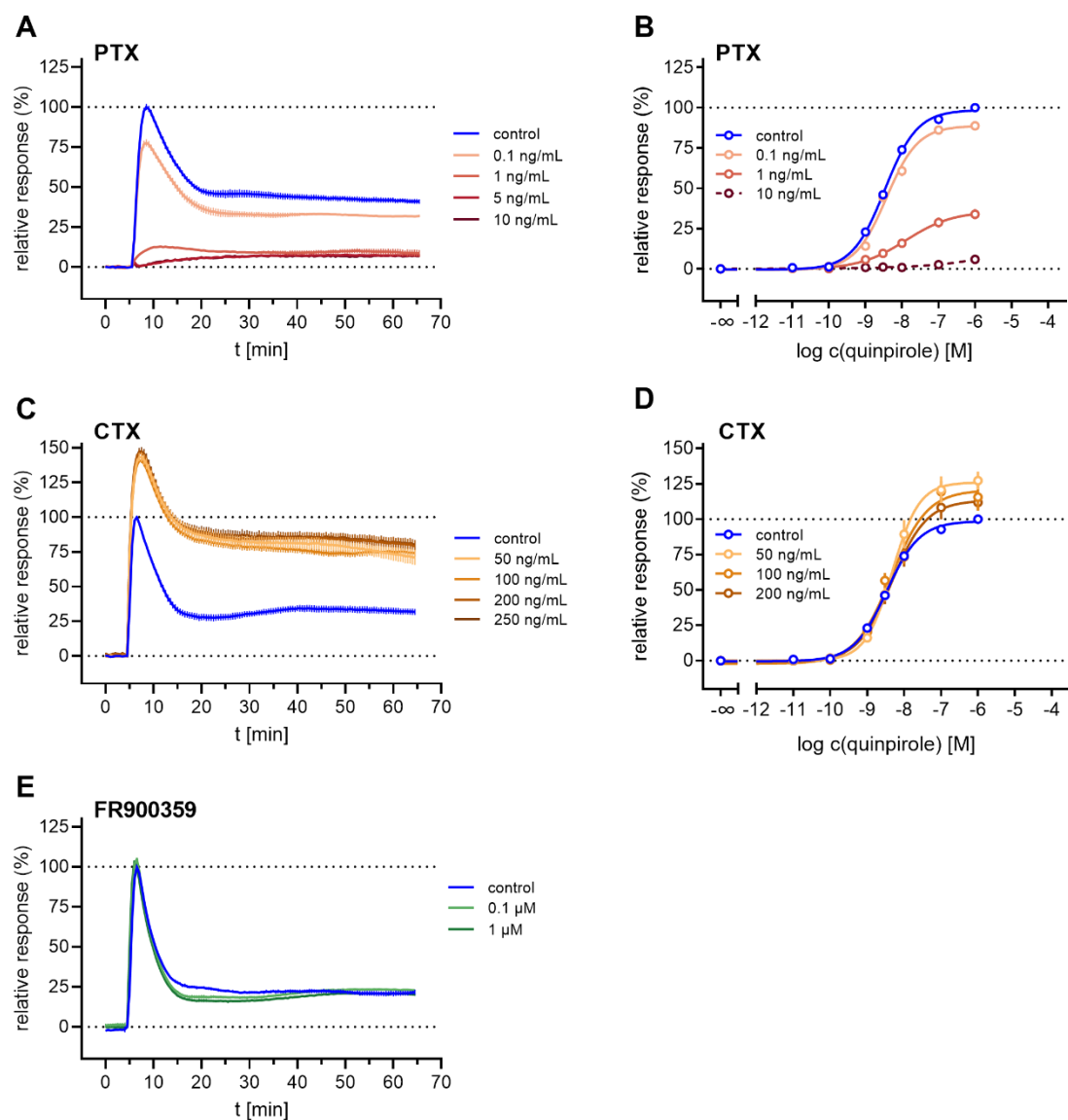
Figure 4.12. Effects of PTX, CTX and FR900359, capable of silencing G$_{i/o}$, G$_s$ and G$_q$ signaling, respectively, on the quinpirole induced DMR response in CHO-K1 hD$_{2long}$R cells. **A,C,E**: representative recordings of the quinpirole (1 µM) induced response of untreated cells (control) and cells pretreated with pertussis toxin (PTX) (**A**), cholera toxin (CTX) (**C**) or FR900359 (**E**). Data were normalized to the maximum change in wavelength shift induced by quinpirole (1 µM) observed in untreated CHO-K1 hD$_{2long}$R cells (100%) and a buffer control (0%). **B**: concentration-response curves of quinpirole resulting from DMR measurements in the absence (control) or presence of PTX at different concentrations. Cells were pretreated with PTX for about 20 h. **D**: concentration-response curves of quinpirole resulting from DMR measurements in the absence (control) or presence of CTX at different concentrations. Cells were pretreated with CTX for about 20 h. In the case of blocking G$_q$ signaling by FR900359 (**E**), cells were incubated with FR900359 for 2 h before the addition of quinpirole and subsequent measurement. Data in **B** and **D** represent means ± SEM of three independent experiments, each performed in triplicate.

Table 4.6. Potencies of quinpirole determined at CHO-K1 hD$_{2long}$R cells by DMR in the presence of pertussis toxin (PTX) or cholera toxin (CTX).

		pEC$_{50}$ ± SEM	% E$_{max}$ ± SEM
PTX	control	8.46 ± 0.05	100
	0.1 ng/mL	8.43 ± 0.05	89 ± 4
	1 ng/mL	7.88 ± 0.07	34 ± 5
	10 ng/mL	-	6 ± 1
CTX	control	8.46 ± 0.05	100
	50 ng/mL	8.36 ± 0.06	130 ± 10
	100 ng/mL	8.32 ± 0.13	130 ± 16
	200 ng/mL	8.34 ± 0.13	110 ± 9

Data are presented as mean ± SEM from three independent experiments, each performed in triplicate.

4.2.4.2   *Effect of elevated adenylyl cyclase activity on the D$_{2long}$R-mediated DMR response*

An increase in quinpirole efficacy, observed after treating the hD$_{2long}$R expressing CHO-K1 cells with CTX, was also found when the cells were incubated with forskolin before the addition of the agonist quinpirole, as shown in **Figure 4.13**. Both agents, CTX and forskolin, lead to an increase in adenylyl cyclase activity and thus to an elevated cellular cAMP level, but via distinct mechanisms. As mentioned above, CTX transfers an ADP-ribosyl residue to the Gα_s subunit, resulting in an inhibition of the GTPase activity of Gα_s, which is thus constitutively active[53]. Consequently, cellular cAMP-levels are elevated[55].
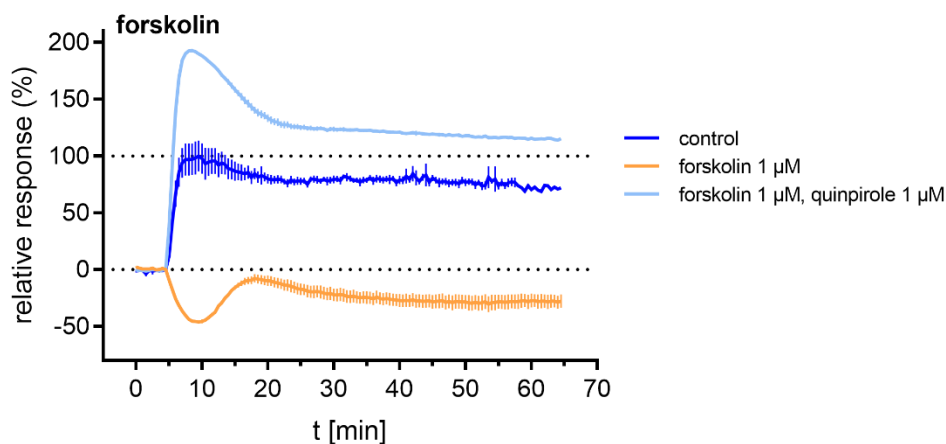

Figure 4.13. Effect of forskolin on the quinpirole-induced DMR response of D$_{2long}$R expressing CHO-K1 cells. The cells were stimulated with quinpirole (1 µM, control) or forskolin (1 µM) alone or incubated with forskolin (1 µM) for 40 min and then stimulated with quinpirole (1 µM). Data were normalized to the maximum change in wavelength shift induced by quinpirole (1 µM) observed in untreated CHO-K1 hD$_{2long}$R cells (100%) and a buffer control (0%). Data shown are means ± SEM of representative recordings performed in triplicate of at least three independent experiments.

Forskolin increases the production of cAMP by directly activating the adenylyl cyclase[56]. It was reported that after prolonged forskolin treatment of D$_{2long}$R expressing Ltk$^-$ cells, quinpirole showed increased

inhibitory efficacy in cAMP accumulation assays[57]. This effect was observed already after 1 h of forskolin treatment[57]. For the same Ltk⁻ cells, it was shown that forskolin treatment for 16 h caused an up-regulation of hD$_{2long}$R expression, due to enhanced cAMP-dependent transcription[58]. Whether treatment of the CHO-K1 hD$_{2long}$R cells with forskolin or CTX resulted in higher receptor expression was investigated by radioligand binding experiments. For this purpose, CHO-K1 hD$_{2long}$R cells were treated with forskolin (1 μM) for 40 min or 20 h or with CTX (100 ng/mL) for 20 h and the binding of [³H]N-methylspiperone (1 nM) was compared to that of untreated CHO-K1 hD$_{2long}$R cells. As shown in **Figure 4.14**, incubating the cells with forskolin for 40 min did not exhibit a marked effect on the receptor expression. However, prolonged treatment with forskolin for 20 h resulted in a strong increase in specific radioligand binding, being in line with the observations reported in the literature[58].
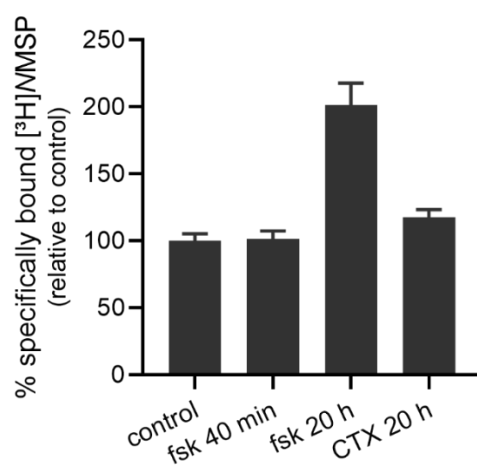

Figure 4.14. Comparison of [³H]N-methylspiperone binding to the hD$_{2long}$R expressed in CHO-K1 cells after treatment with forskolin (fsk) or CTX with [³H]N-methylspiperone binding to untreated cells. Cells were grown over night and treated with forskolin (1 μM) for 20 h or 40 min or with CTX (100 ng/mL) for 20 h. In a 96-well plate, 16 000 cells per well were incubated with [³H]N-methylspiperone (1 nM) for 60 min. Non-specific binding was determined in the presence of (+)-butaclamol (2 μM). Data are normalized to radioligand binding to untreated cells (100%, control) and non-specific binding (0%). Presented are means ± SEM from two independent experiments.

Incubation of the cells with CTX for 20 h exhibited a less pronounced effect but the observed increase in specific [³H]N-methylspiperone binding was significant (p = 0.014, two-tailed t-test), indicating a slight up-regulation of the hD$_{2long}$R. This could account for the increase in wavelength shift depicted in **Figure 4.12C**. However, these results do not explain the marked increase in quinpirole-induced DMR response in CHO-K1 hD$_{2long}$R cells observed after treating the cells with forskolin for 40 min and the underlying mechanisms remain unclear.

Forskolin alone mediated a negative DMR signal (**Figure 4.13**) with a minimum at about 5 min. The signal then increased and reached a plateau below the initial baseline, similar to the forskolin-induced DMR signal reported for CHO-K1 cells[59].

4.2.4.3 Effects of calcium depletion on the hD$_{2long}$R-mediated DMR response

The data shown in **Figure 4.12E** suggested that the Gα$_{q/11}$ protein, mediating a strong increase in cytosolic calcium upon activation[60], is not activated by the D$_{2long}$R. However, it was reported that D$_{2long}$R signaling increases intracellular calcium levels in a neuronal cell line through Gβγ-mediated activation of the phospholipase C resulting in the release of Ca^{2+} from intracellular stores[16]. Whether calcium also played a role in the formation of the quinpirole-induced DMR traces in CHO-K1 D$_{2long}$R cells was investigated by depleting the extra- or both the extra- and intracellular calcium pools. For this purpose, EGTA was added alone or in combination with thapsigargin, a specific inhibitor of the endoplasmic reticulum Ca^{2+}-ATPase[61]. EGTA is a metal ion chelating agent, which cannot permeate the cell membrane and shows higher specificity for Ca^{2+}-ions compared to Mg^{2+}-ions. Complexation of Ca^{2+} by EGTA leads to a Ca^{2+} depletion in the extracellular medium[62]. The combination with the membrane-permeable agent thapsigargin leads to an additional depletion of [Ca^{2+}]$_i$.[63]. Surprisingly, both conditions completely abrogated the quinpirole-induced response of CHO-K1 hD$_{2long}$R cells observed in DMR measurements (**Figures 4.15A+B**). **Figure 4.15C** shows the signal induced by the addition of thapsigargin to the cells equilibrated in EGTA containing assay buffer. A rapidly decreasing negative DMR signal was observed, reaching a plateau after ca. 15 min. The lack of a detectable DMR response under conditions of calcium depletion was further investigated and the changes of [Ca^{2+}]$_i$ after stimulating the hD$_{2long}$R expressed in CHO-K1 cells with quinpirole was explored by performing a Fura-2 calcium assay. Only high concentrations of quinpirole (1 µM and 10 µM) induced a low increase in intracellular Ca^{2+} concentration in CHO-K1 hD$_{2long}$R cells over the buffer control (1.7-fold, *cf*. **Figure A11**, Appendix). For comparison, activation of the muscarinic M$_3$ receptor, a G$_{q/11}$-coupled receptor, results in an about 10-fold increase in intracellular Ca^{2+}-concentration in CHO-hM$_3$R cells as detected by a Fura-2 assay[64]. Consequently, the abrogation of the DMR response by treatment with EGTA and/or thapsigargin must have different underlying mechanisms. A potential effect of Ca^{2+} depletion on the binding of quinpirole to the receptor was considered a possible reason. Therefore, radioligand competition binding experiments were performed in the presence of EGTA (2 mM). However, the results showed that chelation of Ca^{2+} ions by EGTA had no marked effect on the binding of quinpirole to the hD$_{2long}$R. (*cf*. Appendix **Figure A12**).
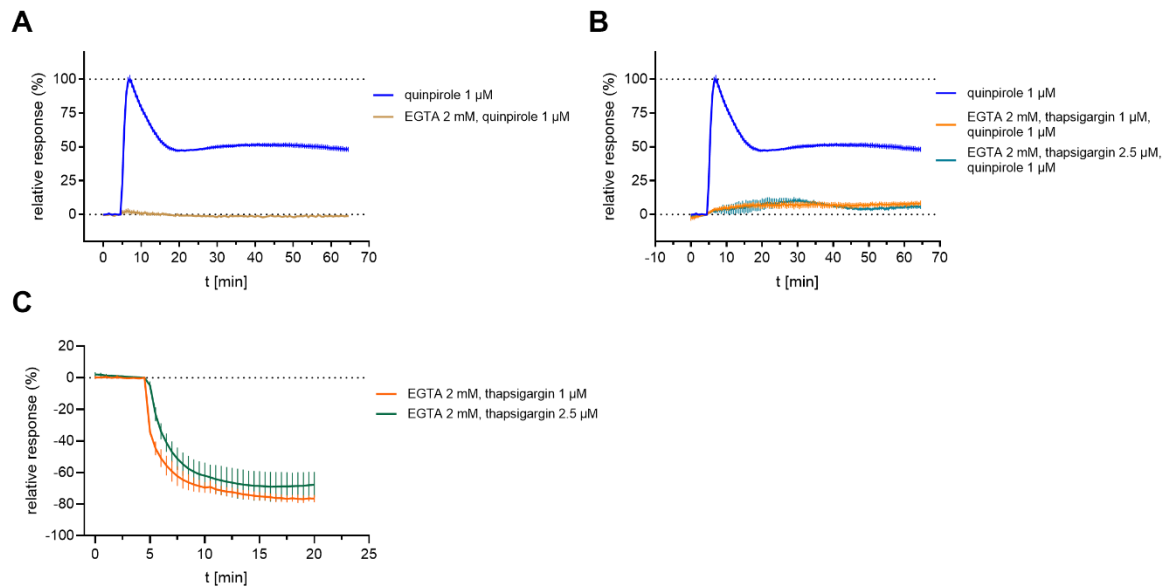
Figure 4.15. Effects of calcium depletion on the quinpirole-induced DMR traces of D$_{2long}$R expressing CHO-K1 cells. **A**: Response induced by quinpirole (1 µM) in the absence or in the presence of EGTA (2 mM) in the assay buffer. **B**: Cells were pre-incubated with thapsigargin (1 µM or 2 µM) for 20 min before the addition of quinpirole (1 µM). EGTA (2 mM) was present in the assay buffer. **C**: Thapsigargin-induced effect on CHO-K1 D$_{2long}$R cells. The assay buffer was supplemented with EGTA (2 mM). In all experiments, after replacement of the medium by the EGTA-containing buffer, cells were allowed to condition in the pre-heated plate reader (28 °C) for 2 h. Data were normalized to the maximum change in wavelength shift induced by quinpirole (1 µM) observed in untreated CHO-K1 hD$_{2long}$R cells (100%) and a buffer control (0%). Data shown are means ± SEM of representative recordings performed in triplicate of three independent experiments.

In conclusion, extracellular or extra- and intracellular depletion of calcium resulted in conditions under which either the hD$_{2long}$R cannot be activated or the hD$_{2long}$R-mediated signaling cannot be detected by DMR measurements. Calcium is a ubiquitous intracellular second messenger[65] which is involved in numerous cellular processes including the modulation of actin[66]. Since the DMR readout is based on actin-dependent cytoskeleton rearrangements or changes in cellular shape, depletion of Ca^{2+} could interfere with the measurement at this level. However, the underlying mechanism leading to a complete abrogation of the quinpirole-induced DMR response remains unclear.

4.3   Materials and Methods

4.3.1   Materials

Dulbecco's modified Eagle's medium/nutrient mixture F-12 Ham (DMEM/F-12) with phenol red, L-glutamine and sodium bicarbonate was purchased from Sigma (Taufkirchen, Germany). Fetal calf serum (FCS), trypsin/EDTA and geneticin (G418) were from Merck Biochrom (Darmstadt, Germany). Fura-2 AM was from Merck Biochrom (Darmstadt, Germany). Leibovitz' L-15 medium (L-15) was from Fisher Scientific (Nidderau, Germany). Pertussis toxin was from Bio-Techne GmbH (Wiesbaden, Germany), FR900359 (UBO-QIC) was purchased from the University of Bonn (Germany) and cholera toxin was from Enzo Life Sciences GmbH (Lörrach, Germany). Thapsigargin was purchased from Tocris Bioscience (Bristol, United Kingdom), EGTA and forskolin were from Sigma-Aldrich GmbH (Taufkirchen, Germany).

4.3.2   Generation of plasmids

Molecular cloning of the plasmids containing the mGsi protein fused to the N-terminal fragment of the NanoLuc (NLucN) and the dopamine $hD_{2long}R$ fused to the C-terminal fragment of the NanoLuc (NLucC) were performed by Carina Höring as described elsewhere[45] with modifications. The human codon-optimized cDNA fragment encoding the mini-Gsi protein was synthesized by Eurofins Genomics (Ebersberg, Germany). Plasmids containing the split-NanoLuc fragments were from Promega (Mannheim, Germany). The cDNA of the $hD_{2long}R$ was kindly provided by Dr. Harald Hübner (Department of Chemistry and Pharmacy, Friedrich-Alexander-University, Erlangen). All cDNAs were amplified by PCR and the mGsi protein, which was fused to the respective split luciferase fragment (NLucN, large NanoLuc fragment), was cloned into a pIRESpuro3 vector (Clontech, Saint-Germain-en-Laye, France) by standard molecular cloning techniques[45]. The $hD_{2long}R$ was cloned into a pcDNA3.1 vector (Thermo Scientific, Nidderau, Germany) via Gibson assembly. The pcDNA3.1 H_1R-NLucC[45] was used as a template. The vector was linearized using standard PCR techniques and the sequence of the human dopamine D_{2long} receptor was amplified and simultaneously, overlaps complementary to the insertion site were attached using specific primers. Subsequently, the receptor was cloned into pcDNA3.1 according to the NEBuilder HiFi DNA Assembly Reaction Protocol (New England Biolabs GmbH, Frankfurt/Main, Germany) resulting in a D_{2long} receptor that is C-terminally fused to the NLucC (small NanoLuc fragment). All sequences were verified by sequencing performed by Eurofins Genomics.

4.3.3   Cell culture

CHO-K1 $hD_{2long}R$ cells[67] were a kind gift from Dr. Harald Hübner (Department of Chemistry and Pharmacy, Friedrich-Alexander-University, Erlangen). These cells were cultured in DMEM/F-12 supplemented with 10% FCS and 600 µg/mL G418 at 37 °C in a water-saturated atmosphere containing

5% CO_2. HEK293T NLucN-mGsi hD_{2long}R-NLucC cells were cultured in DMEM supplemented with 10% FCS, 1 µg/mL puromycin and 600 µg/mL G418 at 37 °C in a water-saturated atmosphere containing 5% CO_2. Cells were routinely tested for mycoplasma contamination using the Venor GeM Mycoplasma Detection Kit (Minerva Biolabs, Germany).

4.3.4   Generation of stable transfectants

Transfection of the HEK293T cells for the mini-G protein recruitment assay was performed by Carina Höring (Lehrstuhl für Pharmazeutische und Medizinische CHemie II, Institut für Pharmazie, Universität Regensburg). HEK293T cells obtained as a gift from Prof. Dr. Wulf Schneider (Institute for Medical Microbiology and Hygiene, Regensburg, Germany) were consecutively transfected with the pIRESpuro3 vector encoding the NLucN-mGsi protein and the pcDNA3.1 plasmid encoding the hD_{2long}R-NLucC fusion protein according to the XtremeGene HP transfection protocol (Merck, Darmstadt, Germany).

4.3.5   Dynamic mass redistribution assay

Dynamic mass redistribution monitoring was performed with an EnSpire multimode reader (Perkin Elmer, Waltham, USA), equipped with the Corning EPIC label-free technology using a resonance waveguide grating (RWG). CHO-K1 hD_{2long}R cells were detached from a 25-cm² flask by trypsinization and centrifuged (22 ± 1 °C, 700 g, 5 min). The pellet was resuspended in DMEM/F-12 containing 10% FCS and the cell density was adjusted to $0.6 \cdot 10^6$ cells/mL. 90 µL of this cell suspension were seeded into 96-well EnSpire label-free sensor plates (cat # 6055408, Perkin Elmer), resulting in 54 000 cells per well. When 384-well plates (cat # 6057408, Perkin Elmer) were used, 50 µL of a cell suspension with a density of $0.32 \cdot 10^6$ cells/mL were seeded, resulting in 16 000 cells per well. Cells were incubated at 37 °C in a humidified atmosphere containing 5% CO_2 overnight. The next day, the culture medium was removed and the cells were gently rinsed with 70 µL (96-well plates) or 30 µL (384-well plates) of serum-free L-15 medium supplemented with 10 mM HEPES and 0.1% DMSO (assay buffer). Subsequently, 90 µL (agonist mode) or 80 µL (antagonist mode) of assay buffer were added per well in the 96-well plates. When 384-well plates were used, 45 µL of assay buffer were added. The cells were incubated in the assay buffer for 2 h in the pre-heated plate reader (28 °C or 37 °C for assay optimization experiments) before a 5 min baseline was recorded. Afterwards, 10 µL (96-well plate) or 5 µL (384-well plate) of compound diluted in assay buffer (10-fold concentrated, 96-well plate) were added and DMR signals were acquired every 30 s for a period of 60 min. The readout is presented as the shift of resonance wavelength over time $\Delta\lambda(t)$, obtained by subtracting the last baseline measurement ($\lambda(0)$) from the raw data of the final read at time t ($\lambda(t)$): $\Delta\lambda(t) = \lambda(t) - \lambda(0)$. Concentration-response curves were constructed by plotting the maximum wavelength shift ($\Delta\lambda_{max}$, pm) against the logarithmic ligand concentrations. The data were normalized to the maximum response induced by

1 μM quinpirole (100%) and the buffer control (0%) and fitted according to a four-parameter logistic equation (log(agonist) vs. response - variable slope, GraphPad Prism 9.0) to obtain EC_{50} values. Means were calculated from individual pEC_{50} values. Data obtained from experiments with antagonists were normalized to the maximum response induced by quinpirole corresponding to the EC_{80} (30 nM; 100%) and the buffer control (0%; L-15, supplemented with 0.1% DMSO) and fitted according to a four-parameter logistic equation(log(inhibitor) vs. response - variable slope, GraphPad Prism 9.0) to obtain IC_{50} values. IC_{50} values were used to calculate K_b values according to a modified Cheng-Prusoff equation, described by Leff and Dougall[44]:

$$K_b = \frac{IC_{50}}{(2+\left(\frac{[QP]}{EC50}\right)^n)^{\frac{1}{n}})-1},$$

where [QP] corresponds to the applied concentration of quinpirole, $[EC_{50}]$ is the concentration of quinpirole producing 50% of the maximal response and n is the Hill coefficient of the concentration-response curve. Means were calculated from individual pK_b values.

4.3.6   Mini-G protein recruitment assay

HEK293T cells coexpressing the $D_{2long}R$-NLucC and the NLucN-mGsi fusion proteins were cultured in 75-cm^2 culture flasks. One day prior to the experiment, cells were detached by trypsinization (0.05% trypsin, 0.02% EDTA in PBS) and centrifuged (800 g, 5 min). Subsequently, the cells were resuspended in L-15 supplemented with 10 mM HEPES (Serva, Heidelberg, Germany) and 5% FCS. The density of the cell suspension was adjusted to $1.25 \cdot 10^6$ cells/mL and 80 μL/well were seeded into a white flat-bottom 96-well microtiter plate (Cat. No. 781965, Brand GmbH + CoKG, Wertheim, Germany). Cells were incubated at 37 °C in a water-saturated atmosphere without additional CO_2 overnight. Shortly before the measurement, the substrate furimazine (Promega, Mannheim, Germany) or coelenterazine h (Biosynth AG, Staad, Switzerland) (2 mM stock) was diluted in L-15 and 10 μL were added to the cells (final dilution of the (delivered) stock: 1:1000). The plate was transferred to a pre-heated (37 °C) EnSpire plate reader (Perkin Elmer Inc., Rodgau, Germany) and the basal luminescence was recorded for 15 min. Then, 10 μL of the agonist serial dilutions were added to the cells (to give a final volume of 100 μL) and luminescence traces were recorded for 45 min (agonist mode). In antagonist mode, the antagonist dilutions were added and the baseline was recorded for 15 min before the reference agonist quinpirole (EC_{80} concentration; 150 nM) was added. Luminescence was captured with an integration time of 0.1 s per well. Data were analyzed using GraphPad Prism 9.0 software (San Diego, CA, USA). The relative luminescence units (RLU) were corrected for (slight) inter-well variation caused by differences in cell density and substrate concentration, as well as for baseline drift, by dividing all data by the mean luminescence intensity of the respective L-15 control. AUCs of the luminescence traces for each concentration were calculated and normalized to the maximum response of 1 μM

quinpirole (100% control) and L-15 (0% control) for the agonists. For normalization of the data obtained for antagonists, the maximum response induced by 150 nM quinpirole (100%) and the buffer control (L-15, 0%) were used. The normalized intensities were plotted against the logarithmic ligand concentrations and the curves were fitted by four-parameter logistic equation (log(c) vs. response – variable slope). The fits yielded pEC_{50} and E_{max} values in the case of agonists, and IC_{50} values in the case of antagonists, which were used to calculate K_b values according to a modification of the Cheng-Prusoff equation, as described in the preceding section (4.3.5).

4.4 Summary and conclusions

The label-free DMR technology was successfully applied to CHO-K1 cells stably expressing the human dopamine D_{2long} receptor. Experiments performed at different temperatures showed that the kinetics of the agonist-induced DMR response was slightly slower at 28 °C compared to 37 °C and concentration-response curves (CRC) of D_2R agonists were almost not affected by this temperature variation. Therefore, a temperature of 28 °C, being favorable when working with a device without automated liquid handling system, was applied for all subsequent investigations. A set of reference DR ligands was characterized using the DMR assay and robust CRCs were obtained for every studied (partial) agonist as well as high-quality inhibition curves for the antagonists. It could also be shown that the DMR technology allows a discrimination between partial agonists and full agonists. The signal induced by the agonist quinpirole could be antagonized by selective D_2R antagonists, confirming that the observed DMR signal arose from a specific activation of the $D_{2long}R$ receptor.

When comparing the agonistic and antagonistic potencies obtained from DMR measurements with the pharmacological parameters obtained from pathway-specific readouts (β-arrestin2 and mini-G recruitment assay), the rank order was essentially the same. The pEC_{50} and pK_b values determined by the label-free technology tended to be higher than the values obtained from the β-arrestin2 and mini-G recruitment assay, which may be explained by the high sensitivity and the distal readout of the DMR method. However, a different expression system was used for DMR measurements compared to the pathway-specific functional assays (CHO-K1 *vs*. HEK293T cells), which could also account for the observed differences.

The utilization of specific $G\alpha_s$ $G\alpha_{i/o}$ or $G\alpha_q$ silencing agents identified the $G\alpha_{i/o}$ protein as the main proximal trigger of the observed DMR response. However, the underlying mechanisms of the marked increase in wavelength shift after treatment of the cells with forskolin remained unclear.

The present study showed that the DMR technology is a valuable method for the characterization of receptors and their ligands complementary to canonical assays used to study ligand-receptor interactions. The label-free nature of the DMR techniques suggests its use for deorphanization studies of GPCRs, provided that appropriate molecular tools such as specific pathway inhibitors, untransfected (wild type) cells and ideally also selective receptor ligands are included to verify the DMR signal specificity.

4.5   References

1.   R. M. Eglen, Functional G protein-coupled receptor assays for primary and secondary screening. *Comb Chem High Throughput Screen* **8**, 311-318; doi:10.2174/1386207054020813 (2005).

2.   T. P. Kenakin, Cellular assays as portals to seven-transmembrane receptor-based drug discovery. *Nat Rev Drug Discov* **8**, 617-626; doi:10.1038/nrd2838 (2009).

3.   C. Harrison, J. R. Traynor, The [^{35}S]GTPgammaS binding assay: approaches and applications in pharmacology. *Life Sci* **74**, 489-508; doi:10.1016/j.lfs.2003.07.005 (2003).

4.   T. B. Patel, Z. Du, S. Pierre, L. Cartin, K. Scholich, Molecular biological approaches to unravel adenylyl cyclase signaling and function. *Gene* **269**, 13-25; doi:10.1016/s0378-1119(01)00448-6 (2001).

5.   E. Trinquet, R. Bouhelal, M. Dietz, Monitoring G_q-coupled receptor response through inositol phosphate quantification with the IP-One assay. *Expert Opin Drug Discov* **6**, 981-994; doi:10.1517/17460441.2011.608658 (2011).

6.   R. M. Eglen, T. Reisine, Photoproteins: important new tools in drug discovery. *Assay Drug Dev Technol* **6**, 659-671; doi:10.1089/adt.2008.160 (2008).

7.   M. Hattori, M. Tanaka, H. Takakura, K. Aoki, K. Miura, T. Anzai, T. Ozawa, Analysis of temporal patterns of GPCR-beta-arrestin interactions using split luciferase-fragment complementation. *Mol Biosyst* **9**, 957-964; doi:10.1039/c2mb25443c (2013).

8.   R. H. Oakley, S. A. Laporte, J. A. Holt, M. G. Caron, L. S. Barak, Differential affinities of visual arrestin, beta arrestin1, and beta arrestin2 for G protein-coupled receptors delineate two major classes of receptors. *J Biol Chem* **275**, 17201-17210; doi:10.1074/jbc.M910348199 (2000).

9.   T. Littmann, A. Buschauer, G. Bernhardt, Split luciferase-based assay for simultaneous analyses of the ligand concentration- and time-dependent recruitment of beta-arrestin2. *Anal Biochem* **573**, 8-16; doi:10.1016/j.ab.2019.02.023 (2019).

10.   J. A. Allen, J. M. Yost, V. Setola, X. Chen, M. F. Sassano, M. Chen, S. Peterson, P. N. Yadav, X. P. Huang, B. Feng, N. H. Jensen, X. Che, X. Bai, S. V. Frye, W. C. Wetsel, M. G. Caron, J. A. Javitch, B. L. Roth, J. Jin, Discovery of beta-arrestin-biased dopamine D_2 ligands for probing signal transduction pathways essential for antipsychotic efficacy. *Proc Natl Acad Sci USA* **108**, 18488-18493; doi:10.1073/pnas.1104807108 (2011).

11.   S. M. Foord, T. I. Bonner, R. R. Neubig, E. M. Rosser, J. P. Pin, A. P. Davenport, M. Spedding, A. J. Harmar, International Union of Pharmacology. XLVI. G protein-coupled receptor list. *Pharmacol Rev* **57**, 279-288; doi:10.1124/pr.57.2.5 (2005).

12.   A. Sidhu, H. B. Niznik, Coupling of dopamine receptor subtypes to multiple and diverse G proteins. *Int J Dev Neurosci* **18**, 669-677; doi:10.1016/s0736-5748(00)00033-2 (2000).

13.   J. Obadiah, T. Avidor-Reiss, C. S. Fishburn, S. Carmon, M. Bayewitch, Z. Vogel, S. Fuchs, B. Levavi-Sivan, Adenylyl cyclase interaction with the D_2 dopamine receptor family; differential coupling to G_i, G_z, and G_s. *Cell Mol Neurobiol* **19**, 653-664; doi:10.1023/a:1006988603199 (1999).

14.   K. A. Neve, J. K. Seamans, H. Trantham-Davidson, Dopamine receptor signaling. *J Recept Signal Transduct Res* **24**, 165-205; doi:10.1081/rrs-200029981 (2004).

15.   D. Hilger, M. Masureel, B. K. Kobilka, Structure and dynamics of GPCR signaling complexes. *Nat Struct Mol Biol* **25**, 4-12; doi:10.1038/s41594-017-0011-7 (2018).

16.   S. Hernandez-Lopez, T. Tkatch, E. Perez-Garci, E. Galarraga, J. Bargas, H. Hamm, D. J. Surmeier, D_2 dopamine receptors in striatal medium spiny neurons reduce L-type Ca^{2+} currents and excitability via a novel PLC[beta]1-IP3-calcineurin-signaling cascade. *J Neurosci* **20**, 8987-8995; doi:10.1523/JNEUROSCI.20-24-08987.2000 (2000).

17.   J.-M. Beaulieu, S. Espinoza, R. R. Gainetdinov, Dopamine receptors – IUPHAR Review 13. *Br J Pharmacol* **172**, 1-23; doi:10.1111/bph.12906 (2015).

18.   Y. Tadori, R. A. Forbes, R. D. McQuade, T. Kikuchi, In vitro pharmacology of aripiprazole, its metabolite and experimental dopamine partial agonists at human dopamine D_2 and D_3 receptors. *Eur J Pharmacol* **668**, 355-365; doi:10.1016/j.ejphar.2011.07.020 (2011).

19.   N. Tschammer, J. Elsner, A. Goetz, K. Ehrlich, S. Schuster, M. Ruberg, J. Kuhhorn, D. Thompson, J. Whistler, H. Hubner, P. Gmeiner, Highly potent 5-aminotetrahydropyrazolopyridines: enantioselective dopamine D_3 receptor binding, functional selectivity, and analysis of receptor-ligand interactions. *J Med Chem* **54**, 2477-2491; doi:10.1021/jm101639t (2011).

20.   D. A. Hall, P. G. Strange, Evidence that antipsychotic drugs are inverse agonists at D_2 dopamine receptors. *Br J Pharmacol* **121**, 731-736; doi:10.1038/sj.bjp.0701196 (1997).

21.   D. Moller, R. C. Kling, M. Skultety, K. Leuner, H. Hubner, P. Gmeiner, Functionally selective dopamine D(2), D(3) receptor partial agonists. *J Med Chem* **57**, 4861-4875; doi:10.1021/jm5004039 (2014).

22.   B. Gardner, D. A. Hall, P. G. Strange, Pharmacological analysis of dopamine stimulation of [^{35}S]-GTP gamma S binding via human D_{2short} and D_{2long} dopamine receptors expressed in recombinant cells. *Br J Pharmacol* **118**, 1544-1550; doi:10.1111/j.1476-5381.1996.tb15572.x (1996).

23.   D. Weichert, A. Banerjee, C. Hiller, R. C. Kling, H. Hubner, P. Gmeiner, Molecular determinants of biased agonism at the dopamine D(2) receptor. *J Med Chem* **58**, 2703-2717; doi:10.1021/jm501889t (2015).

24.   Y. Fang, A. M. Ferrie, N. H. Fontaine, J. Mauro, J. Balakrishnan, Resonant Waveguide Grating Biosensor for Living Cell Sensing. *Biophys J* **91**, 1925-1940; doi:10.1529/biophysj.105.077818 (2006).

25.   J. A. Steyer, W. Almers, A real-time view of life within 100 nm of the plasma membrane. *Nat Rev Mol Cell Biol* **2**, 268-275; doi:10.1038/35067069 (2001).

26.   N. Yu, J. M. Atienza, J. Bernard, S. Blanc, J. Zhu, X. Wang, X. Xu, Y. A. Abassi, Real-time monitoring of morphological changes in living cells by electronic cell sensor arrays: an approach to study G protein-coupled receptors. *Anal Chem* **78**, 35-43; doi:10.1021/ac051695v (2006).

27.   C. W. Scott, M. F. Peters, Label-free whole-cell assays: expanding the scope of GPCR screening. *Drug Discov Today* **15**, 704-716; doi:10.1016/j.drudis.2010.06.008 (2010).

28.   R. Schroder, J. Schmidt, S. Blattermann, L. Peters, N. Janssen, M. Grundmann, W. Seemann, D. Kaufel, N. Merten, C. Drewke, J. Gomeza, G. Milligan, K. Mohr, E. Kostenis, Applying label-free dynamic mass redistribution technology to frame signaling of G protein-coupled receptors noninvasively in living cells. *Nat Protoc* **6**, 1748-1760; doi:10.1038/nprot.2011.386 (2011).

29.   Y. Fang, Label-free cell-based assays with optical biosensors in drug discovery. *Assay Drug Dev Technol* **4**, 583-595; doi:10.1089/adt.2006.4.583 (2006).

30.   Y. Fang, Non-invasive Optical Biosensor for Probing Cell Signaling. *Sensors (Basel)* **7**, 2316-2329; doi:10.3390/s7102316 (2007).

31.   M. Rocheville, J. C. Jerman, 7TM pharmacology measured by label-free: a holistic approach to cell signalling. *Curr Opin Pharmacol* **9**, 643-649; doi:10.1016/j.coph.2009.06.015 (2009).

32.   S. Lieb, S. Michaelis, N. Plank, G. Bernhardt, A. Buschauer, J. Wegener, Label-free analysis of GPCR-stimulation: The critical impact of cell adhesion. *Pharmacol Res* **108**, 65-74; doi:10.1016/j.phrs.2016.04.026 (2016).

33.   I. H. Lee, S. Saha, A. Polley, H. Huang, S. Mayor, M. Rao, J. T. Groves, Live cell plasma membranes do not exhibit a miscibility phase transition over a wide range of temperatures. *J Physic Chem B* **119**, 4450-4459; doi:10.1021/jp512839q (2015).

34.   M. D. Gottwald, J. L. Bainbridge, G. A. Dowling, M. J. Aminoff, B. K. Alldredge, New pharmacotherapy for Parkinson's disease. *Ann Pharmacother* **31**, 1205-1217; doi:10.1177/106002809703101014 (1997).

35.   M. J. Millan, L. Maiofiss, D. Cussac, V. Audinot, J. A. Boutin, A. Newman-Tancredi, Differential actions of antiparkinson agents at multiple classes of monoaminergic receptor. I. A multivariate analysis of the binding profiles of 14 drugs at 21 native and cloned human receptor subtypes. *J Pharmacol Exp Ther* **303**, 791-804; doi:10.1124/jpet.102.039867 (2002).

36. A. Newman-Tancredi, D. Cussac, V. Audinot, J. P. Nicolas, F. De Ceuninck, J. A. Boutin, M. J. Millan, Differential actions of antiparkinson agents at multiple classes of monoaminergic receptor. II. Agonist and antagonist properties at subtypes of dopamine D(2)-like receptor and alpha(1)/alpha(2)-adrenoceptor. *J Pharmacol Exp Ther* **303**, 805-814; doi:10.1124/jpet.102.039875 (2002).

37. R. B. Mailman, V. Murthy, Third generation antipsychotic drugs: partial agonism or receptor functional selectivity? *Curr Pharm Des* **16**, 488-501; doi:10.2174/138161210790361461 (2010).

38. T. F. Brust, M. P. Hayes, D. L. Roman, V. J. Watts, New functional activity of aripiprazole revealed: Robust antagonism of D$_2$ dopamine receptor-stimulated Gbetagamma signaling. *Biochem Pharmacol* **93**, 85-91; doi:10.1016/j.bcp.2014.10.014 (2015).

39. F. Ye, G. F. Anthony, V. Ronald, Label-Free Cell-Based Assays for GPCR Screening. *Comb Chem High Throughput Screen* **11**, 357-369; doi: 10.2174/138620708784534789 (2008).

40. P. H. Lee, A. Gao, C. van Staden, J. Ly, J. Salon, A. Xu, Y. Fang, R. Verkleeren, Evaluation of dynamic mass redistribution technology for pharmacological studies of recombinant and endogenously expressed g protein-coupled receptors. *Assay Drug Dev Technol* **6**, 83-94; doi:10.1089/adt.2007.126 (2008).

41. R. Schroder, N. Janssen, J. Schmidt, A. Kebig, N. Merten, S. Hennen, A. Muller, S. Blattermann, M. Mohr-Andra, S. Zahn, J. Wenzel, N. J. Smith, J. Gomeza, C. Drewke, G. Milligan, K. Mohr, E. Kostenis, Deconvolution of complex G protein-coupled receptor signaling in live cells using dynamic mass redistribution measurements. *Nat Biotechnol* **28**, 943-949; doi:10.1038/nbt.1671 (2010).

42. T. F. Brust, M. P. Hayes, D. L. Roman, K. D. Burris, V. J. Watts, Bias analyses of preclinical and clinical D$_2$ dopamine ligands: studies with immediate and complex signaling pathways. *J Pharmacol Exp Ther* **352**, 480-493; doi:10.1124/jpet.114.220293 (2015).

43. B. Gardner, P. G. Strange, Agonist action at D$_2$(long) dopamine receptors: ligand binding and functional assays. *Br J Pharmacol* **124**, 978-984; doi:10.1038/sj.bjp.0701926 (1998).

44. P. Leff, I. G. Dougall, Further concerns over Cheng-Prusoff analysis. *Trends Pharmacol Sci* **14**, 110-112; doi:10.1016/0165-6147(93)90080-4 (1993).

45. C. Horing, U. Seibel, K. Tropmann, L. Gratz, D. Monnich, S. Pitzl, G. Bernhardt, S. Pockes, A. Strasser, A Dynamic, Split-Luciferase-Based Mini-G Protein Sensor to Functionally Characterize Ligands at All Four Histamine Receptor Subtypes. *Int J Mol Sci* **21**; doi:10.3390/ijms21228440 (2020).

46. R. Nehme, B. Carpenter, A. Singhal, A. Strege, P. C. Edwards, C. F. White, H. Du, R. Grisshammer, C. G. Tate, Mini-G proteins: Novel tools for studying GPCRs in their active conformation. *PloS one* **12**, e0175642; doi:10.1371/journal.pone.0175642 (2017).

47. M. P. Hall, J. Unch, B. F. Binkowski, M. P. Valley, B. L. Butler, M. G. Wood, P. Otto, K. Zimmerman, G. Vidugiris, T. Machleidt, M. B. Robers, H. A. Benink, C. T. Eggers, M. R. Slater, P. L. Meisenheimer, D. H. Klaubert, F. Fan, L. P. Encell, K. V. Wood, Engineered luciferase reporter from a deep sea shrimp utilizing a novel imidazopyrazinone substrate. *ACS Chem Biol* **7**, 1848-1857; doi:10.1021/cb3002478 (2012).

48. J. D. Urban, W. P. Clarke, M. von Zastrow, D. E. Nichols, B. Kobilka, H. Weinstein, J. A. Javitch, B. L. Roth, A. Christopoulos, P. M. Sexton, K. J. Miller, M. Spedding, R. B. Mailman, Functional selectivity and classical concepts of quantitative pharmacology. *J Pharmacol Exp Ther* **320**, 1-13; doi:10.1124/jpet.106.104463 (2007).

49. T. Kenakin, C. Watson, V. Muniz-Medina, A. Christopoulos, S. Novick, A Simple Method for Quantifying Functional Selectivity and Agonist Bias. *ACS Chem Neurosci* **3**, 193-203; doi:10.1021/cn200111m (2012).

50. S. Wilson, J. K. Chambers, J. E. Park, A. Ladurner, D. W. Cronk, C. G. Chapman, H. Kallender, M. J. Browne, G. J. Murphy, P. W. Young, Agonist potency at the cloned human beta-3 adrenoceptor depends on receptor expression level and nature of assay. *J Pharmacol Exp Ther* **279**, 214-221(1996).

51. K. D. Burris, T. F. Molski, C. Xu, E. Ryan, K. Tottori, T. Kikuchi, F. D. Yocca, P. B. Molinoff, Aripiprazole, a novel antipsychotic, is a high-affinity partial agonist at human dopamine D$_2$ receptors. *J Pharmacol Exp Ther* **302**, 381-389; doi:10.1124/jpet.102.033175 (2002).

52. C. Locht, R. Antoine, A proposed mechanism of ADP-ribosylation catalyzed by the pertussis toxin S1 subunit. *Biochimie* **77**, 333-340; doi:10.1016/0300-9084(96)88143-0 (1995).

53. S. Mangmool, H. Kurose, G(i/o) protein-dependent and -independent actions of Pertussis Toxin (PTX). *Toxins* **3**, 884-899; doi:10.3390/toxins3070884 (2011).

54. R. Schrage, A. L. Schmitz, E. Gaffal, S. Annala, S. Kehraus, D. Wenzel, K. M. Bullesbach, T. Bald, A. Inoue, Y. Shinjo, S. Galandrin, N. Shridhar, M. Hesse, M. Grundmann, N. Merten, T. H. Charpentier, M. Martz, A. J. Butcher, T. Slodczyk, S. Armando, M. Effern, Y. Namkung, L. Jenkins, V. Horn, A. Stossel, H. Dargatz, D. Tietze, D. Imhof, C. Gales, C. Drewke, C. E. Muller, M. Holzel, G. Milligan, A. B. Tobin, J. Gomeza, H. G. Dohlman, J. Sondek, T. K. Harden, M. Bouvier, S. A. Laporte, J. Aoki, B. K. Fleischmann, K. Mohr, G. M. Konig, T. Tuting, E. Kostenis, The experimental power of FR900359 to study G_q-regulated biological processes. *Nat Commun* **6**, 10156; doi:10.1038/ncomms10156 (2015).

55. K. P. Holbourn, C. C. Shone, K. R. Acharya, A family of killer toxins. Exploring the mechanism of ADP-ribosylating toxins. *FEBS J* **273**, 4579-4593; doi:10.1111/j.1742-4658.2006.05442.x (2006).

56. K. B. Seamon, W. Padgett, J. W. Daly, Forskolin: unique diterpene activator of adenylate cyclase in membranes and in intact cells. *Proc Nat Acad Sci USA* **78**, 3363-3367; doi:10.1073/pnas.78.6.3363 (1981).

57. M. H. Johansson, A. Westlind-Danielsson, Forskolin-induced up-regulation and functional supersensitivity of dopamine D_{2long} receptors expressed by Ltk- cells. *Eur J Pharmacol* **269**, 149-155; doi:10.1016/0922-4106(94)90081-7 (1994).

58. M. H. Wanderoy, A. Westlind-Danielsson, Molecular mechanisms underlying forskolin-mediated up-regulation of human dopamine D_{2L} receptors. *Cell Mol Neurobiol* **17**, 547-555; doi:10.1023/a:1026367023458 (1997).

59. E. Tran, Y. Fang, Label-free optical biosensor for probing integrative role of adenylyl cyclase in G protein-coupled receptor signaling. *J Recept Signal Transduct Res* **29**, 154-162; doi:10.1080/10799890903052544 (2009).

60. D. Kamato, L. Thach, R. Bernard, V. Chan, W. Zheng, H. Kaur, M. Brimble, N. Osman, P. J. Little, Structure, Function, Pharmacology, and Therapeutic Potential of the G Protein, Galpha/q,11. *Front Cardiovasc Med* **2**, 14; doi:10.3389/fcvm.2015.00014 (2015).

61. O. Thastrup, P. J. Cullen, B. K. Drobak, M. R. Hanley, A. P. Dawson, Thapsigargin, a tumor promoter, discharges intracellular Ca^{2+} stores by specific inhibition of the endoplasmic reticulum Ca2(+)-ATPase. *Proc Nat Acad Sci USA* **87**, 2466-2470; doi:10.1073/pnas.87.7.2466 (1990).

62. Y. S. Kao, J. C. Fong, Thapsigargin and EGTA inhibit endothelin-1-induced glucose transport. *J Biomed Sci* **11**, 206-213; doi:10.1007/BF02256564 (2004).

63. S. Lavenus, E. Simard, E. Besserer-Offroy, U. Froehlich, R. Leduc, M. Grandbois, Label-free cell signaling pathway deconvolution of Angiotensin type 1 receptor reveals time-resolved G-protein activity and distinct AngII and AngIII\IV responses. *Pharmacol Res*; doi:10.1016/j.phrs.2018.06.027 (2018).

64. J. L. Edelman, M. Kajimura, E. Woldemussie, G. Sachs, Differential effects of carbachol on calcium entry and release in CHO cells expressing the m3 muscarinic receptor. *Cell calcium* **16**, 181-193; doi:10.1016/0143-4160(94)90021-3 (1994).

65. M. J. Berridge, P. Lipp, M. D. Bootman, The versatility and universality of calcium signalling. *Nat Rev Mol Cell Biol* **1**, 11-21; doi:10.1038/35036035 (2000).

66. R. Zaidel-Bar, G. Zhenhuan, C. Luxenburg, The contractome--a systems view of actomyosin contractility in non-muscle cells. *J Cell Sci* **128**, 2209-2217; doi:10.1242/jcs.170068 (2015).

67. G. Hayes, T. J. Biden, L. A. Selbie, J. Shine, Structural subtypes of the dopamine D_2 receptor are functionally distinct: expression of the cloned D_{2A} and D_{2B} subtypes in a heterologous cell line. *Mol Endocrinol* **6**, 920-926; doi:10.1210/mend.6.6.1323056 (1992).

Chapter 5
Summary

The family of dopamine D_2-like receptors comprises the D_2, D_3 and D_4 receptor, which exist in different isoforms, due to alternative splicing of the mRNA or polymorphisms in the coding sequence for the respective receptor. The D_2-like receptors are implicated in various pathological conditions, such as schizophrenia, Parkinson's disease, substance abuse or attention deficit hyperactivity disorder (ADHD) among others. This renders them an important target for the development of therapeutic drugs and pharmacological tools, facilitating the elucidation of distinct functions of the receptor subtypes. For the characterization of dopamine receptor ligands regarding their affinities to the receptor subtypes and their functional properties, a variety of technologies is available. This thesis aimed at the establishment of a radioligand binding assay to enable the investigation of ligand affinities at D_{2long}, D_3 and $D_{4.4}$ receptors, the most commonly occurring isoforms. Further, providing a proximal functional readout that enables the determination of agonism or antagonism of ligands, a β-arrestin2 recruitment assay was established. The label-free DMR technology yields a distal readout, generated from the response of whole cells to stimulation of an expressed receptor and was chosen to extend the pharmacological toolbox for the characterization of ligands at D_2 receptors. Label-free methods have the advantage of being less prone to false negatives regarding biased ligands since the whole cell response is detected, compared to the quantification of one distinct signaling event in more traditional functional assays. Unfortunately, it was not possible to establish the DMR assay for the D_3R and the $D_{4.4}R$.

For the binding assay, the high affinity D_2-like receptor antagonist [^{3}H]N-methylspiperone was chosen as radioligand and binding to all three D_2-like receptor subtypes was investigated using whole cells and homogenates prepared from the same cell lines. The utilization of homogenates appeared more useful, especially regarding the investigation of agonists. Agonists distinguish between high and low affinity states of the D_2-like receptors, which appears undetectable when whole cell preparations are used. Further studies were carried out with cell homogenates. The binding kinetics of [^{3}H]N-methylspiperone and the detectability of high affinity states of the $D_{2long}R$, D_3R and $D_{4.4}R$ were investigated. A library of well-known reference ligands was screened and obtained data was compared with literature reports, leading to the conclusion that the established method is a reliable tool for the determination of ligand affinities. Hence, several histamine H_2 receptor agonists generated by our group could be tested for their affinities to the $D_{2long}R$, D_3R and $D_{4.4}R$, supporting the development of histamine H_2 receptor specific compounds.

By developing a β-arrestin2 recruitment assay employing the split Emerald luciferase (ELuc) technique, agonist and antagonistic properties could be determined at the $D_{2long}R$ and the D_3R. At the $D_{4.4}R$, as described in the literature, no β-arrestin recruitment could be determined. Expression of the receptor and the β-arrestin2 fusion proteins with complementary fragments of the ELuc were confirmed by radioligand binding experiments and Western Blotting. Radioligand competition binding studies were

performed and showed that the modification of the receptor does not impact the ligand affinities. β-Arrestin2 recruitment to the $D_{2long}R$ was distinct, yielded excellent signal-to-background ratios and could be monitored in real-time using whole cells. The D_3R recruited β-arrestin2 in a less pronounced manner, but by performing lysis-based endpoint measurements, robust concentration-response and inhibition curves could still be generated.

The DMR assay was established using CHO-K1 cells stably expressing the $hD_{2long}R$, as CHO cells exhibit favorable adhesion properties. Assay conditions were optimized, regarding factors such as the cell seeding density or the assay temperature. Sets of reference (partial) agonists and antagonists were investigated using the DMR technique and the resulting potencies were compared to data obtained from other more conventional assays. Agonists, as well as antagonists exhibited the highest potencies in the DMR assay. The underlying reasons cannot fully be elucidated since different expression systems were used (HEK293T cells or CHO-K1 cells) for the performance of the different assays. However, the DMR assay provides a very distal readout, which is prone to signal amplification and may contribute to the comparably higher potencies. Investigations using pharmacological tools such as pertussis toxin, identified the $G_{i/o}$ protein to be the main trigger of the cell response observed by DMR measurements.

Altogether, the methods described in this thesis in combination with the mini-G protein recruitment assay provide a broad range of assays for the characterization of newly synthesized compounds regarding their affinities and functional properties.

Chapter 6
Appendix

6.1 Appendix to Chapter 2

6.1.1 Supplementary figures
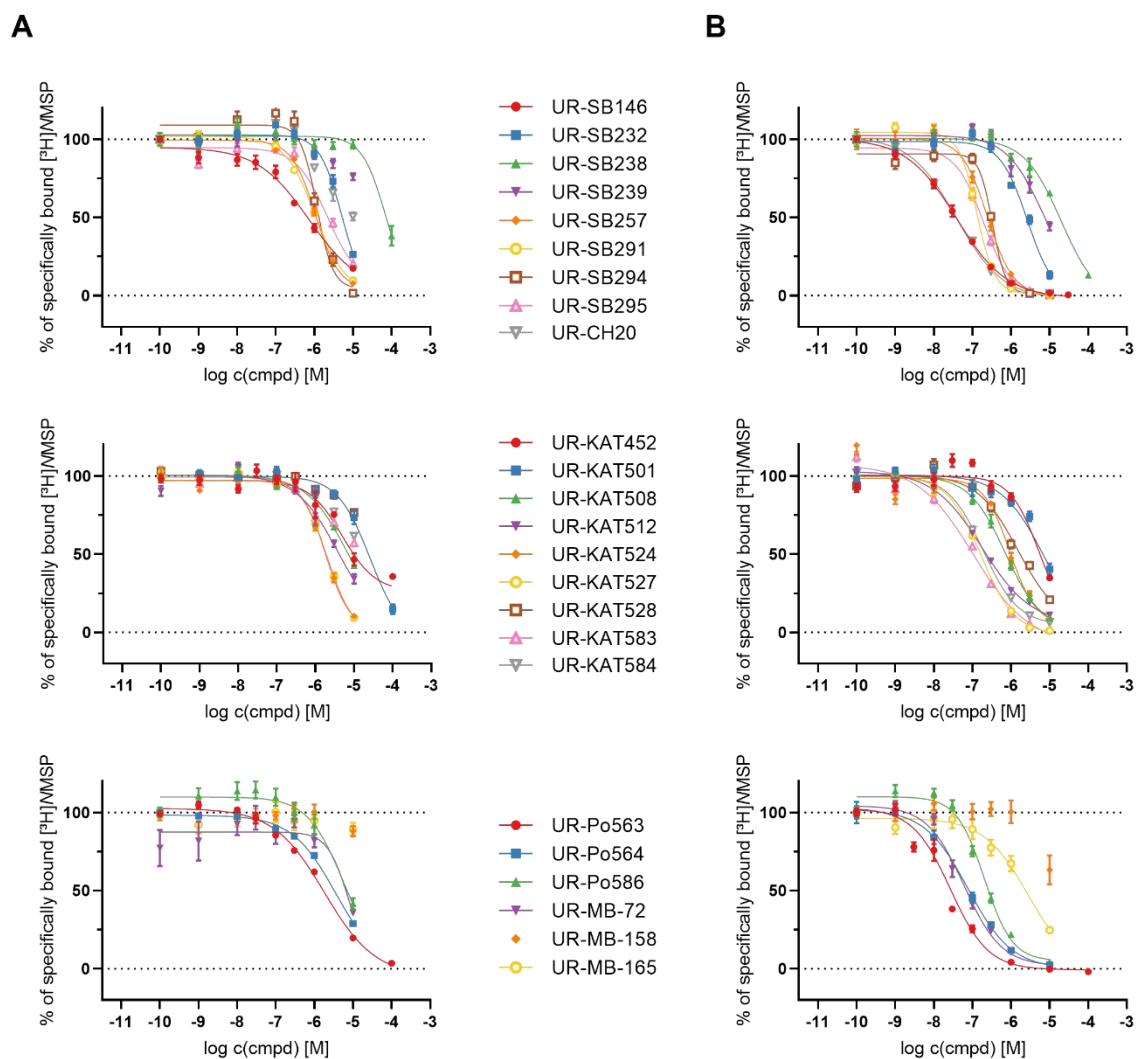
Figure A1. Radioligand displacement curves from competition binding experiments performed with [³H]*N*-methylspiperone ([³H]*N*MSP; 0.25 nM) and carbamoylguanidine- as well as thiocarbamoylguanidine-type histamine H$_2$ receptor ligands (structures see Figure 9) at cell homogenates prepared from HEK293T CRE Luc cells co-expressing the D$_{2long}$R (**A**) or the D$_3$R (**B**). Data represent mean values ± SEM from at least three independent experiments, each performed in triplicate.

6.1.2   Supplementary tables

Table A1. $D_{2long}R$ and D_3R receptor affinities of carbamoylguanidine-type and thiocarbamoylguanidine-type histamine H_2 receptor ligands obtained from [^{3}H]*N*-methylspiperone competition binding studies using HEK293T CRE Luc $hD_{2long}R$ or hD_3R cell homogenates.

cmpd.	$D_{2long}R$ pK_i ± SEM	N	D_3R pK_i ± SEM	N
UR-CH20	<5	3	7.76 ± 0.08	3
UR-SB146	6.62 ± 0.07	3	7.73 ± 0.09	3
UR-SB232	5.63 ± 0.05	3	5.91 ± 0.04	3
UR-SB257	6.30 ± 0.07	3	6.96 ± 0.06	3
UR-SB291	6.30 ± 0.14	3	7.23 ± 0.03	3
UR-SB294	6.32 ± 0.08	3	6.82 ± 0.03	3
UR-SB295	6.15 ± 0.07	3	7.08 ± 0.06	3
UR-KAT452	6.07 ± 0.29	3	5.89 ± 0.12	3
UR-KAT501	5.01 ± 0.11	3	5.54 ± 0.10	4
UR-KAT508	<5	3	6.50 ± 0.09	4
UR-KAT512	<5	3	7.07 ± 0.05	3
UR-KAT524	6.13 ± 0.09	3	6.35 ± 0.05	3
UR-KAT527	6.04 ± 0.10	3	7.13 ± 0.05	3
UR-KAT528	<5	3	6.13 ± 0.04	3
UR-KAT584	<5	3	7.06 ± 0.03	3
UR-Po564	5.86 ± 0.06	3	7.48 ± 0.10	3
UR-Po586	5.63 ± 0.07	3	7.10 ± 0.05	3
UR-MB-72	6.32 ± 0.09	3	7.64 ± 0.14	3
UR-MB-158	<5	3	<5	3
UR-MB-165	<5	3	5.87 ± 0.15	3

Data represent means ± SEM. *N* denotes the number of independent experiments, each performed in triplicate.

6.2　　　Appendix to Chapter 3

6.2.1　　Supplementary figures
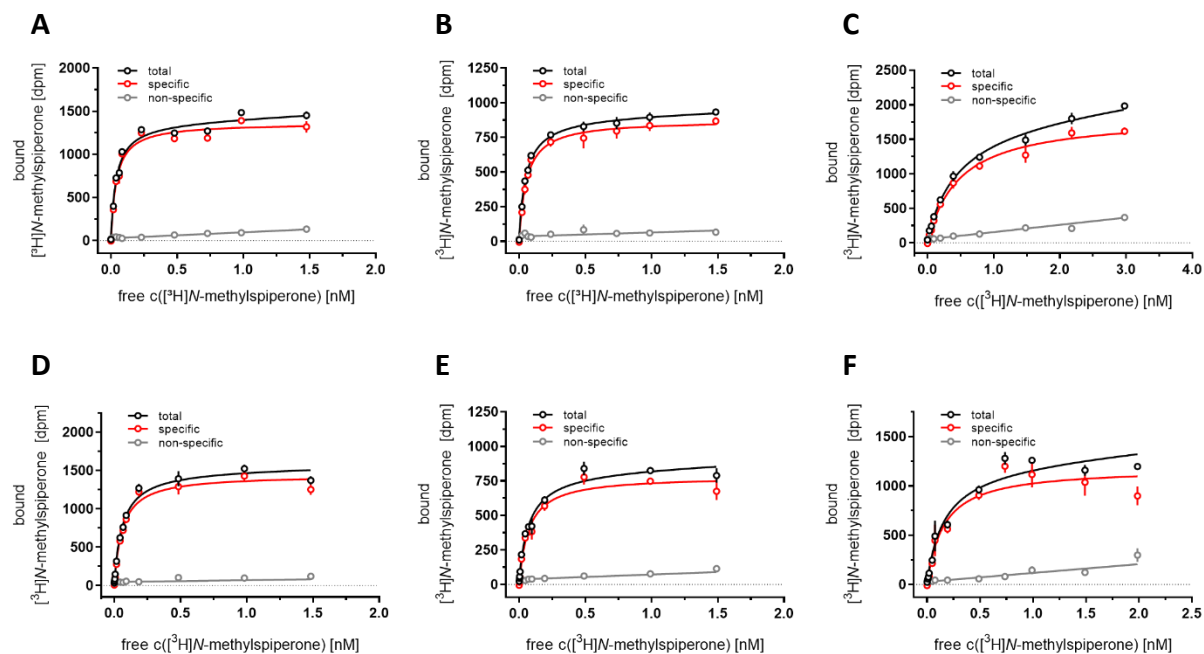
Figure A2. Radioligand binding curves from saturation binding experiments performed with [³H]*N*-methylspiperone at whole HEK293T ELucN-βarr2 cells expressing the hD$_{2long}$R-ELucC (**A**), hD$_3$R-ELucC (**B**) or hD$_{4.4}$R-ELucC (**C**) fusion proteins, and at homogenates from cells expressing the wild-type hD$_{2long}$R (**D**), hD$_3$R (**E**) or hD$_{4.4}$R (**F**). Corresponding dissociation constants are provided in **Table 1** in Chapter 3. Data are representative (means ± SEM) of three independent experiments, each performed in triplicate.

A

MW (kDa)   1   2   3

150 -

100 -   - ELucN-βarr2

75 -

50 -

B

MW (kDa)   1   2   3

100 -

75 -   - D$_{2long}$R-ELucC

                              - D$_3$R-ELucC

50 -

C

MW (kDa)   1   2   3

250 -

150 -

                              - Vinculin

100 -

75 -

D

MW (kDa)   1   2   3

250 -

150 -

                              - Vinculin

100 -

75 -
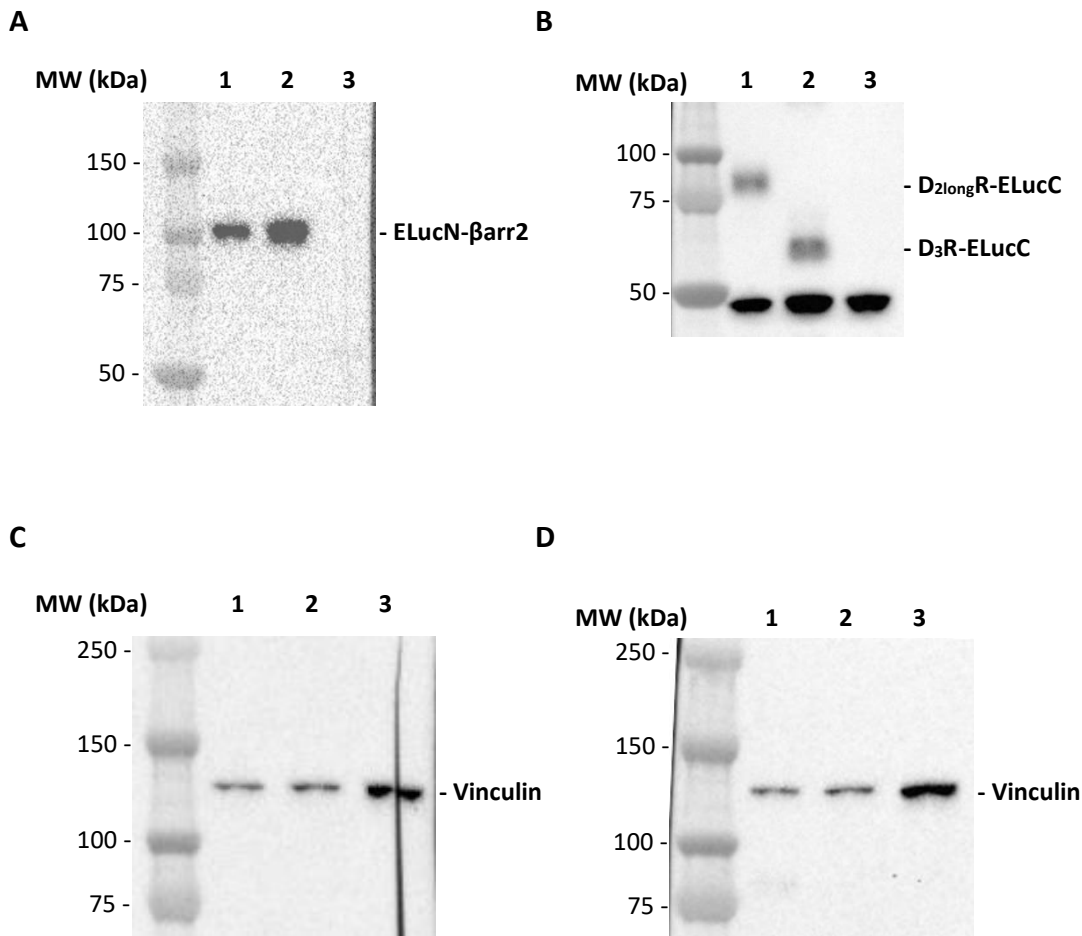
Figure A3. Western blot analysis of lysates of HEK293T cells expressing the ELucN-βarr2 and the hD$_{2long}$R-ELucC (lane 1) or the ELucN-βarr2 and the hD$_3$R-ELucC (lane 2) fusion proteins. A lysate of HEK293T wildtype cells was included in every blot as a negative control (lane 3). For primary staining an anti-myc antibody was used for detection of the ELucN-βarr2 fusion protein (**A**) or an anti-V5 antibody was used for detecting the hD$_{2long}$R-ELucC and the hD$_3$R-ELucC fusion proteins (**B**). An anti-vinculin antibody was used for detecting the housekeeping protein vinculin as a loading control (**C**, **D**). Depicted are superpositions of the chemiluminescent blots with a colorimetric image showing the molecular weight marker. **A**: ELucN-βarr2 has a theoretical molecular weight of 92.3 kDa, calculated from the amino acid sequence. **B**: hD$_{2long}$R-ELucC has a theoretical molecular weight of 67.5 kDa but appears in between the marker bands for 75 and 100 kDa. High levels of posttranslational modifications, such as glycosylation, have been reported for the D$_2$R[1], assumingly causing the appearance of this fusion protein at a higher molecular weight. The calculated molecular weight for the hD$_3$R-ELucC fusion protein is 61 kDa. The anti-V5 antibody revealed unspecific bands just below the 50 kDa in all three lanes. The unspecific binding of this antibody was already described elsewhere[2]. **C** + **D**: The blots shown in **A** and **B** were stripped from all antibodies after detection of chemiluminescence and subsequently treated with an anti-vinculin antibody. Vinculin has a molecular weight of 116 kDa. The procedure is described in detail in section 6.1.3.1.
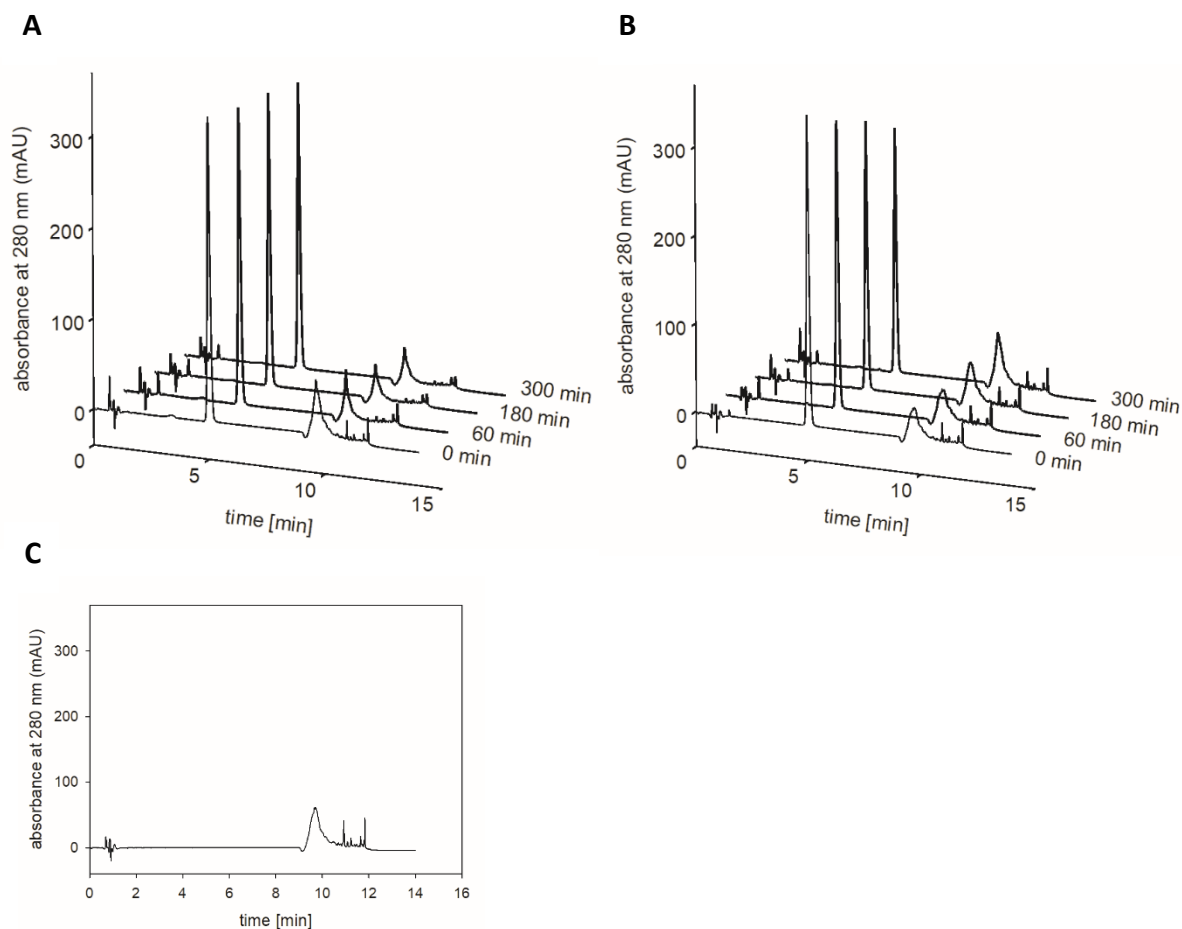
Figure A4. UHPLC chromatograms (λ: 280 nm) of dopamine after different incubation periods at 22 ± 1 °C (**A**) or at 37 °C (**B**) in PBS (pH 7.4). Dopamine is eluted after 5 min. After an incubation period of 300 min at 37 °C, only 78% of the analyte were retrieved. After 9-10 min impurities are eluted, that might originate from the mobile phase, since the peak also appears in the blank run (**C**). The method is described in detail in chapter 5.1.3.2.
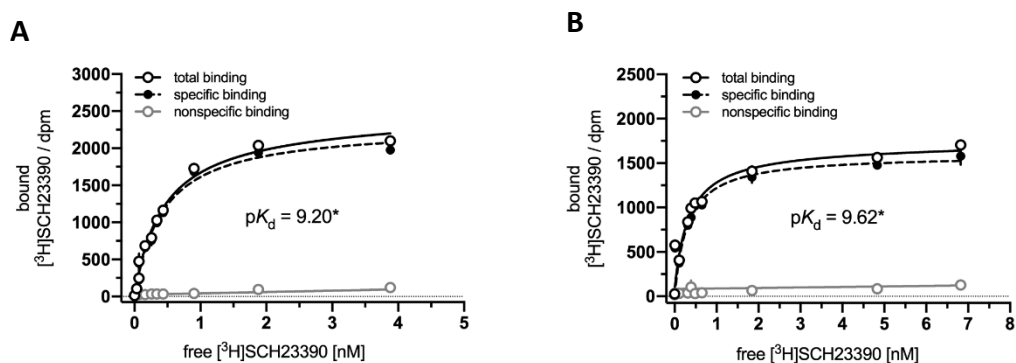

Figure A5. Radioligand saturation binding curves with whole HEK293T ELucN-βarr2 cells expressing the hD$_1$R-ELucC (**A**) fusion protein and homogenates from cells expressing the human wild-type D$_1$R (**B**). Corresponding dissociation constants are provided in **Table A1**. Graphs are representatives (means ± SEM) of three independent experiments, each performed in triplicate. *pK_d values are given as mean from three independent experiments, each performed in triplicate.
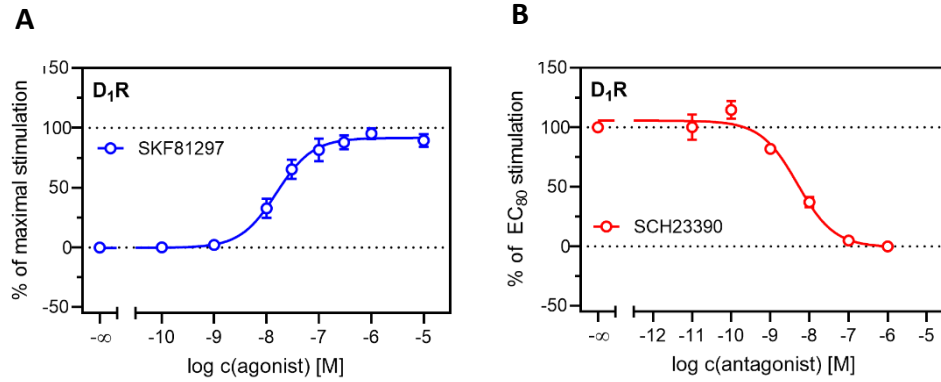
Figure A6. Characterization of the standard agonist SKF81297 and standard antagonist SCH23390 in the β-arrestin2 recruitment assay at the hD_1R. Data of the agonist were normalized to the maximal stimulation (100%) and a solvent control (0%). Antagonist data were normalized to the signal elicited by SKF81297 at a concentration corresponding to the EC_{80} (100%) and a solvent control (0%). Obtained pEC_{50} and pK_b values are presented in **Table A2**. Data represent means ± SEM from at least three independent experiments, each performed in triplicate.

6.2.2   Supplementary tables

Table A2. Dissociation constants (pK_d values) of [³H]SCH23390 determined in radioligand saturation binding experiments at receptors fused to the C-terminal fragment of the Emerald luciferase using whole cells and at wild-type receptors using homogenates.

	D_1R	
	ELucC fusion protein	**wt**
pK_d	9.20 ± 0.09	9.62 ± 0.07

Data represent means ± SEM from three independent experiments, each performed in triplicate.

Table A3. pEC$_{50}$, E$_{max}$ and pK_b values of SKF81297 and SCH23390 analyzed in the newly developed β-arrestin2 recruitment assay at the D_1R. For comparison, pK_i values from published data are included.

receptor	cmpd	β-arrestin2 recruitment		Ref.
		pEC$_{50}$	**pK_b**	**pK_i**
D_1R	SKF81297	7.75 ± 0.15		7.47[3]
	SCH23390		8.84 ± 0.07	9.33[4]

Data represent means ± SEM from 3 independent experiments, each performed in triplicate.

6.2.3   Supplementary methods

6.2.3.1   *Western blot analysis*

Cell lysates of HEK293T cells expressing the ELucN-βarr2 and the D$_{2long}$R-ELucC or the D$_3$R-ELucC fusion proteins (*cf*. section 3.3.5) and untransfected HEK293T cells were cultured in T-175 cell culture flasks to a confluency of about 85%. The cells were washed with phosphate-buffered saline (PBS, containing 137 mM NaCl, 2.7 mM KCl, 10 mM Na$_2$HPO$_4$, 1.8 mM KH$_2$PO$_4$) and harvested with a cell scraper. They were lysed using a RIPA lysis buffer (50 mM Tris, 0.1% sodium dodecyl sulfate, 0.5% sodium deoxycholate, 1% Triton X-100, 150 mM NaCl, pH 7.8) supplemented with protease inhibitors (SigmaFAST Cocktail Tablets, EDTA-free, Sigma-Aldrich, Taufkirchen, Germany) and stored in aliquots at -20 °C to the day of western blot analysis.

For western blots, cell lysates were diluted with RIPA buffer and mixed in a 1:1 ratio with Laemmli 2x buffer supplemented with urea (125 mM Tris-HCl, 20% glycerol, 10% 2-mercaptoethanol, 4% sodium dodecyl sulfate, 0.004% bromphenol blue, 8 M urea, pH 6.8) to a final concentration of 0.75 µg soluble

protein/µL and incubated at 30 °C for 1 h. After incubation, 20 µg of soluble protein per lane were separated on a gradient polyacrylamide gel (Novex WedgeWell 8-16% Tris-Glycine Gel, Thermo Fisher Scientific, Nidderau, Germany), as well as a protein standard (Precision Plus Protein Dual Color Standard, Bio-Rad, Germany). The proteins were electroblotted on a nitrocellulose membrane at 0.1 A for 1 h and the transfer efficiency was monitored by staining the proteins with Ponceau-S. The membrane was rinsed with water and unspecific binding sites were blocked with 5% skim milk powder in PBS-T (PBS, pH 7.4, containing 0.05% Tween 20) for 2 h. For analysis of the proteins of interest an anti-myc antibody (R950-25, Invitrogen, Waltham, MA, USA) and an anti-V5 antibody (R960-25, Invitrogen), both produced in mouse, were used as primary antibodies at a dilution of 1:5000 in PBS-T complemented with 5% skim milk. The membranes were incubated with the antibodies overnight at 4 °C on a roller mixer. The next day, the blots were washed three times with PBS-T and a secondary anti-mouse antibody conjugated to horseradish-peroxidase (HRP) (A0168, Sigma-Aldrich) was applied in a 1:50000 dilution in PBS-T without milk for 2 h. Afterwards, the blots were washed three times with PBS-T and bands were detected using an ECL reagent (Clarity Western ECL Substrate, Bio-Rad). Emitted luminescence was recorded with a ChemiDoc MP imaging system (Bio-Rad) with differing exposure times, depending on the analyte.

Before developing the membranes with an anti-vinculin antibody (MAB6896, Bio-Techne, Minneapolis, MN, USA) as a loading control, the blots were stripped from all antibodies, i. e. the blots were washed with PBS-T and incubated with stripping buffer (15 mM glycine, 3.5 mM SDS, 1% Tween 20, pH 2.2) at room temperature for 10 min. Subsequently, the membranes were washed with PBS and TBS-T (50 mM Tris-HCl, 150 mM NaCl, pH 7.6; 0.05% Tween 20) and then blocked with 5% skim milk powder in PBS-T for 2 h. Primary antibody was added at a 1:500 dilution in PBS-T and incubated at 4 °C over night. Incubation with the secondary antibody and detection of chemiluminescence was carried out as described above.

6.2.3.2   *Dopamine stability in aqueous solution*

The stability of dopamine was investigated in PBS. The solutions were prepared in triplicates in PBS at an initial concentration of 900 µM and incubated at room temperature or 37 °C for a total of 300 min. Samples were taken after 0, 60, 180 and 300 min and diluted 1:1 with the starting gradient immediately before injection. An ion pair chromatography method described by Pramar et al.[5] was applied and modified for this study. The measuring equipment included an agilent 1290 infinity binary pump, an agilent 1290 infinity autosampler and a 1260 infinity diode array detector by which dopamine was detected at 280 nm. The injection volume was 20 µL and separations were carried out using a kinetex C18 column (100 mm x 3.00 mm) by phenomenex (Aschaffenburg, Germany). The mobile phase A, pH 3, was composed of 0.01% glacial acetic acid, 5 mM 1-hexanesulfonic acid (sodium salt; Sigma

Aldrich) in water, whereas mobile phase B was acetonitrile. The following gradient was applied for the UHPLC analysis: 0-8 min: A/B 95:5 (isocratic), 8-11 min: 95:5-80:20, 11-14 min: 80:20 (isocratic), 14-15 min: 80:20-95:5, 15-17 min: 95:5 (isocratic). On each day of measurement, a calibration curve was recorded using dopamine solutions in PBS at different concentrations (100 – 500 µM) and the sample concentrations were calculated using the linear equation of the calibration curve.

# 6.3 Appendix to Chapter 4

6.3.1 Supplementary figures
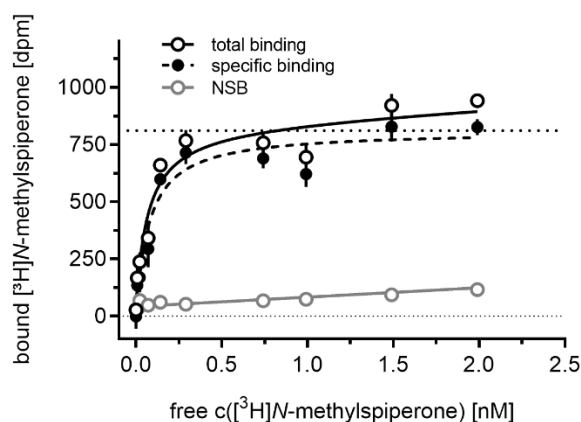
Figure A7. Representative radioligand saturation binding curve obtained from saturation binding experiments with [^{3}H]N-methylspiperone at whole CHO-K1 hD$_{2long}$R cells. Experiments were performed as described in chapter 2, Material and Methods 2.3.6. 35,000 cells per well were applied and non-specific binding was determined in the presence of a 2000-fold excess (+)-butaclamol. Shown is one representative experiment performed in triplicate of two independent experiments. A pK_d value of 10.20 ± 0.07 (mean ± SEM) was determined (for comparison, at whole HEK293T CRE Luc hD$_{2long}$R cells in chapter 2 a pK_d of 10.02 was determined). Error bars of specific binding represent propagated errors. Error bars of total and non-specific binding represent the SEM.
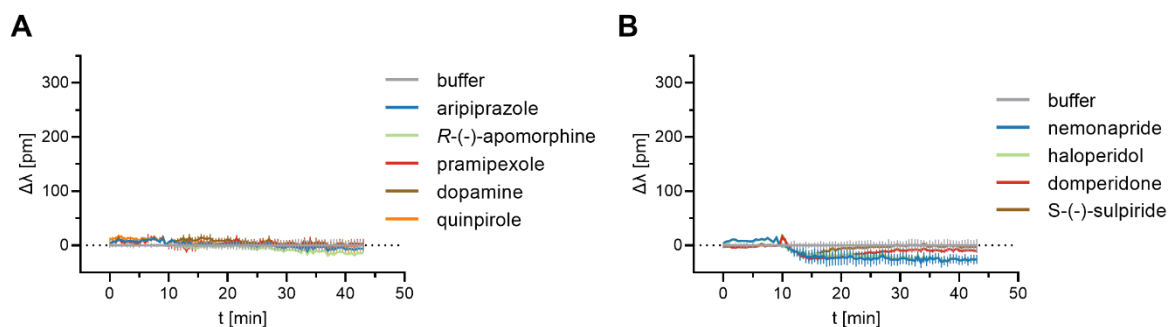

Figure A8. Investigation of the effect of the indicated agonists (**A**) or antagonists (**B**) on CHO-K1 cells in the DMR assay. None of the agonists produced a shift in wavelength. Nemonapride and haloperidol showed a slight negative DMR signal (Δλ about -30 pm). Shown are representatives (means ± SEM) of three independent experiments, each performed in triplicate.
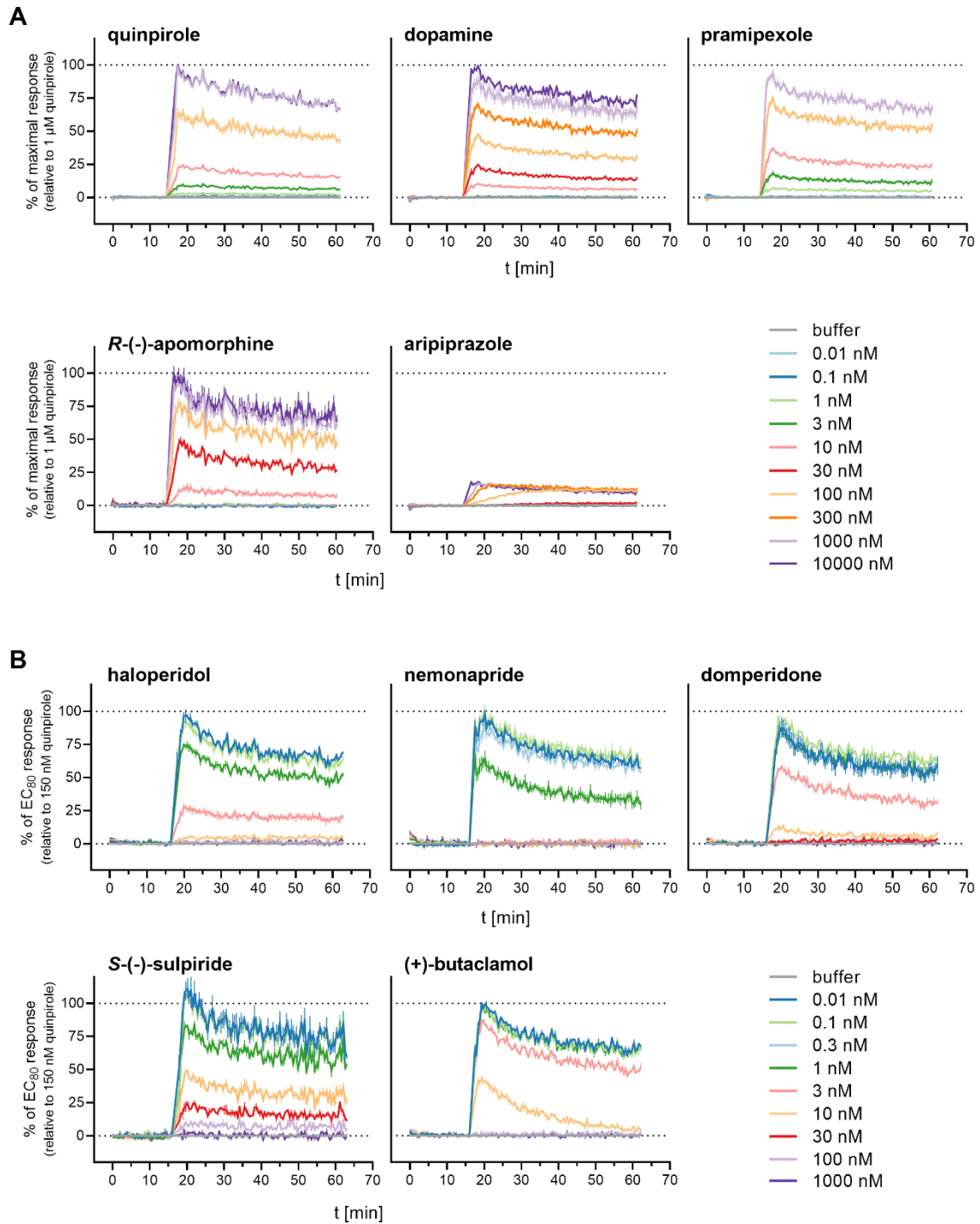
Figure A9. Effect of selected dopamine D_2R agonists and antagonists on mini-Gsi recruitment in HEK293T cells coexpressing the $D_{2long}R$-NLucC and NLucN-mGsi fusion proteins. **A:** representative luminescence traces upon stimulation with agonists. **B:** inhibition of the quinpirole-stimulated mini-Gsi recruitment by antagonists. Data obtained from experiments with agonists (**A**) were normalized to the maximal response induced by 1 µM quinpirole (100%) and L-15 (0%). In antagonist mode (**B**), the experiments were carried out in the presence of quinpirole at a concentration (150 nM) eliciting 80% of the maximal response. The data were normalized to the maximal response elicited by 150 nM quinpirole (100%) and L-15 (0%). Shown are means ± SEM of representative experiments performed in triplicate, of at least three independent experiments.
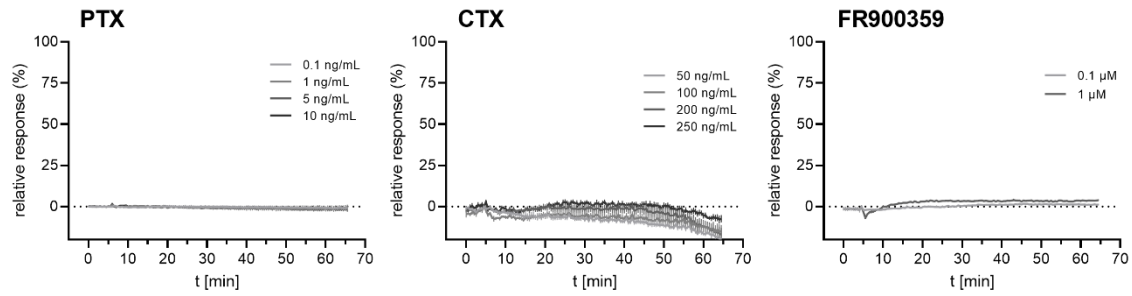
Figure A10. Effect of PTX, CTX or FR900359 on the DMR response of CHO-K1 hD$_{2long}$R cells. Shown are representatives (mean ± SEM) of three independent experiments, each performed in triplicate.
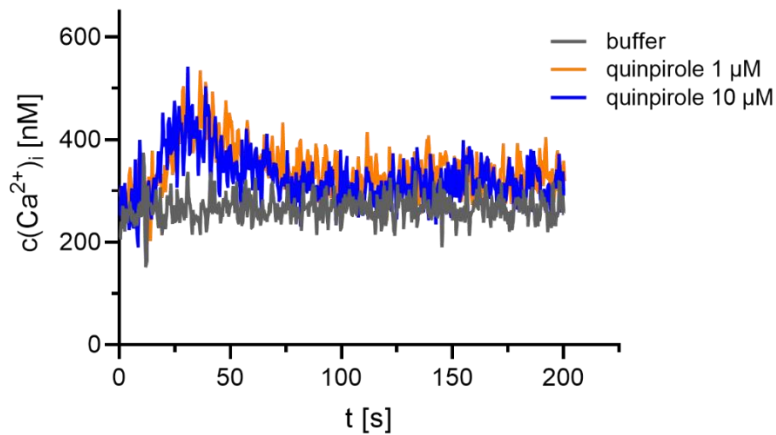

Figure A11. Increase in intracellular Ca^{2+} upon stimulation of CHO-K1 hD$_{2long}$R cells with quinpirole (10 and 1 µM) determined in a Fura-2 calcium assay. Shown is one representative experiment of three independent measurements. The Fura-2 calcium assay was performed as previously described with a LS50 B luminescence spectrophotometer (Perkin Elmer, Rodgau, Germany)[6].
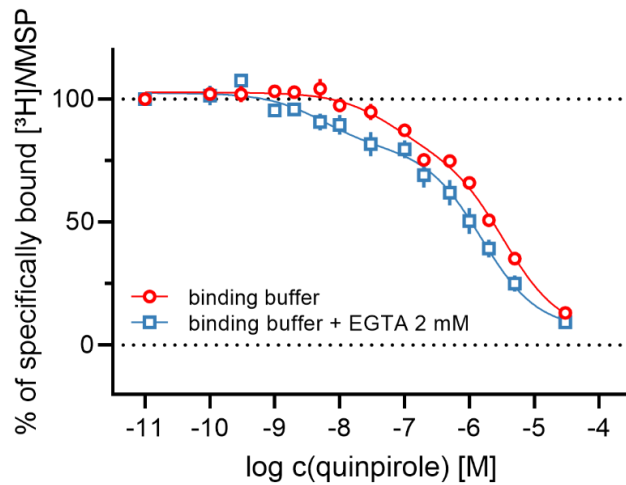
Figure A12. Comparison of radioligand displacement curves obtained from competition binding experiments with [³H]*N*-methylspiperone ([³H]*N*MSP; 0.05 nM) and quinpirole under regular conditions (red line, as described in chapter 2, section 2.3.6) and in the presence of EGTA (2 mM, blue line). The experiments were performed as described in section 2.3.6 using homogenates prepared from HEK293T CRE Luc hD$_{2long}$R cells. Data are means ± SEM of three independent experiments, each performed in triplicate.

6.4 References

1. T. Stojanovic, M. Orlova, F. J. Sialana, H. Hoger, S. Stuchlik, I. Milenkovic, J. Aradska, G. Lubec, Validation of dopamine receptor DRD1 and DRD2 antibodies using receptor deficient mice. *Amino Acids* **49**, 1101-1109; doi:10.1007/s00726-017-2408-3 (2017).

2. J. Felixberger, Luciferase complementation for the determination of arrestin recruitment: Investigations at histamine and NPY receptors. Dissertation, University of Regensburg, Regensburg; doi:10.5283/epub.31292 (2014).

3. P. H. Andersen, J. A. Jansen, Dopamine receptor agonists: selectivity and dopamine D_1 receptor efficacy. *Eur J Pharmacol* **188**, 335-347; doi:10.1016/0922-4106(90)90194-3 (1990).

4. R. K. Sunahara, H. C. Guan, B. F. O'Dowd, P. Seeman, L. G. Laurier, G. Ng, S. R. George, J. Torchia, H. H. Van Tol, H. B. Niznik, Cloning of the gene for a human dopamine D_5 receptor with higher affinity for dopamine than D_1. *Nature* **350**, 614-619; doi:10.1038/350614a0 (1991).

5. Y. Pramar, V. Das Gupta, S. N. Gardner, B. Yau, Stabilities of dobutamine, dopamine, nitroglycerin and sodium nitroprusside in disposable plastic syringes. *J Clin Pharm Ther* **16**, 203-207; doi:10.1111/j.1365-2710.1991.tb00305.x (1991).

6. M. Muller, S. Knieps, K. Gessele, S. Dove, G. Bernhardt, A. Buschauer, Synthesis and neuropeptide Y Y1 receptor antagonistic activity of N,N-disubstituted omega-guanidino- and omega-aminoalkanoic acid amides. *Arch Pharm (Weinheim)* **330**, 333-342; doi:10.1002/ardp.19973301104 (1997).

Abbreviations

1,4-DAP	1,4-disubstituted aromatic piperazines and piperidines
AC	adenylyl cyclase
ADHD	attention deficit hyperactivity disorder
ATP	adenosine-5'-triphosphate
AUC	area under the curve
B_{max}	maximum number of binding sites
BRET	bioluminescence resonance energy transfer
CamKII	Ca^{2+}/calmodulin-dependent protein kinase II
cAMP	3'-5'-cyclic adenosine monophosphate
CDK5	cyclin-dependent kinase 5
CHO	Chinese hamster ovary cells
cpd101	Takeda compound 101
CNS	central nervous system
CRC	concentration-response curve
CRE	cAMP response element
CTX	cholera toxin
DAG	diacyl glycerol
DARPP-32	32-kDa dopamine and cAMP regulated phosphoprotein
DMEM	Dulbecco's modified Eagle's medium
DMR	dynamic mass redistribution
dpm	disintegrations per minute
DR	dopamine receptor
EC_{50}	concentration of an agonist that induces 50% of its maximal response
ECIS	electric cell-substrate impedance sensing
ECL	extracellular loop
ELuc	engineered Emerald luciferase from the click beetle *Pyrearinus termitilluminans*
E_{max}	maximal response of a compound in a functional assay
FCS	fetal calf serum
fsk	forskolin

G416	geneticin
GDP	guanosine diphosphate
GIRK	G protein-coupled inwardly rectifying potassium channels
GPCR	G protein-coupled receptor
Gpp(NH)p	guanylylimidodiphosphate
GRK	G protein-coupled receptor kinase
GSK3	glycogen synthase kinase 3
GTP	guanosine-5'-triphosphate
hD_1R	human dopamine D_1 receptor
hD_2R	human dopamine D_2 receptor
hD_3R	human dopamine D_3 receptor
hD_4R	human dopamine D_4 receptor
HEK293T	human embryonic kidney cells
IC_{50}	inhibitor concentration, that displaces 50% of a labeled ligand from the binding site or antagonist concentration, that suppresses 50% of the agonist induced response
ICL	intracellular loop
K_b	dissociation constant of a ligand determined in a functional assay
K_d	equilibrium dissociation constant
K_i	equilibrium dissociation constant of a ligand determined in a competition binding assay
k_{obs}	observed association rate constant
k_{off}	dissociation rate constant
k_{on}	association rate constant
L-15	Leibovitz' L-15 medium
mGluR1	metabotropic glutamate receptor-1
mRNA	messenger RNA (ribonucleic acid)
NLuc	NanoLuc® luciferase
NMSP	N-methylspiperone
NSB	non-specific binding
OBS	orthosteric binding site
PBS	phosphate buffered saline

PCR	polymerase chain reaction
PKA	protein kinase A
PLC	phospholipase C
PP1	protein phosphatase 1
PP2A	protein phosphatase 2A
PTX	pertussis toxin
RWG	resonant waveguide grating
S/B	signal-to-background ratio
SP	signal peptide
TM	transmembrane
UHPLC	ultra high performance liquid chromatography

Eidesstattliche Erklärung

Ich erkläre hiermit an Eides statt, dass ich die vorliegende Arbeit ohne unzulässige Hilfe Dritter und ohne Benutzung anderer als der angegebenen Hilfsmittel angefertigt habe; die aus anderen Quellen direkt oder indirekt übernommenen Daten und Konzepte sind unter Angabe des Literaturzitats gekennzeichnet.

Einige der experimentellen Arbeiten wurden in Zusammenarbeit mit anderen Institutionen und Personen durchgeführt. Vermerke zu den Beiträgen der betreffenden Personen finden sich in den jeweiligen Kapiteln.

Weitere Personen waren an der inhaltlich-materiellen Herstellung der vorliegenden Arbeit nicht beteiligt. Insbesondere habe ich hierfür nicht die entgeltliche Hilfe eines Promotionsberaters oder anderer Personen in Anspruch genommen. Niemand hat von mir weder unmittelbar noch mittelbar geldwerte Leistungen für Arbeiten erhalten, die im Zusammenhang mit dem Inhalt der vorgelegten Dissertation stehen.

Die Arbeit wurde bisher weder im In- noch im Ausland in gleicher oder ähnlicher Form einer anderen Prüfungsbehörde vorgelegt.

Regensburg, den   _____

                                                                              Lisa Forster